Brake Steer Torque Optimized Corner Braking of Motorcycles

Bremslenkmomentoptimierte Kurvenbremsung von Motorrädern

Am Fachbereich Maschinenbau an der
Technischen Universität Darmstadt
zur Erlangung des Grades eines
Doktor-Ingenieurs (Dr.-Ing.)
genehmigte

Dissertation

vorgelegt von

Dipl.-Ing. Kai Gerd Schröter
aus Gelnhausen

Berichterstatter:	Prof. Dr. rer. nat. Hermann Winner
Mitberichterstatter:	Prof. Dr.-Ing. Markus Lienkamp
Tag der Einreichung:	02.12.2014
Tag der mündlichen Prüfung:	04.02.2015

Darmstadt 2016

D 17

Acknowledgements

This thesis presents the results of my work performed as a research assistant at the Institute of Automotive Engineering *FZD* at the Technische Universität Darmstadt, Germany. It would not have been possible without the support of many people, to all of whom I would like to express my sincere gratitude.

I am especially thankful to Professor Dr. rer. nat. Hermann Winner, head of *FZD*, for the trust he put in me and for the freedom I was granted working in the field of motorcycle research. His guidance and stimulations, his patience and continuous support despite some hardships along the way were indispensable for the completion of this thesis.

For his interest in the project and his support as my co-examiner, I thank Professor Dr.-Ing. Markus Lienkamp, head of the Institute of Automotive Engineering *FTM* at Technische Universität München, Germany.

I am lacking the words to express my gratitude to Dr.-Ing. Alois Weidele, lecturer for motorcycles at *FZD*, for everything he taught me during our many years of fruitful co-operation, but most of all for his continuous encouragement, inspiring discussions and friendship. As the inventor of the Brake Steer Torque Avoidance Mechanism, the core element of this study, I thank him and his former research team under supervision of Professor em. Bert Breuer, for dreaming and thinking thus far ahead.

To the partners at Honda, in particular Kazuhiko Tani, Yasuhiro Uchiike, and Oliver Fuchs, I am thankful for giving these dreams wings in many ways, not only by funding the core research project and sponsoring the base motorcycle, but also for the numerous beneficial discussions and unbureaucratic support with whatever was needed.

Concerning the equipment of the research motorcycle, I am grateful to FAG/Schaeffler Technologies for providing a pair of unique steering head bearings, to Adalbert Hammer Feinwerktechnik for the absolutely perfect application of strain gauges, and to GSG Mototechnik as well as MaxXxware Germany for their generous discounts.

The invaluable support of many students was a key factor for the success of the presented research and I hope that all of them may feel my deep gratitude when reading this thesis. However, I also want to highlight the extraordinary engagement of Michael Wallisch, Raphael Pleß, Jean-Eric Schleiffer, Oleg Vasylyev, Nils Magiera, Simon Frisch, Timm Schröder, Daniel András, and Peter Lauche, to whom I am deeply indebted.

Furthermore, I would like to extend my gratefulness to all of my colleagues at *FZD* for the pleasant working environment, the stimulating discussions and their friendship.

I am especially thankful to my mentor Dr.-Ing. Patrick Seiniger for introducing me to the fascinating research world of “flying on level zero”, to Dr.-Ing. Benedikt Lattke as further fellow motorcycle researcher, and all those diligently working in the background:

To the members of the mechanical workshop under leadership of Robert Korndörfer, in particular Sven Müller, Michael Augustin, Christine Szuska, Jörg Eberlein, and Thomas Glock, for their passion about the project and all the encouraging “bike-talks” in between.

To Harald Bathke, Nico Cianciaruso, Pia Bossong and the complete IT team, for their straightforward 24/7-support, especially in unconventional and urgent situations.

To Fred Becker, Marco Gerner, and Dr. Rolf Boelcke of the electronics workshop, as well as Dr.-Ing. Nico Steinhardt, for their help concerning electronics.

To Rita Delp, Anke Mehm, Anne Hüther, and Monika Stelzer, as well as chief engineer Dr.-Ing. Norbert Fecher, for their perfect organizational support and ever cheerful spirit.

Undoubtedly, this thesis would be poorer in various aspects, without the vivid discussion in the motorcycle research community and expert interviews. In this context I want to express my thanks vicariously to Dr.-Ing. Achim Kuschefski and Matthias Haasper of the Institute for Motorcycle Safety e.V. (*ifz*) and the participants of their annual scientists’ seminars as well as Hans-Albert Wagner of BMW Motorrad, Gerald Matschl of KTM, again Oliver Fuchs of Honda, and Dr. Markus Lemejda of Bosch. I am moreover grateful to Prof. Dr.-Ing. J. Stefan Bald, head of the Road Research Institute at TU Darmstadt, and Prof. Bernt Spiegel for sharing fascinating insights on road design respectively on the psychology of the “upper half of the motorcycle” that are so intricately interwoven. For valuable detail-information on the historical prototype parts of BSTAM, I thank Stefan Scharting of Schaeffler Technologies, who created lots of them when still a student.

Almost last, but definitely not least, my deepest gratitude goes to my friends and family, for all their encouragement, prayers, and strong backing. In particular, I thank my parents Gerd and Elke for their upbringing, fostering my gifts and paving the way for this excellent education, as well as my beloved wife Miriam for sustaining me with their unconditional support and love, especially during the most sacrificial times on the finish line of this thesis. You are wonderful.

Finally, I praise God whom I cannot thank enough for revealing a glimpse at the beauty of creation concealed in motorcycle dynamics and for making this daring adventure possible for me.

Dear reader, may He bless you richly and always keep you safe on the road.

And now: Enjoy reading!

Kai Schröter Mühltal, in December 2014

Contents

List of Abbreviations ..... **IX**

List of Symbols and Indices ..... **X**

Summary ..... **XIII**

1 Introduction and Aims **1**
1.1 Motivation 1
1.2 Working Hypothesis and the Brake Steer Torque Avoidance Mechanism 6
1.3 Research Objectives 7
1.4 Methodology & Structure of this Thesis 9

2 The BST Chain of Effects and State of the Art Countermeasures **11**
2.1 Fundamentals of Motorcycle Dynamics 11
2.1.1 Coordinate Systems and Basic Chassis Geometry 12
2.1.2 Roll Equilibrium, Tire Scrub Radius & Riding Styles 14
2.1.3 Influences on Steering Torque Demand 17
2.1.4 Tire Road Interaction 18
2.1.5 Steering Kinematics and Steering Angle 20
2.1.6 Bi-Directional Coupling of Steer & Roll (Stabilization & Maneuvering) 24
2.1.7 Tire Forces and Ideal Brake Force Distribution during Corner Braking 29
2.1.8 Braking Stability 33
2.2 The BST Chain of Effects 36
2.2.1 The Main Chain of Effects 37
2.2.2 Further Primary and Secondary Influences 37
2.2.3 The Influence of Riding Style 38
2.2.4 The Inverse Effect 38
2.2.5 The Role of the Rider as a Controller 39
2.3 State of the Art of BST-Countermeasures 40
2.3.1 Avoiding BST-Critical Situations 41
2.3.2 Training the Rider 48
2.3.3 Influencing the Brake Force 49
2.3.4 Influencing the Lever Arm(s) 53
2.3.5 Influencing Wheel Load and Chassis Geometry Changes 59
2.3.6 Influencing Secondary Effects on Steering Torque 60
2.3.7 Influencing the Steering Torque and Movement 61
2.3.8 Influencing the Rolling Moment and Movement 64
2.3.9 Using Multi-Track Tilting Vehicles with Two Front Wheels 65
2.4 Conclusions 69

3 Analytic Considerations on the Kinematic Layout and Effectiveness of BSTAM 71
3.1 Force Transmission Ratios of a Generic BSTAM and Standard Chassis 72
3.2 Steering Torque Demand (STD) of a Standard Chassis 76
3.3 Layout and STD of a BSTAM with Laterally Inclined Steering Axis (KPI) 80
3.3.1 Remarks on the STD of a BSTAM with Parallel Steering Axis Offset 81
3.3.2 Definition & STD of a BSTAM Optimized for Neutral Free Cornering ... 82
3.3.3 The Influence of Pitch on the STD and BSTAM Layout 85
3.3.4 STD of the BSTAM Realized in the Prototype Motorcycle 90
3.3.5 Discussion of Neglected Influences on STD 91
3.3.6 The Inertia Effect Created Through a BSTAM with KPI 95
3.4 Layout and STD of a BSTAM with Parallel Steering Axis Offset 98
3.4.1 Optimization Potential of a Parallel BSTAM for Neutral Free Cornering 98
3.4.2 Considerations on Effectiveness of Multi-Lever Steering 102
3.5 Conclusions on Optimal BSTAM Design 104
3.6 Effectiveness Comparison of BSTAM and Standard Chassis 106
3.6.1 Model Extensions & Overview of Simulated Experiments 107
3.6.2 Maximal Braking on Constant Radius 109
3.6.3 Partial Braking on Constant Radius with Different BFD 113
3.6.4 Partial Front Braking under Special Conditions 116
3.6.5 Conclusions on the Effectiveness of Different BFD 118
3.6.6 Comparison of Simulated and Real BFD 119
3.7 Hypotheses for Riding Experiments and Concluding Remarks 123
3.7.1 Hypotheses on the Expected Performance of Standard Chassis and BSTAM in Riding Tests 123
3.7.2 Concluding Remarks 124

4 Implementing BSTAM in a Motorcycle 125
4.1 General Considerations on Mechanical Setup 125
4.1.1 Basic Kinematic Concepts of a BSTAM 126
4.1.2 Combining BSTAM with Different Chassis Designs 128
4.1.3 Bearing Trajectory and Actuation Concept 131
4.1.4 Alternative BSTAM Actuation Concepts 134
4.2 Mechanical Setup of the BSTAM Prototype 139
4.2.1 Definition of Prototype Motorcycle and Choice of BSTAM Concept 139
4.2.2 Excentricity Layout 141
4.2.3 Simple Geometric Control Algorithm and Computation of Lever Arms . 144
4.2.4 Chassis Geometry Changes through BSTAM 147
4.3 Overview of the BSTAM Prototype 149
4.4 Measurement and Control Setup 151
4.4.1 Overview of Main Components 151
4.4.2 Accuracy of Relevant Measurements 152
4.4.3 Data Sampling and Post Processing 152
4.4.4 System Performance 153

4.4.5 Extended Control Algorithms 155
4.4.6 Relevance of Elevated Curve Detection 156
4.5 Concluding Remarks 156

5 Driving Tests 157
5.1 Test Design 157
5.1.1 General Requirements 157
5.1.2 Test Track Definition 157
5.1.3 Test Maneuver and Riding Task 159
5.1.4 Test Setups and Maneuver Variations 159
5.1.5 Comments on the Conduct of Tests 160
5.2 Criteria for Evaluation 161
5.2.1 Definition of Characteristic Values 161
5.2.2 Exemplary Comparison of Characteristic Values in Corner Braking Experiments with Standard Chassis vs. BSTAM 167
5.2.3 Arrangement and Display of Results 174
5.3 Global Analysis of All Test Results 174
5.3.1 Correlation Analysis of Characteristic Values 175
5.3.2 Performance of Centered Steering Axis vs. BSTAM 178
5.3.3 Interim Conclusions from Global Analysis 182
5.4 Detailed Analysis of Individual Test Results 183
5.4.1 Test Setup Nomenclature of Abbreviations 183
5.4.2 ABS Braking with Standard Steering under Variation of Brake Application, Riding Style, and Steering Damper 184
5.4.3 Partial Front Braking with Standard Steering vs. BSTAM 190
5.5 Concluding Remarks 204

6 Discussion and Outlook 206
6.1 Results 206
6.2 Transferability of Results 210
6.3 Relevance of Results for other Systems and Stakeholders 214
6.4 Outlook 216

A Appendix 221
A.1 Appendix to Chapter 1 221
A.2 Appendix to Chapter 2 222
A.3 Appendix to Chapter 3 223
A.3.1 Equation Set for the Derivation of the Optimized Instantaneous Center of Steering Axis Inclination of OPT BSTAM 223
A.3.2 Equation Set for the Computation of Tire Contact Forces with different Brake Force Distributions (BFD) 226
A.3.3 Equation Set for the Computation of Measured Brake Force Distributions for the Entry in the BFD Diagram 235

A.4 Appendix to Chapter 4 236
A.4.1 Alternative Actuation Concepts 236
A.4.2 Technical Data of the Prototype Motorcycle 241
A.4.3 Considerations on Steering Torque Measurement 242
A.4.4 Considerations on Roll Angle Measurement 242
A.4.5 Definition of Filter Parameters 243
A.5 Appendix to Chapter 5 248
A.5.1 Results of Global Analysis in CDF-Plot Format 248
A.5.2 Correlation Tables for ALL Experiments 250
A.5.3 Correlation Tables for Exp. with Centered Steering Axis 252
A.5.4 Correlation Tables for Exp. with BSTAM Active 254

Bibliography 256

Own Publications 263

Student Research Work 265

List of Abbreviations

Abbreviation	Description
ABS	Antilock Brake System
ACT.	Actuator (i.e. BSTAM actuator)
AEB	Autonomous Emergency Braking
ARAS	Advanced Rider Assistance System (cf. ADAS for passenger cars, with D for driver)
BFD (CA-BFD)	(Cornering Adaptive) Brake Force Distribution
BPM	Brake Pitch Moment
BST	Brake Steer Torque
(//)BSTAM	Brake Steer Torque Avoidance Mechanism (with parallel steering axis offset)
OPT BSTAM	BSTAM with optimized instantaneous center of steering axis inclination
BYM	Brake Yaw Moment
CBS	Combined Brake System
C-ABS	Combined Antilock Brake System (Brake-by-Wire)
CoG	Center of Gravity
CoSy	Coordinate System
CTR	A chassis setup with centered steering axis (either standard, or passive BSTAM)
DoF	Degree of Freedom
DS	Displacement Sensitivity
EEF	Excentricity Enlargement Factor
EXP	Experiments
FZD	Institute of Automotive Engineering Darmstadt
GPS	Global Positioning System
HESD	Honda Electronic Steering Damper
IMU	Inertial Measurement Unit
KPI	King-Pin Inclination (angle between (projected) steering axis and symmetry plane)
MBS	Multi Body Simulation
MSC	Motorcycle Stability Control
PBA	Predictive Brake Assist
PMC	Prototype Motorcycle
PTW	Powered Two (and Three) Wheeler
RLP	Rear Wheel Lift-Off Protection
RMS	Root Mean Square
STA	Standard setup / Standard chassis with centered steering axis
STD	Steering Torque Demand
TCS	Traction Control System
TU Darmstadt	Technische Universität Darmstadt
VRU	Vulnerable Road User

Abbreviations that occur only once are explained in context and not contained in this list.

List of Symbols and Indices

Symbol	Unit	Description
a_x	m/s² | g	longitudinal acceleration, mainly: deceleration
a_y	m/s² | g	lateral acceleration
bd	m	bearing distance (perpendicular distance between the kinematic center points of the steering bearings measured along the fork legs / conventional steering axis, in z'_{st}-direction)
c_w	-	aerodynamic drag coefficient
c_l	-	aerodynamic lift coefficient
c_p	-	aerodynamic pitch moment coefficient
c_{roll}	-	rolling resistance coefficient
d	m	displacement, offset, diameter
e	m	BSTAM excentricity
ecr	% | -	effective compensation ratio
f	Hz	frequency
fl	m	fork length (perpendicular distance between the kinematic center of the lower steering bearing and front wheel hub, measured along the fork legs)
fo	m	fork (yoke) offset (perpendicular distance between standard steering axis and front wheel axle, measured along x'_{st}-axis)
g	m/s², N/kg	gravitational acceleration, gravity constant
g_1, g_2	various	slope and axis intercept parameters of linear regression of data correlations
gcr	% | -	geometric compensation ratio
h	m	height
i	A	electrical current
l	m	length, geometric chassis parameter, lever arm, wheelbase
$l_{x,y,z}$	m	lever arms of front tire longitudinal, lateral, and vertical contact forces towards the steering axis
ℓ_{yz}	-	lever ratio (of lateral and normal force levers)
$\mathcal{L}$, $\mathcal{L}_x$, $\mathcal{L}_{yz}$	-	relative lever ratio (ratio of lever ratios of different setups)
m	kg	mass
n	m	trail
nt	m	normal trail
p	bar | -	pressure, brake pressure, tire inflation pressure | probability of a correlation
r	m	tire rolling radius in center position ($\lambda = 0$)
r_c	m	tire contour (or: cross-section) radius
r_r	m	roll angle dependent tire rolling radius
s	% | -	tire (brake) slip
sr	m	scrub radius (lateral lever arm from tire contact point towards steering axis)
t	s	time
tcr	% | -	target compensation ratio
$trigger$	-	trigger signal from the brake light switch
v	m/s | km/h	velocity, speed (vehicle or front wheel circumferential speed)

Symbol	Unit	Description
x, y	various	abscissa and ordinate parameters for correlation analysis and linear regression
A	m²	Area (i.e. the projected frontal area of the vehicle with rider and equipment)
DS	mm/°	Displacement Sensitivity
EEF	-	Excentricity Enlargement Factor
F	N	force
I	kgm²	mass moment of inertia
L	-	length of a straight road | length of whiskers in box-plots (rel. to data spread)
M	Nm	moment
Q	-	quartile (eg. Q_1 and Q_3 for the 25th and 75th percentile of data)
R	m | -	curve radius | correlation coefficient
T	Nm	torque, steering torque, braking torque, driving torque
α	°	(tire) sideslip angle | curve opening angle
β	°	vehicle sideslip angle
χ	°	rider lean angle (relative to motorcycle frame)
δ	°	steering angle
ε	°	BSTAM excenter actuation angle
γ	°	steering axis inclination angle from vertical (x-z-plane)
λ	°	roll angle
μ	-	(available or utilized) friction potential
ν	°	pitch angle
σ	° | -	king-pin inclination angle of steering axis relative to vehicle symmetry plane (x'-z'-plane) | standard deviation of data (separately indicated)
ρ	kg/m³	air density
τ	°	steering head (or caster) angle
ω	°/s | rad/s	angular velocity
ψ	°	yaw angle
Δ	-	Difference
a, c, e	N	Substitute coefficients
b, d, f	kg	Substitute coefficients

Some of the utilized symbols are also used as indices and are therefore not necessarily repeated in the list of indices.

Index	Description
0	initial condition, at the beginning of an experiment ($t = 0$), or upright vehicle position ($\lambda = 0$)
Ackermann	concerning the Ackermann condition (i.e. the Ackermann steering angle)
(//)BSTAM	related to a (//) BSTAM
BPM	Brake Pitch Moment
BYM	Brake Yaw Moment
STA, sta	(related to the) standard setup with centered steering axis
ac	related to the aerodynamic center
aero	concerning an aerodynamic influence
available	available portion (e.g. of the friction potential μ)
brk, brake	related to brakes or braking
cg, CoG	(related to the) center of gravity

Index	Description
demand	demand
drag	concerning aerodynamic drag
drive	related to driving forces or torques
dyn	dynamic
eff	effective
end	related to the end of an experiment
friction	concerning friction / friction limits
ft	front
gyro	related to a gyroscope
i	general index parameter
inertia	concerning the “Inertia Effect”
is	concerning the “is” value of a measured variable at a certain point in time
lift	concerning aerodynamic lift
limit	concerning a limiting value
lower	lower threshold value
max	maximal
mean	mean, averaged value
opt	optimal, optimized, related to (the definition of) an optimized (OPT) BSTAM
partial	partial
pitch	concerning the pitch degree of freedom
precession	concerning the precession of a gyroscope
red	reduced
ref	reference
rel	relative
rider	(related to the) rider
rlp	concerning rear wheel lift-off conditions
roll	concerning the roll degree of freedom | concerning the rolling resistance of tires
rr	rear
spin	concerning the spinning of a gyroscope
st	related to steering / the steering system
target	concerning a target value
th	theoretical, physically active (referring to the roll angle)
tir, tire	related to tires (typically the front tire)
tot	total
upper	upper threshold value
used	used or utilized portion (e.g. of the friction potential μ)
whl, wheel	related to a wheel (typically the front wheel)
x, y, z	in/from x-direction (longitudinal), y-direction (lateral), z-direction (vertical)
yaw	concerning the yaw degree of freedom

Summary

Motorcyclists account for an alarmingly high share among traffic fatalities and severely injured. Especially in unforeseen or hazardous corner braking situations, riders often show a limited capability to balance their brake action and compensation of the Brake Steer Torque (BST) instantaneously. In many cases, the subsequent stand-up tendency of the vehicle can further confuse the rider which might run off track or into oncoming traffic. Since the BST mainly arises as a product of the front brake force with the roll angle dependent tire scrub radius as lateral lever arm, Weidele proposed the so-called BST Avoidance Mechanism (BSTAM), inhibiting BST generation by lateral inclination of the steering axis. The system was however never analyzed or practically tested beyond the demonstration of mechanical feasibility in the early 1990s. Therefore, research objectives lie in the evaluation of a BSTAM's performance and benefit for the rider before the background of the past decades' tremendous improvements in state-of-the-art technology, as well as to find criteria for a favorable system design.

As starting point, influence factors on the BST chain of effects are identified and used as classification scheme for countermeasures, ranging from possibilities of rider training or road design to technical measures on the vehicle. Besides BSTAM, a counter steering actuator, Cornering Adaptive Brake Force Distribution (CA-BFD), semi-active steering dampers, and multi-lever steering are identified as promising.

Focusing on the transmission ratios of front tire contact forces towards the steering axis as the main contributes affected by BSTAM, a simple mathematical model is used to analyze the steering torque demand (STD) of a generic BSTAM against that of the baseline chassis. The balance between normal and lateral force is found to be crucial for a "neutral" steering. Compensation of the tire scrub radius through BSTAM not only eliminates the disturbing influence of the brake force, but also diminishes helpful aligning steering torque components generated by the normal and lateral force, leading to an undesired increase in STD. Kinematic optimization resolves this trade-off for steering axis inclination angles in the order of 10° with an optimal instantaneous center of steering axis rotation located at the intersection of the original steering axis with the vertical connection from tire contact point to wheel hub in upright position. Small steering disturbances arising from the deceleration of wheel spin inertia and inertial forces on the steering system can be accounted for through limitation of front brake pressure gradients and by keeping the instantaneous center of steering axis inclination close to the steering system's center of gravity. An analysis of BSTAM concepts with parallel steering axis adjustment yields acceptable steering balance only for unusually large caster angles and fork offsets (around 50° and 140 mm). However, these setups suffer consid-

erable disturbances through longitudinal accelerations on the steering system (in the order of 10 Nm) and were not further pursued. Also an exemplary analysis of multi-lever steering (i.e. a four-bar linkage) showed no benefits regarding the BST.

Using methods of product design, key aspects of incorporating an optimized BSTAM into a vehicle are investigated and four classes of alternative actuation concepts proposed, that may be favorably incorporated basing on a king-pin or hub-center steering.

For the first time ever, a Honda CBR 600 RR super-sport motorcycle with Combined-ABS and a conventional telescopic fork is equipped with a BSTAM according to Weidele's original design with double excentric adjustment of the upper steering head bearing and tested against the baseline in comparative riding tests.

Correlation analysis of all conducted tests confirms the BST chain of effects, interconnecting disturbances in steering torque, steering angle, roll angle, and also rider lean angle. Moreover, it shows a strong dependency of the disturbance values on the initial brake pressure increase rate and mean deceleration for centered steering axis, while BSTAM eliminates this correlation to a great extend.

In line with predictions from model calculations, riding tests with the baseline chassis confirm a positive influence of "lean in" riding style. For maximal braking, the "stand-up" of the vehicle matches well with the required reductions in roll angle towards lower speeds, provided the maneuver is done intentionally on the test track.

Comparison of baseline and BSTAM in partial front braking maneuvers fully confirms the behavior expected from model calculations. On one hand, handling is compromised due to increases in caster angle and trail (handling index 3.0-3.3 vs. 4.9 $^{Ncm}/_{(m°/s^2)}$) and the stationary STD is significantly increased (5.3 vs. 20.9 Nm). On the other, significant reductions are obtained in steering torque deviations upon brake kick-in (21.2 vs. 13.4 Nm), followed by significant improvements in all other disturbance values. Moreover, BSTAM eases directional controllability for braking on narrowing radius turns.

Even though BSTAM proves already effective in the prototype setup and further improvements are expected from the proposed optimizations, especially concerning stationary STD, stability and handling characteristics require further investigations. Moreover, a simulation study reveals, that Cornering Adaptive Brake Force Distribution already reduces the expected disturbance values in partial braking to such low absolute levels, that this measure alone bears the potential to address a great deal of BST relevant situations in real traffic and might further be complimented by advanced semi-active steering damper control. However, before the background of current discussions on the implementation of predictive brake assist or even autonomous emergency braking into powered two wheelers, effective BST countermeasures are a necessary prerequisite. In these regards, a model based counter steering torque actuator as an add-on to the well understood conventional chassis is regarded as to be superior compared to BSTAM.

I dedicate this thesis to

GOD, the creator of heaven and earth,

JESUS CHRIST, my Lord and Savior, through whom all things are made, and to the

HOLY SPIRIT, eternal inspiration for every good work.

SOLI DEO GLORIA.

1 Introduction and Aims

1.1 Motivation

General Accident Situation of Powered Two Wheelers (PTW)

In 2010 the governments of the world declared 2011–2020 as the "Decade of Action for Road Safety" with a special focus on Vulnearble Road Users (VRU) which include pedestrians, cyclists, and users of Powered Two (and Three) Wheelers (PTW). The latter group alone accounts for 23% of road fatalities worldwide, with a natural black spot in the rapidly motorizing countries of the Asia / Pacific region (> 33%) but also alarmingly high shares in the European Union (EU, 12%) and further high income regions[1].

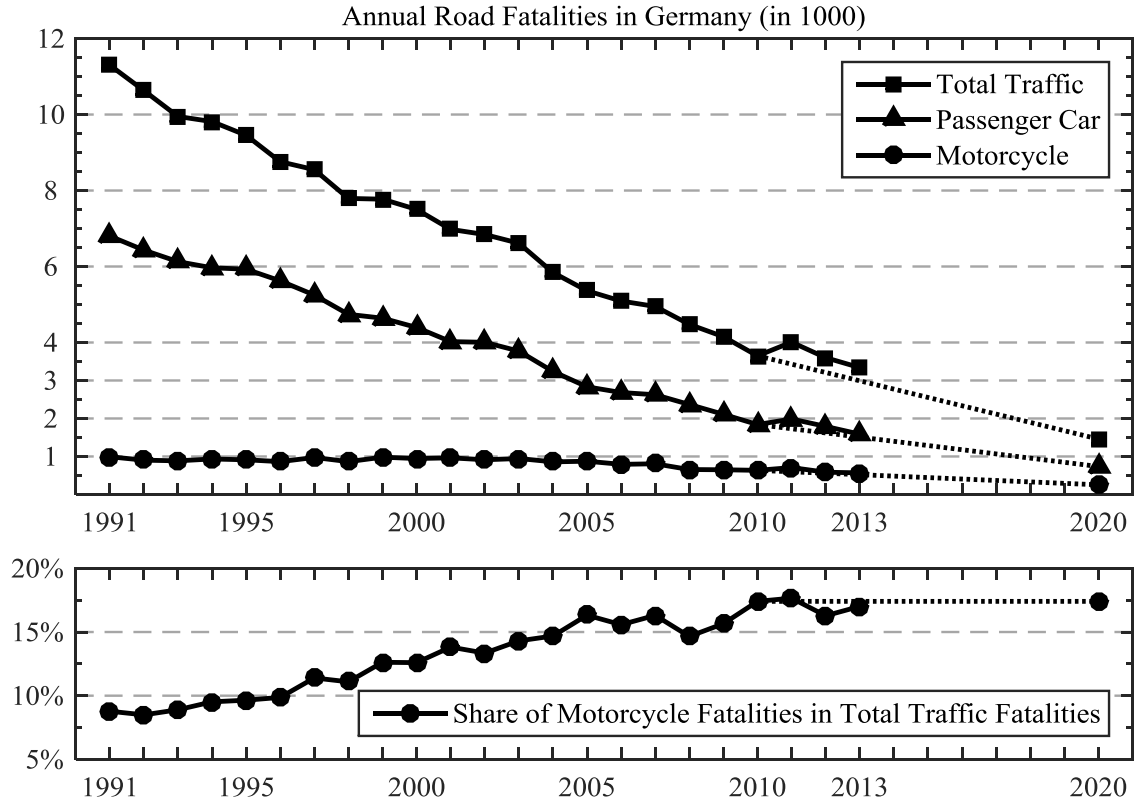

Figure 1.1: Road Fatalities in Germany with 40% Reduction Targets and Trend Lines for 2020[2]

[1] WHO (2013): Global status report on road safety 2013, Section 1, Figure 7, p. 6

[2] DESTATIS (2014): Verkehrsunfälle Zeitreihen 2013, Section 5.1.2 (2), p. 122

While other vehicle transport modes have shown significant decreases in fatalities and serious injuries over the past years, the numbers for motorcyclists fell much slower or remained even static. Thus, the share of killed motorcyclists has constantly been rising in the past decades, as exemplarily illustrated for Germany in Figure 1.1.

Measured against the annual distance travelled, the risk to be severely injured or killed as a motorcyclist in Germany is more than 18 times higher than for passenger car occupants[3]. Through mandatory equipment of motorcycles with advanced brake systems starting from 2016[4] and various other measures[5], the aim of halving road deaths in the EU[6] and cutting them by 40% in Germany[7] until 2020 seams within reach.

However, before the background of declining fossil energy reserves, rising fuel costs and congested cities, there is a trend of rapidly rising motorcycling activity[8]. Since this has recently even led to increasing casualty numbers, for instance in the United States of America and Australia[9], further research to identify and improve typical accident scenarios of PTW is of utmost importance.

Running Wide on Curve Accidents

Going back to Germany as an example, annual accident statistics for motorcycles show an overrepresentation of single vehicle crashes (47.8%) while in the second biggest group the hazard was an interference with parallel or oncoming traffic (20.2%)[10]. With 14%, the accident scenario with the highest share of severely and fatally injured riders is running wide in left turns on rural roads, where 68% of the reported cases led to severe injuries or fatalities and the rider was always the main responsible for the crash[11].

---

[3] DESTATIS (2014): Verkehrsunfälle Zeitreihen 2013, Section 5.1.2 (2), p. 122, and Section 7.4, p. 171, based on figures for 2012.

[4] European Parliament and Council (2013): Regulation (EU) No. 168/2013, Annex VIII

[5] European Commission (2010): Road Safety Programme 2011-2020

[6] European Commission (2010): Towards a European road safety area

[7] BMVBS (2011): Road Safety Programme 2011, p. 12

[8] For instance, between 2000 and 2010, the estimated number of motorcycle vehicle-kilometers travelled in Australia increased by 82% and contributed to a 17% increase in rider fatalities. Cf. footnote 9.

[9] IRTAD (2013): Road Safety Annual Report 2013, Sections on Australia (p. 50ff) and USA (p. 441ff)

[10] DESTATIS (2014): Zweiradunfälle im Straßenverkehr 2013, p. 21

[11] Kühn (2008): Analyse des Motorradunfallgeschehens

There are apparently many reasons for running wide on turns. However, an analysis of in depth accident studies (like Hurt's Report[12] or MAIDS[13]) shows, that throughout the decades braking is one of the dominant pre-crash actions taken by riders. Moreover, they reveal, that when a loss of control was involved, it was "mostly related to braking and a subsequent change in vehicle dynamics[13]".

The picture series in Figure 1.2 shows a real world example, where unexpected braking in a right turn led to a departure of the own lane and almost caused a head-on collision.

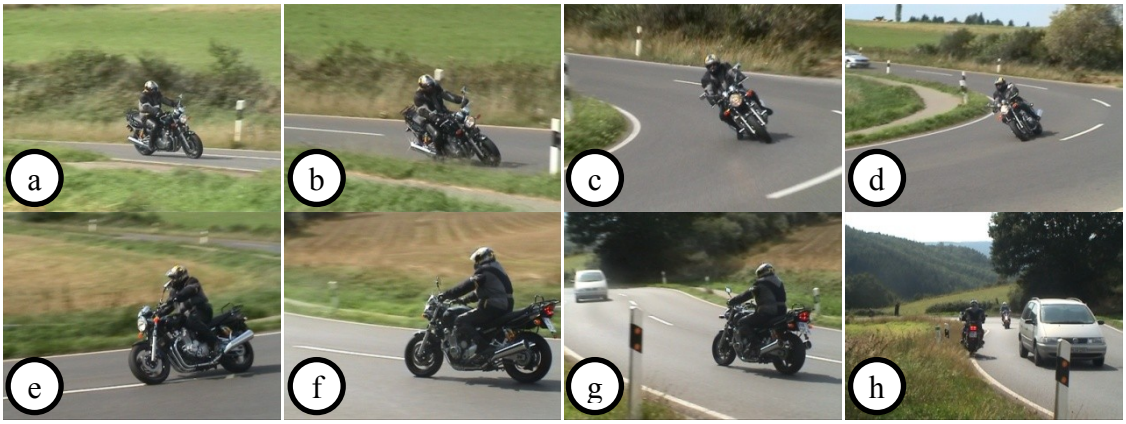

Figure 1.2: Motorcycle running wide on a right turn due to unexpected braking action captured during a motorcycle safety trip for rider training in real traffic[14] (explanation in the main text)

The rider enters the turn a little too close to the inside of his lane (a, b). Realizing that he is already tending towards the opposing lane, he recognizes oncoming traffic (c). Possibly amplified by reaching his mental roll angle limit[15], as a startle reaction he applies the brakes (c, d). The subsequent upward roll movement and increase in turn radius of his motorcycle not only leads to a tangential departure of his own lane (e, f), but also to further confusion of the rider. Like paralyzed, he takes no further action but to remain on the brakes and head straight towards the oncoming car (g). Fortunately, the car driver reacted quick enough to pass the motorcycle safely (h).

The presented case illustrates five key aspects of this accident type, some of which were additionally confirmed by a survey conducted among 311 motorcyclists[16].

---

[12] Hurt et al. (1981): Motorcycle Accident Cause Factors, Section 7.17 Motorcycle Rider Collision Avoidance Performance, p. 142, and Section 7.18 Motorcycle Rider Loss of Control, pp. 151-152

[13] ACEM (2009): MAIDS, Section 5.0 Vehicles, Collision Dynamics, p. 63

[14] Pictures taken from a video by courtesy of Wolfgang Stern, cf. Stern (2006): Motorcycle Safety Trips, proceedings pp. 271-288

[15] Spiegel (2010): The Upper Half of the Motorcycle, Part 1, pp. 34-36, Part 4, pp. 112-116, and 133-136

[16] Hämel (2010): Survey on Corner Braking Behavior, Bachelor-Thesis, cf. appendix A.1

- Running wide on right turns practically does not appear in statistics, because the opposing lane offers additional reaction time and space to return to the intended trajectory – if there is no oncoming traffic. In case there is, the accident type to be recorded will very likely be a head-on collision.
- There is a high number of unreported cases with no or just little personal injury as well as an even greater number of potentially dangerous situations and near accidents.
- The majority of riders rarely train effective emergency braking and avoid braking in turns almost completely for fear of front wheel lock (cf. chapter 2.1.8). In consequence, their brake application in a threatening situation will either lead to exactly that feared locking and direct fall, or be rather low, achieving only partial decelerations[17] as is typical for the concerned accident type[18].
- As a further consequence, such riders are not familiar with the vehicle reaction or possibilities to resolve the situation (e.g. by increasing the roll angle through a determined steering impulse (cf. chapter 2.1) and optionally releasing the brakes). Hence, the stand-up itself can become the trigger for a (mental) blockade or a whole cascade of errors[19].
- Even riders that know about the driving dynamic backgrounds and their options for action can repeatedly get into such situations, because the potential to really train their startle reactions in unexpected, hazardous situations is limited, however still existing (cf. chapter 2.3.2).

Altogether, this motivates to take a closer look at the underlying driving dynamics in order to identify potential technical measures to assist the rider.

Brake Steer Torque Induced Stand-Up Tendency

From a driving dynamic point of view, the genesis of the presented accident type is closely linked to the inherent bi-directional coupling of steer- and roll-motion of PTW[20], which is essential for dynamic stabilization and maneuverability (see chapter 2.1.6). It helps to understand the main chain of effects leading to the so-called Brake Steer Torque (BST) induced stand-up tendency as illustrated in Figure 1.3 and described in the following.

---

[17] cf. Weidele (1994): Bremsverhalten von Motorrädern, and Präckel (1999): Die Motorradbremsung im System, Chapter 6.1 p. 83 ff, e.g. Bild 35, p. 103

[18] Bauer et al. (2014): Retrospective analysis of fatal motorcycle accidents, proceedings pp. 116-127

[19] Spiegel (2010): The Upper Half of the Motorcycle, Part 2, p. 83, Part 4, pp. 133-136

[20] Among others, cf. Cossalter et al. (2010): Steering Torque Decomposition, and Cossalter (2006): Motorcycle Dynamics

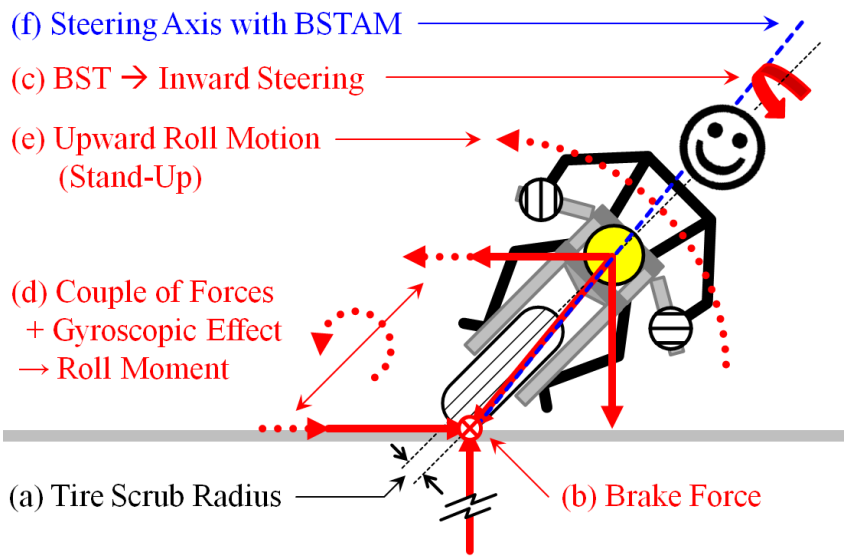

Figure 1.3: Genesis of the BST induced Stand-Up Tendency and Principle of the BSTAM

In stationary cornering, the resultant of weight force and centrifugal force is pointing through the tire contact patch line. The vehicle is in roll equilibrium. Due to the width and contour of the tires, the contact patches move out of the symmetry plane by the so-called tire scrub radius (a). If, for instance in a moment of surprise or even shock, the rider applies a sudden brake force on the front wheel (b), it multiplies with the scrub radius (a) as lever arm and causes a misaligning (that is: turning the steering to the inside of the curve) Brake Steering Torque (BST, c). If this is not fully compensated by the rider, it is leading to an increase of steering angle, a temporary decrease in cornering radius at an initially almost not reduced speed and thus an enlargement of centrifugal force at the center of gravity. Acting as a force couple in conjunction with an enlarged sideslip lateral force on the front wheel and superimposed by a roll moment caused by the gyroscopic effect of the front wheel (d), an upward roll motion (stand-up, e) is induced, which is finally also leading to the undesired increase in turning radius.

In addition to the suddenness of the initial stand-up that can confuse the rider, as illustrated in the previous section, the elevated level of steering torque demand during the braking process is making it more difficult to increase the roll angle again. I.e., the required outward steering impulse needs to be much stronger than in free cornering.

Finally, in context of current discussions on the effectiveness of applying Predictive Braking Assist (PBA) or even Autonomous Emergency Braking (AEB) technology to motorcycles[21], research on technical countermeasures against the presented phenomenon is of utmost importance.

[21] DEKRA (2010): Verkehrssicherheitsreport Motorrad

1.2 Working Hypothesis and the Brake Steer Torque Avoidance Mechanism

In brief, the causation chain of effects of Brake Steering Torque induced accidents can be summarized as illustrated in Figure 1.4.

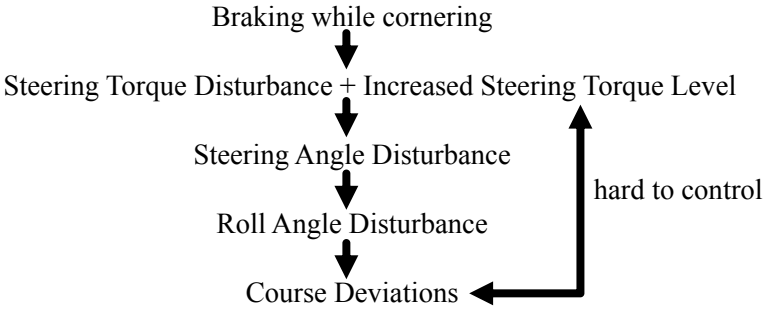

Figure 1.4: The BST Chain of Effects

Braking while cornering is leading to a disturbance in steering torque and consequently in steering angle, roll angle, and finally to course deviations, that are additionally hard to control for the rider due to the elevated level of steering torque demand.

Since the disturbances in steering torque are triggering the complete subsequent chain, the following general hypotheses can be derived:

H_{0a}: A technical device that minimizes the steering torque disturbances for a given corner braking maneuver (especially at the beginning) will as well minimize the disturbances in steering angle, roll angle, and deviations in course.

H_{0b}: A technical device that lowers the steering torque demand during the duration of a given corner braking maneuver will enhance the capability of the rider to keep the intended cornering line or even make course corrections, i.e. increase the roll angle to follow a narrowing radius turn.

In order to address the twin-fold character of these general hypotheses, Weidele[22] derived the concept of the so-called Brake Steer Torque Avoidance Mechanism (BSTAM), a mechatronic device that allows to move the kinematic steering axis in such a way, that it always points through the tire contact patch line (see Figure 1.3, f). At first sight, the elimination of the scrub radius (a) as the brake force's lever arm towards the steering axis avoids the generation of the disturbing BST and hence promises improved controllability especially in unforeseen curve braking maneuvers.

[22] cf. Weidele (1990): Compensated Steering for Motorcycle. Patent Application DE3933058A1, and Weidele (1994): Bremsverhalten von Motorrädern, Chapters 6.4, 7, and 8, pp. 173-182

While the mechanical feasibility of the BSTAM concept has already been proven by a lab prototype in the early 1990s that realizes the required deflection of the kinematic steering axis by a double excentric configuration of the upper steering head bearing (see Figure 2.21 and Figure 4.7), it was never practically tested or theoretically analyzed beyond the prior simple considerations from a driving dynamic point of view.

Before the background of its potential effectiveness against the said accident types or as a necessary pre-requisite for future measures like PBA and AEB, this motivates to carry out further research on BSTAM under the following specified working hypotheses:

For a given corner braking situation (mainly defined by speed, path curvature, lateral acceleration, deceleration, brake force gradients and distribution), a motorcycle equipped with a properly designed BSTAM will benefit the rider in two ways compared to the baseline vehicle:

H_{Wa}: It will show less initial disturbance in steering torque demand, and, following the chain of effects, less deviations in steering angle, roll angle, and course (cf. H_{0a}).

H_{Wb}: It will exhibit a lower level of steering torque demand during the corner braking process and thus ease directional control (in the sense of H_{0b}).

1.3 Research Objectives

Before the background of the hypotheses, the objectives are clustered in three fields:

Field 1: BST Effect and Countermeasures

Besides the simple explanation presented in the previous chapter, there are various other influence factors along the BST chain of effects. Many of them have already been studied and understood separately, but not yet brought together into a unified big picture.

Therefore, it seems very likely that further technical countermeasures beyond BSTAM can systematically be found and the aims in this first research field are set as follows:

Aim 1.1 The fragmented knowledge about the BST chain of effects is collected from literature, complimented by own findings and brought into a unified big picture.

Aim 1.2 Using this understanding as a classification scheme, the entire field of BST countermeasures is identified, including existing state of the art concepts that already address the BST effect (often implicitly).

Aim 1.3 An estimation of the effectiveness, feasibility and practicability of the various concepts is given, as far as directly possible with the available information.

Field 2: Feasibility and Layout of BSTAM

The mechanical feasibility of BSTAM has already been demonstrated by an exemplary solution and is therefore out of question. However, the fact that typical caster angles have arrived to differ only by fractions of a degree between manufacturers of super sports motorcycles underlines that steering kinematics are very sensible to changes. Since these are greatly altered by BSTAM, downsides in terms of interferences with driving dynamics, e.g. in terms of stability, handling, or especially steering torque demand as a sensible control and feedback channel for the rider, are to be expected.

Therefore, the first aims in this research field are set as follows:

Aim 2.1 The main influences of BSTAM on driving dynamics and potentially inacceptable downsides are identified in comparative analysis with the standard steering.

Aim 2.2 Criteria for an optimized kinematic layout are derived, that helps to keep potential downsides as low as possible, at least within an acceptable range.

Aim 2.3 The working hypotheses are refined with regards to the driving dynamic performance to be expected from a BSTAM in practical testing (both for an optimized and the exemplary prototype design addressed in the third research field).

If such an optimized BSTAM design can be found, it is no use, if engineering constraints, like construction space, tire sprung mass, or driving dynamic restrictions, forbid its practical implementation. Hence, further aims in this field are set as follows:

Aim 2.4 The main aspects of incorporating a BSTAM into a real vehicle are addressed from product development view, without claim to be exhaustive or complete.

Aim 2.5 At least one exemplary solution for the mechanical implementation of a BSTAM with optimized kinematics is proposed.

Aim 2.6 The key aspects of the implementation of a BSTAM into a prototype motorcycle for practical testing (cf. research field 3) are investigated in detail.

Field 3: Effectiveness and Benefit of BSTAM for the Rider

BSTAM was developed at a time when the first generation of motorcycle ABS allowed average riders to achieve higher deceleration levels in curves without fear to lock the front wheel and fall[23], and at the same time confronted them with an amplified BST effect as well as hardly manageable steering fluctuations, roll- and course deviations[24].

[23] This risk is viciously fostered by dynamic over-braking and the kinematic instability, cf. chapter 2.1.8.

[24] cf. Weidele (1994): Bremsverhalten von Motorrädern, Chapter 5.3.5, p. 147 ff, and Chapter 5.3.6, p. 151 ff as well as Seiniger et al.(2006): Roll angle sensor, proceedings pp. 369-388

Before the background of improved state of the art technology, especially in terms of advanced brake systems (e.g. smooth ABS control and roll angle adaptive brake force distribution, see chapters 2.3.3 and 3.6.6), tires and chassis design, it stands to question, in how far a BSTAM can still bring a significant benefit for the rider.

Therefore, the aims in this research field are set as follows:

Aim 3.1 A realistic driving test design and related performance criteria are defined with regards to the refined working hypothesis derived in field 2 (cf. Aim 2.3).

Aim 3.2 A state of the art motorcycle is tested as baseline and its performance compared to a BSTAM prototype in real driving tests.

Aim 3.3 Measurements and subjective impressions about the riding behavior and feel of BSTAM are evaluated against the refined hypothesis on its expected behavior (cf. Aims 2.3 and 3.1).

Aim 3.4 A conclusion is drawn, whether BST countermeasures beyond the state of the art technology are necessary at all or at least recommendable.

1.4 Methodology & Structure of this Thesis

Figure 1.5 gives an overview, on how the three fields of research objectives are addressed in the different chapters as well as on important interdependencies.

In chapter 2, a comprehensive introduction into the fundamentals of motorcycle dynamics is given and basic information on the BST effect and countermeasures is collected from various sources. The gathered information is combined to an extended BST chain of effects, furthermore used to identify the full field of BST countermeasures and to classify state of the art approaches, which are subsequently described along the chain.

Chassis geometry changes through BSTAM and correlated driving dynamic interferences are investigated against the standard chassis on the basis of a simple analytical model of quasi-stationary corner braking maneuvers in chapter 3. Optimization criteria for the kinematic layout of BSTAM are derived and a performance estimate for both an optimized as well as the later incorporated prototype BSTAM motorcycle are given in conjunction with refined hypotheses to be examined in the real world tests.

General considerations on the practical incorporation of (an optimized) BSTAM in a real motorcycle are presented from a classical product development point of view in chapter 4. Furthermore, the mechanical and electrical (measurement / control) setup of the prototype motorcycle are addressed in detail along with its performance limitations.

Chapter 5 introduces a suitable test design and evaluation criteria for comparative testing of the research motorcycle in baseline and BSTAM prototype setups against the refined hypothesis from chapter 3. The conduct of tests is described and the results evaluated and discussed in two steps. Firstly, on a global basis, using a correlation analysis on the characteristic values derived from all experiments, and secondly, by addressing the single experiment types in separate detail.

Finally, the obtained results are discussed, conclusions are drawn, and a future outlook is given in chapter 6.

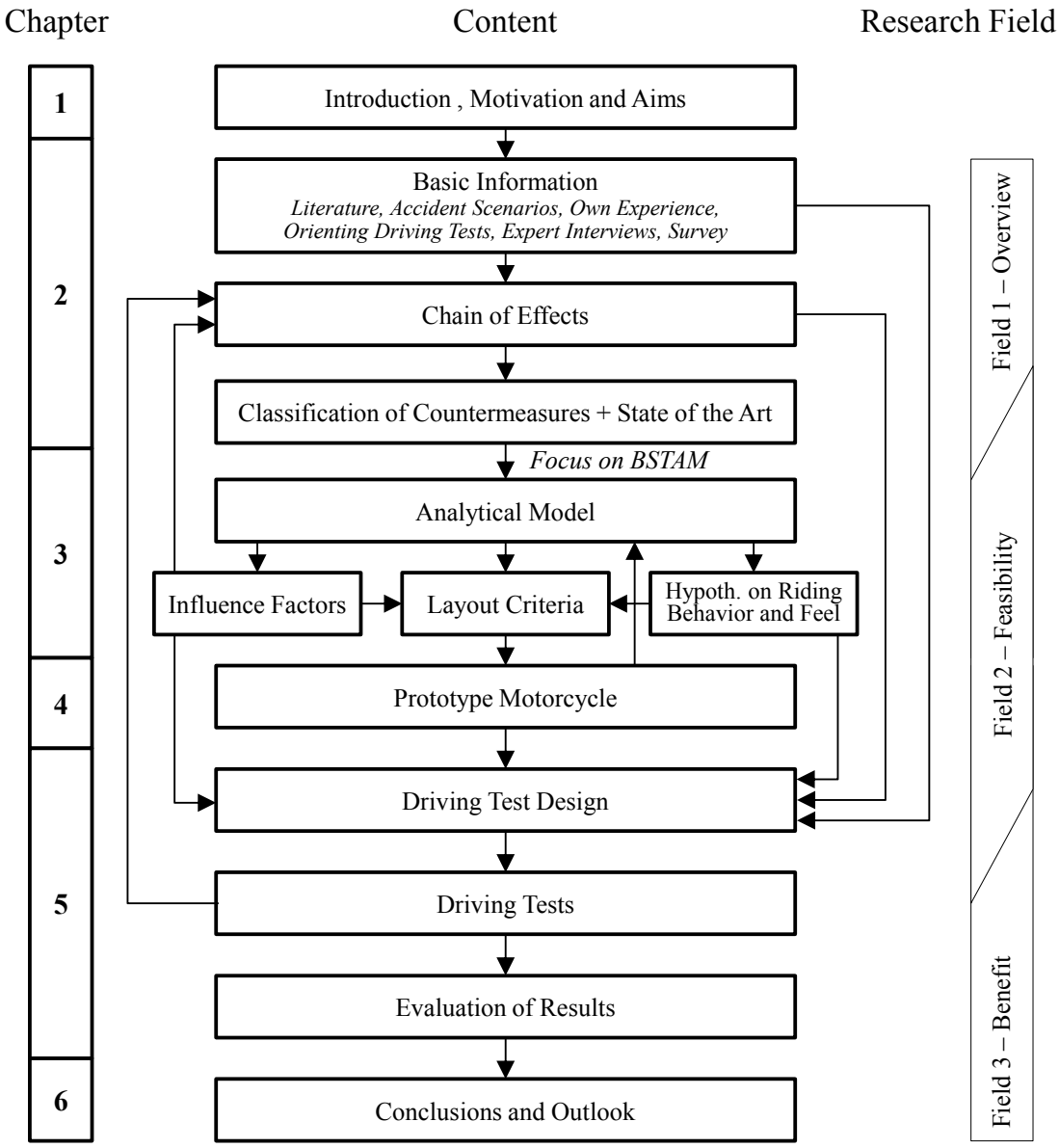

Figure 1.5: Schematic diagram of methodology and structure of the presented research

2 The BST Chain of Effects and State of the Art Countermeasures

In the first section of this chapter, an introduction into the fundamentals of motorcycle dynamics is given. In the second section, an extended BST chain of effects is composed from information found in literature[25] and own findings. It used in the third section as a classification scheme to systematically derive potential BST countermeasures as well as to structure state of the art technology and research in relation to the BST effect.

2.1 Fundamentals of Motorcycle Dynamics

Besides the introduction of some basic definitions, this chapter aims at providing a brief glance at the fundamentals of motorcycle dynamics that play a role in context of the BST effect. The presented information helps to better understand the involvement of a rider's fear and characteristic startle reactions (see chapters 1, 2.2, and 2.3.2), the validity of certain simplifications used in this study (esp. in chapters 3 and 4) and are furthermore handy in interpreting the results of the measurements (see chapter 5).

However, this chapter is mainly addressed at those unfamiliar with motorcycle dynamics in particular or vehicle dynamics in general. The more experienced readers may as well skip or briefly browse it and directly continue with the following chapter 2.2, since all information absolutely essential for understanding of later sections is cross referenced and can also be read in context later.

[25] See mainly: Cossalter et al. (2010): Steering Torque Decomposition, Cossalter (2006): Motorcycle Dynamics, and Weidele (1994): Bremsverhalten von Motorrädern.

2.1.1 Coordinate Systems and Basic Chassis Geometry

Figure 2.1 introduces the three coordinate systems used in this study and gives a schematic overview of important chassis parameters of a motorcycle with standard chassis, using a telescopic fork as front suspension / steering system.

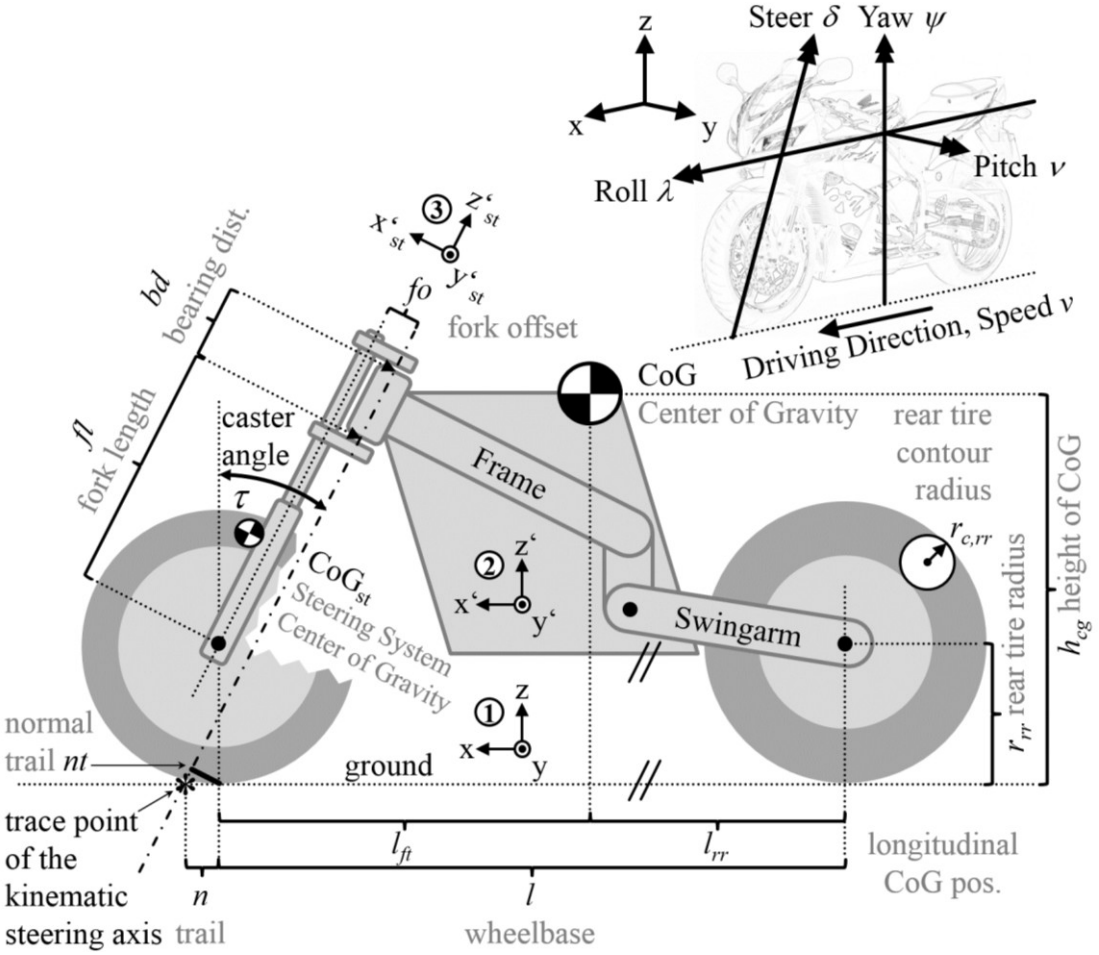

Figure 2.1: Coordinate systems and important geometry parameters of a standard chassis with telescopic fork front suspension / steering system. Dimensions indicated for the rear tire apply analogously for the front. Rear suspension details are omitted. [Motorcycle picture © Honda]

Standard Chassis

It is important to note, that the presented geometry with the fork legs in parallel to the steering axis is the most common on contemporary production motorcycles with telescopic forks. Even if parts of the fork offset (*fo*) are not achieved by means of the fork yokes alone but complimented by an offset at the axle, the kinematics remain the same. However, there are also a few exceptions from this "standard", mainly found in custom made motorcycles of the "chopper" or "cruiser" category. In this context, different offsets at both fork yokes are often used to keep the desired appearance with a very long and flat fork, i.e. a large caster angle (τ), in balance with reasonable amounts of trail (n).

Coordinate Systems

While the regarded chassis parameters are self-explanatory from Figure 2.1, the three coordinate systems (CoSy) are usually only used to describe certain directions rather than absolute positions. Their origin is therefore only fixed to special locations, if it is beneficial in a specific context. The three CoSy are:

1) xyz: Levelled CoSy as a horizontal projection of the motorcycle body CoSy (2) into the x-y-plane, either in parallel to or flat on ground. The x-axis aligns with the projected x'-direction of CoSy (2). Its origin is typically either located in the rear tire contact patch, the CoG or perpendicularly below, projected on ground along the z-axis.
2) x'y'z': Motorcycle body coordinate system, fixed to the motorcycle main frame. It follows all movements of the motorcycle body. Its origin typically lies in the swing arm pivot point or the CoG.
3) $(x'y'z')_{st}$: Coordinate system of the motorcycle steering system. Usually, this system is rotating together with the steering system relative to the body / frame. However, in this definition, the coordinate system is fixed to CoSy (2), so that the y'- and y'_{st}-axes point in the same direction and the z'_{st}-axis points upward along the steering head centerline. Its origin is located in the center of the lower steering bearing or the front wheel hub-center.

Simplifications for Model Calculations

In the presented study, the vehicle is typically considered as an unsprung rigid body bicycle model, where the two steering bearings define the steering axis as a pivotable connection between the steering system (front frame) and the vehicle's main body (rear frame). Moreover, the overall CoG is including the mass of the front frame system as well as the rider, if not otherwise indicated.

As illustrated in the top right image in Figure 2.1 and apart from the spin of the two wheels, the main degrees of freedom are the steering motion around the steering axis, the roll (along the x-axis), pitch (along the y-axis) and yaw (along the z-axis) rotation of the vehicle, further represented by the turn angle variables δ, λ, ν, and ψ, respectively.

For simplified model calculations (esp. in chapters 3 and 4), the vehicle is considered to remain in a static trim condition, with the x'-axis in parallel to the x-axis, as well as a constant caster angle and wheelbase. When pitch is considered, this is done by a reduction in caster angle (τ) and, if applicable, fork length (fl), while the wheelbase and center of gravity (CoG) location are considered invariant for the calculation of tire contact forces in front and rear. – Real changes are estimated to be about 5% at 10° brake pitch and full fork compression of the utilized test motorcycle. - Finally, also the tires are assumed to be non-deflectable and feature constant toroid cross-section radii ($r_{c,ft/rr}$).

2.1.2 Roll Equilibrium, Tire Scrub Radius & Riding Styles

Roll Equilibrium

In this section, a simplified definition of equilibrium roll angle is derived, that is equally used in model calculations for free cornering and "quasi-stationary" corner braking. This means that dynamic influences on the roll angle are neglected and stationary, free cornering conditions are assumed for every point in time also in corner braking.

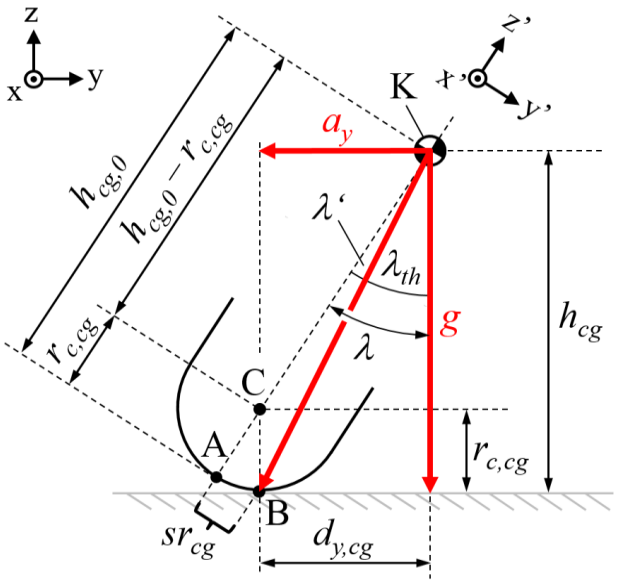

Figure 2.2: Equilibrium roll angle (λ) and tire scrub radius at center of gravity location (sr_{cg})

Figure 2.2 shows the frontal projection of a vehicle cornering at a total geometrical roll angle of $\lambda = 33°$ intersected at its center of gravity (CoG). Demanding that the resultant of accelerations a_y and g is pointing from the center of gravity through the tire contact patch line to obtain equilibrium conditions, the total roll angle λ is in good approximation composed by the physically active / theoretical roll angle λ_{th}, and the tire-width-dependent additional roll angle λ'[26]:

$$\lambda = \lambda_{th} + \lambda' , \tag{2.1}$$

with

$$\lambda_{th} = \arctan\left(\frac{a_y}{g}\right) = \arctan\left(\frac{v^2}{R \cdot g}\right) . \tag{2.2}$$

[26] While λ' is in the order of 10% of λ_{th} and practically relevant, further additional roll angles arise from the nutation of rotating parts and the Coriolis effect. Since these are in the order of only 1% respectively 0.1% of λ_{th}, these are negligible. Cf. to Weidele (1994): Bremsverhalten von Motorrädern, Chapter 3.5, p. 39ff and Chapter 3.6, p. 50ff for more detail, also on dynamic influences on the roll angle.

Since the rear tire width and contour radius are typically larger than in front, the tire contact patch line differs from the intersection line of the vehicle symmetry and ground planes (cf. Figure 2.13). Based on an averaged tire contour radius at CoG location[27]:

$$r_{c,cg} = \frac{r_{c,ft} \cdot l_{rr} + r_{c,rr} \cdot l_{ft}}{l} \tag{2.3}$$

a geometrically consistent formulation of the additional roll angle λ' is obtained as follows. Reformulating the law of sines[28] in triangle (K-C-B) in Figure 2.2 delivers:

$$\sin \lambda' = \frac{r_{c,cg}}{h_{cg,0} - r_{c,cg}} \cdot \sin \lambda_{th} \ . \tag{2.4}$$

Using the equivalent expression for the inverse tangent function:

$$\arctan x = \arcsin \frac{x}{\sqrt{1+x^2}} , \tag{2.5}$$

the theoretical roll angle from equation (2.2) can be expressed as:

$$\lambda_{th} = \arctan\left(\frac{a_y}{g}\right) = \arcsin \frac{a_y}{g \cdot \sqrt{1+\left(\frac{a_y}{g}\right)^2}} = \arcsin \frac{a_y}{\sqrt{g^2+a_y^2}} . \tag{2.6}$$

Inserting of equation (2.6) in equation (2.4), the sine and arcsine cancel each other out and the tire width dependent additional roll angle is finally expressed as a function of geometry and acceleration properties:

$$\lambda' = \arcsin\left(\frac{r_{c,cg}}{h_{cg,0} - r_{c,cg}} \cdot \frac{a_y}{\sqrt{g^2 + a_y^2}}\right) \tag{2.7}$$

Combining equations (2.1), (2.2), and (2.7), the total roll angle becomes:

$$\lambda = \lambda_{th} + \lambda' = \arctan\left(\frac{a_y}{g}\right) + \arcsin\left(\frac{r_{c,cg}}{h_{cg,0} - r_{c,cg}} \cdot \frac{a_y}{\sqrt{g^2+a_y^2}}\right) . \tag{2.8}$$

While this precise formulation is required for the analytical solution of model calculations (cf. chapters 3 and 4), the following approximation has been found to show the order of the additional roll angle λ' for the research motorcycle (cf. chapter 4) in good accordance with literature[26] and experiment:

$$\lambda = \lambda_{th} + \lambda' \approx 1.115 \cdot \lambda_{th} \ . \tag{2.9}$$

Already when regarding the definition of the theoretical roll angle in eq. (2.2) it becomes clear, that a reduction of roll angle is necessary during a corner-braking maneu-

[27] Bayer (1986): Das Pendeln und Flattern

[28] Merziger et al. (2001): Formeln + Hilfen. Chapter 2, p. 18

ver to maintain equilibrium. Consequently, a certain stand-up tendency that matches the deceleration level is even desired and should be considered for the layout of potential countermeasures against the Brake Steering Torque (BST) and its effects.

Tire Scrub Radius and Influences of Riding Style

Even though Figure 2.2 shows a cross-section of the motorcycle at center of gravity location, it can as well be used to describe the effect of roll angle on the tire scrub radii (*sr*) at the front and rear wheel with thier different contour radii (r_c):

$$sr_{ft/rr/cg} = r_{c,ft/rr/cg} \cdot \sin\lambda \,. \tag{2.10}$$

Since the rider and possibly passenger are representing a great portion of the overall mass of the man-machine system and can perform movements relative to the vehicle, they can dynamically influence the overall center of gravity location and hence also the roll angle of a motorcycle for a given riding situation. In an exaggerated way, Figure 2.3 exemplarily shows the potential to decrease the vehicle roll angle through the riding style lean in (LI) or increase it through the riding style lean out (LO) with regards to the centered classical lean with (LW) riding style.

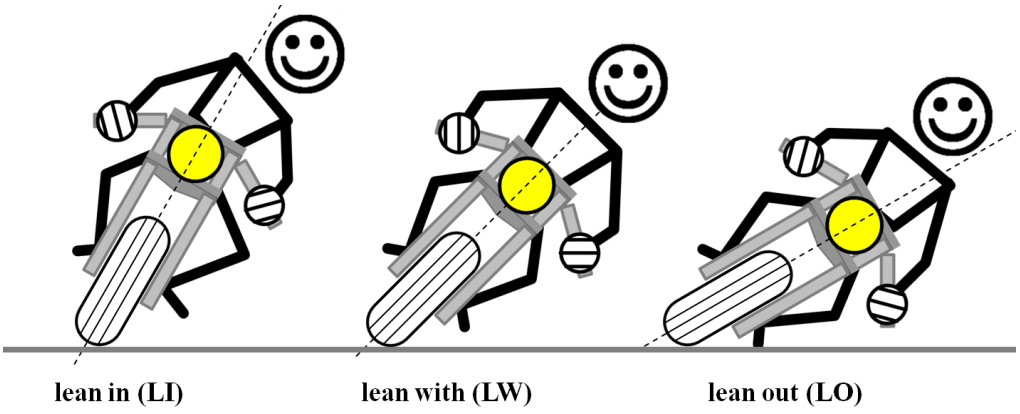

Figure 2.3: Influence of riding style on roll angle and tire scrub radius

Depending on the man / machine mass ratio and geometrical parameters such as the vehicle's center of gravity location, tire contour radii and seating position, a single rider can achieve roll angle variations in the order of 5-10% for typical rural road riding with a touring or sports motorcycle. As directly apparent from eq. (2.10), a reduction (or increase) in vehicle roll angle will also reduce (or increase) the tire scrub radius and thus the effective lever arm of a front brake force. In conclusion, a lean in riding style seems generally favorable, as far as the BST effect in corner braking is concerned. However, in certain situations, such as quick swerving around an obstacle, also the lean out riding style has its benefits. Finally, even though still greater reductions in vehicle roll angle and scrub radius are possible with the radical "hanging-off" riding style, it should be reserved for racing purposes on closed tracks with their predictable boundary

conditions and is not recommended for use on public roads for several reasons. Firstly, it requires a lot of practice and expertise to really master this technique well enough to perform unexpected changes in trajectory as they frequently arise in real traffic. Secondly, if an unforeseen situation occurs during the transition phase of one seating position to another, the loose coupling of the rider to the vehicle is likely to negatively affect the required emergency maneuver performance (cf. chapters 2.2.5 and 2.3.2). Thirdly, hanging-off is also more fatiguing for the rider, which is not desirable in public traffic.

2.1.3 Influences on Steering Torque Demand

The steering torque is at the same time the main control input for maneuvering a motorcycle and an important feedback for the rider about the current driving condition. Figure 2.4 illustrates, how the steering torque demand (STD) to be covered by the rider's steering effort in a given free cornering or corner braking situation is composed by superimposition of aligning and misaligning effects that respectively tend to decrease or increase the steering angle (outward or inward the turn).

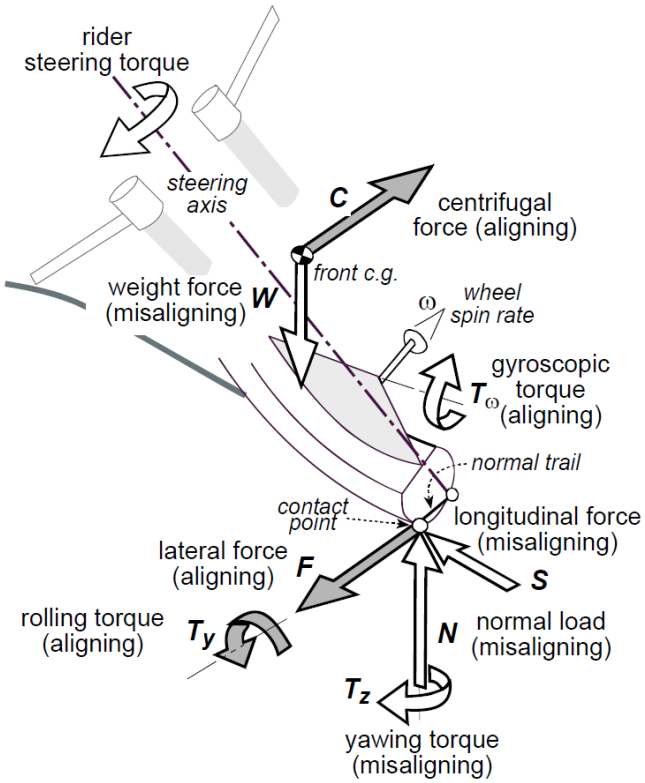

Figure 2.4: Influences on steering torque demand[29]. Note, that in contrast to the nomenclature of this thesis, the "normal trail" in the figure is defined as the perpendicular connection between tire contact point and steering axis. It is thus equal to the vectorial superimposition of the scrub radius (sr_{ft}) and normal trail (nt) as defined in Figure 2.1, Figure 2.2, and eq. (2.10).

[29] Cossalter et al. (2010): Steering Torque Decomposition, Fig. 4: Equilibrium of the front frame.

For a well designed conventional chassis with "neutral" layout, all steering torque components are balanced in such a way, that the rider typically needs to exercise a slight steering torque outward the curve during free cornering which will further increase with rising deceleration. A BSTAM is however changing the steering geometry and transfer ratios of the different steering torque components, mainly of the dominating tire contact forces (cf. Figure 3.8). Hence, special attention needs to be paid during its layout to maintain the sensible balance of the base vehicle. This is treated in detail in chapter 3.

2.1.4 Tire Road Interaction

The presence of sufficient force transfer potential between tire and road is essential for riding stability as well as maneuvering, especially when braking while cornering.

In a very simplified form, the maximum transferrable longitudinal and lateral tire forces for a given normal force can be expressed using Kamm's friction circle:

$$\sqrt{F_x^2 + F_y^2} = \mu_0 \cdot F_z \,, \tag{2.11}$$

with F_x, F_y, and F_z representing the tire longitudinal, lateral, and normal forces, and μ_0 the maximal friction coefficient of the given tire road combination. An alternative notation is given by:

$$\sqrt{a_x^2 + a_y^2} = \mu_0 \cdot g \,, \text{ or } \sqrt{\left(\frac{a_x}{g}\right)^2 + \left(\frac{a_y}{g}\right)^2} = \mu_0 \,, \tag{2.12}$$

with a_x, a_y, and g being the longitudinal, lateral and gravitational acceleration, which leads to the graphical representation of the friction circle with radius μ_0 in Figure 2.5.

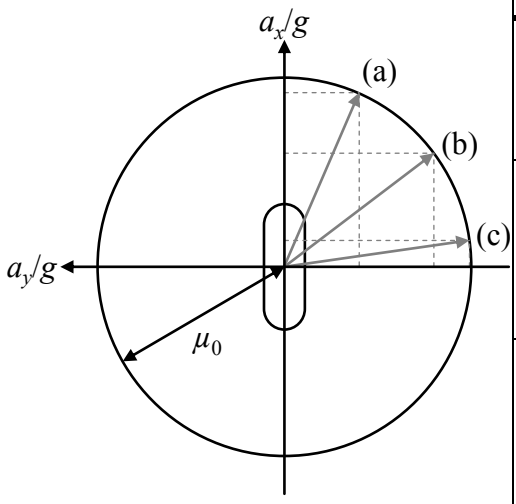

Case	(a)	(b)	(c)
used lateral force transfer (or acceleration)	40.0%	80.0%	99.0%
corresponding geometrical (and theoretical) roll angle for $\mu_0 = 1$	24.3° (21.8°)	43.1° (38.7°)	49.9° (44.7°)
remaining longitudinal force transfer (or acceleration / deceleration) potential	91.7%	60.0%	14.1%

Figure 2.5: Friction circle with example combinations of lateral and longitudinal force transfer

Thanks to the vectorial addition of lateral and longitudinal forces, a huge potential to transfer longitudinal forces remains even for quite impressive lateral accelerations as exemplarily showcased in the table contained in Figure 2.5. For instance, when cornering at 80% of the maximum lateral acceleration in case (b), which correlates to a roll angle of more than 43° on the utilized test motorcycle, still 60% of the straight running deceleration potential remain available. Given the fact that the majority of riders typically does not even utilize such deceleration levels even in straight running[30], this underlines the huge potential of effective corner braking as pointed out by Weidele[31].

While the transfer of longitudinal forces is related to driving or braking slip:

$$\begin{aligned} s_{drive} &= \frac{v_{tire}-v}{v}\text{, with } v_{tire} > v \text{ and} \\ s_{brake} &= \frac{v-v_{tire}}{v}\text{, with } v_{tire} < v, \end{aligned} \tag{2.13}$$

with v being the forward vehicle speed and v_{tire} the circumferential tire speed, lateral forces are generated by a superimposition of camber and sideslip lateral forces:

$$F_y = F_{y,\lambda} + F_{y,\alpha}\,, \tag{2.14}$$

with $F_{y,\lambda}$ being the camber and $F_{y,\alpha}$ the sideslip related component. While the tire camber angle is in good approximation directly attributed to the roll angle λ of the vehicle, the sideslip angle is defined as the leveled projection of the difference angle between the tire symmetry plane and its direction of travel. For a geometrically defined equilibrium roll angle (cf. chapter 2.1.2), the camber lateral force is dominating the sideslip lateral force, which is used to modulate the overall side force balance as to match equilibrium conditions by applying small steering angles (cf. chapter 2.1.6).

Longitudinal and lateral force transfer are interconnected for combined slip conditions as illustrated in Figure 2.6 by measurements of a real tire with a tire measurement trailer under variation of brake slip, sideslip and roll angle. The μ-slip-curve for pure longitudinal slip (solid line, $\lambda = 0$, $\alpha = 0$) exhibits a characteristic shape with a linear increase for low slip values followed by a distinctive peak around 7-8% slip, before falling to significantly lower force transfer capability with increasing slippage in the tire contact patch and a massive drop for a fully locked wheel. When combined with increasing lateral force transfer, be it through camber and / or sideslip, this characteristic shape of the μ-slip-curve is gradually morphing towards a more degressive initial slope, with the peak value being less distinctive, lower and at higher slip values, here of up to 30%. Also the longitudinal force transfer capability is then sinking in accordance with Kamm's friction circle.

[30] Cf. Präckel (1999): Die Motorradbremsung im System, Chapter 6.1, p. 83 ff, e.g. Bild 35, p. 103

[31] Weidele (1994): Bremsverhalten von Motorrädern, Chapter 4, p. 64 ff

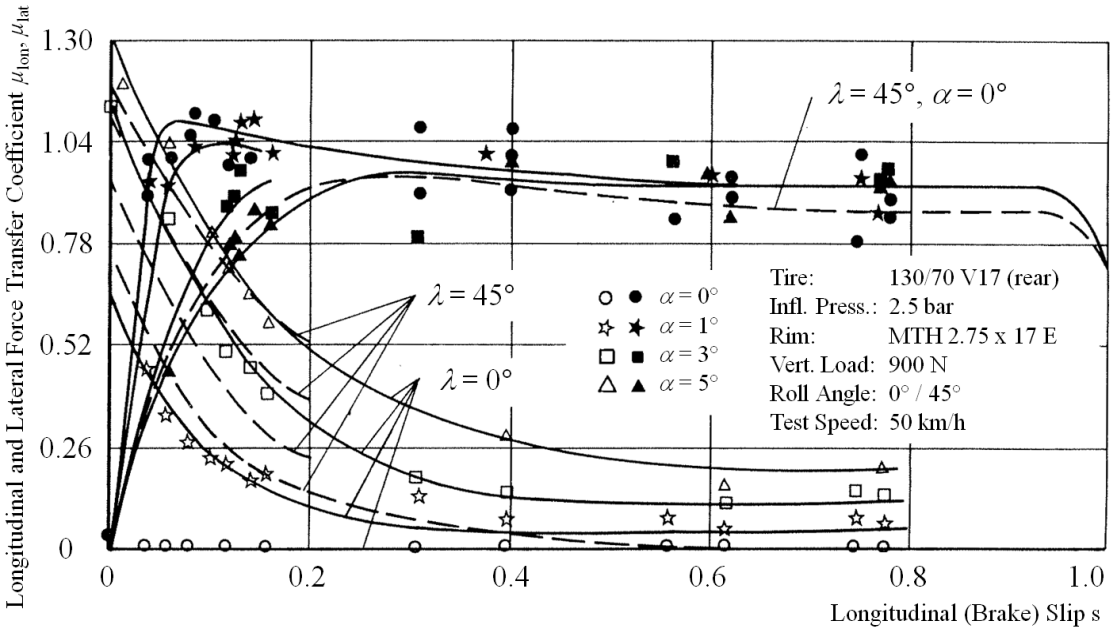

Figure 2.6: Longitudinal and lateral force transfer coefficients as a function of brake slip, sideslip and roll angle[32]

The characteristic degressive shape of the lateral force transfer curves versus increasing brake slip illustrates, that for a given initial roll angle (e.g. $\lambda = 45°$) an increase in side slip angle is required in combined slip situations such as braking while cornering to maintain the lateral force balance and hence roll equilibrium and stability. In this context, also a positive influence of the BST effect can be stated, since it tends to increase the steering angle and directly along with it also the sideslip angle of the front wheel.

2.1.5 Steering Kinematics and Steering Angle

The following simplified considerations illustrate how the characteristic steering kinematics of a motorcycle lead to typically very small steering angles and are still essential for riding stability (cf. chapter 2.1.6).

Figure 2.7 shows the frontal and top view of a motorcycle cornering at roll angle λ. Pushing the motorcycle at infinitesimal small speed around the desired curve center point M at a constant radius R, the roll angle $\lambda = 0$ and the effective front wheel steering angle perpendicular to the road is defined by the Ackermann condition:

$$\delta_{wheel} = \delta_{Ackermann} = \arctan\frac{l}{R}. \tag{2.15}$$

With increasing speed and lateral acceleration also the roll angle λ is increasing. For tires with zero width the total roll angle equals the theoretical one (cf. chapter 2.1.2):

[32] Weidele (1994): Bremsverhalten von Motorrädern, Chapter 5.4.3, Bild 117, p. 161

$$\lambda = \lambda_{th} = \arctan\frac{a_y}{g} = \arctan\frac{v^2}{R \cdot g}\,. \tag{2.16}$$

The motorcycle is then riding in an imaginary banked curve defined by the surface of a cone with tip center M´´ below the road surface. Since the effective radius R' from cone tip to the vehicle is greater than the intended turn radius R, with:

$$R' = \frac{R}{\cos\lambda}\,, \tag{2.17}$$

the perpendicular wheel steering angle δ_{wheel} must be reduced accordingly, as would be the case when going around the turn center M´´ re-projected to M´ on the road plane at radius R' with an upright vehicle according to the Ackermann condition:

$$\delta_{wheel} = \arctan\frac{l}{R'} = \arctan\left(\frac{l}{R} \cdot \cos\lambda\right). \tag{2.18}$$

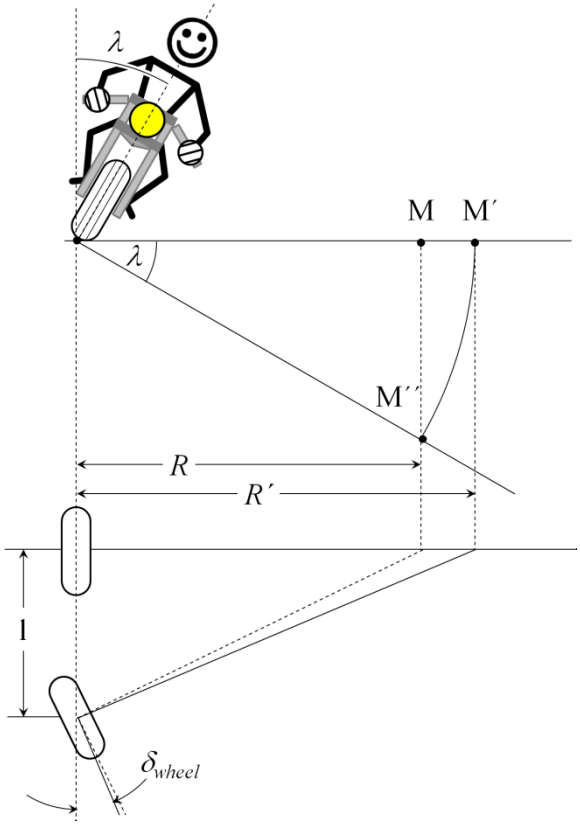

Figure 2.7: Steering angle of a motorcycle while cornering[33]

Due to the inclination of the steering axis by the steering head angle τ, the steering angle δ to be applied at the handlebars is greater than the wheel steering angle δ_{wheel}, as illustrated by the vectorial decomposition of the steering angle in the top left of Figure 2.9:

[33] cf. Bayer (1986): Das Pendeln und Flattern, Chapter 6, pp. 172, Figure 128

$$\delta = \frac{\delta_{wheel}}{\cos\tau} . \tag{2.19}$$

The other portion of steering angle causes the front wheel to camber with respect to the vehicle and thus increase (or decrease) its roll or camber angle towards the road by:

$$\Delta\lambda_{wheel} = \delta \cdot \sin\tau = \delta_{wheel} \cdot \tan\tau . \tag{2.20}$$

As a side note, it is worth pointing out that the effective caster angle τ and prior relationships may be affected by pitch motions as common for conventional chassis with telescopic fork. I.e., when entering a turn "on the brakes", τ is reduced by the forward pitch angle, so the steering transmission ratio in eq. (2.19) is getting more "direct".

A limit value consideration of eq. (2.16) for speeds increasing towards infinity delivers a roll angle of $\lambda = 90°$ and in combination with eq. (2.18) and (2.19) the steering angle becomes zero. This is vividly illustrated by free hand riding in board track motordromes with vertical walls (also called "silodromes" or "walls of death"), which were popular attractions on travelling fairs in the 1920s and 1930s.

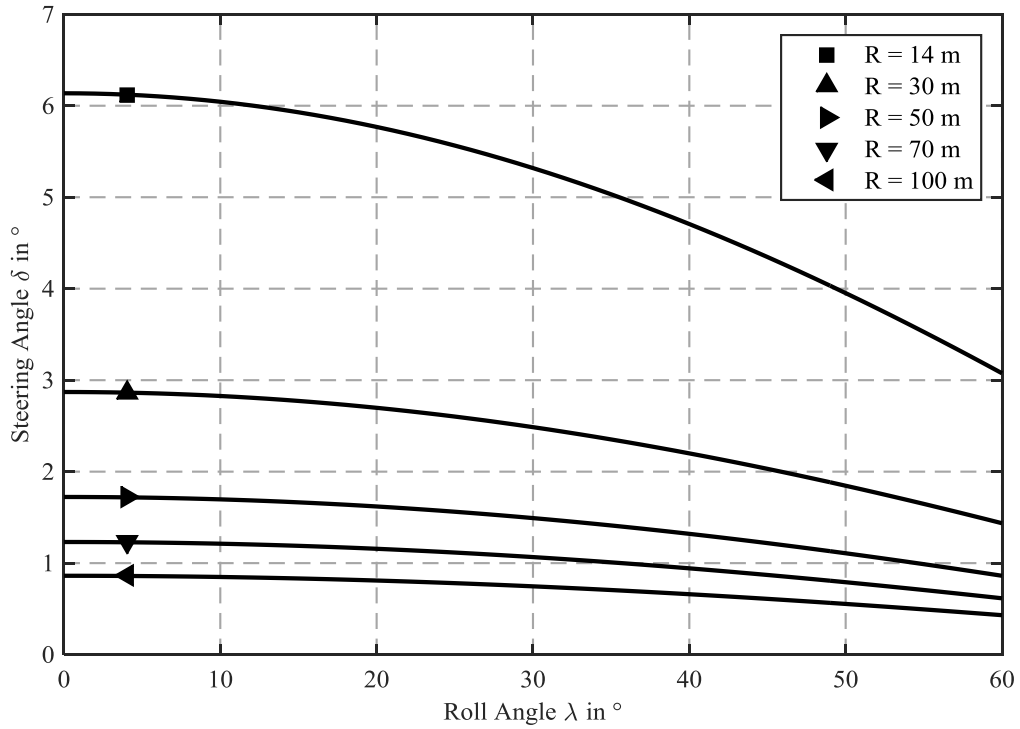

Figure 2.8: Steering angle versus roll angle (simplified model calculation for the Honda CBR 600 RR test motorcycle)

Figure 2.8 shows the results of a parameter variation based on eq. (2.18) and (2.19) for the wheelbase $l = 1.375$ m and caster angle $\tau = 23°55'$of the test motorcycle used in this study. The steering angle stays below 2° for curve radii of $R \geq 50$ m and remains in the order of just 6° even for low roll angles on the smallest turn radius of $R = 14$ m, which might for instance be encountered in hairpins on twisty mountain roads.

In conclusion, small angle approximations for the steering angle are typically valid with good accuracy. This is helpful in analyzing the steering kinematics of a motorcycle which are of utmost importance for stabilization as will be illustrated in chapter 2.1.6.

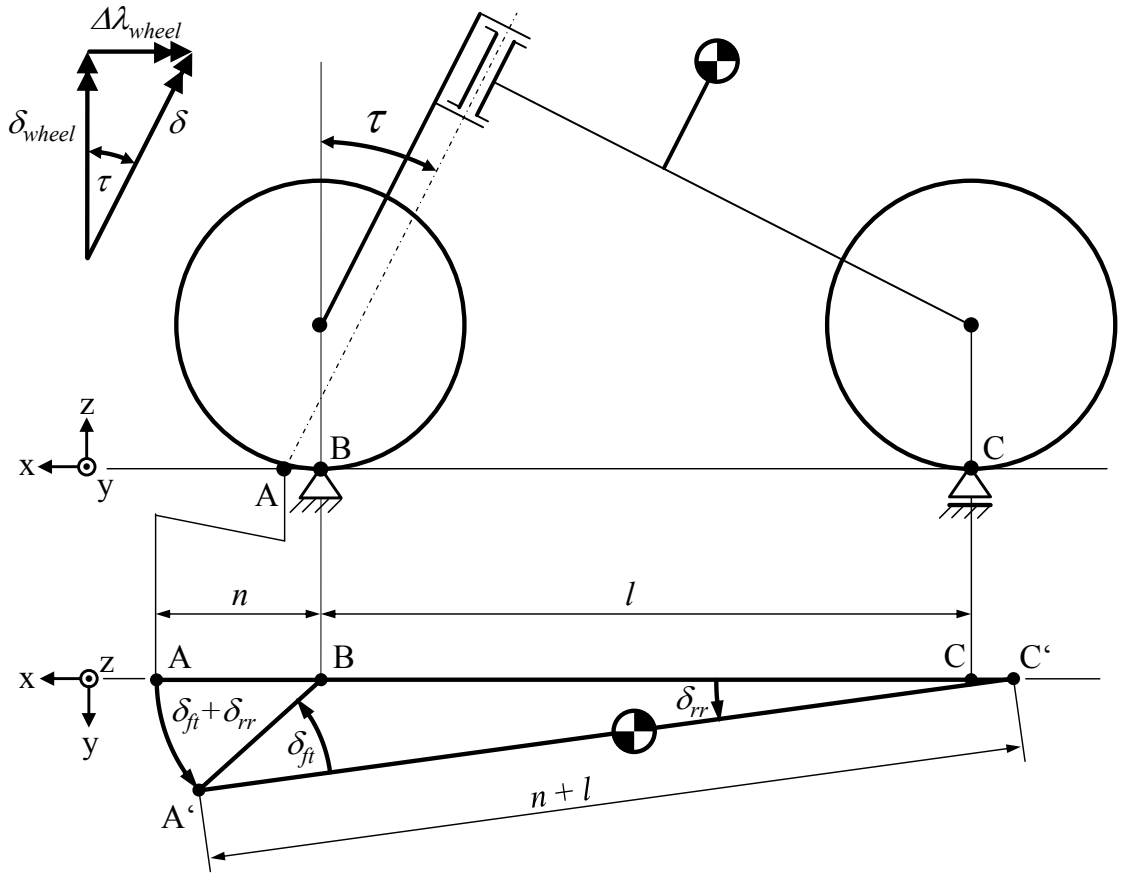

Figure 2.9: Simplified steering kinematics of a motorcycle[34]

Figure 2.9 illustrates the connection between front and rear wheel steering angle and how the vehicle symmetry plane and center of gravity can laterally be moved by steering motions, which is essential for balancing the vehicle at low speeds (cf. 2.1.6).

As shown in the upper half of the illustration, the front tire contact point B is attached to ground through a fixed bearing while the rear wheel contact point C rests on a floating bearing and can move in longitudinal direction. The lower part of the illustration shows the top view with enlarged trail *n* to highlight the desired effect.

Under the simplifying assumption that the front wheel describes a circular path when steered out of the symmetry plane and by making use of small angle approximations[35],

[34] Bayer (1986): Das Pendeln und Flattern, Chapter 6, pp. 172-173, Figures 128 and 129

[35] Bayer (1986): Das Pendeln und Flattern, Chapter 6, p. 173, Eq. 117

the rear wheel steering angle can be expressed as a function of the effective front wheel steering angle as follows:

$$\delta_{rr} = \frac{n}{l} \cdot \delta_{ft} \,. \tag{2.21}$$

Typical values for the quotient n/l are below 0.1, for the test motorcycle $n/l \approx 0.07$. Recalling the typical order of front wheel steering angles from Figure 2.8, illustrates how very small the rear wheel steering angles really are.

This interconnection explains how the front wheel delivers the main contribute to overall gyroscopic stabilization (cf. 2.1.6) while the rear wheel only contributes about 10%, despite the fact that the rear wheel's spinning inertia is typically greater than that of the front wheel (for the test motorcycle by a factor of 30-40% or even more, depending on tire wear (cf. appendix A.4.2, Table A.6).

Since steering angles and related chassis geometry changes stay typically very small, they are neglected for most geometrical considerations in this thesis.

2.1.6 Bi-Directional Coupling of Steer & Roll (Stabilization & Maneuvering)

The bi-directional coupling of steer and roll motion is not only a key causation factor in the BST chain of effects, but also a fundamental requirement for the dynamic stabilization and maneuvering of single track vehicles and therefore addressed in their context.

Low Speed Stabilization

In analogy to an inverted pendulum, a motorcycle is statically instable and prone to **capsizing** at standstill and low speeds. As illustrated in Figure 2.11 (A), a small perturbation in roll angle (1) creates a lateral offset between the tire contact patch line and the centre of gravity (2) so that the weight force (3) acting on the latter creates a destabilizing roll momentum which further increases with increasing roll. At standstill, the rider balances the vehicle by exerting an additional roll moment through the feet. At low speeds, the steering kinematics as illustrated in Figure 2.9 allow to balance the centre of gravity over the tire contact patch line through **alternating steering motions**, which may be complimented by **movements of the rider's body** in relation to the vehicle.

Dynamic Stabilization

Catching up speed, other well interwoven effects come into play that are responsible for the inherent bi-directional coupling of steering and roll motion of single track vehicles.

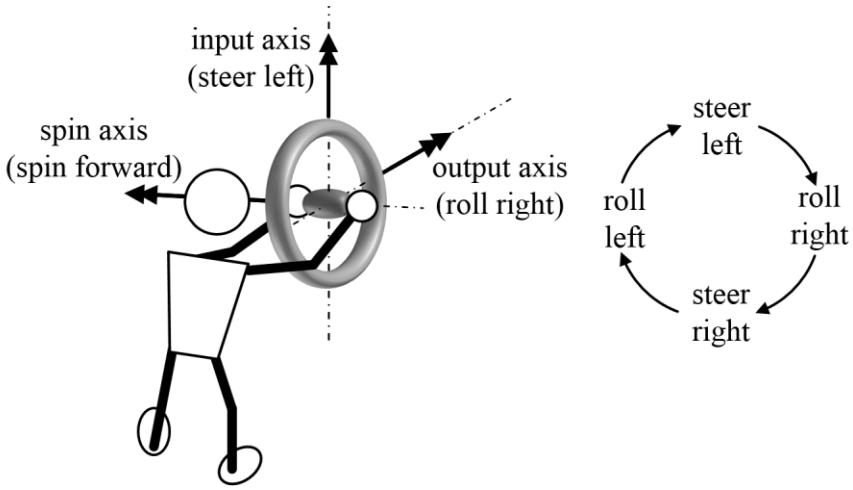

Figure 2.10: The gyroscopic effect and the bi-directional coupling of steer and roll motion

The first is the gyroscopic effect that is illustrated in Figure 2.10 by a person holding a spinning wheel in hands. As a characteristic of a gyroscope, the application of a torque or motion around the input axis (here: steering to the left) causes a proportional reaction torque or motion around the output axis (here: rolling to the right) which is oriented at 90° towards the input axis. Hence, if the input axis in the example is swapped to the roll axis, the output will be around the steering axis. In conclusion, the circular diagram on the right side of Figure 2.10 summarizes all possible in- and outputs.

In fact, the circular diagram is not only characteristic for the gyroscopic effect itself, but also for its interaction with the effects presented in the following, that finally combine to the bi-directional coupling of steer and roll motion as illustrated in Figure 2.11.

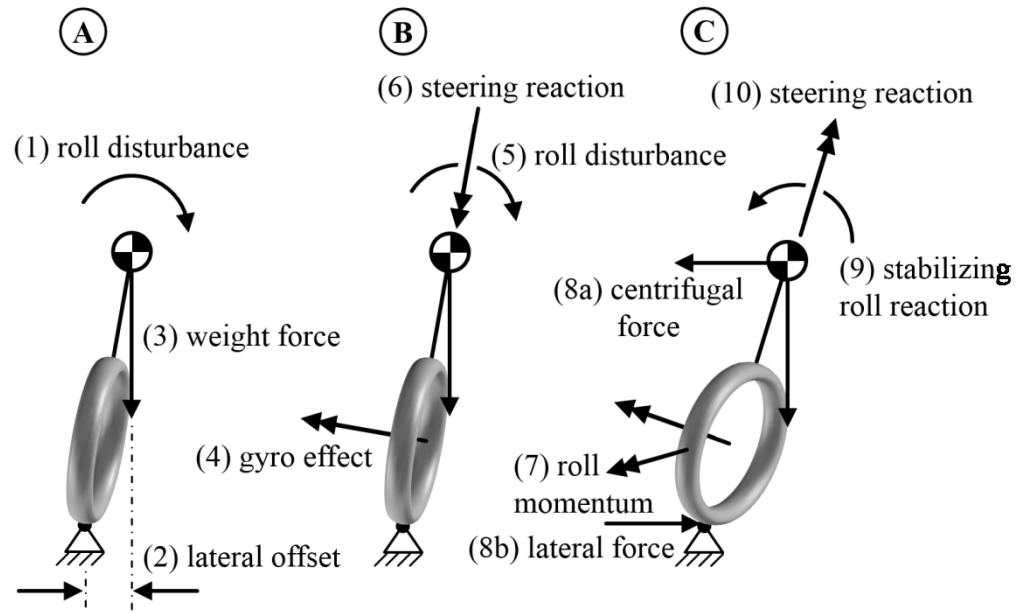

Figure 2.11: Labile equilibrium at low speed (A) and dynamic self stabilization (B, C)

While the labile equilibrium (A) was already discussed in the section on low speed stabilization, introducing a spin rate in (B) establishes the gyroscopic effect (4) which will answer a roll disturbance (5) to the right with a steering reaction to the right (6). Jumping to sketch (C), on one hand, this creates a roll momentum to the left (7) as gyroscopic reaction. On the other hand, with a steering angle being present, the vehicle is riding in a right turn for a short time, creating a centrifugal force on the center of gravity (8a) which is complimented by a lateral force (8b) at the tire contact patch level (both due to camber and sideslip), combining to another left directed roll momentum. All effects together lead to a stabilizing roll reaction of the vehicle to the left (9), while both the gyroscopic coupling and the lateral force (8b) via trail as lever arm initiate a leftward steering reaction (10). In a typical stabilization process, there may be an overshoot in the roll reaction (9), so that the subsequent steering reaction (10) is initiating the same sequence of effects, just for the opposite turn and roll direction. This repeats in an perpetuate manner and even if the amplitudes decay to an invisible level due to damping effects, a dynamically stabilized single track vehicle that seems to be going straight is actually rather driving in a serpentine line. Dynamic stabilization against capsize is typically achieved for speeds of about 30 km/h, with the front wheel contributing about 90% and the rear wheel about 10% to overall gyroscopic stabilization due to kinematic constraints as illustrated in chapter 2.1.5.

Finally, it is worth mentioning, that a single track vehicle can be self-stable without the presence of gyroscopic effects or even trail, for a special configuration of center of gravity locations of rear frame and steering system[36]. However, such a layout is far from practical reality of a motorcycle and the previously described effects remain in order.

Maneuvering

Besides for the stabilization, the described effects are also involved to initiate directional changes and control the roll angle through steering inputs by the rider. In order to achieve roll equilibrium in stationary cornering, the force resulting from centrifugal and weight force needs to point through the tire contact patches (cf. chapter 2.1.2).

As illustrated in Figure 2.12 for a right turn, this means that the path radius of the tire contact patches (grey lines) needs to be somewhat greater than that described by the center of gravity (black lines). In order to move the wheels outside from below the center of gravity, the rider utilizes an **outward steering impulse**, also called **counter steering**.

[36] Kooijman et al. (2011): A bicycle can be self-stable without gyroscopic or caster effects.

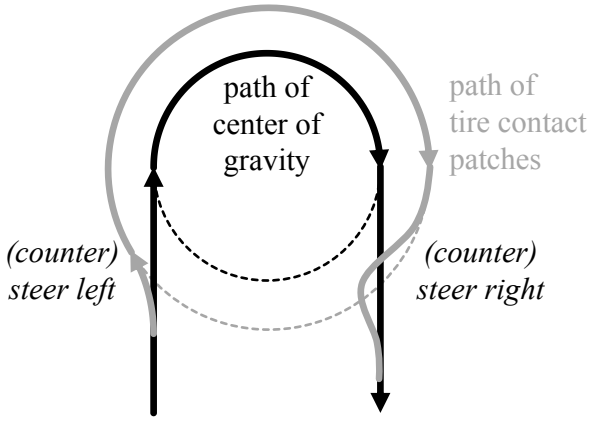

Figure 2.12: Directional changes and control of roll angle through (counter) steering inputs[37,38]

In the example of Figure 2.12, starting from bottom left of the illustration, the right turn is initiated with a steering impulse to the left. This generates a sideslip lateral force that "pulls" the front wheel from below the center of gravity, which continues on its path due to its inertia[38], and at the same time increases the roll angle, following the previously described coupling effects. When achieving the appropriate roll angle after the initial outward steering impulse, the steering angle settles to its equilibrium value (see chapters 2.1.4 and 2.1.5), as does the roll angle (see chapter 2.1.2). In order to leave the turn again, the roll angle needs to be diminished and the contact patches re-aligned with the vehicle symmetry plane, which is achieved by an inward (counter) steering impulse with the already described effects reversed.

A Digression to Instabilities

While the **capsize** of the single track vehicle has already been addressed earlier, also the **wobble**, **weave**, and **kick-back** instabilities are to be mentioned in context of the BST phenomenon, because similarities and characteristic frequencies are re-occurring in corner braking experiments.

Wobble is a natural oscillation of the steering system around the steering axis, with steering inertia and tire reaction forces as resetting component forming an oscillatory system. It is stimulated by dynamic imbalances of the front wheel and also affected by tire wear and inflation pressure. Its first order typically occurs in a speed range of

[37] cf. Spiegel (2010): The Upper Half of the Motorcycle, Part 1, Figures 13 and 14, p. 38

[38] Note that this is a simplified description to illustrate the main physical principle. In reality, the center of gravity's trajectory (black lines) does not necessarily have to remain a straight line in the transition phase from straight driving to cornering conditions, but may as well contain a wavy form.

50-80 km/h at corresponding frequencies of 6-10 Hz. It can be controlled by either detuning the oscillatory system through a tighter grip on the handlebars or by leaving the critical speed range through either acceleration or deceleration. This principally also holds true for the higher orders of the phenomenon, however, the grip on the handlebars is typically already firm enough at these higher speeds to suppress the oscillations.

Weave can be described as a degenerated dynamic stabilization process and as such involves coupled steering, roll, and also yaw oscillations. It typically occurs at speeds greater than 130 km/h (and is hence also referred to as "high speed weave"), with frequencies of about 2-4 Hz. The weave damping sinks with increasing speed, so further acceleration is not appropriate, because it can lead to exceeding the friction limits, e.g. for the lateral front wheel force, and thus cause a fall even in straight running. Since the human body's eigenfrequency lies in the same range, tighter coupling to the handlebars is neither an option, and the only effective countermeasure is careful deceleration.

Kick-back typically occurs when running over a bumpy road under strong acceleration, when large wheel load fluctuations are present at the front wheel, in extreme cases with temporary complete loss of ground contact. During such a "flying" phase, roll control is mainly achieved by the gyroscopic effect of the rotating front wheel, which requires greater steering angles than when the wheel is in road contact and lateral forces are contributing to the job. Touching back on ground with a large sideslip angle, a huge aligning steering torque component is generated and can lead to an even greater overshoot in steering angle to the opposite side during a subsequent flying phase. If the speed, distance and shape of the bumps are "matching", this can literally kick the handlebars out of the rider's hands while reaching the steering angle stops is just a matter of a tenth of a second at characteristic steering angle velocities in the order of 300°/s, as they were observed in experiments[39]. In consequence of the dynamic coupling, a fall is almost inevitable in such cases.

Regarding corner braking experiments with BST effect, the rather low weave frequency can be observed in the steer and roll motion during the initial braking phase with the stand-up, while the wobble eigenfrequency of the steering system and kick-back-like phenomena also occur, especially when in conjunction with dynamic over-braking (see discussions in chapter 5.4).

[39] Weidele (2014): Skriptum Motorräder 2014, Chapter 2.3.5, pp. 38-40

2.1.7 Tire Forces and Ideal Brake Force Distribution during Corner Braking

During corner braking, the tire contact forces are subject to dynamic changes, among which a forward shift in both normal and lateral forces are the dominating effects, which need to be accompanied by an adjustment of the Brake Force Distribution (BFD) between front and rear brake.

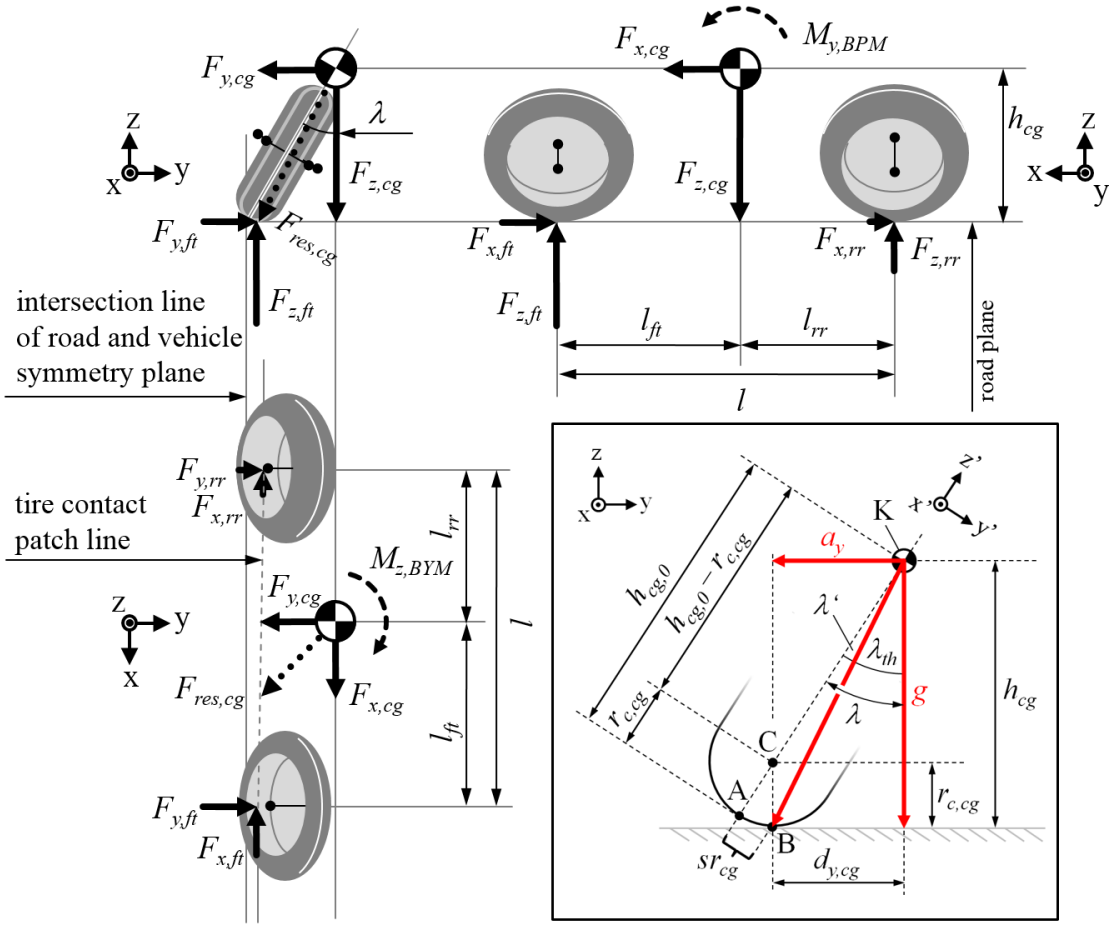

Figure 2.13: Simplified model of a motorcycle in quasi-stationary corner braking. Dimension of arrows representing forces approximately drawn to scale for $\lambda = 30°$ ($a_y \approx 0.5\ g$) and $a_x = 0.5\ g$.

Figure 2.13 shows a simplified model of an unsprung motorcycle with undeformable toroid tires, viewed from left, front and top along with corresponding forces for a quasi-stationary corner braking maneuver in a left turn. “Quasi-stationary” means, that roll equilibrium conditions as defined in Figure 2.2 (see repetition in Figure 2.13 bottom right) are assumed for the whole braking process, while influences through roll dynamics, gyroscopic effects, aerodynamic effects and the like are neglected.

Computation of Tire Contact Forces and Ideal Brake Force Distribution

The inertial forces in all three spatial directions acting on the center of gravity are the deceleration force:

$$F_{x,cg} = a_x \cdot m \,, \tag{2.22}$$

with a_x being the deceleration with a positive value in m/s² and m the overall mass of the vehicle including the rider, the centrifugal force:

$$F_{y,cg} = a_y \cdot m \,, \tag{2.23}$$

with a_y being the lateral acceleration in m/s², and the weight force:

$$F_{z,cg} = g \cdot m \,, \tag{2.24}$$

with g = 9.81 m/s² being the gravitational constant.

In the leveled coordinate system, the deceleration force acts with the height h_{cg} and lateral displacement $d_{y,cg}$ of the center of gravity as lever arms, forming a pitching and yawing moment that lead to a dynamic forward shift of both normal and lateral forces from the rear to the front wheel. Since the lever ratio of these so-called Brake Pitch and Brake Yaw Moments, $M_{y,BPM}$ and $M_{z,BYM}$, is corresponding to the ratio between lateral acceleration and gravity:

$$\frac{d_{y,cg}}{h_{cg}} = \frac{a_y}{g} \,, \tag{2.25}$$

the dynamic normal and lateral forces stay in a fixed relationship for the simple rigid body model and can be expressed as[40]:

$$F_{z,ft/rr} = m \cdot g \cdot \frac{l_{rr/ft}}{l} \pm m \cdot a_x \cdot \frac{h_{cg}}{l} \tag{2.26}$$

$$F_{y,ft/rr} = m \cdot a_y \cdot \frac{l_{rr/ft}}{l} \pm m \cdot a_x \cdot \frac{d_{y,cg}}{l} = \frac{a_y}{g} \cdot F_{z,ft/rr} \tag{2.27}$$

While the dynamic forward shift of normal forces due to the Brake Pitch Moment $M_{y,BPM}$ is well known to increase the force transfer capability of the front wheel under braking, the reduction of the same due to the Brake Yaw Moment $M_{z,BYM}$ with its forward shift of lateral forces must also not be forgotten. It plays an important role, both in terms of stability (cf. chapter 2.1.8) and concerning the Brake Force Distribution (BFD).

Assuming an ideal BFD with equal exploitation of the tire-road friction potential μ_{used} at both wheels according to Kamm's friction circle (see chapter 2.1.4):

[40] cf. Cossalter et al. (2010): Steering Torque Decomposition, Section V

$$\frac{\sqrt{F_{x,ft}^2+F_{y,ft}^2}}{F_{z,ft}} = \frac{\sqrt{F_{x,rr}^2+F_{y,rr}^2}}{F_{z,rr}} = \mu_{used} \,, \tag{2.28}$$

delivers the front and rear brake forces (cf. eq. (A.61), derived in detail in A.3.2):

$$F_{x,ft/rr} = \\ = \frac{\sqrt{\left(m \cdot a_x \cdot F_{z,ft} \cdot F_{z,rr}\right)^2 + \left(F_{y,ft}^2 \cdot F_{z,rr}^2 - F_{y,rr}^2 \cdot F_{z,ft}^2\right) \cdot \left(F_{z,ft}^2 - F_{z,rr}^2\right)} - m \cdot a_x \cdot \ F_{z,ft/rr}^2}{\pm\left(F_{z,rr}^2 - \ F_{z,ft}^2\right)} \tag{2.29}$$

Assuming sufficient available friction potential, a parameter variation of deceleration a_x and lateral acceleration a_y leads to the graphical representation of the ideal BFD with its characteristic "airfoil-like" arrangement[41] as presented in Figure 2.14.

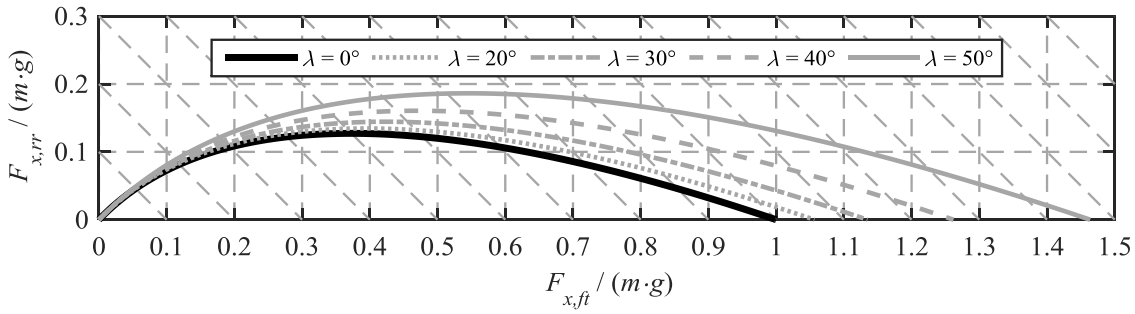

Figure 2.14: Ideal Brake Force Distribution (BFD) of the test motorcycle at different roll angles (model calculation without brake pitch; diagonal lines indicate constant levels of deceleration)

As directly visible from the curves, the ideal BFD becomes more rear wheel oriented for rising lateral accelerations and roll angles and the brake flip-over point moves to higher decelerations due to the lowering of the center of gravity with respect to the road. Keeping in mind the friction circle and a limited friction potential, e.g. of $\mu_0 = 1$, at an exemplary total roll angle of 40° that corresponds to a lateral acceleration of $a_y \approx 0.72g$, also the maximal possible deceleration is reduced to $a_x = \sqrt{1 - 0.72^2}\, g \approx 0.69g$. At such lower deceleration levels, also the differences in the roll angle dependent ideal BFD curves are much lower, than they may appear from the higher deceleration levels.

However, while it is already hardly possible to obtain optimal brake force distributions with the separate controls of a conventional brake even under controlled straight running conditions on a test track[42], it becomes an even more difficult control task for braking while cornering, especially in hazardous real world situations.

---

[41] Weidele (1994): Bremsverhalten von Motorrädern, Chapter 3.6.3, Bild 35, p. 60, and Chapter 4.6, Bild 48, p. 76

[42] Among others, cf. Weidele (1994): Bremsverhalten von Motorrädern, Chapter 5.2.2, p. 116 ff

In order to follow the ideal BFD when starting to brake in a curve, the rider has first to increase both brake forces and then to continue increasing at the front wheel, while reducing actuation at the rear, when getting closer to the flip-over point. With decreasing speed, lateral acceleration and roll angle, the available friction potential allows higher decelerations, while the brake flip-over point is moving to lower decelerations. Hence, either a further increase in front brake actuation may be possible or a reduction necessary, which will in any way need to go along with further reduced rear braking.

Along with the considerations on braking stability presented in chapter 2.1.8, this already underlines the great benefit of a well designed combined brake system, in best case with anti-lock and rear wheel lift-off protection functionalities, as will be addressed in chapters 2.3.3 and 3.6.

Side Note on the Quasi-Stationary Roll Equilibrium

The bottom left sketch in Figure 2.13 illustrates, how the tire contact patch line is laterally inclined due to the different tire contour radii in front and rear and how the averaged tire contour radius $r_{c,cg}$ is derived (cf. eq. (2.3) in chapter 2.1.2).

The same sketch also shows, that the resultant of the inertial, centrifugal and weight forces $F_{x/y/z,cg}$ acting on the center of gravity is no longer pointing exactly through, but a little inside the laterally inclined tire contact patch line for growing decelerations, forming a roll momentum that tends to increase the roll angle:

$$M_x = \left(r_{c,cg} - r_{c,ft}\right) \cdot \tan\lambda \cdot m \cdot g \ . \tag{2.30}$$

For the most extreme situation that will practically not appear due to limitations in friction potential, that is a roll angle of $\lambda = 50°$ and a deceleration at the brake flip-over point, M_x can reach the order of 50 Nm for the parameters of the prototype motorcycle ($r_{c,cg}$ = 79.2 mm, $r_{c,ft}$ = 64.6 mm, and m = 300 kg, including the rider).

The influence of M_x will of cause alter the roll equilibrium and require smaller roll angles. Using $r_{c,ft}$ instead of $r_{c,cg}$ in eq. (2.8) yields maximal roll angle deviations of 3.3% or less over the whole roll angle range. Hence, absolute roll angle deviations with regards to the very simplified quasi-stationary definition remain below 1.65° and justify the neglection of M_x for the model calculations.

However, in a real corner braking experiment, there needs to be a transition from the free cornering to the decelerated roll equilibrium right after brake activation. The harsher the activation and the greater the achieved deceleration, the greater will M_x and the required reduction in roll angle be. Concerning the BST effect, this means two things. On one hand, M_x counteracts the initial stand-up tendency and on the other, the stand-up motion helps to achieve the new roll equilibrium altered by M_x.

In conclusion, and as a hypothesis to be checked in the riding experiments, the stand-up obtained during maximal corner braking could even better match the deceleration than for partial decelerations with rather smooth brake activation (cf. chapter 5.4.2).

2.1.8 Braking Stability

Besides the already challenging task to achieve a good brake force distribution as described in the previous chapter, this section addresses two phenomena, that make effective (corner) braking even more challenging, especially with conventional brakes.

Dynamic Over-Braking of the Front Wheel[43]

Unlike for the idealized unsprung chassis assumed in chapter 2.1.7, the dynamic load transfer to the front wheel under braking on a real sprung motorcycle is typically not in phase with building up brake force and deceleration, but rather delayed.

Taking the standard chassis with its telescopic fork at the front and pulled swingarm in the rear as an example, a great portion of wheel load is transferred through the spring / damper units in proportion to the pitch angle respectively angular velocity. Hence, large pitch motions are necessary, to build up the required wheel load. Even though the pitch tendency of the standard chassis is fostered by its large vertical distance Δh between center of gravity and kinematic pitch center (see Figure 2.15, right), in any case the non-zero pitch inertia of the vehicle body causes the mentioned delay.

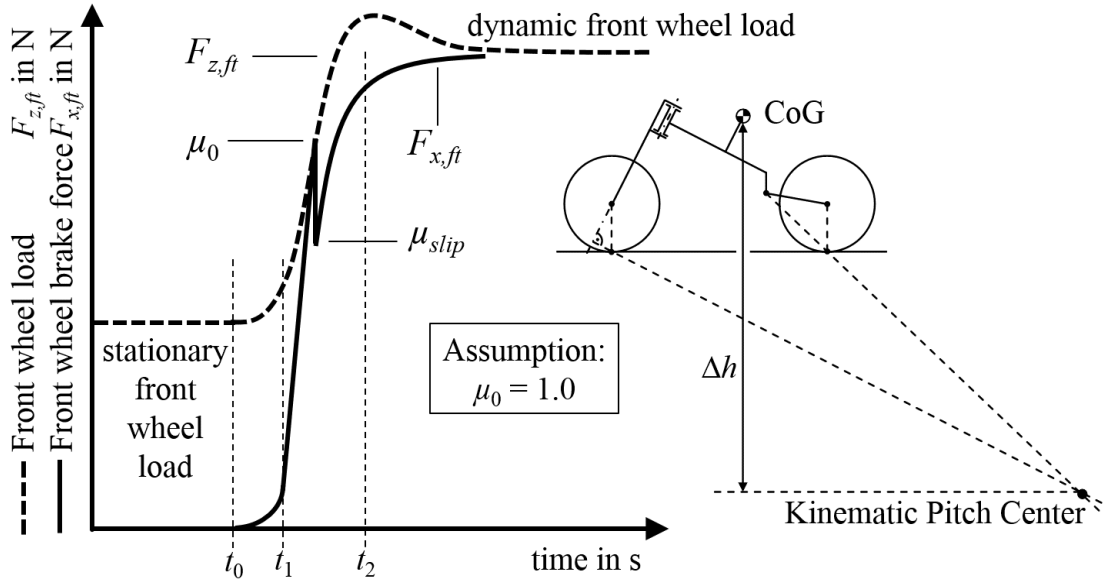

Figure 2.15: Schematic diagram of dynamic over-braking of the front wheel[43]

[43]Weidele (1994): Bremsverhalten von Motorrädern, Chapter 3.4, pp. 36-39, i.e. p. 38, Bild 20

Thus, the rider may easily induce braking force gradients in excess of the wheel load increase and a wheel lock can occur at an unexpectedly low level of brake application.

This effect is schematically illustrated in Figure 2.15, left. At first, the vehicle is traveling at constant speed and stationary front wheel load (dashed line) until the rider starts braking at time t_0. After a short response time of the brake system until t_1, the brake force (solid line) builds up significantly faster than the wheel load. When the maximum transferrable force is reached at full exploitation of the given friction potential μ_0, the front wheel starts to lock and the friction coefficient drops to μ_{slip} (see the characteristic μ-slip-diagram in Figure 2.6). Despite the temporarily reduced friction forces and deceleration, the wheel load continues to rise as the vehicle continues its forward pitch motion due to its pitch inertia. After a small instant, the wheel load has increased sufficiently to let the wheel start spinning again. Finally, both front wheel load and brake force reach their dynamic equilibrium in the full braking phase after t_2.

In a more severe case, the wheel load increase might not suffice to get the front wheel back to spinning without an instantaneous reduction of brake force that can practically only be provided quick enough by ABS control. Without this help, a crash is hardly avoidable, as illustrated in the next section.

Kinematic Braking Instability[44]

The following considerations highlight the criticality of an over-braked or even locked front wheel for the maintenance of riding stability. Figure 2.16 shows a simplified motorcycle model with infinitely slim tires, first in free cornering and then braking with a locked front wheel in three different phases (a, b, and c) from rear view (top illustrations) and top view (bottom illustrations).

In phase (a), the vehicle is in equilibrium steady turning conditions, with the resultant of centrifugal force $F_{y,cg}$ and weight force $F_{z,cg}$ pointing through the tire contact patch line as already discussed in earlier chapters (2.1.2 and 2.1.7).

In phase (b), an excessive front brake force $F_{x,ft}$ is applied that overstresses the available friction potential and locks the wheel. Besides the breakaway of the dynamic stabilization through the gyroscopic effect (see chapter 2.1.6), no lateral force can further be transferred at the front wheel (see chapter 2.1.4), leading to a diminution of centrifugal force $F_{y,cg}$ and an imbalance in roll equilibrium (top image). Moreover, the brake force $F_{x,ft}$ and corresponding inertial force at the center of gravity $F_{x,cg}$ as well as the remaining centrifugal force $F_{y,cg}$ in correspondence with the rear wheel lateral force $F_{y,rr}$ form

[44] cf. Seiniger (2009): Kurvenunfälle von Motorrädern, and Funke (2007): Motorradbremsung

an outward yawing moment (bottom image). Hence, both roll and yaw equilibrium are disturbed towards a downfall with increasing roll and outward yaw angles.

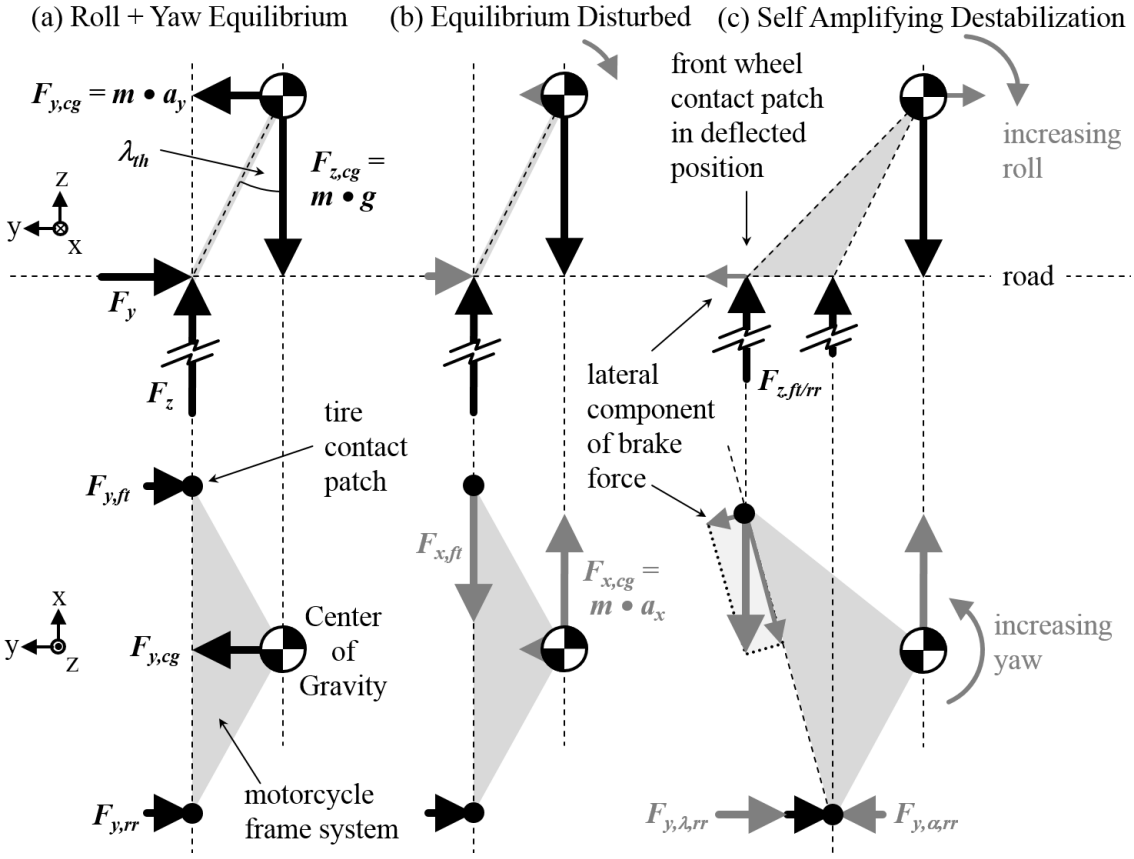

Figure 2.16: Kinematic Braking Instability (own illustration based on Seiniger and Funke[44])

Finally, phase (c) illustrates how this two-fold destabilization is even self-amplifying. Lacking the former lateral force, the front wheel wanders from below the vehicle towards the outside of the turn. Thus, the lever arm between brake force and inertial force, and consequently the outward yawing moment, are growing with increasing roll and yaw. (As an alternative description, this effect can equally be expressed by vectorial decomposition of the brake force that gains an ever growing lateral component that literally is pulling the front end of the vehicle from below the center of gravity.) Lastly, another destabilizing contribution arises from the increase in rear wheel lateral force that results from the fact that the growth of the camber component $F_{y,\lambda,rr}$ exceeds the opposing growth of the side-slip component $F_{y,\alpha,rr}$ already for small perturbations.

Especially when in conjunction with dynamic over-braking, the criticality of the kinematic instability becomes very clear before the background of the brake yawing moment occurring during corner braking (cf. chapter 2.1.7). However, since small roll angles are always present due to the dynamic stabilization process (cf. chapter 2.1.6), the combination of both effects can as well lead to quick fall-downs even from straight running

conditions. The combination of these effects illustrates very well, that most riders "fear to lose the front wheel" while braking for a good reason.

Comments on the Balance of Steering Torque Components

Concerning the balance of steering torque components (cf. 2.1.3) the overstress of longitudinal friction demand at the front wheel leads to a breakdown in the aligning lateral force component. Hence, the steering flips to the inside, often increasing the steering angle until hitting the steering stop in case of a locked wheel. While the lateral force does of cause not recover for this extreme case, this automatic increase in sideslip angle under increasing longitudinal brake slip assists the dynamic equilibrium and stabilization during a more moderate "normal" corner braking situation.

2.2 The BST Chain of Effects

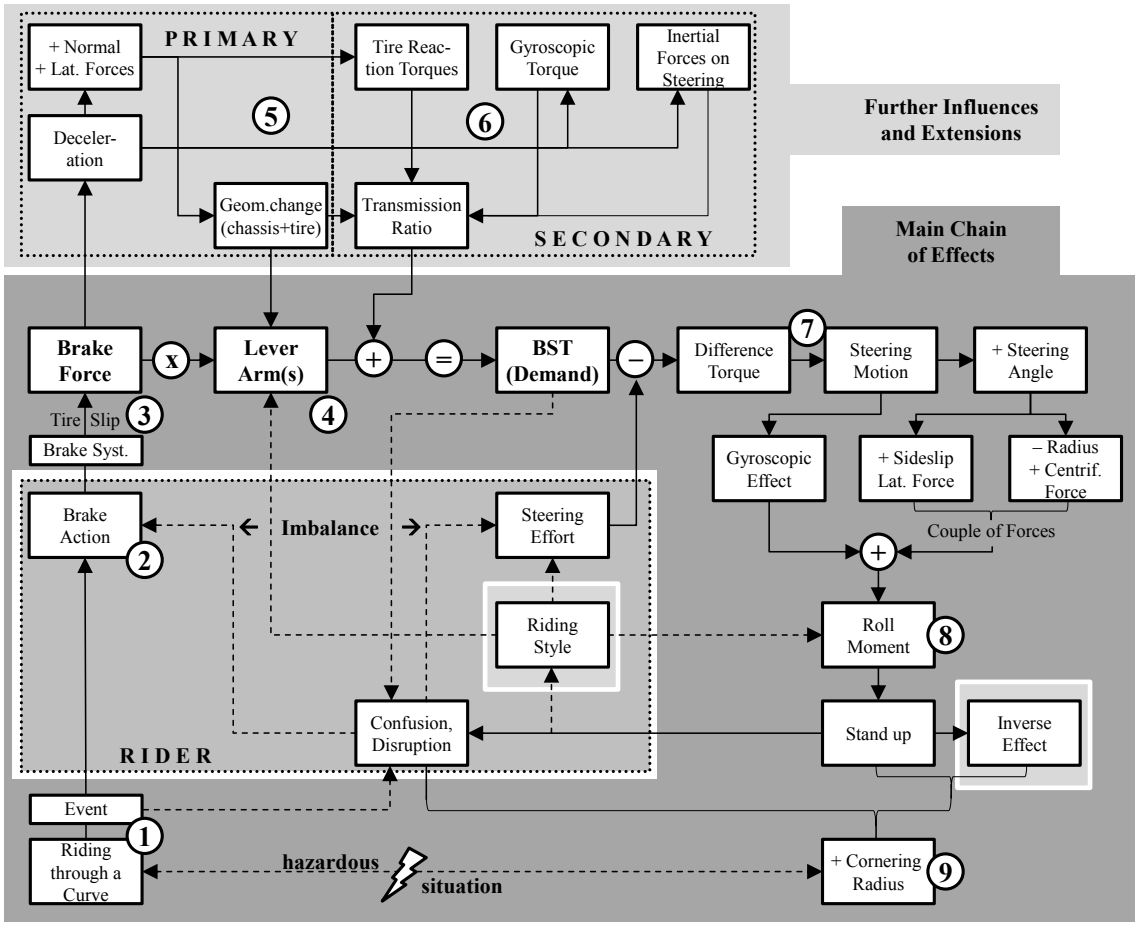

Figure 2.17: Extended BST chain of effects as basis for classification of countermeasures

Before the background of the fundamentals of motorcycle dynamics presented in the previous chapter, the most relevant influence factors on the BST chain of effects were identified. Supported by further findings from literature and own observations, an overview of the extended BST chain of effects (or brief: BST effect) was created as shown in Figure 2.17.

Temporarily ignoring the numbers (1 – 9), which are later used for the classification of BST countermeasures, the schematic diagram can be read as follows.

2.2.1 The Main Chain of Effects

The main chain of effects as illustrated in chapter 1.1 is contained in the lower part of the diagram (dark grey background). It starts in vertical direction from the bottom left corner, with a motorcyclist riding through a curve and being triggered by a certain unexpected event to apply the brakes quickly. The brake system builds up brake pressure and hence brake torque, the tire slip is increasing and a brake force is generated. Following the main path to the right, the brake force multiplies with its lever arm defined by the tire scrub radius, creating the BST. Depending on the balancing quality of the rider's brake and steering action, a difference torque might occur and trigger the already known chain of effects that leads to the stand-up tendency. In order to fully understand the subsequent increase in cornering radius, certain extensions of the main chain are necessary.

2.2.2 Further Primary and Secondary Influences

As one key finding, it is important to regard the overall steering torque the vehicle demands from the rider in a given corner braking situation, rather than considering the brake force induced BST in an isolated way. Leaving the main effect path on the left side of Figure 2.17 towards the extended primary influence factors (top left with light grey background), it is illustrated that the deceleration triggered by the brake force also leads to a dynamic forward shift of both normal and lateral forces[45]. Not only the brake force, but also the normal and lateral front wheel forces have their respective lever arms towards the steering axis. Depending on the chassis type and kinematic brake pitch compensation ratio, the wheel load shift will cause a pitch motion, consequently a change in the chassis geometry and thus also in the transmission ratio of the three wheel forces. The same holds true for the transmission ratio of the three secondary effects[46],

[45] Cf. chapter 2.1.7 on the effect of Brake Pitch and Yaw Moments.

[46] Cf. chapter 2.1.3 and 3.3.5 for an overview of different contributes to the overall steering torque demand and for dimension estimates as an explanation for ranking them "secondary".

tire reaction and gyroscopic torques[47] as well as inertial forces on the steering system (top center in the diagram). Going back to the main chain, these six components combine to the previously mentioned overall Steering Torque Demand (STD) that needs to be covered by the rider's steering effort in order to avoid the BST effect and stand-up tendency. Finally, another small geometry change superimposed to the chassis movement is given through tire deflection under varying load conditions.

2.2.3 The Influence of Riding Style

Jumping back into the main chain of effects, by variation of riding style, the rider has the opportunity to change the geometrical roll angle of the vehicle and along with it also the transmission ratios of the diverse effects as well as the level of steering torque demand within certain limits (cf. chapter 2.1.2). Compared to the classical riding style "lean with", the choice of the riding style "lean in" will decrease the vehicle roll angle and with it the tire scrub radius, while the balance between normal and lateral force components is shifting to be more aligning (cf. chapter 3.2). Both effects will lower the level of STD and thus assist the rider while the opposite holds true for "lean out" riding style. Since the rider's body has a given inertia and is not rigidly fixed to the vehicle, a sudden stand-up of the same during a BST relevant situation may cause his upper body to adopt a more "lean in" position and thus already improve the situation[48].

2.2.4 The Inverse Effect

Furthermore, as an often suppressed link towards the increasing cornering radius at the end of the chain, the initial "stand-up" diminishes the STD due to the same reasons as "lean in" riding style, superimposed by a gyroscopic effect that also tends to turn the steering back outside (cf. chapter 2.1.6). At this point the rider's steering effort often already exceeds the diminishing STD and the bi-directional coupling of steer and roll motion (cf. chapter 2.1.6) leads to further steering, roll and cornering curvature oscillations, until steering torque demand and effort are again in balance. Thus, the tangential departure trajectory from the intended cornering line is typically superimposed by sinuous deviations[49]. Jumping back to the bottom center of the diagram in Figure 2.17, this

[47] While the gyroscopic effect and roll moment arising from the characteristic BST-generated steering impulse at the beginning of braking is a key contributor to the main effect, the base load of quasi-stationary gyroscopic reactions on the steering while cornering belongs to the secondary effects.

[48] This was equally observed during orienting driving tests with different riders on non-instrumented motorcycles as well as during the main driving tests presented in chapters 5.3 and following, i.e. 5.4.2.

[49] See Weidele (1994): Bremsverhalten von Motorrädern, Chapter 3.7, p. 61 ff, and Chapter 5.3.6, p. 151 ff. See also the example measurement for standard chassis in chapter 5.2.2 of this thesis.

mismatch of the curve and increased cornering radius mark the end of the chain of effects with a high likeliness to produce a hazardous situation.

Concerning the inverse effect, another aspect comes into play, when the rider is releasing the brakes during a corner braking maneuver. While a certain amount of steering effort is already applied to compensate the BST, the reduction of brake effort also reduces the steering torque demand. In case the rider's effort is not in the same way reduced right away, it is surpassing the demand, generating an outward steering impulse that increases the roll angle. In contrast to the stand-up tendency when applying the brakes, when releasing them it feels, as if the motorcycle is "falling into the curve" by itself. On one hand, this can consciously be used as a riding technique, but on the other just as much care as for the application needs to be taken not to release the brakes too quickly. In extreme cases, the generated steering impulse and downward roll motion can lead to an accident by exceeding the roll angle limits of the vehicle.

2.2.5 The Role of the Rider as a Controller[50]

As illustrated by the dashed arrow-lines in Figure 2.17, the rider is an integral part of a closed loop control while riding, an intricately interwoven "component" of the man-machine system. Typically, most of his actions are controlled by highly automated (or routinized) action programs without having to pay much conscious attention[51]. Therefore, when intentionally braking into a turn as observed in racing, balancing the steering torque demand and thus the BST effect are not an issue at all.

However, situations with a heightened experience of risk can disrupt this process of effortless riding and bring the challenging sensory-motor control task to more conscious attention. This is especially critical, when fear comes into play, which is often the case in sudden, surprising (i.e. unexpected) events with the subjective threat of potential danger[52]. The triggering event can be almost anything. For a BST relevant example, it might for instance be entering into a right turn that suddenly appears narrower than expected; too narrow for the current speed. While the standard action plan to master the situation would just be to increase the roll angle (cf. chapter 2.3.2), in the moment of fright, the rider does not dare to do so, but rather applies the brakes as a first startle reaction. The subsequent BST effect with its characteristic stand-up tendency and decrease in path curvature may in itself be experienced as another sudden and unexpected event by the rider, ever increasing the pressure of the situation and subjective threat.

---

[50] This text section and the specific termini used therein are based on various passages from Spiegel (2010): The Upper Half of the Motorcycle.

[51] Spiegel (2010): The Upper Half of the Motorcycle, pp. 28ff, 40ff, 54ff, 71ff, 84ff, 106ff, and p. 134

[52] Spiegel (2010): The Upper Half of the Motorcycle, (a) pp. 53ff, 81-83, and (b) pp. 134-136

Hence, also the disruption is amplified, allowing other errors to creep in, such as focusing the view on the potential place of lane departure or collision, rather than on the intended cornering line. Unfortunately, the channel capacity of the conscious interventions required to save the situation is limited[52a] and often on the edge of being too slow. For instance, it might take the rider in the example until he has already crossed over to the opposing lane until he has finally figured out how to resolve the situation, e.g. by overriding the elevated steering torque demand with a decisive steering impulse and/or releasing the brakes to a certain extend and making use of the inverse effect.

The example illustrates very well, how it is not the triggering event or the riding task in itself, but rather a whole cascade of errors, ignited by fear, that finally leads to an accident[52b]. Extreme cases of fear can lead to a total blockade, an abrupt and complete disconnection from all control circuits and total disintegration from the man-machine system. Degraded from an integral "component" to passive "cargo", the tensed-up rider becomes a paralyzed and uninvolved spectator of the further course of actions[52b]; very likely his own upcoming accident. Despite the fact, that some improvements are possible through training the rider (see chapter 2.3.2), the presented psychological background underlines the motivation for research on potential technical assistance.

2.3 State of the Art of BST-Countermeasures

In this chapter, the presented description of the BST chain of effects is utilized to identify potential BST countermeasures along the chain as well as to integrate related state of the art motorcycle technology and research. Tracing the numbers (1 – 9) through the diagram, nine groups of countermeasures as described by the following sub-headlines have been identified. Please note that although tire characteristics influence the BST effect and stand-up tendency in various ways[53], they represent a complex research field of their own[54] and therefore can only be briefly addressed in context of the different groups.

[53] I.e. changing from the original 2010 Bridgestone tires (BT015) to the 2012 successor (S20) on the test motorcycle brought a significant improvement of the stand-up tendency.

[54] Among others, refer to Pacejka (2012): Tire and Vehicle Dynamics, and Cossalter (2006): Motorcycle Dynamics, for further reading.

2.3.1 Avoiding BST-Critical Situations

Road Infrastructure[55]

The general aim of modern road design is to create "self explaining roads", meaning that their perceived appearance intuitively leads motorists to choose an appropriate speed profile and safe driving behavior when following their course[56].

However, such ideal conditions are rarely given on older existing roads in rural areas. An elevated accident risk is especially given, when poor visibility conditions (e.g. due to dim light, shadows, impaired sight lines, etc.) go along with driving dynamic constraints (i.e. friction potential, lateral inclination and road curvature) that require a significant reduction in speed which is not directly apparent to the road user[57].

Concerning motorcyclists, disadvantageous series of curve radii (narrow-wide-narrow), narrowing radius turns, and abrupt transitions to curves after long straights as illustrated in Table 2.1 are typical accident black-spots[58,57], fostering the occurrence of the BST effect (see chapters 1.1 and 2.2) through the application of brakes as a startle reaction.

Table 2.1: Examples of disadvantageous sequences of curve radii[59]

Curve sequence with strongly differing or narrowing radii	Abrupt transition / narrowing radius within a curve	Abrupt transition from a long straight into a curve
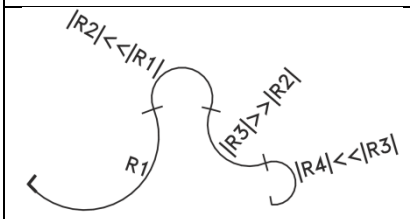	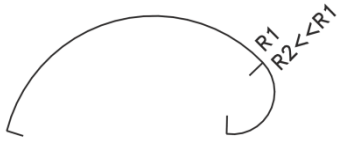	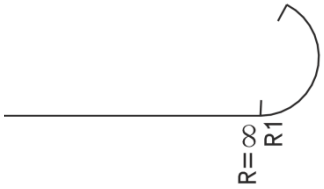

Curves with radii below 100 m[60] and opening angles greater than 30°[57,60] as well as radius ratios of $R_1 > 1.5 \cdot R_2$[57], with R_1 being the leading and R_2 the following curve

[55] Apart from the referenced literature, this section is based on an expert interview with Prof. Dr.-Ing. J. Stefan Bald, head of the Road Research Institute (German: Fachgebiet Straßenwesen) at Technische Universität Darmstadt, Germany, in October 2014.

[56] Bald et al. (2014): HAV, Chapter 2.2.4, p. 87 ff

[57] Bald et al. (2014): HAV, Chapter 6.5, p. 378 ff

[58] FGSV (2007): MVMot, Chapter 2.3, p. 9

[59] FGSV (2007): MVMot, Chapter 2.3.2, Figure 5, p. 9

[60] Ferrero (1988): Fahrverhalten u. Unfallgeschehen auf typischen Motorradstrecken, Chapter 5.4, p. 45 ff

radius, have been identified as critical, with yet rising accident risk for radii below 60 m[61] or opening angles exceeding the range of 72° to 81° (equal to 80 to 90 gon[62])[60].

Besides the geometry of a single curve or series of curves, also the global character of the road stretch they are a part of is a crucial factor in judging their criticality. For example, the same narrow curve may be more critical within a fluently stretched road over wide open flat fields than when embedded into a twisty mountain valley road. This is firstly, because in the latter environment it comes less unexpected than in the former, and secondly, because the curve speed differs much less from the general expected speed level on the twisty road than on the wider one.

Research shows that speed reductions of 5 to 10 km/h, or up to 15 km/h on minor roads, are generally unproblematic, because they are feasible for average passenger car drivers by sole use of the motor brake or only very light braking. This finding allows to derive favorable curve radii following after straights as well as maximal ratios of subsequent curve radii, as incorporated in recent German guidelines for the construction of rural roads[63] and illustrated in Figure 2.18. As apparent from the charts, the construction of roads in accordance with the guidelines will almost completely avoid the aforementioned accident black-spots with radii $R \leq 100$ m in the future.

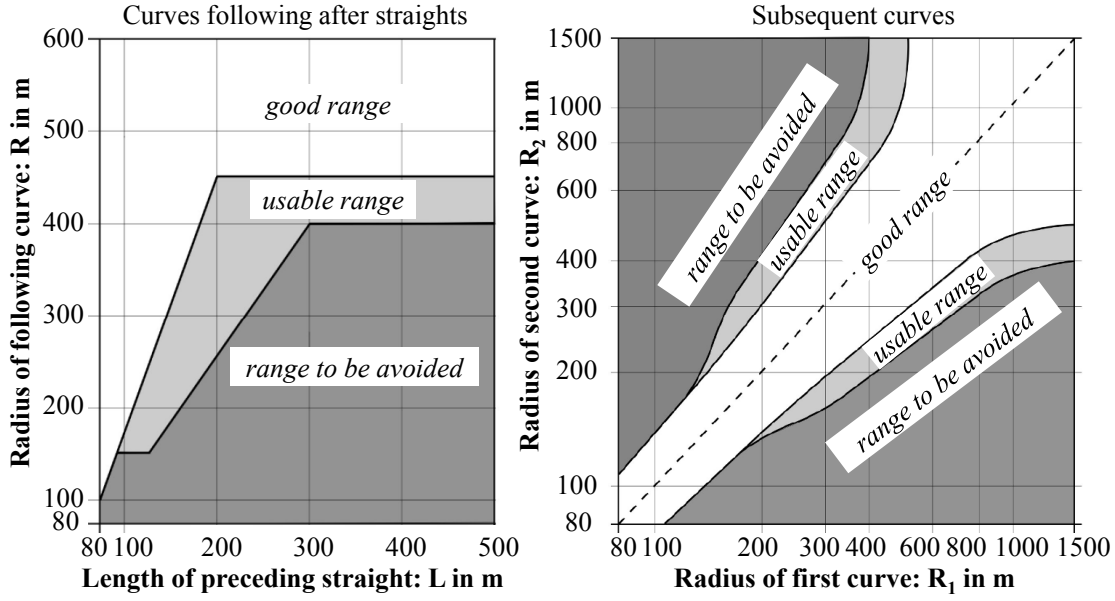

Figure 2.18: Favorable radii of curves following after straights and radius ratios of subsequent curves according to the German guidelines for the construction of rural roads RAL 2012[63]

[61] Bauer et al. (2014): Retrospective analysis of fatal motorcycle accidents, proceedings pp. 116-127

[62] In road construction the gradian is a widespread unit of measurement of an angle: 1 gon is equivalent to $^{1}/_{400}$ of a turn or $^{9}/_{10}$ of a degree. It allows easy identification of right angles as multiples of 100 gon.

[63] FGSV (2012): RAL 2012, Chapter 5, Figures 12 and 13

However, besides the existing roads, in some places, there are topographical constraints that will also force new roads to be constructed with small radii out of these specifications. Since exactly this kind of twisty roads are attracting motorcyclists, a catalogue of five further measure groups to help make them more "self explaining" is addressed in the following[56]. Their general target is to avoid brake maneuvers during cornering by preponing the required speed reduction into the approach phase.

The first measure group is aiming at manipulating the road construction in such a way, that it can be correctly understood and interpreted from a motorist's own perspective, speed and perception of previous motion. For instance, in order to naturally achieve a safe curve speed, the curve should appear a bit more challenging or narrow, than it really is. Special care needs to be taken for curves that run through a sink (that is a concave, pan shaped height profile), since this leads to an optical stretch and consequently to an increase in speed levels, while an optical compression and reduction in speed levels is attributed to curves that run over a crest (that is a convex, dome shaped height profile)[64]. Of cause, this effect can also be applied intentionally when designing and constructing a road, often supported visually by center and edge line markings.

The second measure group is to assist the perception through further optical means, e.g. by using vertical traffic guiding elements such as reflector posts and directional signs. These are especially effective to indicate

- curves with unexpectedly narrow turn radii,
- curves whose curvature is significantly changing during their course, and
- curves covering much greater opening angles than might be expected.

Table 2.2: Distance of reflector posts in curves with narrow radii[65]

	Radius in m	20	30	40	50	60	70	80
	Distance in m	3	3	4	5	6	7	8
	Radius in m	90	100	200	300	400	500	≥ 600
	Distance in m	9	10	15	20	30	40	50

While reflector posts have a typical distance of 50 m on straights and wider roads, a denser positioning is recommended as an indicator of narrower curve radii, see Table 2.2. For $R \leq 200$ m, at least five posts should always be visible on the outer road side, so that a changing post density during a curve is a good indicator of varying curvature.

[64] FGSV (2012): RAL 2012, Chapter 5, Figure 20

[65] FGSV (2007): MVMot, Chapter 4.1.2, Table 6, p. 18

The same effect, but in yet enhanced form, is created by the application of directional boards in either integrated or separated configuration as illustrated in Figure 2.19, left and center. At least two or better three boards of the separate form should always be visible and variations in distance between the elements can be utilized in analogy to the reflector posts to indicate changes in curvature.

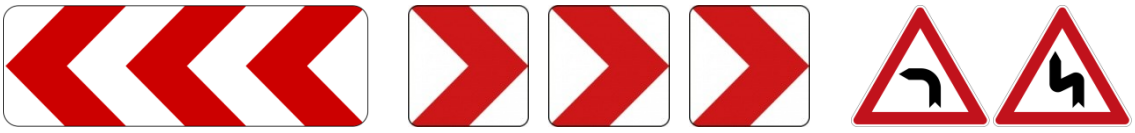

Figure 2.19: Directional boards in integrated (StVO sign no. 625) and separate configuration; Curve warning signs (StVO signs no. 103 and 105)

Even more than the prior measures, these boards use a perception psychological trick to manipulate the approach behavior by creating the impression to drive towards a virtual "super-wall". Since any human will naturally avoid to plainly run into a wall, such a signage is very effective in reducing approach speeds[66].

The third category of measures is warning of unforeseeable dangers[67], using the guidance elements as just described accompanied by curve warning signs for single or multiple sharp turns, see last two illustrations in Figure 2.19. In extreme cases, special measures such as rumble strips across the road can additionally be implemented.

The fourth category is forming action recommendations by combining warning signs with speed recommendations and the fifth category is making use of action instructions and interdictions. The most common ones are – sometimes also motorcycle selective – overtaking bans and speed limits. As a best practice, the latter are typically set to a speed not surpassed by 85% of the uninfluenced passenger car drivers in wet conditions[68]. In last consequence, usage of roads with intolerably high accident rates may be completely prohibited for motorcyclists, favorably during high times of leisure traffic such as during weekends and holidays.

Generally, means of the earlier categories are to be preferred over the latter stages, because the earlier ones are processed in a rather "automated" way (e.g. by making use of subconscious feelings like driving towards a wall), while the later ones require more conscious processing and are therefore less effective.

Moreover, attention needs to be paid, not to overdo the measures. I.e. if a curve is designed to appear much narrower than it really is or a speed limit is set far below what seems reasonable to the motorists, they will naturally disregard the measure.

---

[66] Bald et al. (2014): HAV, Chapter 2.2.5, p 89 ff; Chapter 6.5.3, p. 380

[67] Bald et al. (2014): HAV, Chapter 6.5.4, p. 381

[68] Bald et al. (2014): HAV, Chapter 6.5.5, p. 382

Besides the driving accidents directly addressed by the mentioned measures through pre-adaptation of speed, motorcyclists are also prone to head-on collisions in curves[69]. Other than might be expected before the background of the BST effect, this is not limited to leaving the own lane in right turns, but also very common in left turns[70]. Especially on roads with little expectancy of oncoming traffic, narrow radii and poor visibility, motorcyclists have the tendency to choose a cornering line too far to the inside of the road[71]. Given a decent roll angle, especially their heads and upper bodies may reach out into the opposing lane, even when the tire contact patches are remaining on the own. In addition, the outer contour of heavy oncoming traffic such as busses or trucks is likely to overlap with the motorcyclist's lane, as illustrated in Figure 2.20, left.

Figure 2.20: Photomontage of a motorcycle with oncoming bus and elliptic floor markings in two different left turns[72]

Swerving around the oncoming vehicle and subsequently staying on track requires conscious involvement in a challenging sequence of quick and well coordinated actions, first decreasing roll angle and curvature and then increasing both again.

As this is a prime example for an unexpected hazardous situation that is likely to overburden the rider's limited conscious processing capabilities and lead to an error or even a whole cascade of errors[73], a short digression to the driving dynamics and involvement of BST effect lies at hand. If braking is involved right from the beginning of the evasive action, the stand-up created through the BST effect can be helping in the first part of the maneuver, as long as especially the front wheel is not over-braked and stability is maintained. However, in a startle reaction, riders tend to hold firmly onto the brakes instead

[69] FGSV (2007): MVMot, Chapter 2.3.1, p. 9

[70] The argumentation is based on right-hand traffic, but holds similarly true for left-hand traffic, if left- and right-hand curves are interchanged.

[71] Spiegel (2010): The Upper Half of the Motorcycle, Part 1, p. 21, and discussions on the so-called "risk-composite", pp. 73, 116, 171

[72] Winkelbauer (2014): Riding Left Hand Corners, proceedings pp. 44-61

[73] Spiegel (2010): The Upper Half of the Motorcycle, p. 134

of releasing them again. Hence, the BST is also elevating the steering torque demand for the later required increase in roll angle and curvature, making this second maneuver even more difficult (cf. chapters 1.1 and 1.2).

If the first evasive action is straightening up the vehicle through a dedicated inward steering impulse, two options for the second maneuver are likely. Either, the rider is directly starting to brake in a startle reaction and heading towards the outer edge of the lane due to the BST effect, or the rider manages to counter-steer and increase the roll angle again significantly, which is often achieved by using "lean out" riding style. In case this was not sufficient to manage the situation, e.g. when the mental roll angle limit is reached[74], braking may be a startle reaction with even worsened BST effect as will be illustrated in chapters 3.2 and 3.6.

From a road infrastructure point of view, the classical approach to keep motorists away from oncoming traffic is the application of solid center line markings, banning overtaking and corner-cutting that includes the opposing lane. These are typically required for turn radii $R \leq 180$ m and compulsory for narrow turns with $R \leq 80$ m and should ideally commence 50 m before the curve or earlier. If the road width allows, the separation effect of solid center line markings can be amplified by using double solid center lines with a lateral distance of 0.5 m[75]. However, since this is typically not possible on narrow and twisty mountain roads, an advanced approach has recently been investigated and effectively field-tested in Austria[72].

The proposed solution to keep the motorcyclists in a safe zone on a wider line within their own lane is the application of additional road markings next to the centerline. It makes use of the psychological trick that motorcyclists avoid riding over road markings because they are considered as slippery. Therefore, the markings proved to work stunningly well for all three tested configurations, with either a v-shaped arrangement of straight strips, lots of dots, or an elliptic design, as shown in Figure 2.20, right.

While all road measures described in this section are aiming at avoiding critical situations or even accidents, guidelines and recommendations for road constructions also address numerous measures to mitigate the severity of injury in case of a crash[76]. Concerning motorcyclists, typical measures are targeted at avoiding collisions with hard objects such as signposts, trees, walls, etc. in direct environment of the road and potential trajectory of a fallen rider or to mitigate these – if unavoidable – e.g. by use of styrofoam-shells on guard rail posts or even double guard rails (see Figure 2.20, left).

---

[74] Spiegel (2010): The Upper Half of the Motorcycle, Part 1, pp. 34-36, Part 4, pp. 112-116, and 133-136

[75] FGSV (2007): MVMot, Chapter 4.1.1, table 5, p. 17

[76] Detailed information can be found in FGSV (2007): MVMot, and DEKRA (2010): Verkehrssicherheitsreport Motorrad, pp. 51-57.

Assisted Anticipation

Besides training the rider, different means can assist anticipatory driving and adaptation of speed before the potentially BST critical curve. The simplest way is a well-prepared road book like in rallye sports or a good GPS device with detailed moving maps. Both already allow estimation of oncoming turn radii and thus pre-adaptation of speed. The research project "Powered Two Wheeler Integrated Safety" (PISa)[77] on Advanced Rider Assistance Systems (ARAS) and On Bord Information Systems (OBIS) went a step further. Besides providing speed alerts based on map data when exceeding legal limits, also a curve warning function was developed, that derives a risk potential from the predicted own speed profile and upcoming curve in order to generate a warning and give a speed recommendation. Among others, these functionalities are supposed to be complimented by traffic and black-spot warnings, leading to the next level of assistance offered by Bike2X vehicular communication, which allows to warn the rider still earlier[78]. However, since all these systems generate additional information to be processed by the rider with his limited channel capacity, they all bear the potential risk to distract the rider from his primary riding task, making the situation more dangerous or even creating dangerous situations by themselves. Hence, the development of appropriate Human Machine Interfaces (HMI) is of utmost importance and subject of current research and scientific discussion[77,78,79].

Environment Perception and Predictive Braking

Finally, there are also technologies under development that are based on environment perception. Functions like Predictive Brake Assist (PBA, meaning either an automatic pre-fill of brakes, from no up to medium decelerations, plus brake boosting when the rider confirms the automatic action by applying the brakes) and even Autonomous Emergency Braking (AEB) are currently being investigated for motorcycles[80]. These offer a high theoretical potential of accident prevention or at least reduction in crash speeds and injury level, but are however not directly addressed to curve braking accidents. In contrast to passenger cars, where the occupants are typically more or less fixed by safety belts which even allow further tightening in critical situations, the rather loose coupling and interaction between rider and motorcycle is the most challenging task yet

[77] PISa – virtual: www.pisa-project.eu, last access: 2014-11-20

[78] Lattke (2012): Ein kommunikationsbasiertes Gefahrstellenwarnsystem für Motorräder

[79] Guth (2014): Absicherung von Anzeige-Bedien-Konzepten, proceedings pp. 440-459

[80] Among others, refer to: DEKRA (2010): Verkehrssicherheitsreport Motorrad, pp. 41-45, Roll et al. (2010): Safety benefits of electronic brake-control systems, proceedings pp. 423-513, and SafeRider – virtual: www.saferider-eu.org, last access: 2014-11-20.

to be solved for such measures[81]. However, especially in case an AEB is triggered while riding through a curve, such predictive measures might even create BST critical situations themselves, making the development of BST countermeasures even more interesting for the future.

2.3.2 Training the Rider

The integral role of the rider was already addressed briefly in chapter 2.2. Apart from aiming to avoid potentially dangerous situations through training in anticipatory driving with a good guidance of view and advance trajectory planning, Spiegel[82] also proposes a method to deal with startle reactions involving fear. According to him, as already mentioned, an event needs to fulfill three criteria to trigger them. At the same time, it needs to be sudden, surprising (i.e. unexpected), and have a threat of potential danger. While the suddenness cannot be influenced, the other two aspects can – to a certain degree – be mitigated through education and training, both practical and mental.

Firstly, teaching the rider about the driving dynamic backgrounds and chain of effects in conjunction with the psychological aspects is essential to understand, that the situation can actually be mastered. As a prime example, it is for instance important to know about the existence of a natural mental roll angle limit of typically 20° that occurs for running on natural surfaces, which is not exceeded by riders in many accident scenarios despite the fact that the traction potential of modern motorcycle tires by far allows to do so[83,84].

Secondly, before this background, the requirement of regular training becomes evident, addressing both riding at large roll angles and curve braking maneuvers alike. Practical training under controlled conditions (in best case with ABS and a professional instructor) helps to familiarize with driving dynamics and vehicle reactions. Thus, suddenly required increases in roll angle or curve braking maneuvers are losing a great deal of their surprising as well as threatening components and appropriate reaction patterns can be acquired. Experience shows, that in most cases an increase in roll angle is absolutely sufficient and braking is not even necessary to master the situation[84].

---

[81] Note that there are a few examples of special powered two wheelers, such as cabin motorcycles or the BMW C1 scooter, that feature a safety cell and seatbelts like a car. E.g., see Kompass et al. (1998): The Safety Concept of BMW C1, proceedings pp. 223-241. – Seatbelts for "ordinary" motorcycles are primarily investigated as safety measures to mitigate crash injuries. Among others, see Murri et al. (2008): Sicherheitsgurt für Motorradfahrer, proceedings pp. 418-429, and Unger (2010): Sicherheitskonzept, proceedings pp. 2-48.

[82] Spiegel (2010): The Upper Half of the Motorcycle, Part 4, p. 134 ff

[83] Spiegel (2010): The Upper Half of the Motorcycle, Part 1, pp. 34-36, Part 4, pp. 112-116, and 133-136

[84] Bauer et al. (2014): Retrospective analysis of fatal motorcycle accidents, proceedings pp. 116-127

Practically, the rider in the example case presented in Figure 1.2 could have stayed on his own lane by increasing the roll angle through application of an outward steering impulse in three moments. Either as a first reaction even before applying the brakes, while applying the brakes and overriding the BST, or by making use of the "inverse effect" through release of the brakes as described in chapter 2.2. Thirdly, mental training can be used to think through and prepare reaction patterns even for worst case crash scenarios that cannot be physically exercised. For further information on this interesting field and useful tips for daily training, please refer to Spiegel[85].

2.3.3 Influencing the Brake Force

During cornering, the ideal Brake Force Distribution (BFD) becomes more rear wheel oriented (cf. chapter 2.1.7). While the rear brake force does not contribute much to the BST effect, the disturbance is mainly generated from the product of front brake force and lever arm[86]. Concerning an emergency-brake maneuver that requires deceleration at the physical limits, reducing the front brake force in order to mitigate the BST will also compromise the achievable braking distance (cf. chapter 3.6). However, the analysis of typical situations reveals that besides steep brake actuation gradients mostly only partial decelerations far below the ABS activation threshold are applied. E.g. the rider showcased in Figure 1.2 only had a single finger on the brake lever! Therefore, a brake system could assist the rider in BST relevant situations by unloading the front wheel from brake effort, both in terms of gradients and absolute level. With the BST chain of effects in mind, the following strategy – from initial brake application to full ABS controlled deceleration – lies at hand:

- After activation of either brake, first build up brake pressure in the rear, where also steep gradients are not an issue in terms of stability and BST.
- Continue to operate with rear wheel oriented BFD, i.e. a higher exploitation of friction potential at the rear wheel compared to the front wheel $\mu_{used,rr} > \mu_{used,ft}$[87], especially for partial decelerations.

---

[85] Spiegel (2010): The Upper Half of the Motorcycle

[86] Cf. chapter 3 and Weidele (1994): Bremsverhalten von Motorrädern, Chapter 3.7, p. 61ff, i.e. eq. 69

[87] This strategy has already been suggested by Weidele (1994): Bremsverhalten von Motorrädern, Chapter 6, pp. 167-176.

- Let the brake force on the front wheel be built up with a gradient limited to an acceptable level[88]. Depending on the brake force demand of the rider, also a time delay may be incorporated, as long as the front brake application is early enough to avoid destabilizing slides through ABS activation on the rear wheel.
- Finally, for high decelerations, a smooth ABS control is required to diminish BST fluctuations and thus improve course stability and controllability. Since the traction limits set by modern tires[89] even allow a brake flip-over at large roll angles, a Rear wheel Lift-off Protection (RLP) respectively mitigation function should also be incorporated in the ABS control[90], meaning a release of front brake pressure when a lift-off tendency of the rear wheel is detected.

While the ABS functionality is the essential basis for a fully cornering approved brake system (cf. chapter 2.1.8), the complete realization of this strategy ideally requires:

- Assessment of the rider's brake demand.
- Active brake force generation, at least at the rear wheel.
- Rear wheel lift-off mitigation.
- Assessment of the cornering state (i.e. the roll angle).

Apart from this, it is worth noting, that already a hydro-mechanical combined brake system (CBS) like the Honda Dual-CBS[91] is a benefit with regards to the BST effect. Linking the rear brake also to the front brake lever unloads the front wheel from brake effort and, in case a delay valve is featured, also the rear brake lever activated rise in front brake effort is eased.

However, in the following it shall exemplarily be illustrated, in how far two of the most recent brake systems available on the market address the defined requirements.

---

[88] Roll (2010): Safety benefits of electronic brake-control systems, proceedings pp. 423-513, i.e. p. 463, Figure 25

[89] Weidele / Schmieder (1990): Power transfer between motorcycle tyres and real road surfaces

[90] Depending on the brake system manufacturer, this functionality is given different names. The most frequently encountered are Rear wheel Lift-off Protection (RLP, Continental), and rear wheel lift-up mitigation (Bosch). Also combined forms like rear wheel lift-off mitigation are widespread, while Honda speaks of pitching control for their C-ABS system. From a physical point of view, none of the systems can guarantee to protect the rear wheel from lifting from road contact under any circumstance, and all of them are rather mitigation functions. However, in this study all terminologies are used as suited to the context of the addressed systems, while RLP is generally used as the abbreviated form.

[91] Nishimoto et al. (1991): Research on Combined Brake System, proceedings pp. 327-345

Honda C-ABS Brake-by-Wire

Super-sport motorcycles typically feature a short wheelbase and relatively high center of gravity. Under strong braking, they are therefore prone to large pitching motion and flip-over tendency. Introduced in 2009, Honda's electronically controlled Combined-ABS (C-ABS) in Brake-by-Wire architecture was the first in this vehicle category to address this issue[92].

Driving experiments revealed a correlation and time lag between brake inputs and resulting pitch effect. Moreover, it was found, that when the slip ratio at the front wheel was increasing during that narrow time window, the undesired pitching did not occur. Creating such a configuration on purpose was not possible with conventional brake systems and therefore the Brake-by-Wire architecture was chosen. The occurrence of pitching is forecasted from the rate of pressure increase, and a reaction is triggered in two steps: Firstly, a very quick increase in front brake pressure reduces the brake force in the tire contact patch through increasing slip. Secondly, this triggers a subsequent pressure reduction through activation of ABS functionality, which is achieved earlier than for contemporary conventional ABS / RLP configurations.

The used hardware setup is as follows and for packaging reasons subdivided into five components: The Electronic Control Unit (ECU) as well as a valve and power unit for each brake circuit. While the valve units contain switching valves, the so-called "stroke-simulators" and pressure sensors, the power units are electrically driven master cylinders. Under operation, the hydraulic connection between the rider's master cylinders and calipers is disconnected by switching valves, while the brake demand is measured by pressure sensors and ordinary lever feel is generated by the stroke-simulators. Finally, output pressure is generated by the power units and monitored by further pressure sensors, while ABS functionality is triggered by wheel speed sensors.

The by-wire architecture allows the implementation of arbitrary brake force distributions (BFD) and combined functions upon activation of either brake lever[93]. The rear brake is always actuated in advance. Front braking leads to a front wheel oriented BFD with a typically rather low and constant contribution from the rear wheel, while strong rear braking also activates the front brake a great deal, yet with reasonable gradients (see also chapter 3.6.6). Moreover, in contrast to conventional CBS, the BFD during brake actuation can be different from that during brake release.

---

[92] Nishikawa et al. (2008): Pitching Control using Brake-by-Wire, proceedings pp. 430-446

[93] To a certain degree, the meanwhile discontinued first generation BMW Integral-ABS with integrated electric brake booster would also have offered this option from a hardware point of view. Among others, see: Stoffregen (2010): Motorradtechnik, Chapter 11, pp. 384-386.

Compared with the previously defined requirements and strategy for BST optimized corner braking, the C-ABS is only lacking the integration of roll angle information to allow further adaptations to the cornering state. Despite this theoretical limitation, its corner braking performance with easy controllability up to high decelerations was well approved both in racing[94] and the test drives in context of this study (cf. chapter 5).

Bosch Motorcycle Stability Control (MSC)

Following the series introduction of a roll angle sensor for traction control systems in 2009[95], the use of this sensor information for a cornering approved brake system was just a question of time. In 2013, Bosch presented their Motorcycle Stability Control (MSC) together with KTM[96]. The system is based on the enhanced version of Bosch's ABS 9 generation of motorcycle brake systems (ABS 9 ME[97]), that follows the standard layout with valves and pump known from the Electronic Stability Control (ESC) hydro units of passenger cars, but is just much smaller. In the debut version of MSC, active pressure generation is only implemented for the rear and a sensor cluster is used that measures two turn rates and accelerations in all three dimensions of space. Through an inclined mounting position in the vehicle, rotated by 45° around the pitch axis, one gyroscope is measuring the pitch-rate and the other a combination of roll- and yaw-rate. This arrangement allows to compute information for all six degrees of motion, especially roll and pitch[98], which are considered both in the adaptive BFD (called eCBS) and ABS control. Moreover, as an alternative approach to the Honda C-ABS, pitch rate and deceleration signal can be used to improve rear wheel lift-up mitigation.

Even though only very few details about the control strategy of MSC have so far been published[99], it fulfills all previously defined requirements for BST optimized corner braking. First tests by motorcycle journalists[100,101] revealed a significant reduction in stand-up tendency and in general, that MSC operates smoother than the standard system under cornering in order to avoid everything that might disturb stability close to the physical limits.

---

[94] Tani et al. (2010): Brake-by-Wire System for Race Motorcycle, proceedings pp. 378-395

[95] Landerl et al. (2010): Enhanced rider assistance, proceedings pp. 362-377

[96] BOSCH (2013): Bosch motorcycle stability control, Bosch Press-Release PI 8314 CC

[97] BOSCH (2011): New Bosch ABS for all motorcycle types, Press-Release PI 7438 CC

[98] Willig et al. (2012): New Inertial Sensor Unit for Dynamic Stabilizing Systems, proceedings pp. 66-84

[99] Matschl et al. (2014): Motorcycle Stability Control, proceedings pp. 128-154

[100] Bergmann (2013): Kurvenwunder. In: Motorrad News 11/2013, pp. 10-11

[101] Schneider (2013): Vollbremsung in Schräglage. In: Motorrad 23/2013, pp. 52-55

Comparing tests between the same vehicle with and without MSC showed that experienced riders under controlled conditions and high friction road surface can achieve the same corner braking performance without the assistance of MSC. Moreover, it was found that the control quality of the standard Bosch ABS (or equally sensitive contemporary systems) already allows safe full lever braking for roll angles up to 35° on roads with "normal" friction coefficient[102].

However, this just holds true when the maneuver is done intentionally. Before the background of the BST chain of effects involving startle reactions and confusion of the rider, it is well to be expected, that the improved functionality of MSC will be a great help in a real world BST critical situation.

Furthermore, as the name MSC already suggests, it is much more than just a cornering sensitive brake system. Including the engine management, it also features advanced Motorcycle Traction Control (MTC), allowing add-on functions like launch- or wheelie control. In the sense of a scalable system architecture, it is further already prepared to include additional control systems, such as semi-active suspensions[103].

Finally, the inertial measurement of MSC theoretically also offers the possibility to manipulate roll and yaw motion of the vehicle in terms of controlled drifting by strong over-braking of the rear wheel, which could be applicable at the end of the BST chain of effects. However, such a measure brings along all insecurities of rider coupling, motion, and not least acceptance that were already addressed in context of predictive and autonomous brake systems in chapter 2.3.1.

More details on state of the art of motorcycle brake systems and technology can be found in literature[104]. Just for completeness, also the dynamic tire characteristics under transient combined slip[105] conditions have an influence, but are not further addressed.

2.3.4 Influencing the Lever Arm(s)

Technical measures in this category mainly aim at reducing the effective lever arm between tire contact patch and steering axis in order to tackle the BST generation. As

[102] Schneider (2014): Schrecklage und Schrägbremsen. In: Motorrad 04/2014, pp. 38-41, where the level of "normal" friction coefficient is not further specified.

[103] Yildirim et al. (2013): Modern Brake Control Systems and Sensor Systems for PTW

[104] E.g. refer to the respective last updates of Winner et al. (ed., 2016): Handbook of Driver Assistance Systems, or in German: Winner et al. (ed., 2015): Handbuch Fahrerassistenzsysteme, as well as Breuer / Bill (ed., 2012): Bremsenhandbuch, and Stoffregen (2010 ff): Motorradtechnik.

[105] cf. Weidele (1994): Bremsverhalten von Motorrädern, and Pacejka (2012): Tire and Vehicle Dynamics

shown in chapter 3, this may also influence the transmission ratio of other steering torque components and special care needs to be taken to keep them in desired balance.

Handlebar Width

As an exception from the description in the general introduction, a very simple measure is to improve the rider's capability to counterbalance the BST by increasing the handlebar width, leading to reduced handlebar forces for a given steering torque demand. However, for any vehicle type, there are engineering, ergonomic, and styling constraints on the handlebar design and width, so that other solutions need to be found.

Tire Variations

The simplest way to reduce the roll angle dependent tire scrub radius seems to be the reduction of tire width, possibly accompanied by adaptations in contour or even flexibility, aiming to reduce lateral deformations when cornering. However, in many cases this is not an option for production motorcycles, because the tire characteristics are subject to engineering constraints in terms of force transfer, handling, stability, and wear characteristics. Finally, even if a slimmer tire might suffice from engineering side, it might not be acceptable for styling reasons.

Brake Steer Torque Avoidance Mechanism (BSTAM)

The BSTAM concept as introduced by Weidele[106] for use with conventional front fork suspensions has already been briefly described (cf. chapter 1.1) and will be regarded in more detail throughout this thesis (i.e. chapters 3 and 4). From a mechanical point of view, the deflection of the kinematic steering axis by means of the double excentric adjustment of the upper steering bearing (see Figure 2.21, right) has several benefits.

Firstly, at zero steering angle the fork is exactly remaining in design position for all excenter positions. Even in case of steering angle overlay, only small movements of the fork assembly occur and the actuation power is mainly provided by the rider's steering input, rather than from the actuator. Secondly, since the kinematic steering axis is just the massless connection line of the kinematic centers of the two steering head bearings, a low power actuator (in the order of those in a portable electric drill) is sufficient to overcome friction and inertia of the moving parts. Thirdly, the use of planetary gear sets as differential gear eliminates steering disturbances through actuation (cf. Figure 4.7 and Figure A.1).

---

[106] cf. Weidele (1990): Compensated Steering for Motorcycle. Patent Application DE3933058A1, and Weidele (1994): Bremsverhalten von Motorrädern, Chapters 6.4, 7, and 8, pp. 173-182

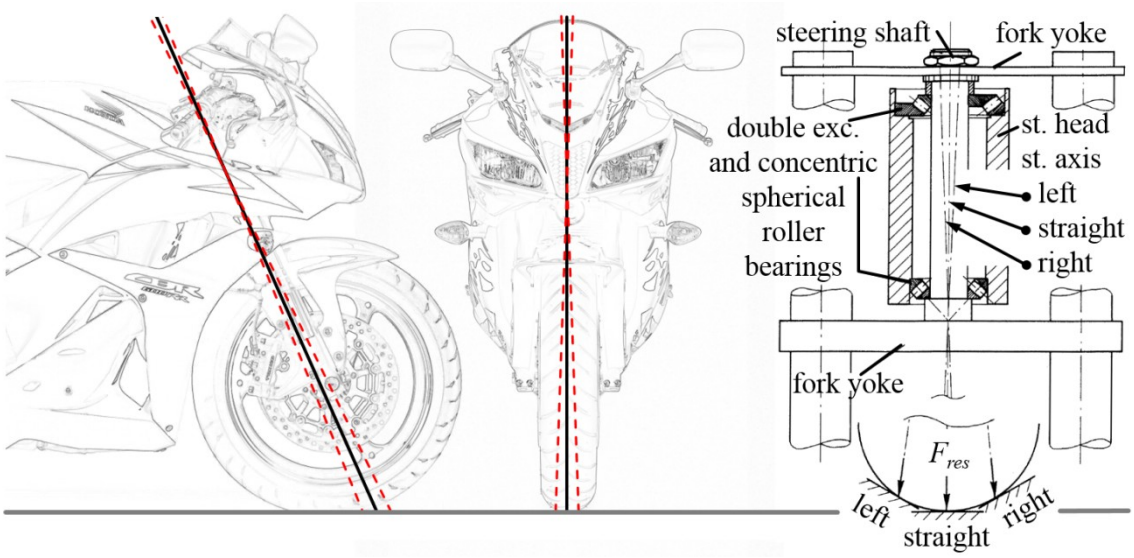

Figure 2.21: Weidele's original BSTAM design with double excentric adjustment of the upper steering head bearing and corresponding manipulation of steering axis orientation as realized in the prototype motorcycle [Motorcycle pictures © Honda, principle sketch © Weidele[106]]

It is worth noting, that this description holds fully true only for front suspension systems with a conventional steering head that allows the use of small excentricity and steering axis inclination angles. The larger the chosen excentricity and inclination, the bigger will the deviations in fork (or generally steering system) orientation be for steering angles significantly different from zero.

Finally, if BSTAM is not directly considered during the frame design of a vehicle but retrofitted to an existing one as done for the prototype motorcycle, the caster angle and trail in straight running will either be increased or decreased (see Figure 2.21, left), while both will come closer to the design values again for growing excenter angles. While the setup with small caster angle and short trail provides a more direct steering (cf. chapter 2.1.5, eq. (2.19)) and easier handling at the cost of decreased stability (cf. chapter 2.1.6), the opposite holds true for the long trail setup with increased caster angle, that was utilized for the driving tests in the presented study (cf. chapter 5).

Fork Inclination

In contrast to the BSTAM with its double excentric layout of the upper steering head bearing, another invention aimed at "stabilizing the vehicle in a critical driving situation" features ball joints in a conventional steering head that allow single excentric adjustment of the upper bearing center relative to the fork yoke, see Figure 2.22.

In contrast to the BSTAM, the steering axis remains in the symmetry plane of the vehicle's main body and the whole steering assembly (i.e. the front fork and wheel) needs to be moved, in order to compensate the scrub radius. This does not only require a much more powerful actuator than the BSTAM, but also cause larger chassis geometry varia-

tions for a given excentricity. Since the illustrated layout suggests, that the rider will need to deal with disturbing actuator back torque superimposed on the steering torque, the BSTAM concept is regarded as superior in all these aspects.

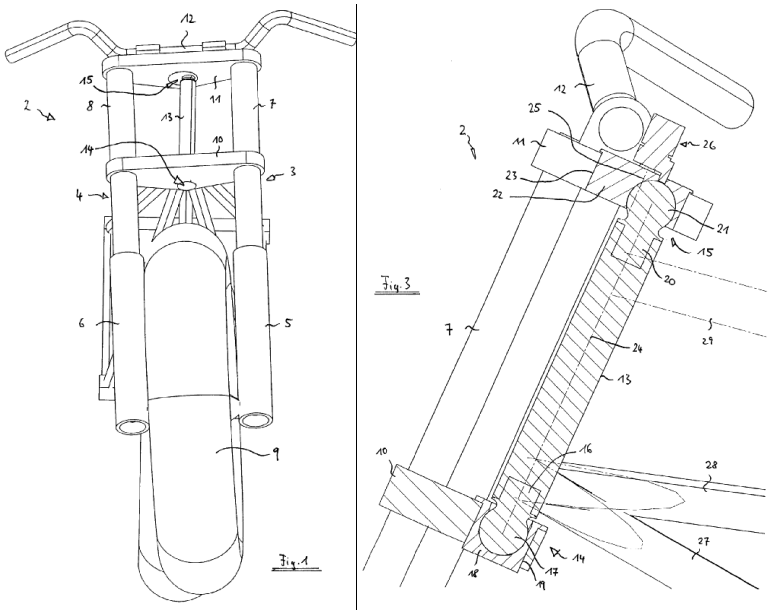

Figure 2.22: Fork inclination through single excentric upper steering bearing[107]

Multi-Lever Steering

While the use of multiple joint suspension / steering systems is widespread in the passenger car sector, it is quite uncommon in the PTW world. For given steering and suspension deflections it offers huge degrees of freedom in designing virtual steering axes, allowing to control various chassis properties – like tire contact patch position, trail, king-pin offset and inclination, camber and bump steer, and others.

In order to be helpful against the BST effect, the kinematic steering axis would need to wander further towards the inside of the curve with increasing roll angle. However, the lateral steering axis deflection of multi-lever steering primarily depends on the steering angle. Now, steering angles on PTW are usually rather small (in the order of 1° or 2°) for typical cornering situations (cf. chapter 2.1.5). In some cases, they can even be slightly negative[108], while braking in cornering conditions typically requires small increases to generate additional side slip angle at the front wheel.

[107] Seidl (2007): Motorrad. Patent Application DE102006024326A1

[108] This is the case, when the tires are generating excess camber lateral forces at a given equilibrium roll angle and the side force is reduced to the equilibrium requirements by application of a negative side-slip angle, i.e. outward steering.

The kinematic layout of a multi-lever steering must therefore provide a sensitive compromise between the following three trade-offs:

- Supply a sufficient lateral deflection of steering axis for BST mitigation at typical steering angles (through virtual king-pin offset and / or inclination).
- Leave a safety margin for additional sideslip angles in order to avoid overcompensation, which might lead to a change of sign in steering torque demand.
- Avoid negative steering angles as far possible, because they lead to an increase of effective lever arm, worsening the BST effect.

In conclusion, such measures can only mitigate the BST effect, but they are however still attractive in terms of functional safety considerations, because their purely mechanical layout naturally does not involve safety-critical electronic control circuits.

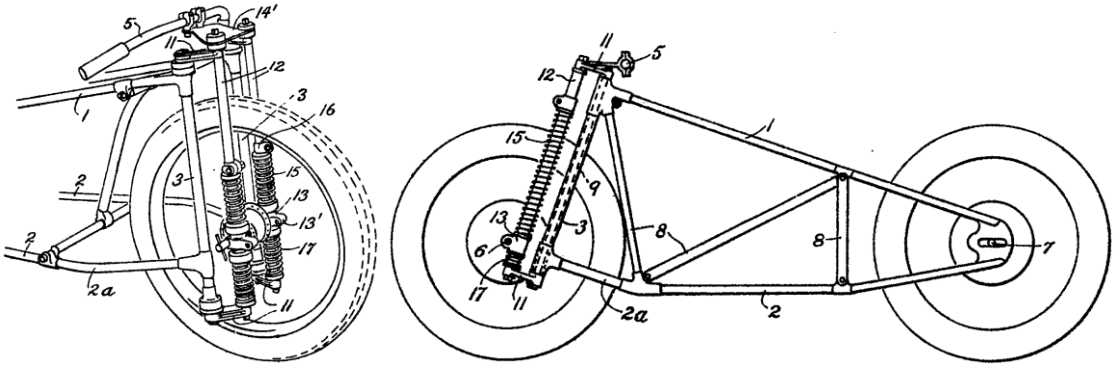

Figure 2.23: Duplex Steering of OEC[109]

Concerning the BST effect, the four-bar linkage incorporated in the first series solution by the British company OEC[109] in the 1930s was moving the steering axis to the wrong side (Figure 2.23). However, it was famous for its superior performance in side cars. Firstly, it enhances curve braking stability due to the same self-stabilizing steering effect that a negative king-pin offset promises for split-μ-braking in cars. Secondly, trail is long for good straight running stability and decreases with increasing steering angles, such lowering the steering torque demand under cornering. Lastly, it also features superior lateral stiffness compared to contemporary girder and telescopic forks.

While the aim to improve suspension stiffness and lower a motorcycle's center of gravity by banning the massive steering head lead to variations of the principle in 1973[110], the possibility to introduce camber steer was considered in a front wheel steering for a three wheeled vehicle in 1982[111]. The benefit of long trail in conjunction with compact

[109] Osborn / Wood (1930): Lenkvorrichtung. Patent Application DE494664A, Figures 5 and 1

[110] King / Pizzey (1973): Motor Bicycle Assemblies. Patent Application GB1319703A

[111] Weldy (1982): Steering and suspension system. Patent Application US4353567A

construction space makes four-bar linkages also attractive for other applications. While the "Automatic Safe Steering" of a meanwhile discontinued baby stroller led to superior maneuverability at "high speed" jogging conditions[112], a steering mechanism similar to the OEC design allows to go off-road with radio controlled motorcycle models[113].

However, concerning the BST effect, these solutions are all still featuring the wrong side setup. The kinematic inversion of the principle capable to address the BST phenomenon was finally introduced by Seidl[114] of BMW in 1990 and most recently refined by US based TIER Motorsports[115], incorporating a four-bar linkage into a hub-steering.

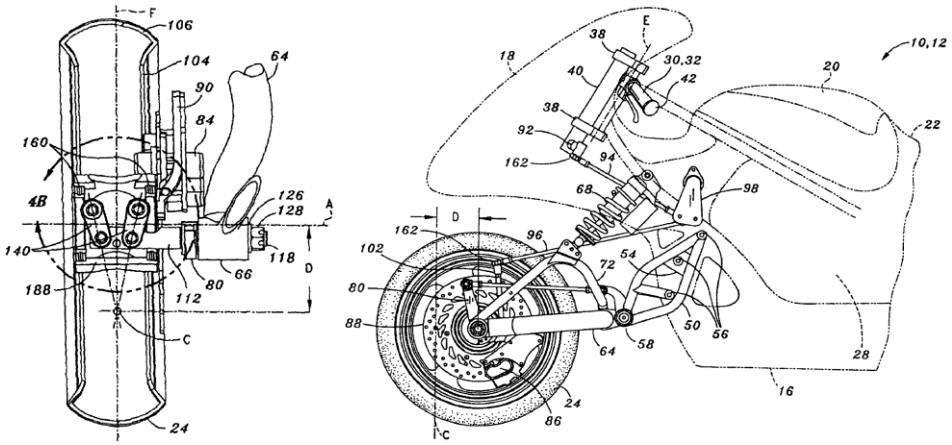

Figure 2.24: Hub-Center Steering with Four-Bar Linkage[115]

While the utilized single or double sided swing arm suspensions offer about 50% brake pitch compensation, the long trail and vertical steering axis ($\tau = 0$) promise superior off-road handling (no bump steer or moments of inversed trail). Moreover, the considerably reduced mass and inertia of steering components is claimed to eliminate wobble and the system is said to guarantee "very light and precise steering" also on the racetrack.

Since no publications on the effectiveness against BST are known to the author, this question is dealt with by simple model calculations alongside the detailed analysis of BSTAM in chapter 3.4.

---

[112] Quinny –virtual: "Automatic Safe Steering" of the "Quinny Formula 3 Synergy" jogging buggy. http://dohnal.comnex.net/jogger/quinny.htm, last access: 2014-05-06

[113] For instance "ARX 540 Cross" of AR Racing, see ARX – virtual: www.armodelling.com, last access: 2014-05-06

[114] Seidl (1990): Lenkung für ein Fahrzeugrad. Patent Application DE3914050A1

[115] TIER – virtual: www.tiermotor.com, last access: 2014-11-15, and Thiers (2011): Motorcycle Steering. Patent Application US7887077B2, Figures 4a and 2

2.3.5 Influencing Wheel Load and Chassis Geometry Changes

Typically, the geometric layout of a conventional chassis aims at keeping all steering torque components in balance for free cornering to provide a neutral steering behavior and low stationary steering torque demand[116] (cf. chapters 2.1.3 and 3). However, geometry and transmission ratios of the various components may change due to chassis movements. Apart from modulations arising from an uneven road surface, the suspensions are compressed under cornering and – depending on the chassis layout – a forward pitch motion is occurring when braking. The pitch characteristics influence both the transmission ratio of steering torque components as well as dynamic wheel load changes (cf. chapter 2.1.7) and slip conditions, especially when applying the brakes.

A standard chassis with telescopic fork features a negative brake pitch compensation ratio and is therefore prone to dynamic over-braking and great pitch movements (cf. chapter 2.1.8, Figure 2.15). For a well balanced chassis, the reduction in effective steering head angle and trail can be purposefully considered to make handling behavior more agile, e.g. when entering a turn "on the brakes", like observed in racing (cf. also chapter 3.2). However, for the said reasons of dynamic wheel load transfer it seems more desirable to keep brake pitch motion and related chassis geometry variations small.

Miscellaneous anti-dive measures became very popular in the 1970s and 1980s as add-ons to the telescopic fork. Mechanical anti-dive is typically implemented by brake calipers that can pivot around the wheel axis and deliver their reaction-torque to the lower fork yoke through pushrods and sometimes also an additional linkage for the adjustment of fork dive compensation ratio. Also hydraulic anti-dive that manipulates the fork damping through adjustable valves when the front brake is actuated was available in mainly two forms with different principles of function. The first form makes direct use of the hydraulic pressure and brake fluid volume of the front brake to adjust the fork damping valves. Since this inevitably goes along with variations in the brake pressure point and an indifferent feel on the sensible front brake, it quickly disappeared from the market again. The second form, namely the different versions of Honda's Torque Reactive Anti-dive Control (TRAC), is eliminating this downside by using indirect adjustment of the damping valves through a pivotable caliper, either with direct mechanical coupling or via a secondary hydraulic circuit. Since the floating caliper and secondary hydraulic circuit are anyway present with a Dual-CBS brake system[117], the system is still found on some of today's Honda models, such as the Gold-Wing series.

Further than that, alternative suspension systems as presented in chapter 4, Figure 4.1, allow to design a kinematic brake pitch compensation of up to 100%. In order to keep a

[116] Cossalter et al. (2010): Steering Torque Decomposition

[117] Nishimoto et al. (1991): Research on Combined Brake System, proceedings pp. 327-345

certain degree of the usual feedback about the deceleration level for the rider, only about 70% of brake pitch are compensated in practical applications.

While changing the spring pre-tension (e.g. via an electric motor) or spring stiffness (e.g. by switching a steel and elastomeric spring in a series system[118]) are too slow channels of reacting on a brake application under cornering, switching variable air volumes, using semi-active[119] or even active suspensions[120] allows to influence the sequence in time that dynamic lateral and normal forces and thus the steering torque demand are build up. While all mentioned measures can directly address the initial phase of the BST kick-in, the improvements against the elevated steering torque demand in the second "quasi-stationary" phase of braking are typically only marginal, due to usually more constant caster angle and trail during that phase (cf. chapter 3.2).

Concluding with some remarks on tires, it has to be stated, that also the different tire widths and contours in front and rear lead to small geometric pitch and yaw angles with increasing roll angle. Moreover, the tires are deflecting under load and thus changing their contact patch shape and centre, force transfer behavior as well as their reaction torques[121]. However, compared to the geometric changes generated by chassis movements, those attributed to tire influences are small and therefore neglected in this study.

2.3.6 Influencing Secondary Effects on Steering Torque

This field comprises tire reaction torques, gyroscopic torque and inertial forces on the steering system. While their transmission ratios towards the steering axis and changes therein originating from BSTAM are addressed in detail in chapter 3, tire characteristics are regarded as given and only possibilities of influencing the latter two effects remain to be discussed.

The mass and inertia properties of the front wheel are essential for dynamic stabilization and handling of the vehicle. Realizing a suspension system with good responsiveness to road irregularities and low wheel load fluctuations requires low tire sprung mass and agile longitudinal dynamics call for low spin inertia of the wheels. As a trade-off, a certain amount of inertia needs to be present for dynamic stabilization, even for a completely worn tire. In fact, the tire contributes a great deal to the front wheel's mass (39.4% in new condition) and spinning inertia (63.7%), while tire wear is reducing the

[118] I.e. BMW Electronic Suspension Adjustment (ESA) of the second generation, ESA II

[119] E.g. BMW Dynamic Damping Control (DDC) or Dynamic ESA, with continuously variable damping

[120] BOSE – virtual: www.bose.com → Automotive Technologies → Suspension System, last access: 2016-11-11

[121] Cossalter (2006): Motorcycle Dynamics, Chapter 2, Motorcycle Tires, pp. 37-72

latter quite a lot compared to a new tire (reductions greater 16% were measured for the Honda CBR 600 RR test motorcycle, cf. appendix A.4.2, Table A.6, for detailed values). Summing up, mass and inertia of the front wheel are subject to engineering constraints and typically already well optimized for a given vehicle. Therefore, this possibility of influencing the BST effect is of minor importance and not further analyzed.

Also the mass and inertia properties of a given front suspension / steering system are subject to engineering constraints concerning wobble and weave stability. However, laying aside stability concerns, inertial forces on an asymmetric mass could provide a certain counter steering torque. In order to estimate the effectiveness of such a measure, an experiment of thought is conducted. On a modern street motorcycle, the weights mounted at the ends of the handlebar to mitigate vibrations can easily have a mass of 0.5 kg or more on either side. Assuming this amount of mass to be transferrable from one side to the other (e.g. by means of a high density liquid), 1 kg of mass could asymmetrically be placed on the inner side of the handlebar, without changing the overall inertia of the steering system or the balance between the centrifugal and weight forces acting thereon (cf. chapter 2.1.3). Assuming a 0.8 m wide handle bar and a deceleration of 10 m/s² delivers 4 Nm of counter steering torque, further reduced through steering axis inclination through the caster angle by another 10%. Measured against a steering torque demand of presumably 40 Nm or more in contrast to the much larger functional potential of other means and before the background of impending negative interference with driving stability, also this idea is not further pursued.

2.3.7 Influencing the Steering Torque and Movement

Active Counter Steering

Among all possibilities to address the BST effect, providing an active counter steer torque is one of the most promising. At the same time, it offers full compensation of the BST and zero interference with the standard riding behavior. The latter is well understood for motorcycles with conventional chassis[122]. Therefore, the required prediction of steering torque demand in a given corner braking situation should easily be possible from sensor inputs such as roll angle and brake pressure (gradients) or even more available signals. Beyond improving corner braking behavior, a steering actuator could further be used to manipulate the vehicle's trajectory in terms of a combined emergency brake / swerve maneuver aimed at avoiding or mitigating a collision. However, such a powerful device also requires appropriate measures on the functional safety side, especially in terms of interaction with the rider and also legal aspects might play a role.

[122] Among others, cf. Cossalter (2006): Motorcycle Dynamics

Currently, there are no such systems on the market. However, Honda patented the following two systems, which are only implicitly addressing the BST effect, but from hardware point of view could be fully effective. Firstly, the generic Steering Conversion Mechanism[123] allows to convert arbitrary steering inputs (at the handlebars) into arbitrary steering outputs (at the fork or other front wheel system), both in terms of torque and angle. This is achieved by a power assist mechanism and a variable ratio steering mechanism, both powered by electric motors. Secondly, the Steering Assist System[124] features a hydraulic actuator that can overlay steering torques in both turn directions and at the same time be used as a hydraulic steering damper. The main aims of the invention are the compensation of roll disturbances and wobble due to external influences, such as side wind and bumpy road surface. However, the sensory setup suggests, that also a certain effectiveness against the BST could already be given. While the functional integration of steering actuator and damping function lie at hand for the hydraulic setup in the latter example, the realization of steering damping through an electric actuator could offer new possibilities.

Steering Damper Measures

Typically, a steering damper is limiting the steering rate and can therefore only mitigate the BST effect in its initial phase but not reduce the steering torque demand for the duration of the brake maneuver (cf. working hypotheses in chapter 1.2). Manually adjustable steering dampers with frictional or hydraulic damping are state of the art in either linear or rotational motion setups. Such devices can be made automatically adjustable by adding small electric (stepper) motors to the adjustment wrenches, however, with still too low actuation speeds regarding BST kick-ins. A faster reaction is promised by dampers that make use of a seismic mass to switch hydraulic channels for excessive steering angle gradients[125]. However, publications on its effectiveness are not to the author's knowledge.

The most promising solutions in this field are offered by extended semi-active steering damper control. Current semi-active hydraulic steering dampers such as the Honda Electronic Steering Damper (HESD) were designed to eliminate kick-back (through high damping) without compromising the low speed handling (by keeping the damping low)[126]. In order to achieve this, speed and acceleration are used as input parameters to

[123] Hikichi et al. (2009): Motorcycle steering system. Patent Application EP2085307A1, and others

[124] Suzuki (2009): Steering assist system. Patent Application US2009/0139793A1, and others

[125] Uden (2010): Lenkungsdämpfer mit veränderbarer Wirkung. Patent Application DE102006036135B4

[126] Wakabayashi et al. (2004): Development of electronically controlled steering damper, proceedings pp. 489-509

identify kick-back relevant situations and trigger an electric solenoid valve that is used to control the damping intensity accordingly. Extending the current inputs by roll angle and brake pressure (gradient) information would also allow quick reaction to BST relevant situations. Other hardware options for a fast reaction to desired changes in damping rate can be incorporated by the use of fluids with variable viscosity such as electro-rheological[127] or magneto-rheological fluids. Moreover, BMW presented a ball joint with variable friction damping realized by means of an electromagnet[128] which is predestined for the use in alternative chassis designs such as exemplarily shown in chapter 4.1.2. Finally, as a BST effect specific characteristic, an advanced semi active steering damper control could be designed to be direction selective. That means, that when a BST relevant situation is predicted or detected, high damping against misaligning (inward) steering motion resulting from the BST is provided, while damping against aligning (outward) steering motion is kept low, so that desired steering impulses needed to increase the roll angle in accordance with the situation are not negatively affected. In case opposing course corrections should be necessary, the BST is helping the rider to act against the elevated damping ratio.

Stability Control Measures: The Inerter

In this group, various inventions address stability issues by actively taking influence on the steering torque and motion by use of the former two groups of hardware. However, a less familiar component called “inerter” must not be forgotten. It allows the synthesis of arbitrary passive mechanical impedances and might help to generate more sophisticated mechanical solutions in the future[129]. A simulation study of a steering compensator composed of a spring, damper and inerter already revealed significant improvements compared to a standard steering damper in terms of wobble and weave oscillations over the full range of roll angles[130]. Despite these promising results, further research is required to draw valid conclusions about the effectiveness of such systems against the BST effect.

---

[127] Funke et al. (2010): Electrorheological Dampers, proceedings pp. 211-224

[128] Seidl / Heyl (2004): Kugelgelenk. Patent Application DE10245983A1

[129] Smith (2003-2010): Force-controlling mechanical device. Patent Applications WO2003005142A1, EP1402327B1, US20050034943, US7316303B2, and others

[130] Evangelou et al. (2004): Steering compensation, proceedings pp. 749-754

2.3.8 Influencing the Rolling Moment and Movement

Even though measures of this field intervene rather late in the BST chain of effects, current developments are worth a closer look. The simplest idea to generate a supportive roll moment is to push an additional wheel onto the ground. This seems to be especially attractive for cabin motorcycles like the Swiss MonoTracer[131] that already features retractable support wheels. However, experience in riding conventional motorcycles with wheeled outriggers shows that this is forbidding from a driving dynamic point of view in BST critical situations, because the unexpected transition from single track to multi-track vehicle steering response (i.e. from counter steering to direct steering) can hardly be managed by a further confused rider (cf. chapter 2.2.5).

The next level is to always keep one or more additional wheels on the ground, which can be achieved by multi-track tilting vehicles, as addressed in chapter 2.3.9.

Finally, gyro-stabilization through a pair of gimbaled flywheels offers another possibility to control the roll of a "real" single track vehicle in an elegant way without support of additional wheels. The technology was originally developed for monorail trains at the beginning of the 20th century[132] and recently refined and patented by the American company LIT Motors[133] for use in an electric cabin motorcycle, see Figure 2.25.

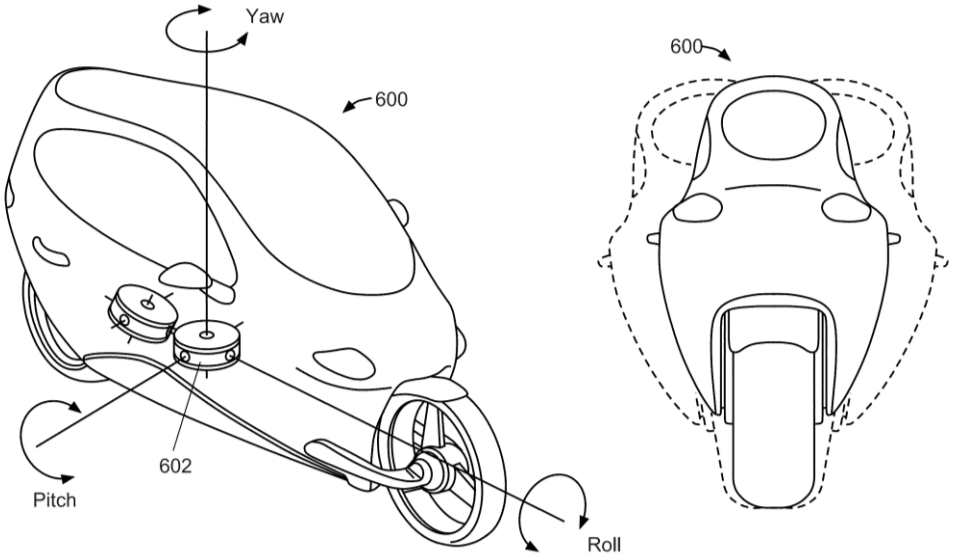

Figure 2.25: Schematic diagram of roll stabilization through gimbaled flywheel assembly[134]

[131] MonoTracer – virtual: https://peraves.wordpress.com/, last access: 2016-11-11

[132] Among others, see: Flacke (1912): Gyrostatic Mechanism. Patent Application US1048817A

[133] LIT Motors – virtual: litmotors.com, last access: 2016-11-11, see also Kim et al. (2013): Gyroscopic stabilized vehicle. Patent Application US8532915B2

[134] Kim (2013): Dynamically balanced flywheel. Patent Application US20130233100A1, FIG 6A

The two gyros spin in opposite directions around the vertical axis and can individually be inclined against the chassis in a pitch motion. While the gyroscopic reaction torques cancel each other out in normal driving, an enormous roll momentum can be generated by opposed inclination of the gyros, as illustrated by the following model calculation[135].

Assuming a vehicle at low speed close to standstill to have a mass of $m = 500$ kg, an upright height of center of gravity of $h_{cg} = 0.75$ m inclined by $\lambda = 30°$ from vertical, with gravity $g = 9.81$ m/s², it will produce a roll moment of approximately:

$$M_x = m \cdot g \cdot h_{cg} \cdot \sin(\lambda) \approx 1.8 \text{ kNm} \tag{2.31}$$

Reasonably dimensioned equal gyros (e.g. with spinning inertia $I_{gyro} = 0.07$ kgm²) spinning at $\omega_{spin} = 570$ rad/s (≈ 15.000 rpm) and precessing at $\omega_{precession} = 10.47$ rad/s (≈ 100 rpm) in still undeflected orientation will (temporarily) be able to balance the vehicle by delivering the following output roll momentum:

$$M_x = 2 \cdot I_{gyro} \cdot \omega_{spin} \cdot \omega_{precession} \approx 2.3 \text{ kNm} \tag{2.32}$$

Apart from the low speed stabilization, the system is also supposed to be powerful enough, to keep the vehicle upright during a typical urban intersection lateral impact crash, thus increasing occupant safety. Furthermore, the energy efficiency of the electric vehicle can be enhanced by linking the gyros to a recuperative brake system. Letting them spin quicker covers the high stabilization demand at low speeds, while their kinetic energy is used for propulsion at higher speeds, when stabilization through the spinning wheels is sufficient.

Regarded from the perspective of a potential safety measure in BST critical situations, the said reduction in spin rate is of course counterproductive. Moreover, the desired effect is decreasing with increasing precession angle and only present for up to 90° of deflection, which limits the actuation time frame to about 0.15 s at the above mentioned precession speed. Before this background it remains to be seen, in how far this technology – that also seems promising for autonomous braking applications (cf. chapter 2.3.1) – will prove effective in the cabin motorcycle. Even if it will be a success there, it is rather unlikely that it will ever be transferred to ordinary motorcycles with their extremely limited construction space, weight and packaging constraints.

2.3.9 Using Multi-Track Tilting Vehicles with Two Front Wheels

This rapidly developing vehicle category features three and four wheeled vehicles (like the Piaggio MP3 or Quadro 4D scooters) whose chassis constructions allow roll motion

[135] Model calculation and figures are based on LIT Motors' patent of Kim et al. (2013): Gyroscopic stabilized vehicle. Patent Application US8532915B2, column 4, p.17.

and motorcycle-like driving dynamics with superior braking stability on slippery surfaces[136], but still include the BST effect. In order to avoid relative lateral movements between the two front wheels that would generate disturbing sideslip forces from roll or suspension movement, all solutions known to the author are keeping the wheels and suspension travel (more or less) parallel to the vehicle symmetry plane and at (approximately) constant track width. Moreover, the roll degree of freedom can typically be locked at low speeds or standstill, so that the rider does not need to take off the feet and no stands are required for parking.

Given these pre-conditions, there are theoretically three potential ways of using left / right asymmetries – in normal and brake forces as well as scrub radii – to influence the BST effect. These were studied on the basis of simplified quasi-stationary simulations[137] in the framework of the presented research and are discussed in the following.

Influencing the Normal Forces

There is a great variety of roll-lock mechanisms. While Piaggio's MP3 features a mechanical disk brake segment, Quadro realizes the roll-lock by closing a valve in the fluid flow between left and right cylinders of their Hydraulic Tilting System (HTS). Both types could therefore be easily modified to transfer surplus roll moment to the outer wheel during a stand-up phase late in the BST chain of effects (No. 8 in Figure 2.17). However, the possibility to create temporary asymmetry in wheel load – if required by active components – could also interact beneficially with the following two measures.

Influencing the Brake Forces

As illustrated in Figure 2.26 (a), asymmetric braking of the outer wheel can mitigate the BST as follows. The brake force (dashed arrow) multiplies with the scrub radius and generates a misaligning steering torque demand (STD_{BST}, dashed arrow) around the steering axis (black dot). However, the brake force and inertial force on the center of gravity form a couple of forces and generate an outward Brake Yaw Moment[138] ($M_{z,BYM}$, dashed arrow), which needs to be counter-balanced by a difference in side forces front / rear ($\Delta F_{y,BYM}$, dotted arrows). Multiplied by trail n (i.e. the normal trail nt for $\tau \neq 0$), the additional side forces on the front wheels generate an aligning steering torque demand component (STD_{BYM}, dotted arrow) around the steering axis. In theory, this

[136] Especially regarding the kinematic braking instability, cf. chapter 2.1.8.

[137] Frisch (2011): Countermeasures against BST in Three Wheel Tilting Vehicles, Bachelor-Thesis

[138] For more detailed information about the BYM and how the wheel forces translate to the steering axis on a conventional powered two wheeler, refer to chapters 2.1.7 and 3, respectively.

sounds promising, but comes along with practical limitations. Even though the decrease in lateral force at the rear wheel allows shifting the brake force distribution (BFD) a bit more rearward, the force transfer limits of the outer front wheel are reached very soon. Even when its wheel load could temporarily be increased, this measure can only address partial decelerations. Finally, the generation of an outward Brake Yaw Moment stands in direct contrast to the aim of keeping a given cornering radius that would rather require braking of the inner wheel in the sense of an Electronic Stability Control (ESC) known from passenger cars. However, besides its undesired reduction or even change of sign in the aligning steering torque demand component that is induced by the Brake Yaw Moment (STD_{BYM}), a super-elevation of the inner normal force is not as easily possible as for the outer, since the centrifugal forces under cornering are naturally directed outward the curve. This limits such a strategy to even lower partial deceleration levels.

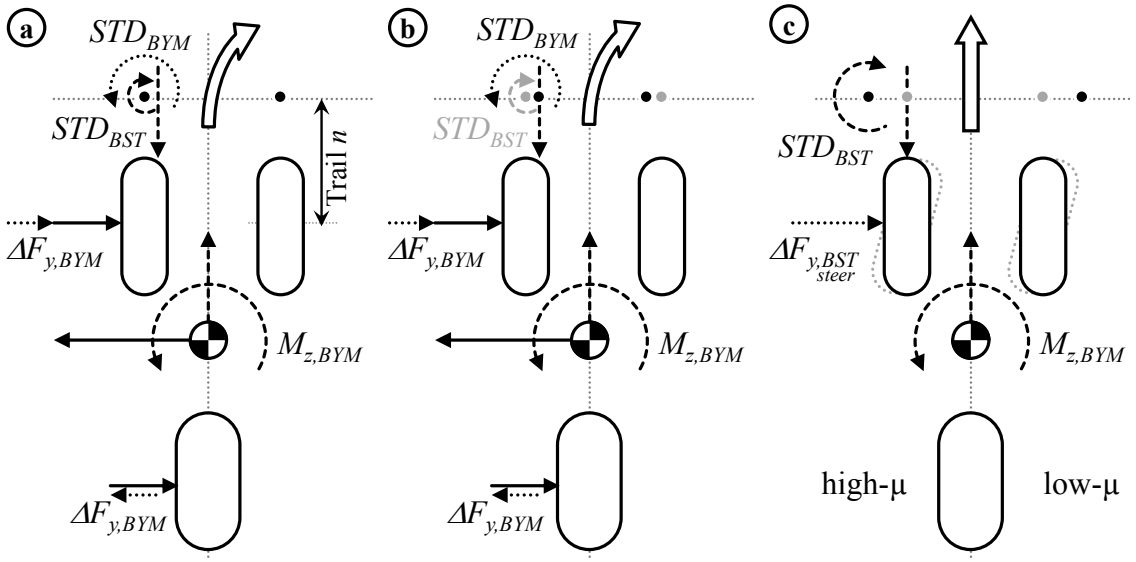

Figure 2.26: BST mitigation through asymmetric braking and king-pin offset on a tilting vehicle

Influencing the Scrub Radii

Introducing a king-pin offset and / or inclination (KPI) generates asymmetric scrub radii under cornering. Applying more brake force – and in assistance potentially also more normal force – to the wheel with the smaller scrub radius will in total decrease the BST level and STD. Figure 2.26 (b) illustrates this strategy for positive king-pin offset (old centered steering axes in grey, new offset ones in black). Keeping the same strategy of braking the outer wheel as in case (a), the aligning influence of STD_{BYM} is maintained, while the applied brake force does in this ideal case no longer generate a misaligning STD_{BST} (greyed out).

The strategy of braking the inner wheel more – with its disadvantages concerning the STD_{BYM} effect – would require negative king-pin offset, as would straight braking under split-μ conditions illustrated in Figure 2.26 (c). In this particular case, the STD_{BST} is even desired to generate a steering motion and side-slip lateral forces ($\Delta F_{y,BST,steer}$, dotted arrow) towards the low-friction side, in order to compensate the disturbing effect of $M_{z,BYM}$ towards the high-friction side.

Due to this trade-off between case (b) and (c), all concepts currently known to the author keep the steering axes more or less centered with respect to each wheel. However, this trade-off may be solved, by introducing roll angle dependent differences in left and right scrub radii. A quite interesting but very likely also mechanically complicated approach could be based on the BSTAM technology by using the roll movement of the suspension parts relative to the chassis as a purely mechanical input. Theoretically, a more simple way of achieving the same aim is to use tires with asymmetric contour radii for left and right, as illustrated in Figure 2.27.

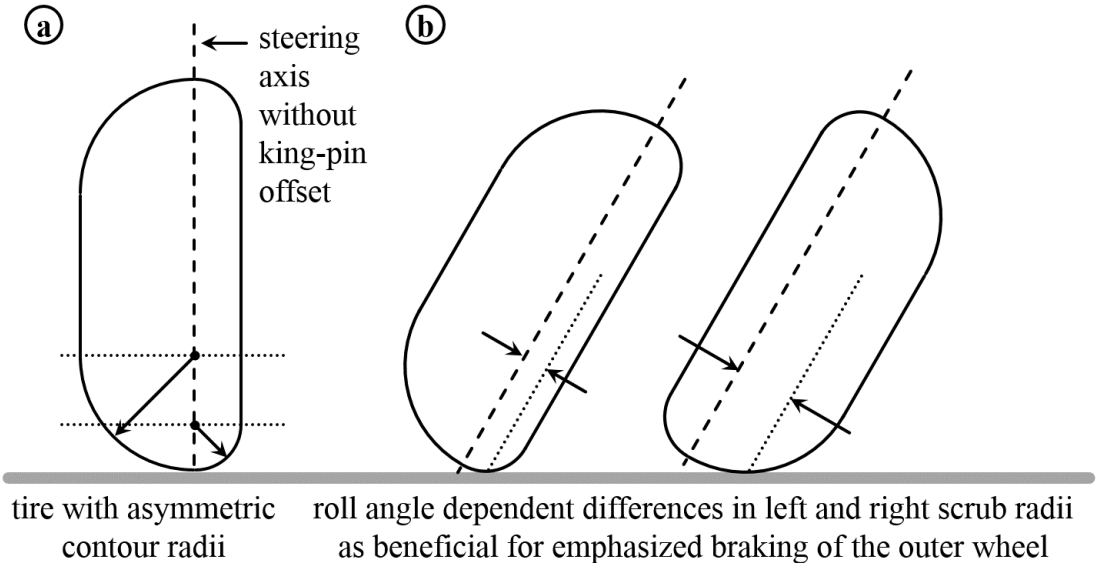

Figure 2.27: Tire with asymmetric contour radii

While the presented case is set up to go along with the emphasized braking of the outer wheel, interchanging left and right tire in Figure 2.27 (b) achieves the same for the inner-wheel braking strategy. In order to enhance split-μ braking performance, an additional negative king-pin offset could also be introduced as illustrated in Figure 2.26 (c). Even though similar tires have already been manufactured in the past for the Mercedes Benz F400 Carving research car with active wheel cambering[139], it is not known to the author, if this will practically be also feasible for motorcycle tires.

[139] Mercedes Benz – virtual: www.fanmercedesbenz.com/2001-mercedes-benz-f400-carving/, last access: 2016-09-08

Finally, also for symmetric tires and brake force distribution, a benefit concerning the BST can be achieved against conventional PTW, because the force transfer through two front tires allows to use slimmer tires with smaller scrub radii (cf. chapter 2.3.4).

Safety In Motion (SIM) Prototype Piaggio MP3

Among other measures contributing to the integrated approach for motorcycle safety of the SIM project, Piaggio MP3 vehicles were equipped with semi-active suspension, an active three channel ABS brake system[140] as well as measurement of roll angle, yaw rate and lateral acceleration. A cornering sensitive brake strategy with roll angle dependent slip thresholds, brake force distribution and limitation of brake force gradients for reasons of BST has been implemented as well as an ESC-like yaw control, mitigating power over-steer through traction control at the rear wheel[141]. The coordination of semi-active suspension and brake system was further used for bad road recognition and optimizing parameter adaptations. Thus, measures of influencing both the normal and the brake force have already been successfully implemented. So finally, it is left to further investigations to reveal, whether the presented options of using modified roll-lock in conjunction with asymmetric brake forces and scrub radii can be of further benefit.

2.4 Conclusions

The BST chain of effects has been described in detail and a complete field of potential countermeasures has been systematically derived, including state of the art motorcycle technology into the classification scheme.

Regarding the driving dynamics along the chain of effects, the following solutions have been identified as the most promising for conventional Powered Two Wheelers:

1. Rear wheel oriented Cornering Adaptive Brake Force Distribution (CA-BFD) and limited front brake force gradients
2. Reduced lever arm (scrub radius) through BSTAM or multi-lever steering
3. Counter steering torque actuator
4. Semi-active steering damper with additional sensor inputs (like roll angle and brake pressure, respectively gradients).

[140] Pieve et al. (2010): Safety In Motion (SIM), proceedings pp. 167-185

[141] Roll et al. (2010): Safety benefits of electronic brake-control systems, proceedings pp 423-513

While the market introduction of cornering sensitive brake systems (1) like Bosch's MSC was just a matter of time even at the beginning of the presented research[142], and a semi-active steering damper (4) can only mitigate the BST effect, reducing the lever arm (2) or applying a counter steering torque (3) both promise a complete cure of the issue. Realizing the latter on the basis of the well understood driving dynamics of a conventional chassis[143] should be a question of diligent work and in addition offers the most degrees of freedom up to active trajectory manipulation during autonomous emergency braking maneuvers. However, as a downside of these possibilities, an erroneous actuation bears the potential risk to instantly throw off the rider. This requires extensive efforts on the side of functional safety, while a BSTAM always maintains a certain degree of steerability and an incorrect actuation is per se excluded for the purely mechanical multi-lever steering. Since the mechatronic layout of BSTAM is more flexible in terms of system adaptation than multi-lever steering, it was chosen as the main focus of the presented research and multi-lever steering is exemplarily regarded alongside.

Beyond the already addressed measures, four further ones with expected positive influence on the BST chain of effects should not be forgotten. These are:

5. (Semi-)Active suspensions, promising improvements in initial effect dynamics.
6. Steering compensation based on inerters, promising better effectiveness than conventional steering dampers.
7. Gyro stabilization, intervening very late in the chain of effects and coming with massive packaging downsides.
8. Use of multi-track tilting vehicles that do not only allow yaw control in analogy to the ESC used in passenger cars, but also diverse measures to profit from the possibility to create asymmetries in wheel loads, brake forces and scrub radii.

Synchronizing the results of the presented chapter with the initially formulated three aims in research field 1, which comprise the provision of a unified big picture on the BST chain of effects, a classification of state of the art countermeasures and identification of potentially new ones, as well as an estimate of their effectiveness and feasibility (cf. chapter 1.3), these aims have almost completely been achieved.

While the outstanding estimate on the effectiveness of multi-lever steering is briefly addressed in chapter 3.4, the same is done for the Cornering Adaptive Brake Force Distribution (CA-BFD) in chapter 3.6.

[142] Seiniger et al.(2006): Roll angle sensor, proceedings pp. 369-388

[143] E.g. Cossalter (2006): Motorcycle Dynamics

3 Analytic Considerations on the Kinematic Layout and Effectiveness of BSTAM

This chapter mainly addresses the first three aims in the second research field on the feasibility and layout of BSTAM (cf. chapters 1.3 and 1.4): Identifying the main influence factors of BSTAM on driving dynamics and potential downsides in a comparative analysis with the standard steering, deriving criteria for an optimized kinematic layout as well as to refine the working hypotheses for investigations on BSTAM in practical testing (cf. chapter 5). Moreover, the remaining open questions on the effectiveness of multi-lever steering and Cornering Adaptive Brake Force Distribution (CA-BFD) from the third aim in the first research field are addressed alongside (cf. chapters 3.4 and 3.6).

BSTAM Design for "Neutral" Free Cornering

As already briefly discussed in chapter 2.1.3, the steering torque is at the same time the main control input for maneuvering a motorcycle and an important feedback for the rider about the current driving condition. According to Figure 2.4, it is mainly composed by a superimposition of portions resulting from the tire contact forces (in all three spatial directions) with gyroscopic and tire reaction moments as well as inertial effects on the steering system. For a well designed conventional chassis with "neutral" layout, all steering torque components are balanced in such a way, that the rider needs to exercise a steering torque slightly outward the curve during free cornering which will further increase with rising deceleration[144]. Thus, a change of sign in steering torque demand (STD) when applying the brakes while cornering is effectively avoided.

However, the reduction of scrub radius through a BSTAM in its original design (cf. Figure 2.21) is altering the transfer ratios of all three tire forces towards the steering axis and greatly impairing the said balance, while small steering axis inclination angles lead to only minor distortions in the transfer ratios of the remaining steering torque contributes (cf. chapter 3.3.5).

Therefore, the focus of the following chapters is put on the front tire contact forces and how they translate towards the steering axis, while pursuing the aim to mitigate the BST effect through scrub radius compensation and at the same time keep the "neutral" steering balance of the baseline chassis.

[144] Cossalter et al. (2010): Steering Torque Decomposition

3.1 Force Transmission Ratios of a Generic BSTAM and Standard Chassis

In the following, different BSTAM layouts are compared with the standard chassis on the basis of their steering torque demand T_F arising from the front tire contact forces $F_{x/y/z}$ and their respective lever arms $l_{x/y/z}$ towards the steering axis. It is defined as:

$$T_F = \sum_{i=x,y,z} T_i = \sum_{i=x,y,z} F_i \cdot l_i \,. \tag{3.1}$$

While a simple model to compute roll equilibrium and tire forces during corner braking was already introduced (cf. 2.1.2 and 2.1.7), the lever arms remain to be defined.

Effective Lever Arms (or Force Transmission Ratios)

Since the original double excentric BSTAM design produces changes in caster angle τ and trail n that is further modulated by fork travel (cf. chapter 4), moving the steering axis in its original y'$_{st}$-z'$_{st}$-plane through purely lateral displacement of one or both steering bearings is avoiding these downsides. Hence, as illustrated in Figure 3.1, the lever arms are defined on the basis of a generic BSTAM chassis, which allows the kinematic steering axis to be freely moved (laterally and rotationally) in this plane.

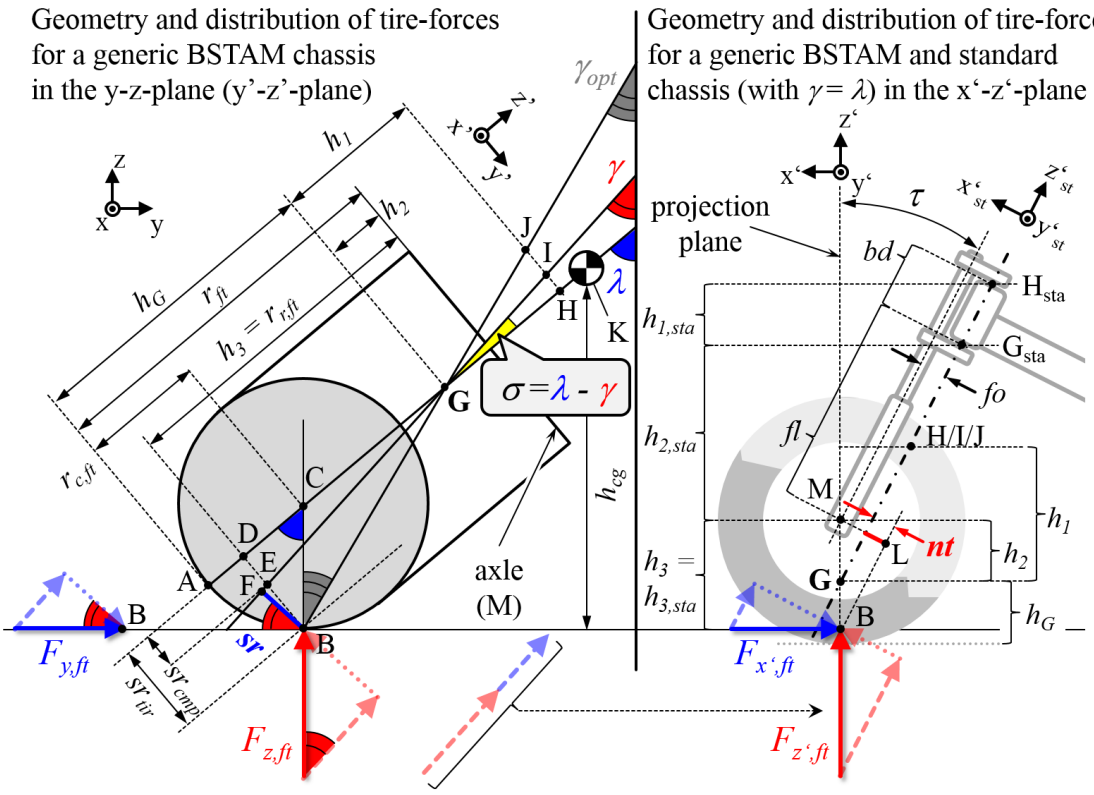

Figure 3.1: Geometry and force transmission of a generic BSTAM and a standard chassis

Table 3.1: Explanation of Symbols and abbreviations used in Figure 3.1

Symbol	Explanation
bd	Bearing distance = distance between upper and lower steering bearing
fl	Fork length = distance between front wheel hub-center and lower steering bearing along the z'_{st}-axis (depends on fork travel)
h_{cg}	Height of center of gravity over ground (only for graphical reasons, the arrow tip does not go all the way up until the center point K)
h_1 / $h_{1,sta}$	Projected vertical bearing distance (along z')
h_2 / $h_{2,sta}$	Projected vertical distance between the lower steering bearing and the front wheel hub-center (along z') Note that the lower steering bearing (G) is below the wheel axle and h_2 and h_3 overlap for the generic BSTAM, while they do not for the standard chassis, with both steering bearings (G_{sta} and H_{sta}) located firmly above the axle in the steering head.
$h_3 = r_{r,ft}$	Projected vertical distance between the front wheel hub-center and the tire contact point (along z'); equal to the current front tire rolling radius
h_G	Height of optimal instantaneous center of steering axis inclination (G) over ground in upright vehicle position (along z'- or z-direction)
r_{ft} / $r_{c,ft}$ / $r_{r,ft}$	Free center radius / contour radius / and roll angle dependent rolling radius of the front tire
sr	Scrub radius = perpendicular distance between tire contact point and projected BSTAM steering axis
sr_{tir}	Roll angle dependent tire scrub radius = lateral distance between tire contact point and projected standard steering axis, respectively vehicle symmetry plane
sr_{cmp}	Compensated portion of sr_{tir}
γ / γ_{opt} / γ_{red}	(Optimal / reduced) inclination angle of the projected BSTAM steering axis from vertical (in leveled coordinates, i.e. the z-axis)
λ	Roll angle of the vehicle
σ / σ_{opt} / σ_{red}	(Optimal / reduced) inclination angle of the projected BSTAM steering axis from the vehicle symmetry plane (king-pin inclination angle)
τ	Steering head (or caster) angle

The left side of Figure 3.1 schematically shows the frontal view of the front wheel cross-section (from below the wheel axle, M) in the y-z-plane of the leveled coordinate system. While the vehicle symmetry plane and standard steering axis (A-H) are inclined by the total roll angle λ from vertical, the projection of the BSTAM steering axis (I-G)

into the y-z-plane is inclined by the angle γ from vertical, and by the king-pin inclination (KPI) angle σ from the vehicle symmetry plane, with:

$$\sigma = \lambda - \gamma \tag{3.2}$$

The current tire rolling radius $r_{r,ft}$ decreases with increasing roll and can be computed with the tire's rolling radius in upright position r_{ft} and its contour radius $r_{c,ft}$ as follows:

$$r_{r,ft} = r_{ft} - (1 - \cos\lambda) \cdot r_{c,ft} \tag{3.3}$$

The lateral displacement of the tire contact point towards the symmetry plane is growing with increasing roll angle (point A to B) and defines the tire scrub radius (line B-D):

$$sr_{tir} = \sin\lambda \cdot r_{c,ft} \tag{3.4}$$

A geometric compensation ratio (*gcr*) for BSTAM is defined by the intersection point (E) and the ratio of the projected steering axis (I-G-E) to the said lever arm (B-D):

$$gcr = \frac{sr_{cmp}}{sr_{tir}} \tag{3.5}$$

with sr_{cmp} being the compensated portion (D-E) of the tire scrub radius sr_{tir} (B-D)[145].

The closer the intersection point (E) is moving towards the tire contact point (B), the greater is the geometric compensation ratio. In case both points coincide, $gcr = 1$. With this definition, the effective scrub radius *sr* of the generic BSTAM can be calculated within triangle (B-E-F) in Figure 3.1, left, as follows:

$$sr = \left((1 - gcr) \cdot sr_{tir}\right) \cdot \cos(|\lambda - \gamma|) \tag{3.6}$$

For the conventional steering axis (H-G-A, $\gamma = \lambda$, $gcr = 0$) the effective scrub radius *sr* is identical with the tire scrub radius sr_{tir}.

The right side of Figure 3.1 shows the lateral view (in negative y'-direction) of the vehicle-fixed x'-z'-plane and the projection of a second parallel plane in the foreground that runs through the tire contact point (and is thus displaced by sr_{tir} in y'-direction). Based on the previously defined tire rolling radius $r_{r,ft}$, the steering head angle τ and the fork offset *fo*, the effective normal trail *nt* can be derived from triangle (B-L-M):

$$nt = r_{r,ft} \cdot \sin\tau - fo \tag{3.7}$$

[145] Note that besides for *gcr*, the same definition holds true for the target (*tcr*) and effective compensation ratio (*ecr*) used in context of real incorporations of BSTAM in later chapters. While a controller can only target at achieving a set geometrical *tcr*, the effective outcome in positioning the steering axis and hence the *ecr* may differ, be it through limitations in controller or actuator performance or geometric constraints in terms of limited displacement (i.e. excentricity) or interferences with suspension travel.

The front wheel contact forces in all three spatial directions $F_{x/y/z}$ are counted positive in arrow direction as defined in Figure 3.1 and their lever arms $l_{x/y/z}$ towards the steering axis are described by the following set of equations, where positive components have a misaligning effect (turning inward the curve, increasing the steering angle) and those with negative sign an aligning one (turning outward, decreasing the steering angle):

$$l_x = +\cos\tau \cdot sr \tag{3.8}$$

$$l_y = -\cos\gamma \cdot nt - \sin\gamma \cdot \sin\tau \cdot sr \tag{3.9}$$

$$l_z = +\sin\gamma \cdot nt - \cos\gamma \cdot \sin\tau \cdot sr \tag{3.10}$$

Thus, it can already be stated, that the lateral force F_y is always acting in an aligning way and the normal force F_z in a misaligning way through the normal trail *nt*, while both have an aligning influence through the scrub radius *sr* for $\tau \neq 0$, which is decreasing for increasing compensation ratios *gcr*. The following chapters illustrate how this is crucial for the kinematic layout of a BSTAM that aims at compensating the scrub radius and keeping the steering torque in "neutral" balance at the same time.

Tire Forces in Reference Corner Braking Situation

The front tire contact forces are computed on the basis of the equation sets provided for quasi-stationary corner braking, as introduced in chapters 2.1.2 and 2.1.7 and the chassis geometry properties of the test motorcycle as provided in appendix A.4.2.

Among others, the model implies the following simplifications:

- Undeformable tires with constant contour radius
- Unsprung chassis with constant wheelbase and center of gravity location (estimated deviations to the real sprung chassis are in the order of 5%)
- Zero steering angle (cf. chapter 2.1.5)
- Roll equilibrium as for stationary free cornering (hence "quasi-stationary" corner braking, cf. chapter 2.1.2)
- Aerodynamic effects, rolling resistance, tire reaction and gyroscopic torques, other dynamic effects on wheel loads, and suspension deflections are neglected.

On this basis, the contributions of each front tire force component to T_F as defined in eq. (3.1) are exemplarily compared for different chassis setups for the following reference corner braking conditions, that are in line with the conducted driving tests (cf. chapter 5) and a typical example of BST relevant situations in the real world:

- Initial lateral acceleration of a_y = 6 m/s², corresponding to an
- Initial roll angle of $\lambda \approx 35°$ for the test motorcycle.
- Variations in deceleration a_x.

3.2 Steering Torque Demand (STD) of a Standard Chassis

In this chapter, the composition of steering torque demand on a standard chassis with centered steering axis ($\gamma = \lambda$, $gcr = 0$) is analyzed under the influence of riding style and brake pitch in order to draw conclusions for the optimal kinematic layout of a BSTAM.

As a simplification, the tire contact forces derived from the model calculation are assumed to remain the same, regardless of variations in riding style or brake pitch. These are solely considered in terms of varying roll and steering head angles in the lever arm equations, neglecting other geometry changes (shortening of wheelbase, lowering of center of gravity) that would in reality interfere with the roll equilibrium and calculation of tire contact forces. In the chosen example, changing the riding style from "lean with" (LW) to "lean in" (LI) or "lean out" (LO) is addressed by a 10% (3.5°) decrease or increase of the roll angle λ while brake pitch is represented by a reduction of up to 10° in steering head angle τ.

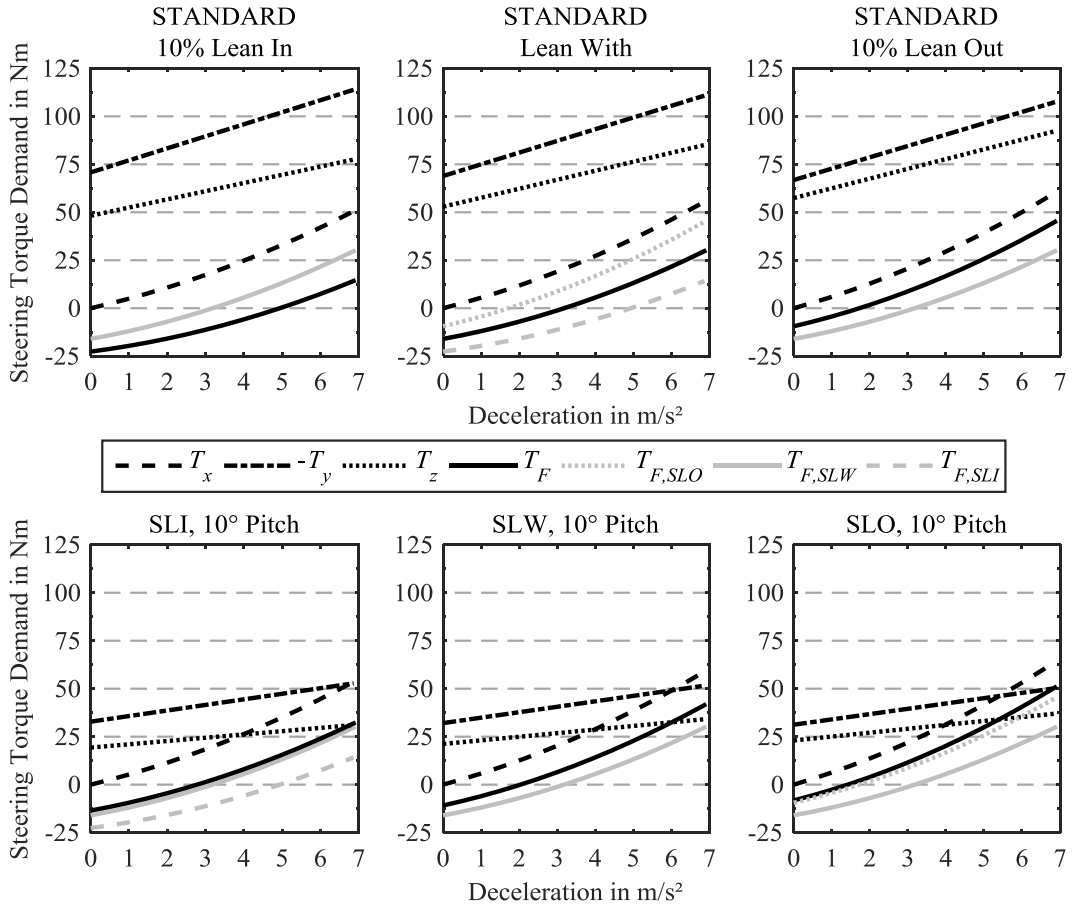

Figure 3.2: Steering Torque Demand generated by front tire forces for the standard chassis at $a_y = 6$ m/s² ($\lambda \approx 35°$) and $a_x = 0 – 7$ m/s² under variation of riding style ($\Delta\lambda \approx \pm 3.5°$) and pitch angle (steering head angle $\Delta\tau = -10°$). Reference case: Standard, Lean With (SLW).

As a result of the model calculations, the top row of Figure 3.2 shows the tire force based steering torque demand T_F and its individual components $T_{x/y/z}$ for the three riding styles LI, LW, and LO and unaltered steering head angle, while the second row presents the same for the reduced steering head angle. Note, that the T_y component is displayed with negative sign for reasons of compactness of the diagrams.

In reality, the values presented in the figure are superimposed by the other steering torque relevant components as described in chapter 2.1.3. Therefore, the results of the model calculation are no absolute values, but rather to be understood in the sense of relative tendencies. The more positive the Steering Torque Demand (STD), the more the rider needs to apply a steering torque outward the curve and vice versa.

Steering Torque Demand under Variation of Riding Style

Starting with the reference case (unaltered steering head angle and "lean with" riding style), the central diagram of the first row in Figure 3.2 shows, that the aligning influence of T_y is dominating the misaligning one of T_z for increasing decelerations. Thus, it leads to a partial compensation of the misaligning T_x resulting from the brake force, which is positive in view of the BST effect.

In context of Figure 3.1 the lever arm equations (3.8) to (3.10) illustrate furthermore, that a more upright orientation of the steering axis (with smaller values of γ) is enforcing the aligning effect of F_y while reducing the misaligning one of F_z.

This is illustrated very well by the top left diagram in Figure 3.2 for the "lean in" riding style, by which the rider can actively reduce the vehicle roll angle λ and with it both the steering axis inclination γ (here identical with λ) as well as the scrub radius sr in a given cornering situation (cf. chapter 2.1.2).

As exemplarily shown in the top row of Figure 3.2, both the stationary STD (T_F at $a_x = 0$) as well as the Brake Steering Torque (BST, in terms of total STD under braking, T_F at $a_x > 0$) for a standard chassis can – to a certain degree – be positively influenced by the riding style "lean in" in comparison to "lean with" (rider upper body in line with vehicle symmetry plane). The opposite holds true for "lean out".

However, the dominance of T_y over T_z and their balance over the complete range of decelerations is common for all three riding styles. Recalling the balance between F_y and F_z through the effects of Brake Pitch and Yaw Moments (cf. chapter 2.1.7, eq. (2.26) and (2.27)), there also seems to be a desirable balance in their respective lever arms l_y and l_z (cf. eq. (3.9) and (3.10)) on a standard chassis. Hence, the lever ratio:

$$\ell_{yz} = \frac{l_y}{l_z} \tag{3.11}$$

is defined for further analysis.

The Influence of Brake Pitch on Chassis Geometry and Lever Arms

Temporarily ignoring the lower row of Figure 3.2, the influence of brake pitch, or in more general, a variation in caster angle, is first studied for characteristic geometry parameters of the standard chassis in the reference corner braking maneuver. From a handling point of view in terms of a direct steering angle transmission ratio, the caster angle should be as low as possible (cf. chapter 2.1.5). However, for reasons of stability (cf. chapter 2.1.6) and robustness of the currently investigated steering balance against brake pitch, a certain range of caster angle is clearly preferable in combination with a given fork offset (*fo*).

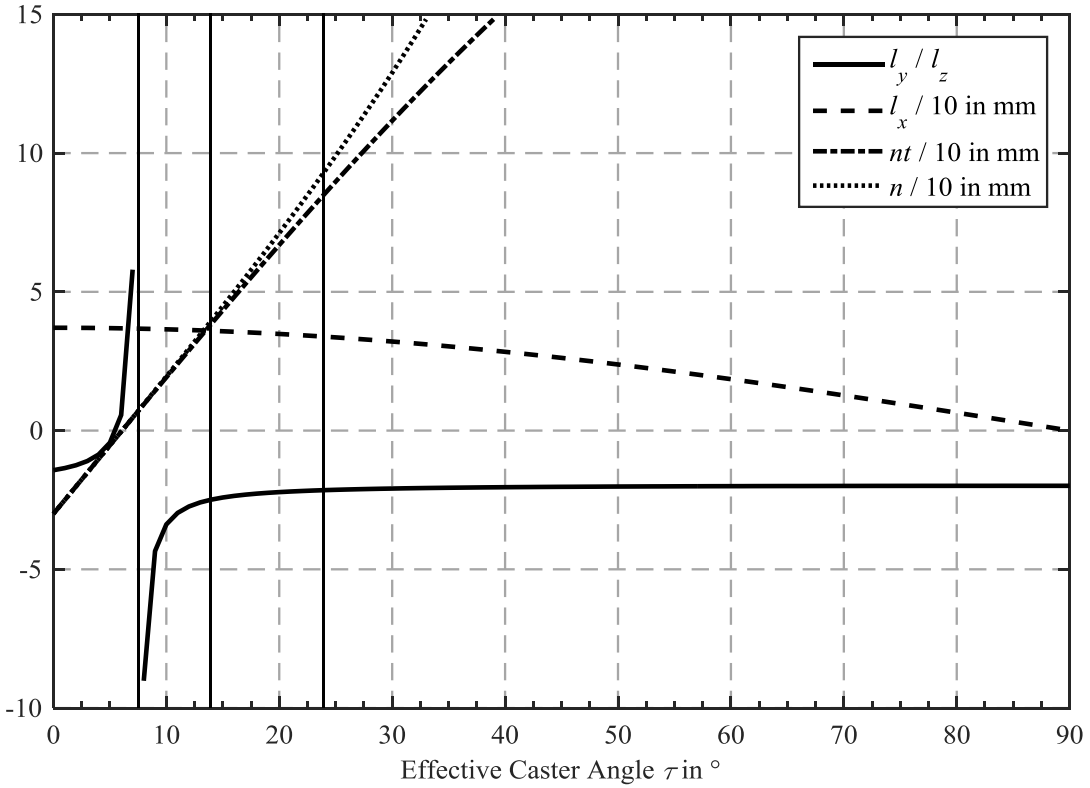

Figure 3.3: Variation of characteristic geometry parameters of the standard chassis (*fo* = 30 mm) under influence of brake pitch in the reference corner braking situation (a_y = 6 m/s², $\lambda \approx 35°$). From right to left, three black vertical lines indicate the stock caster angle $\tau = 23°55'$, a reduction of the same by 10° through pitch and the transition in lever-ratio at approximately 7.5°.

Starting with an effective caster angle of 90° from the right end of Figure 3.3, the lever ratio l_y/l_z remains constant for a relatively large span of caster angles down to about 33°, before starting to drop slowly for further reductions in caster angle. In the range of the production caster angle and even for a generically defined reduction of 10° through brake pitch (cf. vertical dashed lines), the ratio changes only slightly to more negative values. Concerning the STD, this means, that the aligning effect of T_y is even more dominating the misaligning one of T_z under the influence of brake pitch, which is desirable to help against the BST effect.

For further reductions in caster angle, the lever ratio is dropping ever quicker and finally has a change of sign at about 7.5°, inverting the balance between T_y and T_z. However, this is a theoretical case far beyond lift-off of the rear wheel and indicates, how well the production caster angle of the base vehicle is chosen in terms of both, a direct steering transmission ratio (low caster angle) and keeping away enough from too great variations in lever ratio under brake pitch.

Furthermore, the more direct steering transmission under braking while cornering is also accompanied by an increase in lever arm l_x, eq. (3.7). As illustrated in Figure 3.3, changes in this value are also desirably low for a caster angle in the range of the production value, but still emphasis the misaligning effect of T_x. As a contributing factor to the lever arm ratio, the picture is completed by the respective variations of trail n and normal trail nt, respectively. These drop in a relatively linear manner with reducing caster angles or increasing brake pitch, easing the handling characteristics while maintaining positive values for a reasonable level of stability.

Jumping back to Figure 3.2, the bottom row illustrates how these characteristics help to maintain the balance between T_y and T_z for all three riding styles under the influence of brake pitch. However, since the balance is achieved at much lower absolute values of both components and the transmission ratio of the brake force is becoming more direct with increasing l_x, the overall steering torque demand is rising compared to the reference case without pitch in the first row of the figure. It is worth noting, that a change of riding style from “lean with” to “lean in” during the transition phase from free cornering to corner-braking including the brake pitch effect only leads to marginal increases in steering torque demand (bottom left illustration). This is especially interesting, since the BST induced stand-up of the vehicle after brake kick-in will lead to similar configurations, when the rider previously was riding relaxed and loose enough (cf. chapter 5).

In conclusion of the considerations on the steering torque demand (STD) of the standard chassis, keeping the balance between T_y and T_z and hence the lever ratio l_y/l_z of BSTAM close to that of the baseline geometry for any given constellation of compensation ratio, roll and pitch angles is the primary aim to keep the STD in free cornering as much as possible in a “neutral” balance – despite the reductions in scrub radius and lever arm l_x.

Moreover, since the aligning effect of T_y is increasingly dominating the misaligning one of T_z for growing decelerations and thus already leading to a partial compensation of the misaligning T_x resulting from the brake force, only a partial compensation of the scrub radius may be required, yielding favorable geometric compensation ratios $gcr < 1$.

3.3 Layout and STD of a BSTAM with Laterally Inclined Steering Axis (KPI)

Just like in the previous chapter, also in this chapter different chassis setups are compared on the basis of the composition and level of their steering torque demand (STD) in the reference corner braking situation. In analogy to the graphs in Figure 3.2, the simulation results of five setups are presented in Figure 3.4 and complimented by small illustrations (a-e) that show their steering bearing positioning, steering axis orientation (without and with king-pin inclination, KPI), as well as the remaining scrub radius in frontal projection (cf. Figure 3.1). The five setups will be addressed in sequence along the argumentation of the chapter and are therefore centrally placed at the beginning.

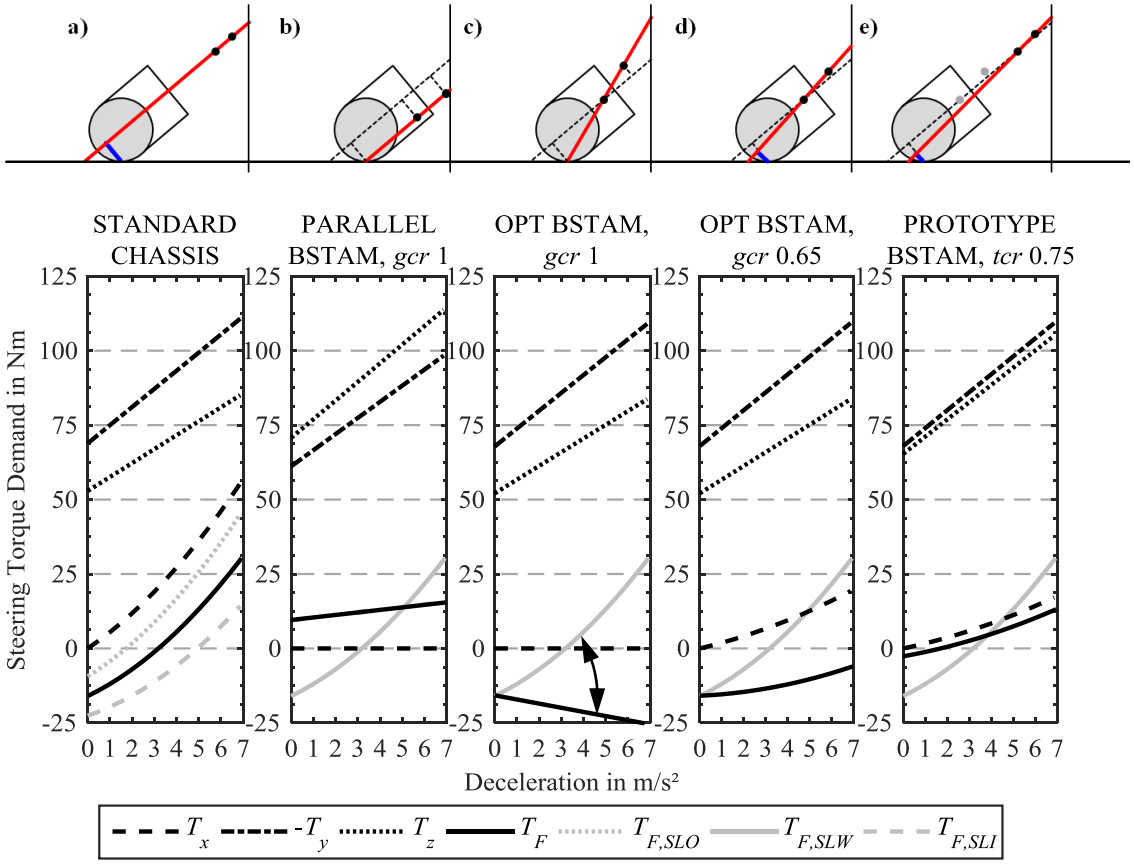

Figure 3.4: Steering Torque Demand (STD) generated by front tire forces for different chassis setups at a_y = 6 m/s² ($\lambda \approx 35°$) and a_x = 0 – 7 m/s² for riding style "lean with". The STD of the standard chassis with this riding style is repeated for reference in all diagrams ($T_{F,SLW}$), and in detail of all contributes in case (a), including the STD of the other two riding styles ($T_{F,SLO\,/\,SLI}$).

As a reference for both the absolute level of Steering Torque Demand T_F and the separate torque contributes resulting from each of the three tire contact forces ($T_{x/y/z}$), the steering torque composition of the standard chassis as discussed in the previous chapter

is repeated in detail in case (a) and its STD for "lean with" riding style $T_{F,SLW}$ is repeated in all following diagrams (solid grey line).

3.3.1 Remarks on the STD of a BSTAM with Parallel Steering Axis Offset

Despite the main headline of chapter 3.3, a BSTAM that moves both bearing points in parallel to the original steering axis ($\sigma = 0$, $\gamma = \lambda$, cf. Figure 3.4 (b) and the dotted line through point B in parallel to (H-G-A) in Figure 3.1, henceforth called a "Parallel BSTAM" or "//BSTAM") promises unchanged transmission ratios for most of the hitherto neglected steering torque components and should therefore be the first option to analyze. However, as proven in the following, a //BSTAM with "neutral" steering balance for full compensation is not feasible and king-pin inclination has to be used.

Setting the geometric compensation ratio $gcr = 1$ for a full compensation of the scrub radius sr, the lever arm equations (3.8) to (3.10) yield the following transfer ratios:

$$l_x = \cancel{+ \cos\tau \cdot sr} = 0 \tag{3.12}$$

$$l_y = -\cos\lambda \cdot nt_{//BSTAM} \cancel{- \sin\lambda \cdot \sin\tau \cdot sr} \tag{3.13}$$

$$l_z = +\sin\lambda \cdot nt_{//BSTAM} \cancel{- \cos\lambda \cdot \sin\tau \cdot sr} \tag{3.14}$$

Besides the desired elimination of l_x, also aligning steering torque contributes from both F_y and F_z are lost. This is already sufficient to swap the balance between the aligning T_y and misaligning T_z of the standard steering so that the latter is dominating the former over the complete deceleration range, as illustrated in Figure 3.4 (b, compared to a).

Regarding free cornering conditions ($a_x = 0$), this leads to an increase of stationary steering torque demand by about 25 Nm compared to the standard steering. Given the fact, that the total STD of the real test vehicle in standard configuration ranges between 5 Nm inward and 10 Nm outward the curve and typically is between 0 and 5 Nm outward (cf. chapter 5.4, experiments on $R = 50$ m turn radius), this means a fatiguing super-elevation by a factor of at least 2.5 to 5 and is therefore unacceptable from a rider's point of view. As a desirable benefit of this //BSTAM configuration, the total tire force generated STD T_F shows considerably lower increase rates with rising decelerations than the standard reference. For decelerations higher than about 5 m/s², the STD T_F of the //BSTAM is moreover falling below that of the standard reference.

Aiming to restore the desired balance between T_y and T_z for a //BSTAM with full compensation, the lever ratios of standard steering (index "sta") and //BSTAM (index "//BSTAM") are equated and reformulated. Inserting equations (3.9) and (3.10) respectively (3.13) and (3.14) into eq. (3.11) with $\gamma = \lambda$ for both setups delivers:

$$\ell_{yz,std} = \frac{\cos\lambda \cdot nt_{sta} + \sin\lambda \cdot \sin\tau \cdot sr_{sta}}{\sin\lambda \cdot nt_{sta} - \cos\lambda \cdot \sin\tau \cdot sr_{sta}} = \frac{\cos\lambda \cdot nt_{//BSTAM}}{\sin\lambda \cdot nt_{//BSTAM}} = \frac{1}{\tan\lambda} = \ell_{yz,//BSTAM} \cdot \quad (3.15)$$

Multiplication of both sides of the equation with the denominator of the leftmost fraction expression for the standard chassis and division by cos(λ) delivers:

$$nt_{sta} + \tan\lambda \cdot \sin\tau \cdot sr_{sta} = nt_{sta} - \frac{1}{\tan\lambda} \cdot \sin\tau \cdot sr_{sta} \quad (3.16)$$

After subtraction of nt_{sta}, both sides of the equation can be reduced through division by $\sin(\tau) \cdot sr_{sta}$, yielding the following contradiction:

$$\tan\lambda = -\frac{1}{\tan\lambda} \quad \text{or} \quad \tan^2(\lambda) = -1 \quad (3.17)$$

This proves, that a parallel BSTAM with "neutral" steering balance for $gcr = 1$ is not feasible at all. As a side note, eq. (3.15) furthermore reveals that the lever ratio of this setup only depends on the roll angle and is invariant to changes in normal trail $nt_{//BSTAM}$, and hence also caster angle τ, and fork offset (fo), cf. eq. (3.7).

With the lever arm equations (3.12) through (3.14) in mind, it lies at hand, that also partial compensations of the scrub radius ($gcr < 1$) will always suffer from the loss of aligning steering torque components and increased steering torque demand in free cornering. Hence another solution to eliminate the tradeoff between neutral steering balance and BST mitigation needs to be sought for as discussed in the following chapter.

However, if the pre-condition of keeping the caster angle and fork offset of the super sport base vehicle is abandoned, also favorable //BSTAM configurations with partial compensation ($gcr < 1$) can be found, see chapter 3.4.

3.3.2 Definition & STD of a BSTAM Optimized for Neutral Free Cornering

As already shown for the "lean in" riding style in context of the analysis of the standard chassis (cf. chapter 3.2), a more upright orientation of the steering axis can influence the balance between T_y and T_z to be more aligning. Introducing a king-pin inclination angle σ (with $\sigma = \lambda - \gamma$ and $\gamma < \lambda$) and again targeting at a full compensation of the scrub radius ($gcr = 1$), the lever ratios of both the standard steering and the BSTAM with king-pin inclination are equated. In analogy to eq. (3.15) this yields:

$$\ell_{yz,std} = \frac{\cos\lambda \cdot nt_{sta} + \sin\lambda \cdot \sin\tau \cdot sr_{sta}}{\sin\lambda \cdot nt_{sta} - \cos\lambda \cdot \sin\tau \cdot sr_{sta}} = \frac{\cos\gamma \cdot nt_{BSTAM}}{\sin\gamma \cdot nt_{BSTAM}} = \frac{1}{\tan\gamma} = \ell_{yz,BSTAM} \cdot \quad (3.18)$$

Since $\gamma = \lambda$ for the standard setup, the standard chassis' lever ratio ratio only depends on the roll angle, while the BSTAM's lever ratio only depends on the steering axis inclination angle γ. Reformulation of eq. (3.18) leads to the target steering axis and king-pin

inclination angles of an optimized BSTAM (further referred to as "OPT BSTAM") with full compensation (*gcr* = 1, steering axis (J-G-B) in Figure 3.1, left):

$$\gamma_{opt}(\lambda) = \arctan\left(\frac{\sin\lambda \cdot nt_{sta} - \cos\lambda \cdot \sin\tau \cdot sr_{sta}}{\cos\lambda \cdot nt_{sta} + \sin\lambda \cdot \sin\tau \cdot sr_{sta}}\right) \tag{3.19}$$

and

$$\sigma_{opt}(\lambda) = \lambda - \gamma_{opt}(\lambda) \tag{3.20}$$

Also the derived king-pin inclination angle σ_{opt} only depends on the roll angle λ and shows a merely slight degression from linear behavior for growing roll angles, cf. the solid black line in Figure 3.6.

For a roll angle of $\lambda = 50°$, it amounts to approximately $\sigma_{opt} \approx 14°$.The intersection point of the projected steering axis inclined by σ_{opt} with the vehicle symmetry plane is universally defining the (projected) instantaneous centre of BSTAM steering axis inclination (G), see Figure 3.1. Its height h_G (line A-G) over the front wheel road contact point in upright vehicle position (A) can be derived from Figure 3.1, left, with the sine rule in triangle (B-C-G) and the tire contour radius $r_{c,ft}$ as follows:

$$h_G = \left(1 + \frac{\sin\gamma_{opt}}{\sin(\lambda - \gamma_{opt})}\right) \cdot r_{c,ft} \tag{3.21}$$

Resolving this expression by inserting all defining equations (3.3), (3.4), (3.7), for the definition of the roll angle dependent normal trail nt_{sta} and scrub radius sr_{sta} of the standard chassis, as well as (3.19) for γ_{opt}, it can analytically be shown, that h_G is even independent of the tire contour radius $r_{c,ft}$, since this value is already contained in the definition of γ_{opt} from eq. (3.19) through eq. (3.3), (3.4), (3.7). The step-by-step reformulation of the equation is presented in appendix A.3.1 and yields:

$$h_G = r_{ft} - \frac{fo}{\sin\tau} \tag{3.22}$$

for the vertical position of the (projected) instantaneous center of steering axis inclination above the tire contact point (A) or, together with Figure 3.1, right:

$$h_2 = \frac{fo}{\sin\tau} \tag{3.23}$$

for its vertical distance below the front axle (M). Since the initial boundary condition was to keep the BSTAM steering axis in the y'_{st}-z'_{st}-plane of the original steering axis through purely lateral displacement of the steering bearings, the instantaneous center of steering axis inclination (G) must also be located in this plane. Comparing the result for h_2 from eq. (3.23) with the side-view sketch of the vehicle in Figure 3.1, right, defines the longitudinal position of (G) as the intersection of the original steering axis (H_{sta}-G_{sta}) with the vertical connection line from the front tire contact point (of the upright vehicle, point A) towards the front axle (M, cf. line B-G-M, since A is not visible).

In case only the upper steering bearing is adjusted, point (G) coincides with the lower steering bearing. For the chassis parameters of the prototype motorcycle, (G) lies $h_2 \approx 74$ mm below the hub-center, which is $h_G \approx 221$ mm above ground for the front wheel with the typical tire dimensions 120/70ZR17 and $r_{ft} = 295$ mm for the upright vehicle. From an engineering point of view, a hub-center or king-pin front suspension / steering system (Figure 4.1) would therefore be beneficial to facilitate the implementation of an OPT BSTAM with full realization of $\sigma_{opt} \approx 14°$. However, given the geometric conditions of the test vehicle's standard chassis with telescopic fork and steering head, the realization of such a high king-pin inclination angle σ in conjunction with the optimal instantaneous center (G) would require lateral displacements of both steering head bearings in the order of 100 to 185 mm in both directions. This is judged to be very unfavorable in terms of construction space, mass, and system dynamics. Finally, also the ideal position of the instantaneous center of steering axis inclination varies under the influence of brake pitch, as will be discussed in detail in chapter 3.3.3.

STD of OPT BSTAM with Full Compensation

Based on the previous definitions on the optimized king-pin inclination angle σ_{opt} and optimal instantaneous center of steering axis inclination (G), the lever arms and steering torque demand (STD) of OPT BSTAM at full compensation ($gcr = 1$) can be computed.

The diagram in Figure 3.4 (c) is showing the according results of the model calculation. Besides the full elimination of T_x, the diagram shows, that the initial balance of T_y and T_z has been restored as to be identical with the standard steering, cf. diagram (a). Consequently, the STD T_F in free cornering ($a_x = 0$) is the same as for the standard steering $T_{F,SLW}$ (solid grey line). However, for growing decelerations, T_F is even sinking, since the aligning effect of T_y is dominating the misaligning one of T_z in the same way as in standard configuration, while T_x is completely cancelled out. Therefore, the rider would be required to apply less and less steering torque towards the outside and finally maybe even to the inside of the curve, the stronger he decelerates. In case of a sudden brake application, his steering effort will be subject to a just as sudden change of sign, which must be avoided in the sense of intuitive controllability and safety.

Coupling of King-Pin Inclination Angle with the Compensation Ratio

Remedy is found in choosing a smaller compensation ratio ($gcr_{red} < 1$) in conjunction with a reduced king-pin inclination angle $\sigma_{red} < \sigma_{opt}$. If this is done by keeping the previously defined instantaneous center (G) for the steering axis inclination motion, the reduced king-pin inclination angle σ_{red} for a given reduced compensation ratio gcr_{red} can be written as follows (see triangles D-B-G and D-E-G in Figure 3.1, left):

$$\sigma_{red} = \arctan\left(gcr_{red} \cdot \tan \sigma_{opt}\right) \tag{3.24}$$

As an example, $gcr_{red} = 0.65$ at a roll angle of $\lambda = 50°$ leads to a value of $\sigma_{red} \approx 9.2°$.

The black lines in Figure 3.6 give an impression for the variation of the king-pin inclination angles σ_{opt} and σ_{red}, which are almost linear over the roll angle range.

STD of OPT BSTAM with Partial Compensation

A variation of the compensation ratio in the range $0 < gcr < 1$ allows to generate steering torque demand curves T_F that lie between those of the OPT BSTAM with full compensation and the standard setting (solid black and grey lines in Figure 3.4 (c)). Figure 3.4 (d) exemplarily shows the results for $gcr_{red} = 0.65$. While the balance between T_y and T_z remains unchanged, a certain amount of T_x that rises with increasing deceleration is allowed through the reduction in compensation ratio. In consequence, the total steering torque demand T_F is now fulfilling the requirement, to be equal with the standard setting for free cornering ($a_x = 0$) and to rise monotonously with increasing deceleration level, however with a much lower gradient, as desired. In the example, the average increase in STD over deceleration amounts to approximately 1.4 $^{Nm}/_{m/s^2}$ For the OPT BSTAM. By a factor of about 4.7, this far below the standard reference with an average increase of more than 6.6 $^{Nm}/_{m/s^2}$.

3.3.3 The Influence of Pitch on the STD and BSTAM Layout

Even though it is derived under the assumption of an unsprung chassis, the mathematical definition of the OPT BSTAM in terms of instantaneous center of steering axis inclination (cf. eq. (3.23)) and king-pin inclination angle (cf. eq. (3.19), (3.20), (3.24)) is universally true for every conventional front suspension / steering system with two steering bearings. Depending on the chassis layout, there may however be practical implications for the implementation of OPT BSTAM on a real sprung chassis.

One such implication arises, when a standard chassis with a telescopic fork front suspension is chosen as baseline, on which the effect of brake pitch causes significant variations in effective caster angle and trail. The mathematical description of the OPT BSTAM remains principally the same, only the caster angle τ has to be replaced in the already known equation set by:

$$\tau_\nu = \tau_0 - \nu \tag{3.25}$$

with τ_0 being the design value of the caster angle in static trim (23°55’ for the test motorcycle) and ν the forward brake pitch angle (set to $\nu = 10°$ for the following example).

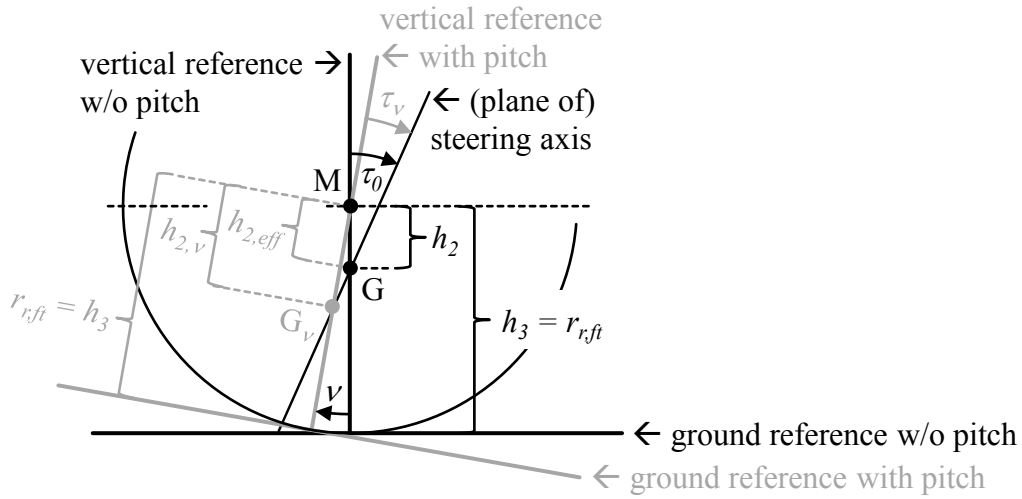

Figure 3.5: Instantaneous center of steering axis inclination of OPT BSTAM under the influence of brake pitch with telescopic fork suspension

Figure 3.5 illustrates, how h_2 (cf. eq. (3.23) and (3.26)) increases under the influence of pitch and the new instantaneous center of steering axis inclination (G_v) moves lower along the vertical connection line between front axle (M) and tire ground contact point:

$$h_{2,\nu} = \frac{fo}{\sin \tau_\nu} \tag{3.26}$$

For the chassis parameters of the test motorcycle and a pitch angle of $\nu = 10°$, $h_{2,\nu} \approx 124.7$ mm compared to the original $h_2 \approx 74.0$ mm in static trim.

In order to achieve the same geometric compensation ratio (*gcr*) with this lower instantaneous center of steering axis inclination (G_v vs. G), the king-pin inclination angle needs to be increased as well. Also this effect is already included in the mathematical definition through replacing the original caster angle τ (in eq. (3.7), (3.19), (3.20), and (3.24)) with τ_v (from eq. (3.25)). It yields the dark grey lines in Figure 3.6 with much higher required inclination angles than for the reference with no pitch, cf. black lines.

Besides implications for the construction space needed for larger displacements of the steering bearing adjustments, this also means, that the control algorithm of an ideal OPT BSTAM with a telescopic fork needs to take the pitch angle into account.

Even though the variable height of instantaneous center of steering axis inclination is theoretically feasible with two independently adjustable steering bearings (cf. Table 4.2, KC 4-6), it stands to question, if this effort is justified by functional superiority of the mathematically ideal to simpler solutions in terms of steering torque demand. In the following, this question is discussed for a “non ideal” OPT BSTAM with a fixed instantaneous center of steering axis inclination and a king-pin inclination angle σ computed on the basis of an invariant baseline caster angle τ_0.

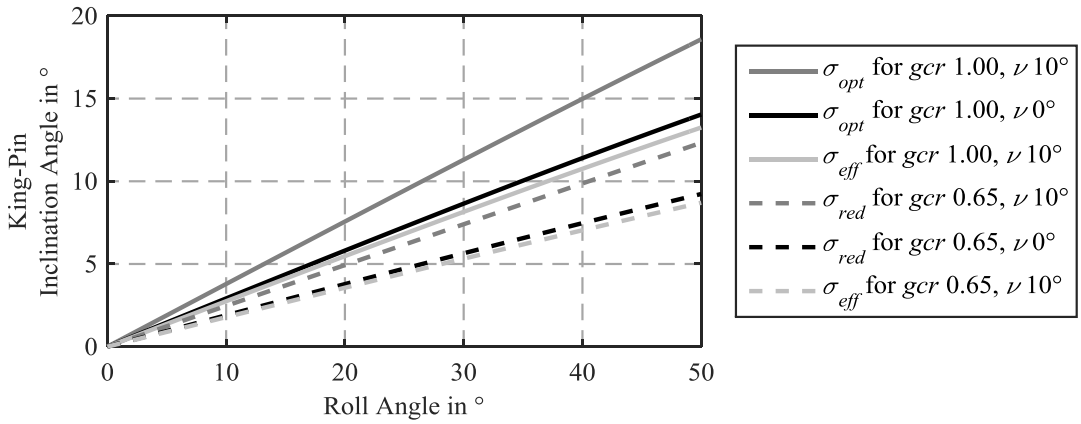

Figure 3.6: King-pin inclination angles in dependency of the roll angle for the OPT BSTAM at full or partial compensation under the influence of brake pitch ($\nu = 10°$) for the mathematically ideal (black and dark grey lines) and non ideal case (light grey lines). Note that the diagram presents effective values in perpendicular frontal projection. The slightly smaller king-pin inclination angles σ_{st} in the steering axis plane can be computed using eq. (3.31).

STD of a Non Ideal OPT BSTAM under the Influence of Pitch

Looking back at Figure 3.5, for this configuration, the effective vertical position of the lower steering bearing in the frontal projection hardly changes under the influence of brake pitch:

$$h_{2,eff} = h_2 \cdot \cos\nu = \frac{fo}{\sin\tau_0} \cdot \cos\nu \tag{3.27}$$

For a pitch angle of $\nu = 10°$, this yields $h_{2,eff} \approx 72.9$ mm (grey reference system), instead of $h_2 \approx 74.0$ mm (black reference system). Since the frontal projection of the instantaneous center is placed slightly higher, also the projected king-pin inclination angle σ needs to be reduced to avoid over-compensation (i.e. $ecr > tcr$, but especially when $ecr > 1$).

Using a twin-fold projection of the original king-pin inclination angle σ (according to equations (3.19), (3.20), and (3.24) and based on τ_0) – from the vertical reference plane (black) to the steering axis plane and back to the new vertical reference (grey) – yields the new effective king-pin inclination angle under brake pitch:

$$\sigma_{eff} = \arctan\left(\tan\sigma \cdot \frac{\cos\tau_0}{\cos\tau_\nu}\right) \tag{3.28}$$

As desired and illustrated in Figure 3.6 (light grey lines), this leads to slightly lower values as in the ideal reference case with no pitch angle (black lines). Referring back to Figure 3.1, left (triangle D-E-G), the compensated portion of the tire scrub radius sr_{cmp} can be computed as follows:

$$sr_{cmp} = \tan\sigma_{eff} \cdot (r_{r,ft} - h_{2,eff}) \tag{3.29}$$

Together with the roll angle dependent tire scrub radius sr_{tir} (eq. (3.4)), the effective compensation ratio *ecr* (cf. eq. (3.5)) is then given by:

$$ecr = \frac{sr_{cmp}}{sr_{tir}} \tag{3.30}$$

yielding slightly lower effective compensation ratios as would be the target $ecr \leq tcr$.

In order to evaluate, what all these deviations from the ideal case mean in terms of steering torque demand, the already known equation set can be used to compute the lever arms and steering torque demand contributes of the front tire contact forces. The results are illustrated in Figure 3.7 for the same boundary conditions as before.

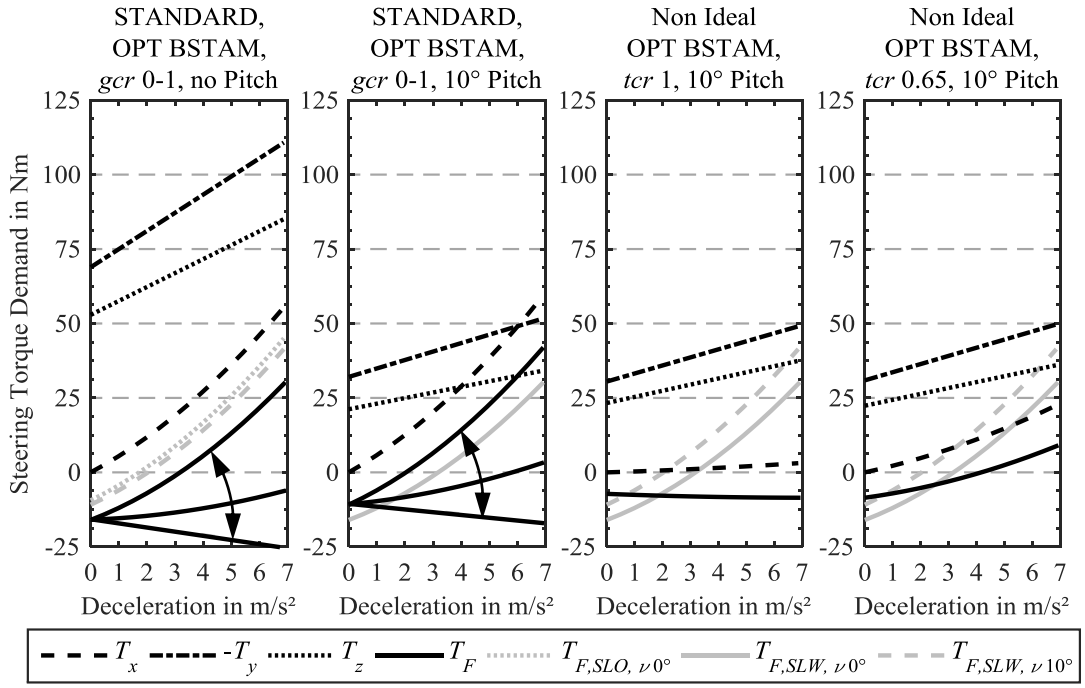

Figure 3.7: Steering Torque Demand generated by front tire forces for different chassis setups at $a_y = 6$ m/s² ($\lambda \approx 35°$) and $a_x = 0 - 7$ m/s² for riding style "lean with" under variation of pitch angle ($\nu = 0$ or 10°). Refer to the main text for a detailed description.

The black lines in the first graph show the STD and its three contributes for the standard chassis with lean with riding style and no pitch. The lowest two solid black lines indicate the STD of the ideal OPT BSTAM at partial ($gcr = 0.65$) and full compensation ($gcr = 1$) while the curved arrow describes the possible field of adjustment. The dashed grey line is the STD of the standard chassis at $\nu = 10°$ brake pitch (cf. second diagram in the figure) which is in the order of 5 to 10 Nm higher than without pitch, but still lower as with 10% lean out riding style and no pitch in the reference corner braking situation, as indicated by the dotted grey line (also cf. Figure 3.2).

In the same manner as for the first diagram in Figure 3.7, the second diagram depicts the situation for the standard chassis and the adjustment field of the ideal OPT BSTAM

under the influence of $v = 10°$ brake pitch. While the more direct transmission ratio of the brake force is to be slightly recognized in the gradient of T_x, the balance of T_y and T_z takes place at lower absolute values and gradients. This leads to an initial offset in STD in comparison with the no pitch reference as indicated by the solid grey line. The mathematically ideal OPT BSTAM is exactly following this offset (of approximately 5.3 Nm in the example, cf. common root of black diagram curves at $a_x = 0$ vs. grey reference).

The third and fourth diagram in Figure 3.7 show the decomposition of steering torque demand contributes for the non ideal OPT BSTAM – with a fixed instantaneous center and pitch angle invariant actuation of steering axis inclination – for full and partial compensation. While the target compensation ratios are $tcr = 1$ and 0.65, the effective compensation ratios that are achieved according to eq. (3.27) through (3.30) are slightly lower, e$cr \approx 0.95$ and 0.62, respectively. The STD of the standard chassis is repeated for reference, the dashed grey line indicating the situation with pitch and the solid grey line the one without.

While, for a given pitch angle, the balance of T_y and T_z remains identical for any compensation ratio $0 \leq gcr \leq 1$ and the corresponding steering axis inclination angles on the ideal OPT BSTAM (cf. first and second diagram in the figure), this does not hold true in the non ideal case, where this balance changes slightly with varying compensation ratio. Therefore, the resulting STD T_F of the non ideal OPT BSTAM starts with a gap towards the standard reference (solid black vs. dashed grey line) in free cornering ($a_x = 0$). Its magnitude is biggest for full compensation and decreases with lower compensation ratios. In the example, it is 3.6 Nm for $tcr = 1$ and 2.3 Nm for $tcr = 0.65$, respectively.

However, it has to be stated, that a pitch angle of 10° does not suddenly occur during free cornering. On the one hand, the absolute pitch angle depends on the deceleration level and on the other, pitching is a transient process that involves a certain time span, due to the motorcycle's pitch inertia. Even for the standard chassis, the resulting steering torque demand curve is therefore always a blend between the model calculations for the situation with pitch and without. Moreover, during free cornering at zero pitch angle (i.e. parallel suspension travel), the geometry of the OPT BSTAM is the same for both the ideal and non ideal case. Consequently, also the stationary steering torque demand is the same, and both curves start from the same origin as for the standard chassis (see first diagram in Figure 3.7).

In the presented example, the "blended" average increase rates from free cornering ($v = 0$, $a_x = 0$) to the end-point of the model calculation ($v = 10°$, $a_x = 0.7g \approx 6.87\ ^{m}/_{s^2}$) are 8.36 $^{Nm}/_{m/s^2}$ for the standard chassis, 2.78 $^{Nm}/_{m/s^2}$ for the ideal OPT BSTAM at $gcr = 0.65$, and 3.61 $^{Nm}/_{m/s^2}$ for the non ideal OPT BSTAM at $tcr = 0.65$ ($ecr \approx 0.62$). This is a reduction by a factor of 3.0 in the ideal case and by 2.3 in the non-ideal case, corresponding to an efficiency of roughly 77% for the non ideal solution, which even allows further improvements through adaptations in compensation ratio.

In conclusion it can be stated, that – despite the strong influence of brake pitch on the steering geometry of a standard chassis with telescopic fork – even a mechanically more simple and mathematically non ideal implementation of the OPT BSTAM concept proves effective to mitigate the BST effect and to provide a stationary steering torque demand (from tire contact forces) very close or even identical to that of the baseline.

Finally, the less sensitive the baseline chassis is to brake pitch and related changes in caster angle and trail, the closer will a simplified practical implementation of OPT BSTAM be to the ideal case. As already mentioned earlier, this can favorably be obtained on the basis of a hub-center or king-pin steering.

Since the practical functionality of a non ideal OPT BSTAM does not deviate too much from the mathematically ideal case and is even identical at zero pitch angle, a rigid chassis remains the simplified basis for further considerations, if not stated otherwise.

3.3.4 STD of the BSTAM Realized in the Prototype Motorcycle

For the sake of completeness and in anticipation of chapter 4, the results of the model calculation are also shown for the finally realized prototype motorcycle with telescopic fork and excentric adjustment of the upper steering head bearing for a target compensation ratio of $tcr = 0.75$ in Figure 3.4 (e). Since its excentricity is limited to only 8 mm by the available construction space, on the one hand the system immanent variations of caster angle stay conceivably low. With the proposed control algorithm that is limiting the actuation angle of the excenter to $\varepsilon = \pm 80°$ (see chapter 4.2.2), the variations in caster angle τ range between + 0.34° for maximal displacement and + 1.97° in straight running (for "long trail" setup, and opposite sign for "short trail", see chapter 4.2.4). On the other hand, the limited excentricity and actuation angle only allow to achieve a projected king-pin inclination angle of $\sigma \approx 2.12°$. Despite a target compensation ratio of $tcr = 0.75$, this only allows an effective compensation ratio of $ecr \approx 0.69$ in the reference situation with static trim or even less, $ecr \approx 0.62$, with fully compressed fork.

Analyzing the results of the model calculation presented in Figure 3.4 (e) reveals, that the aligning influence of T_y hardly outbalances the misaligning one of T_z while T_x is at the same time desirably reduced. Taken in sum, the real BSTAM shows a stationary steering torque demand ($a_x = 0$) that is about 13 Nm increased with regards to the standard reference, while its overall steering torque demand curve T_F is growing at a desirably low rate of less than 2.3 $^{Nm}/_{m/s^2}$, which is by a factor of 2.9 lower compared to the reference of 6.6 $^{Nm}/_{m/s^2}$. While the increase in stationary STD is inacceptable before the background of typical total STD in the order of 0 to 5 Nm in free cornering (cf. chapter 3.3.1), for decelerations greater than 4 m/s², T_F is already lower than for the reference.

Due to the small king-pin inclination angle, the overall steering torque demand T_F of the real BSTAM as just described resembles that of a parallel BSTAM with reduced com-

pensation ratio (cf. chapters 3.3.1 and 3.4, and compare Figure 3.4 (e) with the second diagram in Figure 3.12). For the same reason it may be assumed that all other neglected influences on the steering torque demand still have approximately the same transmission ratio as for the standard chassis.

As an interim conclusion before the background of the working hypothesis (cf. chapter 1.2), the BSTAM prototype is expected to display the following characteristics in driving experiments (cf. chapter 5):

- A significant increase of stationary steering torque in free cornering.
- A significant reduction of BST kick-in when starting to brake in the turn.
- A small reduction also of the total STD, but only for higher decelerations.
- And consequently: Reductions in steering, roll and course deviations.

These considerations will be taken up again in chapter 3.7 for a refined formulation of hypotheses to be tested in the driving experiments after additional considerations on the influence of brake force distribution in chapter 3.6.

3.3.5 Discussion of Neglected Influences on STD

Among the many influences on STD presented in chapter 2.1.3, so far only the main effect of changing the transfer ratio of tire forces through BSTAM was considered. While the simplified model calculation only included the principal quasi-stationary effects of Brake Pitch and Brake Yaw Moments (cf. chapter 2.1.7), in reality, the tire forces are subject to many more influences. Among others, rolling resistance, aerodynamic effects, driving and braking reaction torques (cf. chapter 3.6), roll and steering dynamics[146] as well as chassis movements play an important role.

However, due to the universal geometric definition of the "neutral" OPT BSTAM layout on the basis of lever arm ratios, changes in F_y and F_z tire forces will produce the same changes for both the standard steering and OPT BSTAM on T_y and T_z, keeping them in the desired balance. Any alteration therein would at the most require an adjustment in the compensation ratio to obtain a STD curve with a desired low progression (cf. chapter 3.3.3 on the influence of pitch). One small deviation in the transfer of tire forces results from neglecting the rolling resistance, which is of special interest only in free cornering. Due to the partial compensation of the scrub radius through BSTAM, also the misaligning influence of the rolling resistance is reduced to a certain extend. Since this effect is estimated to be in the negligible order of only 0.5 Nm for the reference riding situation (cf. chapter 3.6), it does not justify an alteration of the instantaneous center of steering axis inclination from its optimized position, which would cause much greater

[146] Weidele (1994): Bremsverhalten von Motorrädern, Chapter 3.6, p. 50 ff

deviations in STD for rising decelerations through imbalances between T_y and T_z. Hence, the qualitative results of the model calculation remain valid, even for changes in the computation of tire contact forces.

In contrast, and before the background of king-pin inclination angles of 10° or more for an OPT BSTAM setup, the transfer of tire reaction torques (esp. twisting torque), gyroscopic torque, and inertial forces on the steering system – as already listed as secondary effects in Figure 2.17 and briefly addressed in chapter 2.3.6. – require a closer look.

For a free cornering situation, Figure 3.8 gives an idea about their typical magnitudes, how they compose to the total steering torque demand (i.e. the torque applied by the rider), and how they relate to the already regarded contributes of the reactive tire forces.

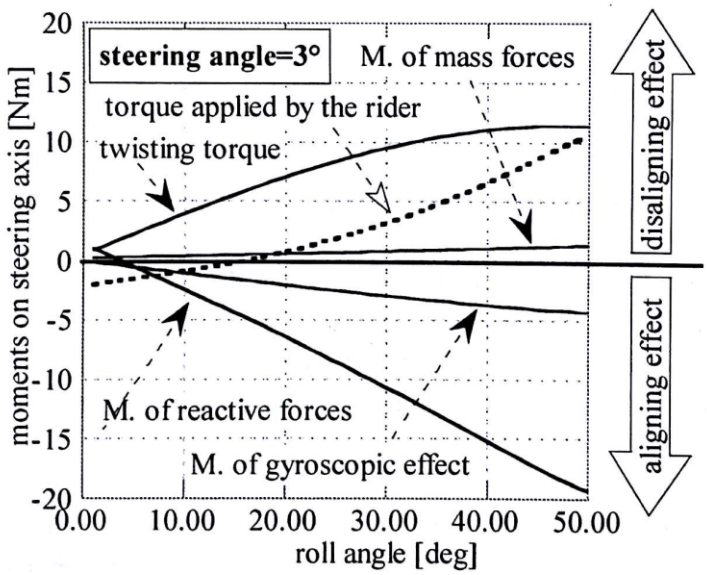

Figure 3.8: Torque applied by the rider and moments exercised around the steering axis[147] in free cornering

Bearing in mind the additional misaligning influence of the BST (T_x component), the tire forces are confirmed to be the dominating effect, directly followed by the twisting torque, with misaligning amplitudes up to 12 Nm, the gyroscopic torque, with aligning amplitudes up to 4 Nm, and the contribute resulting from inertial forces on the steering system's center of gravity, reaching misaligning amplitudes of around 2 Nm.

An estimate for changes in their transfer ratio towards a laterally inclined steering axis is conducted based on the sketches in Figure 3.9 by making use of the mechanical law that torques or moments acting on a rigid body can freely be moved along their perpendicular plane and still exercise the same effect on it.

[147] Cossalter (2006): Motorcycle Dynamics, p. 136, Fig. 4-30

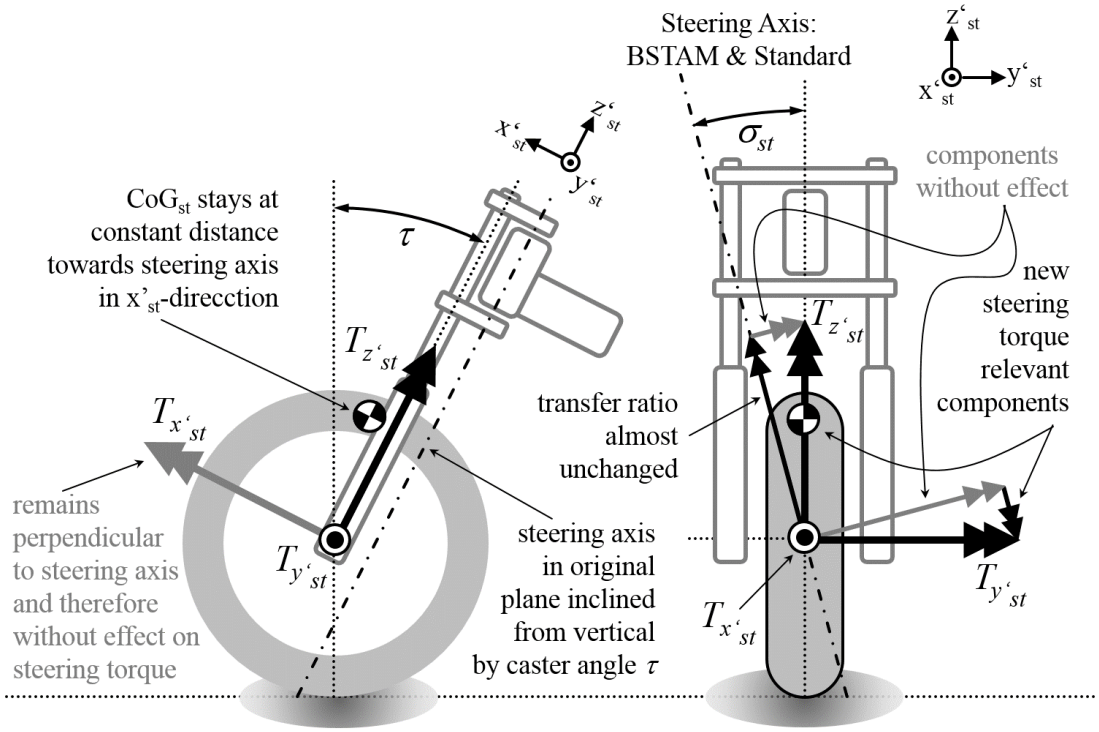

Figure 3.9: Changes in transfer ratio of hitherto neglected steering torque components for an OPT BSTAM chassis with king-pin inclination in a left turn

For a given riding situation and steering angles around zero, the front wheel's orientation and all reaction torques in the wheel hub-center are the same for both OPT BSTAM and standard chassis. Vectorial decomposition of these reaction torques along the steering system's coordinate system (x'_{st}-y'_{st}-z'_{st}) yields three torque components.

Since those in x'_{st}-direction remain perpendicular also towards the inclined steering axis (see Figure 3.9, left), their influence around the steering axis also remains zero. Regarding the transfer ratio of the other two components first requires a re-projection of the king-pin inclination angle σ from the frontal projection plane as defined in Figure 3.1 into the steering axis plane as follows:

$$\sigma_{st} = \arctan(\cos\tau \cdot \tan\sigma) \,, \tag{3.31}$$

yielding slightly smaller inclination angles (e.g. $\sigma_{st} \approx 12.9°$ for $\sigma = 14°$).

Since the y'_{st}-axis coincides with the wheel axle (cf. Figure 3.9, right), the only two paths for a torque transfer between the wheel and fork (or other wheel carrier system) are the friction torque of the brake disks and the negligible friction in the wheel bearings. Their decomposition into the inclined steering axis direction delivers new aligning steering torque relevant components:

$$T_{BSTAM,T_{y'_{st}}} = T_{brake} \cdot \sin\sigma_{st} \,. \tag{3.32}$$

As an experiment of thought concerning a quasi-stationary base brake load, the brake disks can be considered as to be rigidly welded to the calipers in order to balance the tire brake force F_x. Therefore, this quasi-stationary contribute is already considered in the model calculation for the changes in transfer ratios of the tire forces towards the steering axis and does not need to be separately considered. However, the front wheel also needs to be decelerated against its spin inertia which leads to an elevation in brake torque and additional aligning steering torque components during the whole braking process. The effect is however biggest in transient situations, especially when starting to brake, decelerating the wheel inertia in a very short period of time to generate brake slip that subsequently generates the brake force F_x. This phenomenon specific for a BSTAM with king-pin inclination is henceforth called the "inertia effect" and analyzed in detail in the next chapter 3.3.6. After the initial disturbance, the effect could be outbalanced by adjustments in the compensation ratio during the quasi-stationary deceleration phase.

Concerning the final remaining third torque component along the z'_{st}-axis, only marginal changes in transfer ratio are to be expected:

$$T_{BSTAM,T_{z'_{st}}} = T_{z'_{st}} \cdot \cos \sigma_{st} \ . \tag{3.33}$$

With maximal king-pin inclination angles of $\sigma_{st} < 13°$, the cosine delivers reductions of less than 2.6%. While the quasi-stationary torque contributes arising from the tire forces in z'_{st}-direction are already covered in analogy to those in y'_{st}-direction, changes in the additional contributes are not. Exemplarily regarding a maximal twisting torque contribute of 12 Nm from Figure 3.8, the changed transfer ratio means an absolute loss of only 0.3 Nm in the overall steering torque demand for free cornering. This is already negligible, when regarded by itself. Taking into account that $T_{x'st}$ is further reduced through superimposition with the gyroscopic torque, that exceeds the small increasing contribute by the forces acting on the steering system's center of gravity, this effect is even less in free cornering.

However, while the longitudinal distance between the steering system's center of gravity (CoG_{st}) and steering axis along the x'_{st}-axis remains constant through keeping the inclined steering axis in its original plane, a lateral displacement is likely to occur, depending on the chassis type and geometric properties chosen for the realization of BSTAM. As implied in Figure 3.9, right, this may cause additional aligning (or misaligning) effects for a given longitudinal acceleration and vertical position of CoG_{st} towards the instantaneous center of steering axis inclination. For quasi-stationary conditions, these can easily be considered in the choice of compensation ratio. In order to keep steering torque fluctuations low also for quick changes in longitudinal acceleration, it is advisable to keep the steering system's center of gravity CoG_{st} close to the instantaneous center of steering axis inclination, which would for instance be the case for the realization of an OPT BSTAM on the basis of a hub-center or king-pin steering

(cf. Figure 4.1). As a side note, it is impossible to avoid lateral offsets of the steering axis towards the steering system's center of gravity for parallel BSTAM setups, generating aligning disturbances for acceleration and misaligning ones for deceleration which need to be considered in the choice of the compensation ratio.

In interim conclusion of the presented simplified considerations on BSTAM with kingpin inclination, additional quasi-stationary influences might be outbalanced by variations in the transfer ratio of wheel forces, i.e. the choice of compensation ratio for the OPT BSTAM. However, further dynamic influences in transient driving conditions with a real sprung chassis cannot finally be judged with the simplified model.

Therefore, a more detailed analytical model[148] as well as a multi body simulation (MBS) model[149] were created. Both models confirmed the qualitative predictions of the simplified model and that the assumption of similar transfer ratios of the secondary effects towards the steering axis holds especially true for the BSTAM prototype motorcycle with its small steering axis inclination (see chapters 3.3.4 and 4.2). Even though the analysis of the OPT BSTAM in free cornering and corner braking experiments in the MBS generally revealed no significant impact of the secondary effects on the STD, it also confirmed the presence of the "inertia effect" at the beginning of the braking process, which will be addressed in detail in the following chapter.

Moreover, a time-lag in the BSTAM control leads to an inclination of the steering axis to the wrong side when changing from one curve into another of opposite direction. The enlarged effective scrub radius increases the aligning effect of both normal and lateral force (see equations (3.9) and (3.10)). On one hand this facilitates the outward steering impulse necessary to do the directional change; on the other it will (dramatically) worsen the BST effect when a brake maneuver is required[150]. Since the analysis of stand-up tendency and vehicle-rider interaction at BST kick-in require a more sophisticated MBS rider model than the idealized and rigidly coupled one available for this study, this step is finally done in real world experiments as addressed in chapter 5.

3.3.6 The Inertia Effect Created Through a BSTAM with KPI

As pointed out in the previous chapter, the deceleration of the front wheel against its spinning inertia is causing additional aligning steering torque components during the whole braking process for a BSTAM with lateral inclination of the steering axis.

---

[148] Magiera (2011): Simulation Model, Bachelor-Thesis

[149] Vasylyev (2012): Multi Body Simulation, Bachelor-Thesis

[150] This was confirmed in orienting slalom tests with the prototype that required only very little steering input ("almost doing the maneuver all by itself") for a given time lag, speed and cone distance.

While their quasi-stationary portion is anyway overridden by the misaligning BST (i.e. the T_x component) during the steady braking phase and could beneficially be considered through a reduction in compensation ratio, their disturbing influence is biggest in the initial phase of braking. In order to generate the brake force in the contact patch, the tire first needs to build up brake slip. This means, that the brakes are quickly reducing the spinning velocity of the wheel against its inertia and generate the said aligning (outward) steering disturbance just an instant before the brake force and misaligning BST (i.e. T_x) occur and override the effect. The significance of the effect for the layout and riding feel of a BSTAM chassis shall be illustrated by the following rough calculation.

The brake reaction torque that decelerates the front wheel against its spinning inertia is:

$$T_{brake,inertia} = I_{yy} \cdot \ddot{\omega} \tag{3.34}$$

with I_{yy} being the spinning inertia of the front wheel in kgm² and $\ddot{\omega}$ being the reduction in angular velocity in $^{rad}/_{s^2}$ of the same during the initial braking phase.

The initial angular velocity ω_0 of the front wheel in $^{rad}/_{s}$ is defined by the initial velocity v_0 in m/s and the current roll angle dependent tire rolling radius (see eq. (3.3)) in m:

$$\omega_0 = \frac{v_{wheel,ft}}{r_{r,ft}} = \frac{v_0}{r_{r,ft}} \tag{3.35}$$

The percental brake slip s leads to a reduction in wheel speed:

$$\Delta v_{wheel,ft} = s \cdot v_0 \tag{3.36}$$

The time needed to generate the brake slip is limited by the build-up of brake pressure respectively brake torque. In the driving experiments conducted during this study, typical front brake pressure rise times ranged between $0.1 < \Delta t < 0.3$ s, with a higher percentage of lower values close to 0.1 s. Taking these values as reference for a combination of equations (3.35) and (3.36) leads to:

$$\ddot{\omega} = \frac{\Delta v_{wheel,ft}}{r_{r,ft} \cdot \Delta t} = \frac{s \cdot v_0}{r_{r,ft} \cdot \Delta t} \tag{3.37}$$

As already introduced in eq. (3.31), the relationship between the king-pin inclination angle in the frontal projection σ and that in the steering coordinate system σ_{st} is depending on the caster angle τ:

$$\sigma_{st} = \arctan(\cos\tau \cdot \tan\sigma) \tag{3.38}$$

The aligning steering torque disturbance resulting from the generation of initial brake slip is then given as:

$$T_{st,inertia} = T_{brake,inertia} \cdot \sin(\sigma_{st}) \tag{3.39}$$

Filling in from equations (3.3), (3.34), (3.37), and (3.38), it can finally be written as:

$$T_{st,inertia} = I_{yy} \cdot \frac{s \cdot v_0}{(r_{ft} - (1 - \cos\lambda) \cdot r_{c,ft}) \cdot \Delta t} \cdot \sin\left(\arctan(\cos\tau \cdot \tan\sigma)\right) \qquad (3.40)$$

Figure 3.10 shows the results of a parameter study under variation of initial velocity v_0 and king-pin inclination angle σ, conducted under the assumption of a brake slip s = 5%, rise times of 0.1 s respectively 0.3 s, and a roll angle of λ = 35°, for the parameter data of the test motorcycle (cf. appendix A.4.2, with a front wheel inertia of I_{yy} = 0.48 kgm², caster angle τ = 23°55', and tire geometry defined by r_{ft} = 295 mm and $r_{c,ft}$ = 64.6 mm).

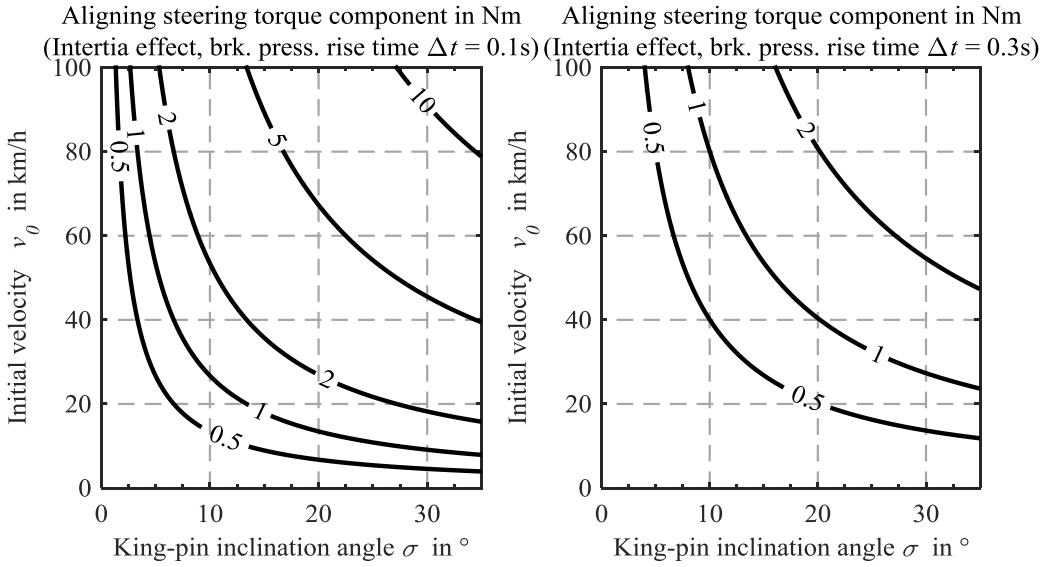

Figure 3.10: Aligning steering disturbance in Nm caused by front wheel inertia while generating 5% brake slip at λ = 35° for a wheel inertia of 0.48 kgm² (average between new and worn tire)

The realized BSTAM prototype features less than 2° projected king-pin inclination angle. For a given initial velocity of 60 to 70 km/h, a steering disturbance in the order of only 0.5 to 1 Nm is to be expected from Figure 3.10, left. It was therefore only very rarely recognized and reported by the test rider and could only once be captured in a measurement (cf. chapter 5.2.2). On one hand, the effect duration is only a few tenths of a second and directly followed by the opposing BST effect. Thus, no real steering angle or even roll angle disturbances occur due to steering system and vehicle roll inertia. On the other hand, capturing of the effect in terms of steering torque measurement requires a relatively pre-tensioned rider. In these regards, the elevated stationary steering torque demand with active BSTAM setups can be seen as a small help, since the test rider typically was very much at ease and relaxed while doing the test rides.

Going back to Figure 3.10 for an OPT BSTAM design, with king-pin inclinations of 5°, 10°, or even more as well as higher speeds of up to 100 km/h not uncommon on rural roads, the effect can assume values of 5 Nm or even more. Even for the short duration,

an unexpected outward steering impulse of that dimension is potentially dangerous, especially when cornering close to the roll angle limits of the vehicle.

Remedy may be found in reducing the front brake pressure increase rates, as exemplarily illustrated in Figure 3.10, right. Choosing a rise time of 0.3 s instead of 0.1 s brings the disturbance to more acceptable levels of only 1 or 2 Nm. Theoretically, this is of cause compromising the minimal achievable braking distance. However, for most practical cases, only partial decelerations are required (and requested by the rider's inputs), so that the reductions in front brake force can be more than outbalanced by a rear-wheel oriented brake force distribution (cf. chapter 3.6), without compromising the braking distance. Moreover, on a real sprung chassis, a braking strategy that activates the rear brake slightly in advance of the front brake is regarded as beneficial. It is triggering a forward shift in wheel load and the pitch process, so that a small misaligning effect on the steering is generated (through T_z) just about the time of the occurrence of the inertia effect. The fact that such a strategy is already incorporated into the C-ABS brake system of the test motorcycle is seen as a further contribute to the rare recognition of the effect.

In conclusion, the inertia effect of a BSTAM with inclined steering axis has the following three facets that need to be considered for the system layout. Firstly, its quasi-stationary portion can beneficially reduce the required compensation ratio – and with it ultimately the construction space. Secondly, the initial aligning disturbance can be mitigated to an acceptable level through limited front brake pressure increase rates and advanced rear brake activation. Finally, also tire wear needs to be considered, since it significantly affects the front wheel inertia and hence the magnitude of the inertia effect (cf. Table A.6).

3.4 Layout and STD of a BSTAM with Parallel Steering Axis Offset

3.4.1 Optimization Potential of a Parallel BSTAM for Neutral Free Cornering

In chapter 3.3.1 the pursuit of a parallel (//) BSTAM was turned down because of the high stationary steering torque demand (STD) in free cornering that arises from such a setup with full compensation ($gcr = 1$). However, it was not yet analyzed, to which extend a //BSTAM can be tuned towards a more "neutral" steering balance.

The first and essential adjustment is a reduction in compensation ratio $0 < gcr < 1$, which allows a certain aligning effect of both F_y and F_z through the remaining effective scrub radius, cf. eq. (3.9) and (3.10) with $\gamma = \lambda$. Despite this measure, the STD in free

cornering will still be increased and further measures need to be taken. Abandoning the pre-condition of keeping the steering axis in the original plane of the super sport base vehicle offers changes in caster angle τ and fork offset *fo* as further tuning options.

In order to find triples of *gcr*, τ, and *fo* which match a more neutral steering behavior, the relative lever ratio has been introduced as optimization criterion on the basis of equations (3.3) through (3.11):

$$\mathcal{L}_{yz} = \frac{\ell_{yz,BSTAM}}{\ell_{yz,sta}} = \frac{\frac{l_{y,BSTAM}}{l_{z,BSTAM}}}{\frac{l_{y,sta}}{l_{z,sta}}} \tag{3.41}$$

It describes, to which degree a modified BSTAM chassis achieves the same balance between the steering torque demand resulting from lateral and normal forces as the standard setup. Figure 3.11 illustrates the results of a parameter study with five different setups of a parallel BSTAM compared to the standard steering geometry.

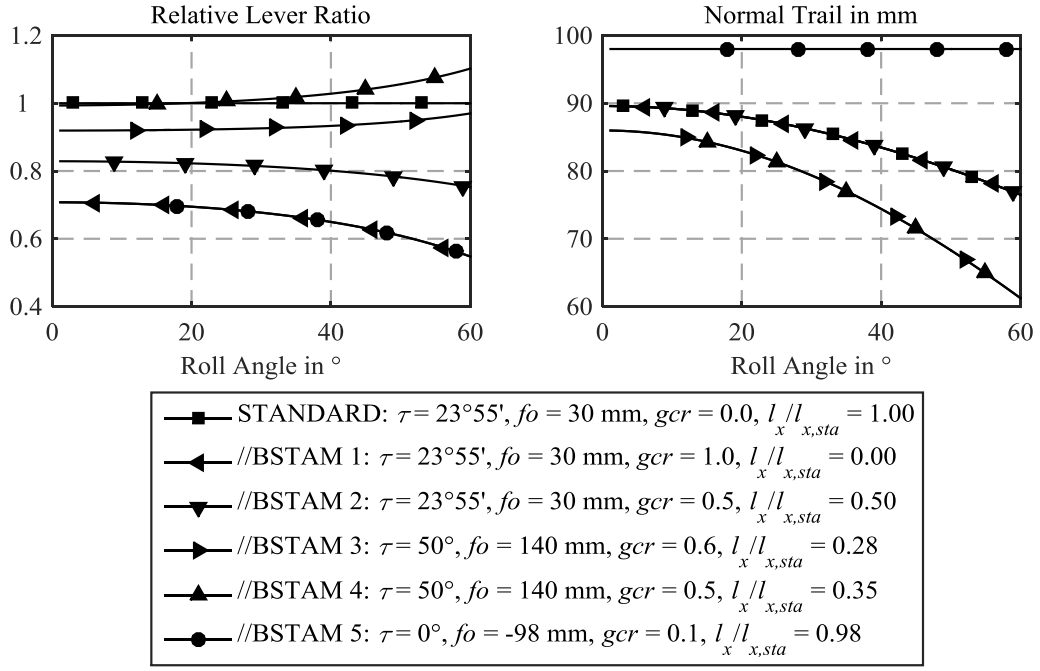

Figure 3.11: Relative lever ratio and normal trail of different parallel BSTAM setups

While the relative lever ratio for the standard setup is necessarily $\mathcal{L}_{yz} = 1$, that of //BSTAM 1 with *gcr* = 1 is strongly decreasing with increasing roll angle. Reducing *gcr* to 0.5 for //BSTAM 2 brings the ratio closer to the neutral target, still with a degression over roll angle. Both, //BSTAM 1 and 2 feature the same degression in normal trail over roll angle as the standard setup. Equations (3.9) and (3.10) show an increase in caster angle τ as a potential means, of weighing the scrub radius *sr* stronger in order to bring the relative lever ratio closer to the neutral target. However, since the normal trail should remain in similar dimensions as for the standard setup for stability and handling

reasons, also the *fo* must be increased along with τ. Setups //BSTAM 3 and 4 show the results for $\tau = 50°$, $fo = 140$ mm and compensation ratios of $gcr = 0.6$ respectively 0.5. This setup produces a progressive curvature of the relative lever ratio over roll angle and for the smaller *gcr* the resulting relative lever ratio even intersects with the target line, which means, that this setup produces "neutral" steering balance for this given roll angle. A systematic variation of the three available design parameters in reasonable bounds ($0 \leq gcr \leq 1$, $0° \leq \tau \leq 90°$, and $-100 \leq fo \leq 200$ mm) revealed, that arbitrary triples of these parameters can be found for the full range of roll angles $0° \leq \lambda \leq 60°$ that fulfill the condition to deviate less than 0.5% from the target in relative lever ratio $\mathcal{L}_{yz}$. However, despite the theoretical feasibility, the physical incorporation of such a strategy would require permanent adjustments in all three variables and make the resulting mechanism far too complex to be practically feasible. Therefore, at the price of higher deviations from the targeted relative lever ratio, such solutions have been sought for that keep constant caster angle τ as well as *fo* and allow adjustments through adaptation of *gcr* only. Such were exemplarily found in the parameters incorporated for setups //BSTAM 3 and 4. As can be seen from Figure 3.11, this is achieved at the cost of a rather strong decrease in normal trail for growing roll angles. Better results concerning the trail value may be achieved by smaller *fo*, however at the cost of neutrality in terms of balance between the aligning influence of the front tire lateral force F_y and normal force F_z. The last extreme parameter variation of //BSTAM 5 is treated in detail in the next chapter, and temporarily laid aside.

Concerning the effectiveness of each solution against the BST, the roll angle invariant lever ratio for the transfer of the brake force F_x is defined by:

$$\mathcal{L}_x = \frac{l_{x,BSTAM}}{l_{x,sta}} . \tag{3.42}$$

It is listed as the last entry for each setup in the legend of Figure 3.11. It is especially worth noting, that despite their rather low compensation ratios, both //BSTAM setups 3 and 4 feature very low values due to the flat caster angle (see equation (3.8)).

In analogy to chapters 3.2 and 3.3, the overall effectiveness of the found solutions is comparatively illustrated on the basis of the STD generated from the front tire forces in the reference free cornering and corner braking situation in Figure 3.12.

The leftmost diagram shows the composition of STD of the standard setup for reference. //BSTAM 2 is maintaining the initial chassis parameters at a reduced compensation ratio of $gcr = 0.5$. Compared to the same setup with full compensation //BSTAM 1 (cf. Figure 3.4 (b)), the aligning influence of T_y is again slightly dominating the misaligning one of T_z, however, not to the same extend, as for the standard reference. Therefore, the stationary steering torque demand ($a_x = 0$) is still unacceptably elevated by about 13 Nm, which is in the same order as for the BSTAM realized in the prototype motorcycle (cf. Figure 3.4 (e)). As a natural consequence of the intermediate compensa-

tion ratio, the increase rate of the overall STD T_F with rising decelerations is also between that of the standard setup and that of //BSTAM 1 with full compensation, leading to a lower STD level for higher decelerations of $a_x > 5.2\ ^{m}/_{s^2}$.

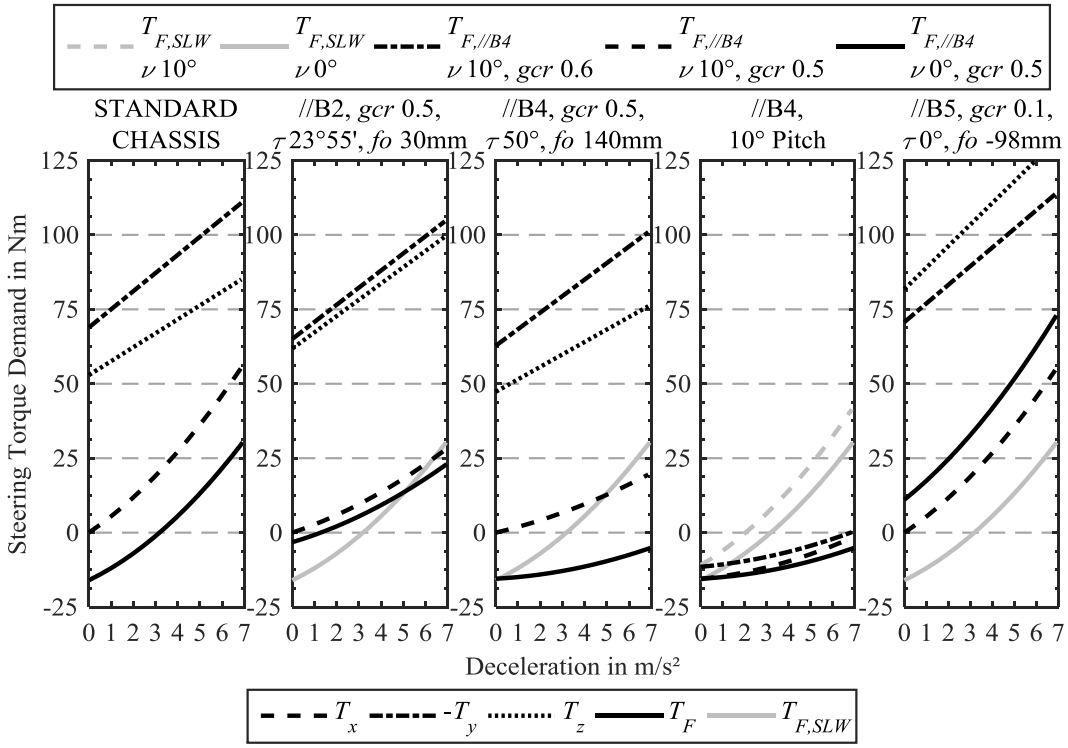

Figure 3.12: Steering Torque Demand generated by front tire forces for different chassis setups at $a_y = 6$ m/s² ($\lambda \approx 35°$) and $a_x = 0 – 7$ m/s². Note that the top legend belongs only to the fourth diagram (//B4, 10° Pitch), while the bottom legend is valid for the other four.

//BSTAM 4 in the central diagram in Figure 3.12 with $\tau = 50°$ shows a stationary steering torque demand close to "neutral" and very desirable small increase in STD with growing deceleration (in average 1.47 $^{Nm}/_{m/s^2}$ compared to 6.6 $^{Nm}/_{m/s^2}$ of the standard setup and 1.4 $^{Nm}/_{m/s^2}$ of the OPT BSTAM with $gcr = 0.65$ in Figure 3.4 (d)). For the chosen setup, this holds qualitatively true over the full range of roll angles from 0° to 60°. However, as shown in the fourth diagram in Figure 3.12, the steering balance of //BSTAM 4 is less sensitive than the standard setup to variations in effective caster angle – like they occur from pitch motions on chassis with telescopic forks. In contrast to the ideal OPT BSTAM layout derived in chapter 3.3.2, which inherently undergoes the same fluctuations as the standard setup, the *gcr* of the presented //BSTAM 4 would need to be adjusted, in that case be increased from $gcr = 0.5$ to 0.6, to compensate a generic caster angle reduction of 10° through brake pitch, if this is at all desired.

Moreover, when bearing in mind that the center of gravity of the steering system will always have a lateral displacement towards the steering axis on a //BSTAM (cf. chapter 3.3.5, Figure 3.9), an additional steering torque component that depends on longitudinal acceleration has to be considered:

$$T_{CoG_{st},//BSTAM} = m_{st} \cdot a_x \cdot \cos\tau \cdot gcr \cdot sr_{tir} \tag{3.43}$$

with m_{st} being the mass of the steering system in kg (including the front wheel), a_x the longitudinal acceleration or deceleration in m/s², τ the effective caster angle in degree, *gcr* the compensation ratio and sr_{tir} the front tire scrub radius according to eq. (3.4).

The following estimate gives an impression of the absolute values to be expected from this effect. Choosing //BSTAM 1 with $\tau = 23°55'$, $fo = 30$ mm, $m_{st} \approx 30$ kg, $a_x = 0.7g$, and full compensation in the reference braking situation delivers a considerable misaligning torque contribute of about 7 Nm, which will be halved for //BSTAM 2. For //BSTAM 3 and 4 with their flat caster angle, it will range between 2.4 and 3 Nm. While this effect could be accounted for by increasing the compensation ratio in dependency of the deceleration level while braking, the effect also occurs with opposite sign (i.e. an aligning influence) when accelerating. The steering torque applied by the rider would then need to be more inward (or less outward).

Finally, the radical geometry of //BSTAM 3 and 4 with their flat caster angle will significantly affect the handling and maneuverability characteristics through a more indirect steering, an increased aligning influence of the gyroscopic torque, and a decreased misaligning one of the twisting torque. Hence it is of utmost importance to consider all these influence factors for the design and layout of a real //BSTAM system.

3.4.2 Considerations on Effectiveness of Multi-Lever Steering

A multi-lever steering like the four-bar linkage presented in chapter 2.3.4 (cf. Figure 2.24), is a special form of //BSTAM, with steering angle dependent lateral steering axis displacement and thus compensation ratio.

The order of typical geometry variations that are possible with such a setup are exemplarily illustrated in Figure 3.13 on the basis of geometry parameters estimated from the patent sketch shown in Figure 2.24. Before the background of the inherently small steering angles of motorcycles (cf. chapter 2.1.5), it seems rather unlikely to achieve considerable compensation ratios and benefits regarding the BST effect. However, for the reason of its purely mechanical design, the system is still worth a closer look.

For the last extreme variation of //BSTAM 5 in Figure 3.11, the chassis parameters have been adapted to approach those of the four-bar linkage presented in Figure 3.13.

The caster angle is set to perpendicular ($\tau = 0$) in conjunction with a negative $fo = -98$ mm, leading to a constant (normal) trail with $n = nt$. As can be seen from equations (3.9) and (3.10), this makes the lever ratio ℓ_{yz} according to eq. (3.11) of the last setup invariant to the current scrub radius *sr* and the *gcr*, leading to the same, only roll angle dependent, lever ratio as for //BSTAM 1 with full compensation, cf. eq. (3.15):

$$\ell_{yz,//BSTAM\,5} = \ell_{yz,//BSTAM\,1} = \frac{\cos\lambda\cdot nt + \sin\lambda\cdot\cancel{\sin\tau}\cdot sr}{\sin\lambda\cdot nt - \cos\lambda\cdot\cancel{\sin\tau}\cdot sr} = \frac{\cos\lambda\cdot nt}{\sin\lambda\cdot nt} = \frac{1}{\tan\lambda}\,. \qquad (3.44)$$

On the one hand, this characteristic is pre-destining a perpendicular caster angle $\tau = 0$ for the use with multi-lever steering systems, with their steering angle dependent compensation ratio and scrub radius (see chapter 2.3.4 and Figure 3.13). However, on the other hand, and in further analogy to //BSTAM 1 (cf. Figure 3.4 (b)), this also leads to an increased stationary steering torque demand, by flipping the balance between the T_y and T_z contributes to the STD in favor of the misaligning effect of T_z (cf. last illustration in Figure 3.12). However, despite the identical lever ratio (cf. eq. (3.44)) and also relative lever ratio (cf. Figure 3.11), the absolute levers and steering torque contributes differ from those of //BSTAM 1 due to the differences in basic chassis parameters. While the increase in stationary steering torque demand by about 25.6 Nm is already unacceptably high for //BSTAM 1, that of //BSTAM 5 is still exceeding it with approximately 27 Nm increase.

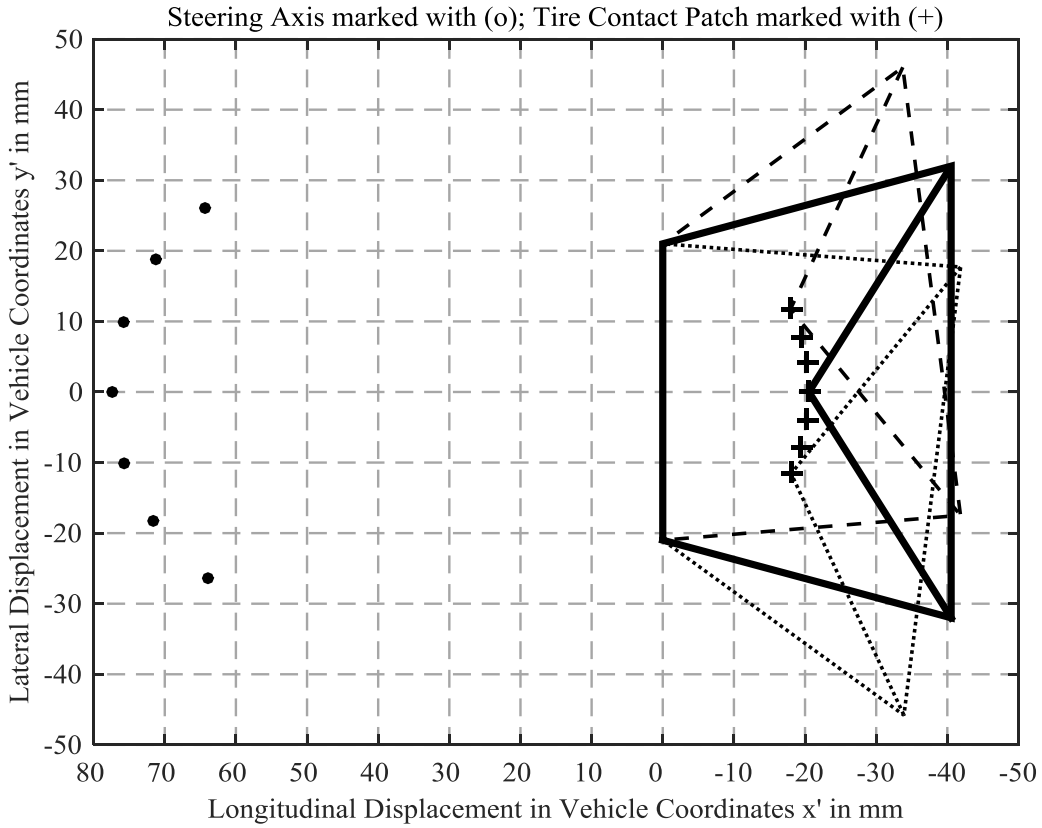

Figure 3.13: Geometry of a Four-Bar Linkage steering system with $\tau = 0$, $n = nt = |fo| = 98$ mm, showing displacements of steering axis and tire contact patch in upright vehicle position for a variation in steering angle over a range of 42°. The slight asymmetry of the diagram results from the connection of the handlebars to one of the connecting rods in the simulation model[151].

[151] Vollmuth (2012): Analysis of Multi-Lever-Suspension, Student Research Project

In order to evaluate the effectiveness against the brake steering torque, the compensation ratio achieved in the reference corner braking maneuver has rather optimistically been set to $gcr = 0.1$. As a downside of the perpendicular caster angle, this only yields a lever ratio for the transfer of the brake force F_x of:

$$\mathcal{L}_{x,//BSTAM\,5} = \frac{l_{x,//BSTAM\,5}}{l_{x,sta}} = 0.9845\ . \tag{3.45}$$

In conjunction with the unfavorably changed balance between T_y and T_z, that yields an even stronger increase in steering torque demand for growing decelerations than for the standard setup (in average 8.9 $^{Nm}/_{m/s^2}$ compared to 6.6 $^{Nm}/_{m/s^2}$, cf. last illustration in Figure 3.12).

Besides its benefits in stability and direct handling characteristics resulting from the perpendicular caster angle and constant trail, that have been well approved on the racetrack and even in off-road use[152], the analyzed multi-lever steering performs even worse than the reference standard chassis concerning both the stationary steering torque demand arising from tire forces as well as the total steering torque level for increasing decelerations. The additional consideration of the hitherto neglected effects is expected to make the situation even worse, since the perpendicular caster angle will lead to a more direct transmission of the misaligning twisting torque and a decoupling from the aligning gyroscopic reaction torque components from the steering (cf. chapter 3.3.5).

3.5 Conclusions on Optimal BSTAM Design

The front tire contact forces in all three spatial directions and their respective lever arms towards the steering axis were identified as the main contributors to the total steering torque demand (STD). The balance between lateral and normal forces was found to be essential for the "neutral" STD of a standard chassis setup in free cornering. While the lateral force F_y acts aligning, the normal Force F_z acts in opposite direction via the normal trail, and both forces have aligning contributes via the scrub radius. If the latter is reduced or fully compensated through a BSTAM in order to reduce the misaligning effect of the brake force F_x, also the aligning portion of both lateral and normal force is breaking away, leading to an increase in STD. Analytical investigations show, that the initial "neutral" balance between F_y and F_z can be restored through BSTAM layouts with either lateral inclination or parallel displacement of the steering axis.

The OPT BSTAM concept keeps caster angle and fork offset of the standard setup and uses roll angle dependent king-pin inclination angles of up to about 10° at a geometrical

[152] TIER – virtual: www.tiermotor.com, last access: 2014-11-15

compensation ratio of $gcr = 0.65$. It is based on a universal analytic definition of instantaneous center of steering axis inclination at the intersection of the original steering axis with the connection line from front wheel hub-center to tire contact point in upright vehicle position, which is typically below the front wheel hub-center, by about 74 mm in the example for the test motorcycle in static trim. In an ideal case, this definition inherently allows to keep the "neutral" standard steering balance of F_y and F_z for all roll angles, compensation ratios and changes in caster angle, as they occur e.g. due to pitch motion (see chapter 3.3.3 for non ideal cases). Despite its analytic elegance and possibility to account for hitherto neglected influences on the STD through adaptations in compensation ratio and king-pin inclination angle, the following boundary conditions need to be considered for practical implementations.

Firstly, an ideal OPT BSTAM that is based on a chassis with telescopic fork requires a variable position of the instantaneous center of steering axis inclination in conjunction with pitch angle dependent compensation ratios. This is theoretically feasible with two independently adjustable steering bearings. However, also more simple solutions – with a fixed instantaneous center, adjustment of only one steering bearing, and pitch angle invariant target compensation ratios – are effective against the BST effect without significant compromises to the neutral steering behavior (cf. chapter 3.3.3).

Secondly, the "inertia effect" that arises from the deceleration of the front wheel inertia has a twin-fold influence. While its quasi-stationary portion can beneficially reduce the required compensation ratio, the aligning disturbance when generating the initial brake slip can be mitigated (from up to about 5 Nm) to an acceptable level (of 1-2 Nm) through limited front brake pressure increase rates and advanced rear brake activation (cf. chapter 3.3.6).

Thirdly, potentially (mis-)aligning influences resulting from longitudinal inertia forces on the steering system's center of gravity (CoG_{st}), can be addressed by choosing a chassis design that allows to keep CoG_{st} close to the instantaneous center of steering axis inclination, such as a hub-center or king-pin steering (cf. chapter 3.3.5).

Finally, the concept suffers a negligible loss in misaligning steering torque resulting from rolling resistance (in the order of 0.5 Nm), that cannot be compensated through adjustment of the compensation ratio in free cornering.

As an alternative solution, also parallel BSTAM concepts were investigated, since the perpendicularity of their steering and wheel axes excludes the disturbances through the inertia effect per definition. Even though "neutral" steering balance cannot be kept for full compensation of scrub radius with parallel BSTAM setups, systematic parameter variations revealed configurations with rather huge caster angles and fork yoke offsets as optimization direction, yet with rather low values in normal trail for large roll angles. Exemplarily, a setup with $\tau = 50°$, a fork offset of $fo = 140$ mm, and compensation ratios

in the range of $0.5 \leq gcr \leq 0.6$ was found to deliver a STD from the tire contact forces that is desirably close to "neutral" as well as being effective against the BST. However, such geometry parameters are rather attributed to vehicles of the chopper / cruiser / custom category. Since they will make the steering transmission more indirect and increase the aligning influence of the gyroscopic torque while decreasing the misaligning one of the twisting torque, the expected handling and maneuverability characteristics are not really promising for a sports motorcycle. As another major downside, parallel BSTAM setups always suffer from steering interferences caused by longitudinal inertia forces on the steering system's center of gravity, which can easily reach disturbance levels in the order of ±7 Nm (aligning for acceleration and misaligning for deceleration) and therefore must be considered during the layout of a system to be incorporated in reality.

In comparison to the standard chassis, an exemplary investigation on the effectiveness of a multi-lever steering (i.e. a four-bar linkage) showed downsides in both the free cornering and corner braking steering torque demand and is not further pursued.

Summing up, both the OPT and parallel BSTAM are effective against the BST, but each version has specific tradeoffs in its layout. As an important note (especially to custom bike builders that might be interested in the BSTAM technology), it must be considered, that all model calculations are based on the steering balance and front tire dimensions of a super sports motorcycle. It is therefore of utmost importance to analyze the desired steering characteristics of the target vehicle and redo the calculations, e.g. for much wider tires or a higher target steering torque demand in free cornering, that better matches the vehicle characteristics, including the typically much wider handlebars.

Finally, as the presented study was based on a strongly simplified quasi-stationary model calculation, it can only be a qualitative hint for the layout of a BSTAM system. Further research is required to account for dynamic effects and all other hitherto neglected influence factors on STD. In the framework of this study, this aspect is addressed by driving experiments as presented in chapter 5.

3.6 Effectiveness Comparison of BSTAM and Standard Chassis

The quasi-stationary model calculations presented in chapter 3.2 revealed, that the riding style "lean in" is favorably reducing the Steering Torque Demand (STD) of the standard chassis in corner braking maneuvers. Further improvements are to be expected from the implementation of Cornering Adaptive Brake Force Distributions (CA-BFD)

as discussed in chapters 2.3.3 and 2.4. Before that background, the question arises, in how far a BSTAM can still benefit the rider beyond a combination of these measures.

In order to address this question and derive hypotheses for the expected behavior of the baseline vehicle compared to the BSTAM prototype in real world experiments, the former corner braking model is extended to facilitate a simulation of a complete braking process with different BFD (cf. Table 3.2) at maximal and also partial decelerations, since these are of special interest regarding typical accident situations (cf. chapter 1.1).

On this basis, the STD arising from the tire forces is comparatively investigated in relevant example cases for the different chassis setups and the simulated brake force distributions are qualitatively compared to real ones captured of the test motorcycle. Finally, conclusions are drawn and refined hypotheses are derived, which are to be tested in the real riding experiments.

3.6.1 Model Extensions & Overview of Simulated Experiments

Model Extensions

While the influence of aerodynamic effects (in terms of drag and lift force as well as aerodynamic pitch moment) and rolling resistance on the tire forces and STD is in the order of only 2% for the considered experiments and was therefore neglected in the previous chapters, they are significantly influencing the braking distance for varying BFD in the order of 10% and are henceforth taken into account.

In addition, the driving torque of the rear wheel has been modeled, allowing to analyze wheel load changes when disengaging the clutch and to perform (front) braking maneuvers with clutch engaged (stalling the engine). Furthermore, also an option to investigate the special challenges of a narrowing radius turn was implemented.

It is important to note, that the extended model is still a quasi-stationary one, calculating the tire contact forces under the simplified assumptions of an unsprung chassis with constant wheelbase and caster angle as well as undeformable tires. Even though the transient phase at the beginning of the braking process, i.e. brake pitch and fork compression, are missing, the qualitative result remains valid (cf. chapter 3.3.3). The utilized mathematical approach and corresponding equation set are presented in appendix A.3.2.

Simulated Test Maneuver and its Initial Conditions

In analogy to the real riding experiments (cf. chapter 5), a simulated corner braking maneuver consists of:

- An initial free cornering phase, with clutch engaged and a driving torque at the rear wheel, that is needed to overcome the aerodynamic and rolling resistances.
- Disengaging the clutch and a free rolling phase, decelerated by aerodynamic and rolling resistances – or leaving the clutch engaged, keeping the initial driving torque also during the brake maneuver.
- The brake maneuver until reaching complete halt.

The initial conditions were chosen to be in line with both the prior simulations and riding experiments. On a turn radius of $R = 50$ m, an initial lateral acceleration of $a_y = 6$ m/s² and roll angle of $\lambda \approx 35°$ are reached for an initial velocity of $v_0 = 10\sqrt{3} \approx 17.32$ m/s² (62.35 km/h). In order to obtain the same speed at the start of the braking phase also for the experiments with clutch disengaged, their beginning speed needs to be slightly increased due to the resistance losses in the free rolling phase. In the example with only 0.5 seconds of free rolling, this speed is $v_{0+} \approx 17.55$ m/s (63.2 km/h). Finally, the available friction coefficient is set to $\mu_0 = 1$.

Overview of Investigated Brake Force Distributions

The investigated variations in brake force distribution and deceleration level comprise the following 9 cases as listed in Table 3.2.

Table 3.2: Overview of Simulated Brake Force Distributions

Case No.	Deceleration Level	Brake Force Distribution (BFD)		Clutch
1	maximal (limited by friction potential or brake flip-over)	bb-eq	Use of both brakes, with equal use of friction potential (“ideal” BFD)	disengaged
2		ft	Front braking only	
3				engaged
4		rr	Rear braking only	disengaged
5	partial $a_{x,target} = 0.5g$ (same limits as above)	bb-eq	Use of both brakes, with equal use of friction potential (“ideal” BFD)	disengaged
6		bb-rr	Use of both brakes, with maximal use of friction potential at the rear	
7		ft	Front braking only	
8				engaged
9		rr	Rear braking only	disengaged

Overview of Investigated Chassis Setups

On the previously presented basis, the STD arising from the tire forces is comparatively investigated in relevant example cases for the following different chassis setups:

- The standard chassis with all three riding styles (lean in, with, and out, with 10% changes in vehicle roll angle for the computation of lever arms at maintained tire forces from lean with case),
- The BSTAM realized in the prototype motorcycle with two different target compensation ratios (*tcr* = 0.5 and 0.75), as well as
- The OPT BSTAM (with a compensation ratio of *gcr* = 0.65).

3.6.2 Maximal Braking on Constant Radius

Just as in the previous quasi-stationary model calculations as a "snap-shot" of the initial conditions, a corner braking maneuver with an ideal BFD and equal levels of friction potential used at both wheels is regarded and discussed as an example, achieving a maximal possible mean deceleration of a_x = 9.51 m/s² (case no. 1).

Figure 3.14 gives an impression of how the characteristic values of the corner braking maneuver develop over the whole time course of the simulated maneuver.

From top to bottom, the left column presents the course of roll angle, speed, deceleration, tire forces in front and rear, and the utilized friction potential at both wheels. It is remarkable to note how quickly the deceleration level is approaching the higher level of straight running conditions with sinking speed and roll angle. Moreover, the changes in tire forces when disengaging the clutch (t = -0.5 s) are clearly visible despite the rough scaling of the graph. Concerning the main steering torque relevant components, the lateral force at the front wheel is growing by 48 N from 863 N to 911 N, while the front wheel normal force is increasing by even 84 N from 1383 N to 1467 N, which results in a clearly recognizable alteration in steering torque demand also in the experiment.

As a result of the maximum target deceleration that is only limited by force transfer or brake flip-over, the rear tire contact forces reach very low values just slightly above zero. Both the normal and lateral force are falling at the same time in a given relationship due to the brake pitch and brake yaw effects (cf. chapter 2.1.7). This explains why the transition to rear wheel lift-off and balancing only on the front wheel can be very smooth in a real world situation and how a rear wheel lift-off mitigation function of the brake system can assist the rider, who possibly may not even be aware of the situation.

The utilized friction potential is slightly elevated at the rear wheel due to the driving force (-1 s< t < -0.5 s), nearly identical to the front wheel's value in the coasting phase (-0.5 s < t < 0 s), and identical during the full deceleration phase afterwards (t > 0 s).

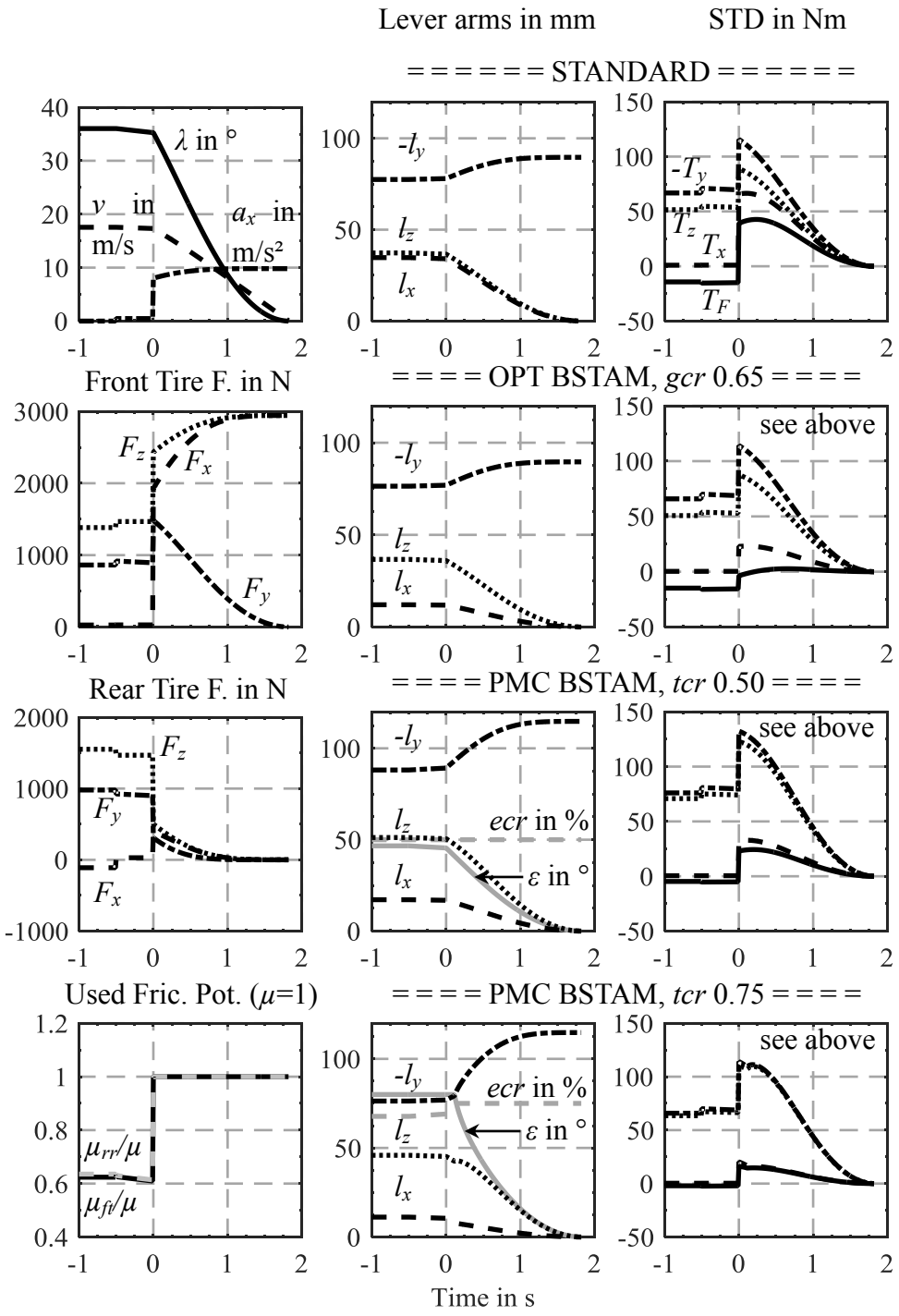

Figure 3.14: Simulated time course of roll angle, speed, deceleration, tire forces, utilized friction potential, lever arms, BSTAM excenter angle, effective compensation ratio, and composition of STD for four chassis setups at max. deceleration (a_x = 9.51 m/s²) with ideal BFD (v_0 = 17.3 m/s on a turn radius of R = 50 m, $a_{y,0}$ = 6 m/s², $\lambda_0 \approx 35°$). Note the negative sign of l_y and T_y.

From top to bottom, the central and right column in Figure 3.14 illustrate, how the lever arms and the composition of tire force based steering torque demand develop over the time course, for the standard chassis setup, the OPT BSTAM (with gcr = 0.65), and the prototype BSTAM with two different compensation ratios (tcr = 0.5 and 0.75). It is

worth noting, that ly and T_y are displayed with a negative sign for reasons of compactness of the illustration. As expected, all BSTAM configurations feature a lower effective lever arm l_x of the front brake force in accordance with their compensation ratios. While the balance between l_y and l_z, and consequently also T_y and T_z, is always kept for the OPT BSTAM, the prototype BSTAM shows the already known divergences (cf. chapter 3.3, Figure 3.4 (e), and chapter 3.3.4).

In the bottom two illustrations of the central column, the excenter adjustment angle ε and effective compensation ratio (*ecr*) of the prototype BSTAM are additionally displayed. While, the lower target compensation ratio ($tcr = 0.5$) can be met right from the beginning of the maneuver, the excenter is reaching its limit angle of $\varepsilon = 80°$ for the higher value ($tcr = 0.75$), leading to a reduction in effective compensation ratio at the beginning of the maneuver (to $ecr \approx 0.69$). As confirmed by the real world experiments, this has recognizable consequences also in the total steering torque demand that will be discussed in the following for the various setups on the basis of the more detailed illustration in Figure 3.15 and corresponding information provided in Table 3.3.

Since the STD arising from the tire forces is in reality superimposed by further contributes, the absolute values of the model calculation are to be regarded as relative tendencies. The lower (the more negative) the values, the less steering torque the rider needs to apply outside the curve and vice versa, as already explained in preceding chapters.

Starting with the standard chassis and lean with riding style (SLW) for reference, the free cornering steering torque demand drops by 1.1 Nm when releasing the clutch ($t = -0.5$ s) and jumps by 54 Nm upon brake kick-in ($t = 0$). After a characteristic peak is reached following a further increase ($t \approx 0.25$ s), the STD demand drops to zero, when straight running conditions and a complete halt are reached.

In addition to Figure 3.15, Table 3.3 contains also results of the prototype BSTAM with passively centered steering axis (BPC). Since its steering torque demand only differs in the order of about 1 Nm from the standard reference (SLW), it is not further discussed.

In accordance with the previous considerations, the STD in free cornering and coasting (T_{crc} and T_0) show a reduction (or increase) for the lean in (or lean out) riding style in the order of 6 to 7 Nm, while the reduction (or increase) in steering torque upon brake kick-in or during the braking process (ΔT_0 and ΔT_{max}) range in the order of 8 to 10 Nm.

The prototype BSTAM shows the already known disadvantageous increases in stationary steering torque demand (T_{crc} and T_0) which are in the order of 9 to 10 Nm for the lower and 12 to 13 Nm for the higher target compensation ratio. The drop in STD upon disengagement of the clutch (ΔT_{clutch}) is however favorably reduced by 0.6 or 0.8 Nm, respectively.

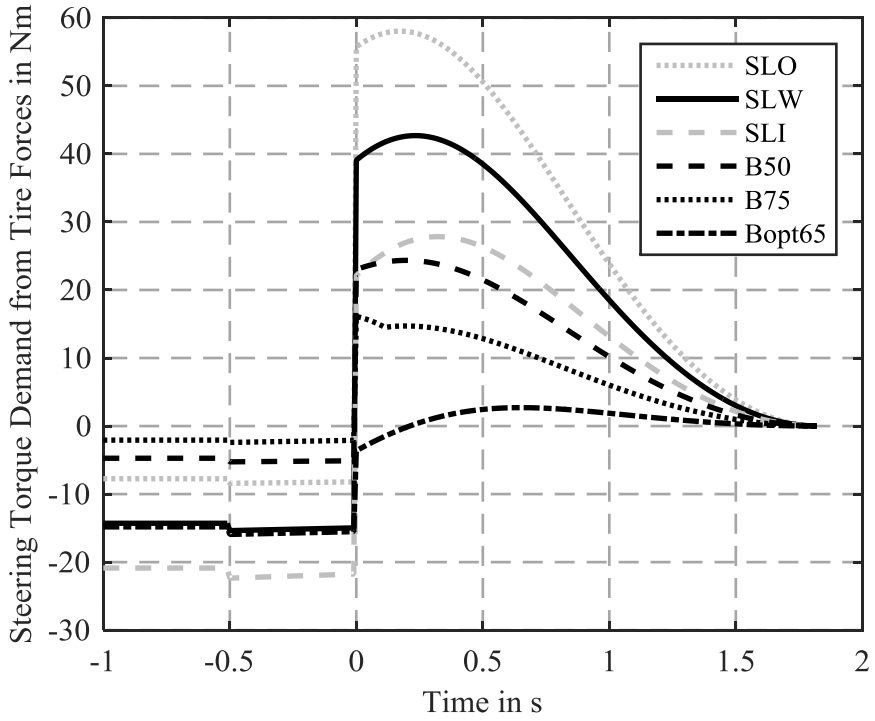

Figure 3.15: Steering torque demand arising from tire forces during maximal corner braking (a_x = 9.51 m/s²) with ideal BFD (from v_0 = 17.3 m/s on a turn radius of R = 50 m, $a_{y,0}$ = 6 m/s², $\lambda_0 \approx 35°$) for different chassis setups (SLO/SLW/SLI: Standard, Lean Out/With/In; B50 and B75: Prototype BSTAM, with *tcr* = 0.5 and 0.75; Bopt65: OPT BSTAM with *gcr* = 0.65)

Table 3.3: Characteristic values corresponding to Figure 3.15. From left to right: Steering torque demand (STD) in free cornering (T_{crc}), changes through disengagement of the clutch (ΔT_{clutch}), the STD at the beginning of braking (T_0), its initial (ΔT_0) and maximal increase (ΔT_{max}) for the different chassis setups (BPC: Prototype BSTAM with passively centered steering axis). The left part of the twin columns contains the absolute (abs.) value of the simulation results and the right one its relative (rel.) value towards the reference case Standard, Lean With (SLW). A negative relative value means a relief for the rider, i.e. a less outward steering torque.

Setup	T_{crc} [Nm]		ΔT_{clutch} [Nm]		T_0 [Nm]		ΔT_0 [Nm]		ΔT_{max} [Nm]	
	abs.	rel.	abs.	rel.	abs.	rel.	abs.	rel.	abs.	rel.
SLO	-7.7	6.6	-0.7	0.4	-8.2	6.8	63.9	9.9	66.3	8.6
SLW	**-14.3**	**0**	**-1.1**	**0**	**-15.0**	**0**	**54.0**	**0**	**57.7**	**0**
SLI	-20.9	-6.6	-1.5	-0.4	-21.8	-6.8	43.9	-10.1	49.6	-8.1
BPC	*-13.4*	*0.9*	*-1.1*	*0.0*	*-14.1*	*0.9*	*53.6*	*-0.4*	*57*	*-0.7*
B50	-4.7	9.6	-0.5	0.6	-5.1	9.9	28.1	-25.9	29.5	-28.2
B75	-2.1	12.2	-0.3	0.8	-2.1	12.9	18.2	-35.8	18.2	-39.5
Bopt65	-14.8	-0.5	-1.1	0.0	-15.5	-0.5	11.9	-42.1	18.2	-39.5

Most importantly, the kick-in of the brake steering torque and maximal increases in STD level (ΔT_0 and ΔT_{max}) can be greatly reduced in the order of 25 Nm to almost 40 Nm, representing a reduction of about 70% compared to the reference (SLW) and a benefit against what can be achieved by lean in riding style (SLI) by a factor of 2.5 to 5. The STD level of the BSTAM setup with $tcr = 0.5$ (B50) over the time course of the maneuver is not far below what can be achieved by the lean in riding style with the standard chassis (SLI), which confirms subjective impressions from the riding tests.

While the latter curve (B50) still shows the characteristic peak in STD, this is no longer the case for $tcr = 0.75$ (B75), because the excenter reaches its adjustment limits (i.e. $\varepsilon = 80°$), producing a characteristic kink in the STD curve, when the excenter finally begins turning with sinking roll angles.

Finally, the OPT BSTAM (Bopt65) is only lacking a misaligning steering torque contribute from the rolling resistance in free cornering, which is in the negligible order of 0.5 Nm (cf. T_{crc} and T_0), while the STD difference upon clutch release is the same as for the reference (SLW). It achieves 42.1 Nm or almost 78% reduction in initial STD deviation (ΔT_0) and shows the lowest STD level of all setups over the whole time course.

While these findings only support the previous statements, the analysis becomes more interesting for partial decelerations with changing BFD and experiment type.

3.6.3 Partial Braking on Constant Radius with Different BFD

While the initial free cornering conditions, including the disengagement of the clutch and the free coasting phase, are identical to the previously presented maximal braking example, the influence of the brake force distribution (BFD) on the steering torque demand (STD) level shall be taken into focus.

Starting with the standard chassis reference (SLW), the characteristic peak in the torque curve is vanishing, if only the front brake is applied (cf. case no. 7 on the left in both Figure 3.16 and Table 3.4). Despite the lower deceleration level of only 0.5g, the STD jumps by 39.5 Nm, which is still 73% of the 54 Nm to be dealt with for maximal deceleration and ideal BFD, as shown in the previous section. Choosing an ideal BFD (case no. 5, center) already lowers the kick-in to 25.7 Nm, while a rear-oriented BFD with full exploitation of the available friction potential can release the front wheel even from more brake load and reduces the jump to only 15.9 Nm, which is a 60% reduction compared to using only the front brake (case no. 6, cf. Figure 3.16 and Table 3.4, right).

The same holds qualitatively also true for the other setups, with kick-in reductions for lean in riding style and active BSTAM setups vs. a super-elevation for lean out. While the latter (for SLO) is in the order of 4.5 to 6.5 Nm, equivalent to 28% or 16% increase compared to the reference (SLW), the benefit of lean in (SLI) ranges in the same order.

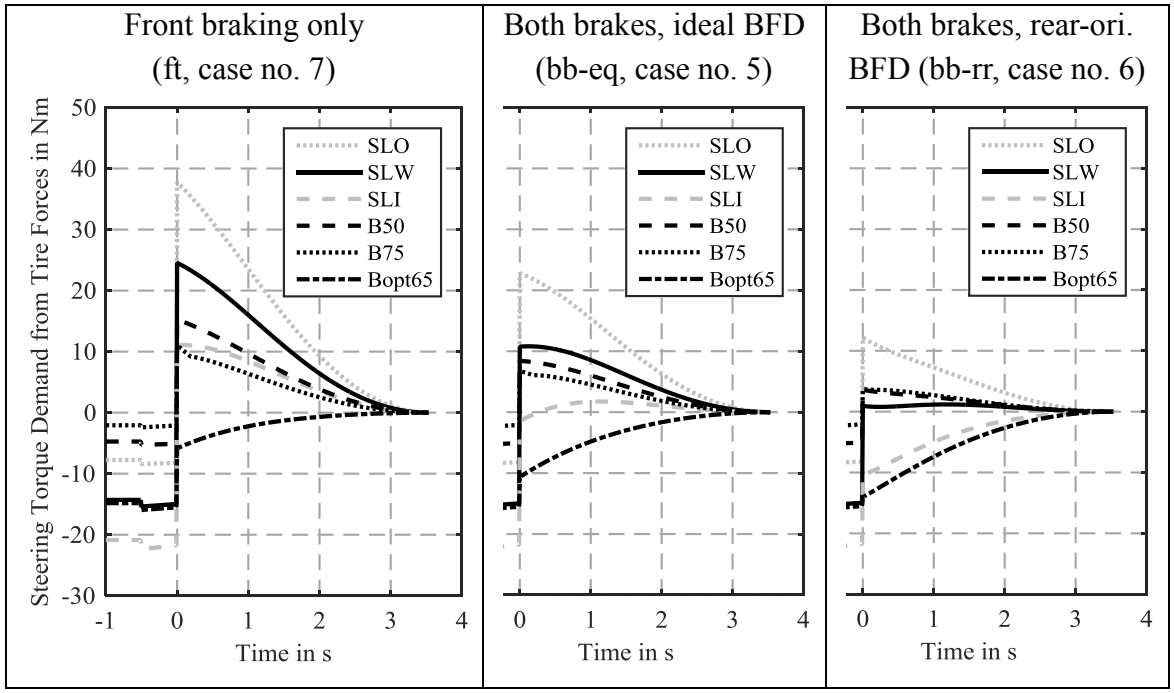

Figure 3.16: Steering torque demand arising from tire forces during partial braking with a_x = 0.5g and three different BFD (from v_0 = 17.3 m/s on a turn radius of R = 50 m, $a_{y,0}$ = 6 m/s², $\lambda_0 \approx 35°$) for different chassis setups (SLO/SLW/SLI: Standard, Lean Out/With/In; B50 and B75: Prototype BSTAM, with *tcr* = 0.5 and 0.75; Bopt65: OPT BSTAM with *gcr* = 0.65)

Table 3.4: Characteristic values corresponding to Figure 3.16. From left to right: Steering torque demand (T_0) and its initial increase (ΔT_0) at the beginning of braking for the different chassis setups. The left part of the twin columns contains the absolute (abs.) value of the simulation results and the right one its relative (rel.) value towards the reference case (SLW). A negative relative value means a relief for the rider, i.e. a less outward steering torque.

		Brake Force Distribution (BFD)					
		ft (case no. 7)		bb-eq (case no. 5)		bb-rr (case no. 6)	
Setup	T_0 [Nm]	ΔT_0 [Nm]		ΔT_0 [Nm]		ΔT_0 [Nm]	
	rel.	abs.	rel.	abs.	rel.	abs.	rel.
SLO	6.8	46.0	6.5	31.0	5.3	20.4	4.5
SLW	**-15.0** (abs.)	**39.5**	**0**	**25.7**	**0**	**15.9**	**0**
SLI	-6.8	32.8	-6.7	20.3	-5.4	11.4	-4.5
B50	9.9	20.3	-19.2	13.5	-12.2	8.7	-7.2
B75	12.9	13.1	-26.4	8.8	-16.9	5.8	-10.1
B65opt	-0.5	9.7	-29.8	4.9	-20.8	1.5	-14.4

It is worth noting, that the STD level of the lean in riding style (SLI) is generally lower than that of the prototype BSTAM with *tcr* = 0.5 (B50) for all three BFD and even lower than that of the BSTAM with *tcr* = 0.75 (B75) for the latter two BFD.

However, the reductions in steering torque kick-in on the prototype BSTAM are in the impressive order of 45% to 48% for the lower compensation ratio and 63% to 67% for the higher one. Moreover, with a kick-in of only 13.1 Nm for the worst BFD with front braking only (case no. 7, left) and lean with riding style, the BSTAM (B75) is already reaching similar levels as the 11.4 Nm which are possible for lean in and the best BFD (case no. 6, right).

Finally, the OPT BSTAM is even topping this, with a kick-in of only 9.7 Nm for pure front braking (case no 7, left) and just 1.5 Nm for the rear oriented BFD (case no 6, right), which corresponds to reductions of 75% to 90% compared to the reference (SLW). Since its STD curve is now no longer showing a characteristic peak but rather approaching its endpoint at standstill from below the zero line in the graph shows a limitation of the model calculation. In such cases, it is no longer valid to compute an absolute difference in STD, since this will always be the zero endpoint, which is practically not relevant.

In conclusion it can be stated, that a Cornering Adaptive BFD, be it in terms of an ideal BFD or stronger rear-orientation of the brake balance, is already greatly reducing both the kick-in and level of steering torque demand (STD). In conjunction with lean in riding style on the standard chassis (SLI), the rear-oriented BFD (case no. 6) almost reaches kick-ins just as low as the OPT BSTAM for pure front braking and lean with riding style. However, for a given BFD, all BSTAM concepts still show considerable benefits in the steering torque kick-in. While the OPT BSTAM is also generally offering a lower level of STD over the whole braking process, the prototype BSTAM is suffering from its increased STD in free cornering and may even show a higher STD level than the reference (SLW) in dependency of the chosen BFD (see Figure 3.16).

Even though the total steering torque demand is subject to further dynamic influences that were hitherto neglected, the absolute gaps concerning kick-ins and STD level between OPT BSTAM and the standard chassis's performance with rear wheel oriented BFD and riding style lean with are already as low as 10 Nm in the simplified simulation. Before the background, that further improvements seem possible by means of limited front brake pressure gradients and that a certain deceleration-proportional level of STD should be kept as a feedback for the rider, the true benefit of BSTAM with sophisticated Cornering Adaptive BFD can only be evaluated through more detailed simulations, or finally, riding experiments.

3.6.4 Partial Front Braking under Special Conditions

The simulations presented in the following for variations in pure front braking will not be analyzed in numerical detail. They shall rather provide a qualitative impression of changes in the steering torque demand that occur when the clutch is not disengaged during braking (stalling the engine), when encountering a narrowing radius turn, or both at the same time. The reference experiment is pure front corner braking on a constant radius with clutch disengaged, as presented in the previous section.

Figure 3.17 shows the results for all possible combinations, clutch disengaged in the left column, engaged on the right, constant radius in top row, narrowing radius in bottom row. While the initial conditions are the same as for the prior simulations, the narrowing radius is represented by a transition from the initial turn radius $R_1 = 50$ m to $R_2 = 30$ m over a path distance of $\Delta x = 20$ m. This is in line with radius ratios typically considered as critical (with $R_1 > 1.5 \cdot R_2$, cf. chapter 2.3.1) and fully within the braking distance of 30.65 m achieved during the maneuver performed at $a_x = 0.5g$ in all cases.

As an experiment of thought, it is possible, to ride through a curve with constant speed, while braking at the front and driving at the rear. Compensation of the propulsion force through front braking will lead to an elevated STD without achieving any deceleration. While the additional demand in friction potential will lead to a prolongation of the braking distance concerning maximal braking, this does not have to be the case for partial braking. Rather, both an elevation in steering torque kick-in and super-elevation over the duration of the maneuver are to be expected and were confirmed by the simulation results, see top row in Figure 3.17. For the presented example and reference setup (SLW), both values increase by about 5 Nm or in the order of about 13% for the kick-in. As a side note, also the STD when the braking is initiated (T_0) is slightly elevated by about 1.1 Nm through the presence of the driving force.

Directly jumping to the second row of Figure 3.17 illustrates how the narrowing radius is stretching the steering torque demand curves over the duration of the braking process. For increased starting speeds and roll angles of the same experiment (e.g. $v_0 = 19.44$ m/s = 70 km/h and $\lambda_0 \approx 40°$ instead of $v_0 = 17.32$ m/s = 62.35 km/h and $\lambda_0 \approx 35°$), the STD curves even develop a decisive peak at $t \approx 1.5$ s in excess of the initial STD level.

These characteristics, the super-elevation in STD with clutch engaged and the stretching or even increase of STD level over the duration of the braking process through a narrowing radius hold qualitatively also true for the other BFD, however at lower levels.

Just as for the previously regarded experiments, lean out riding style is worsening the situation, while lean in or BSTAM setups are bringing improvements, both for the kick-in and stationary steering torque demand level. While keeping the cornering line during a braking maneuver is already a challenging task on a constant radius, the benefit of BSTAM for easier maneuverability through the lower STD is expected to be especially

strong on narrowing radius turns. This is particularly illustrative when considering that the STD of the prototype BSTAM on the narrowing radius with clutch engaged (B75 in Figure 3.17, bottom right) remains below the constant radius reference with clutch disengaged (SLW in Figure 3.17, top left) over the whole braking process.

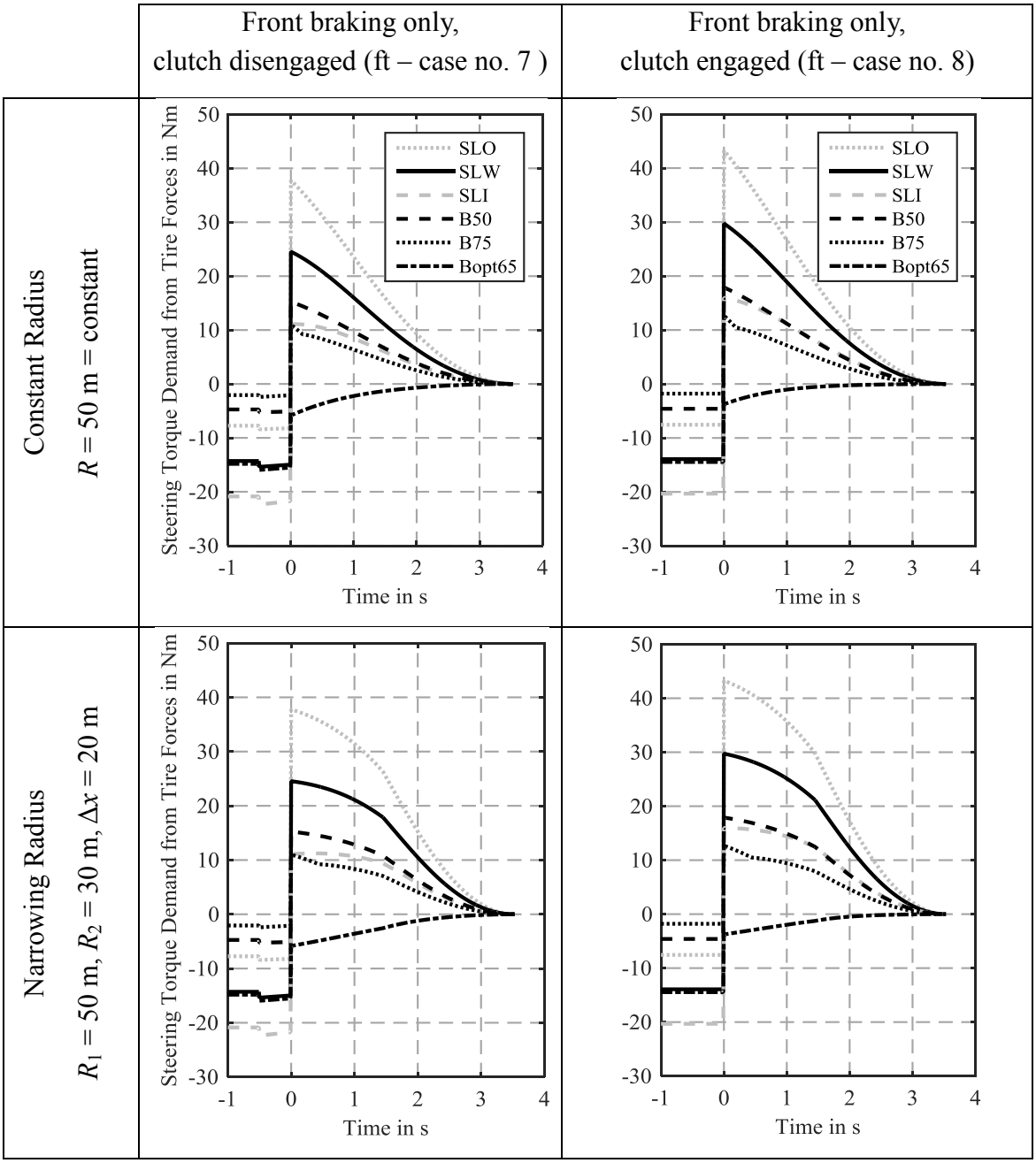

Figure 3.17: Steering torque demand arising from tire forces during partial front braking with $a_x = 0.5g$ and clutch engaged / disengaged on constant or narrowing radius turn (starting from $v_0 = 17.3$ m/s on a turn radius of $R = 50$ m, $a_{y,0} = 6$ m/s², $\lambda_0 \approx 35°$) for different chassis setups (SLO/SLW/SLI: Standard, Lean Out/With/In; B50 and B75: Prototype BSTAM, with *tcr* = 0.5 and 0.75; Bopt65: OPT BSTAM with *gcr* = 0.65. The legend is the same for all four diagrams.)

3.6.5 Conclusions on the Effectiveness of Different BFD

Table 3.5 gives a global overview of the simulation results achieved for the nine different cases of brake force distribution (BFD), including the steering torque demand (STD) of the reference setup (standard chassis and lean with riding style, SLW).

Table 3.5: Overview of simulation results concerning the performance of different BFD in terms of braking distance, time and mean deceleration, as well as STD for the standard chassis and lean with riding style (R = 50 m, v_0 = 17.3 m/s², $a_{y,0}$ = 6 m/s², $\lambda_0 \approx 35°$)

Case No.	Brake Mode	Clutch Mode	Braking		Mean Deceleration [m/s²]	STD Standard Chassis, LW		
			Distance [m]	Time [s]		T_0 [Nm]	ΔT_0 [Nm]	ΔT_{max} [Nm]
Maximal Deceleration								
1	bb-eq	diseng.	16.31	1.82	9.51 (100%)	-15.0	54.0	57.7
2	ft		18.26	1.96	8.83 (93%)		50.1	54.4
3	ft	eng.	20.63	2.21	7.84 (82%)	-13.9	47.4	51.1
4	rr	diseng.	43.78	5.05	3.43 (36%)	-15.0	-3.8	(15.0)
Partial Deceleration. Target: $a_x = 0.5g \approx 4.91$ m/s²								
5	bb-eq	diseng.	30.65	3.53	4.91	-15.0	25.7	25.8
6	bb-rr						15.9	16.2
7	ft						39.5	
8	ft	eng.	30.67			-13.9	43.7	
9	rr	diseng.	identical to case 4, since a_x-target cannot be achieved					

Concerning maximal braking performance (cases No. 1-4) in terms of braking distance, time, and deceleration level, the ideal BFD (No. 1) clearly dominates sole front (No. 2 and 3) and rear braking (No. 4), with only 36% of possible deceleration for the latter. However, the higher decelerations with ideal BFD also create a greater forward shift in wheel loads and thus the highest deviations and levels in STD over the braking process.

Concerning partial decelerations, up to a certain level, equal deceleration performances can be achieved by various BFD. In that case, the equal use of friction potential through an ideal BFD is providing the largest reserves in terms of braking stability and already providing significant reductions in STD kick-in and level over the whole braking process compared to sole front braking, that will suffer further increases, when the clutch is not disengaged during the braking process. Concerning the STD, further benefits can be

achieved through a rear wheel oriented BFD and limitations in front brake pressure increase rates. This is however done at the cost of decreased rear wheel stability and, depending on the desired deceleration level, also an increase in braking distance.

All in all, a combined anti-lock brake system (ABS / CBS) with a Cornering Adaptive BFD, be it an ideal one or a more rear wheel oriented one, is to be highly recommended, in terms of stability, maximal deceleration, and mitigation of the BST effect alike.

3.6.6 Comparison of Simulated and Real BFD

In order to check the transferability of simulation results to the real experiments and get an impression of the brake force distributions (BFD) practically realized by the C-ABS brake-by-wire system of the test motorcycle (Honda CBR 600 RR), the simulated BFD are qualitatively compared to randomly captured BFD from real riding experiments in the form of BFD diagrams. It is important to note, that the entry of data points from the experiments is derived from brake pressure measurements under the assumption of constant friction characteristics of the brake pad / disk combinations, undeformable tire contours, and an unsprung chassis. Moreover, the excess brake torque needed to decelerate the wheel's spinning inertia is not considered, which may altogether lead to deviations from the actual BFD. However, a qualitative comparison is still valid, despite these limitations. The simplified calculation for the entry of measured data into the BFD diagram is explained along with parameters of the brake system in appendix A.3.3.

Simulated Brake Force Distributions

Figure 3.18 presents the 9 different cases of simulated BFD. While rear only braking coincides for both the maximal and partial braking experiment (cases 4 and 9) and includes the rolling resistance force at the front wheel, the partial braking experiments with $a_x = 0.5g$ remain left of the respective line of constant deceleration level and the maximal braking maneuvers are found right of it. It is important to note, that this line starts at a value of 0.6 (instead of 0.5) on the axis of the relative front brake force (x-axis) of the graph, since the front braking cases with clutch engaged and a driving force at the rear (cases 3 and 8) require a prolongation of the diagram in negative vertical direction. As a side note, the rear wheel driving force, which is based on keeping constant the initial driving torque at the rear wheel, is sinking for the partial deceleration in case 3, while it is growing for the maximal deceleration in case 8. On one hand, the tire rolling radius increases with decreasing roll angles, which leads to a diminution of driving force for the constant torque. On the other, the rear wheel is unloaded due to the deceleration, leading to lower rolling resistance. Since its initial value is covered in the driving torque and the rear wheel is almost completely unloaded due to the high deceleration in case 8, this effect is dominating and leading to the increase in driving force.

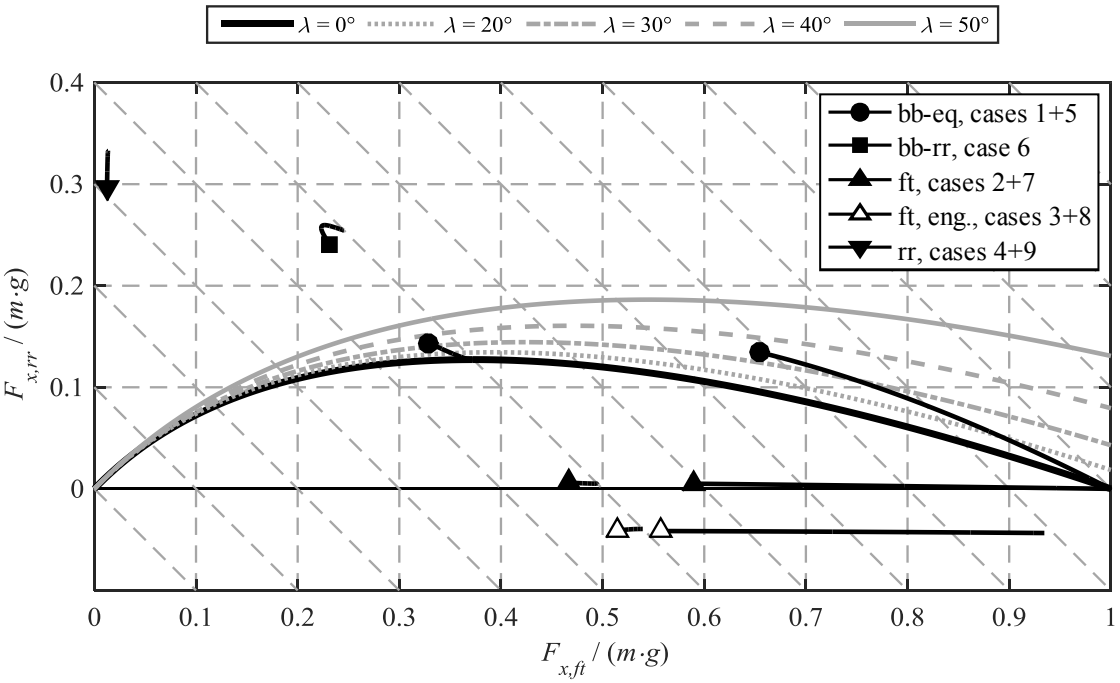

Figure 3.18: Simulated brake force distributions of the 9 different cases. Markers indicate the beginning of the braking process. Further explanation is given in the running text.

While the ideal BFD (cases 1 and 5) nicely follows the "airfoil-like" shape of the ideal BFD curves, starting with a roll angle of $\lambda_0 = 35°$ and ending with straight conditions, the rear-oriented Cornering Adaptive BFD (case 6) operates firmly above, at the rear wheel's friction limits, and all front braking BFD (cases 2, 3, 7, and 8) stay firmly below the ideal reference curves.

Real Brake Force Distributions in Maximal Straight Braking

The real BFD obtained for maximal straight braking with the test motorcycle are compared against the ideal BFD curve in Figure 3.19. Even the sole activation of the front brake initially leads to a rather quick build-up of brake force at the rear wheel. After a first ABS-intervention, be it due to dynamic over-braking or for reasons of rear wheel lift-off mitigation respectively pitch control, the rear brake force is kept at an almost constant low level. After only 0.3 to 0.4 seconds of braking, also the front brake force has settled, delivering a smooth braking control with a clearly front wheel oriented BFD and achieving a mean deceleration of 0.75*g* in the presented example. The distinctively high values occur after halting the vehicle, before releasing the brake again.

The sole activation of the rear brake leads to an even sharper increase in rear brake force, but starts to involve also the front brake with more modest increase rates after about 0.2 s of braking. After about 0.6 s of braking, the BFD has settled at its operation point. It remains clearly rear wheel oriented, but through application of the front brake

already allows to achieve a mean deceleration of 0.59*g* in the example, which is about the typical deceleration level reached by average riders[153].

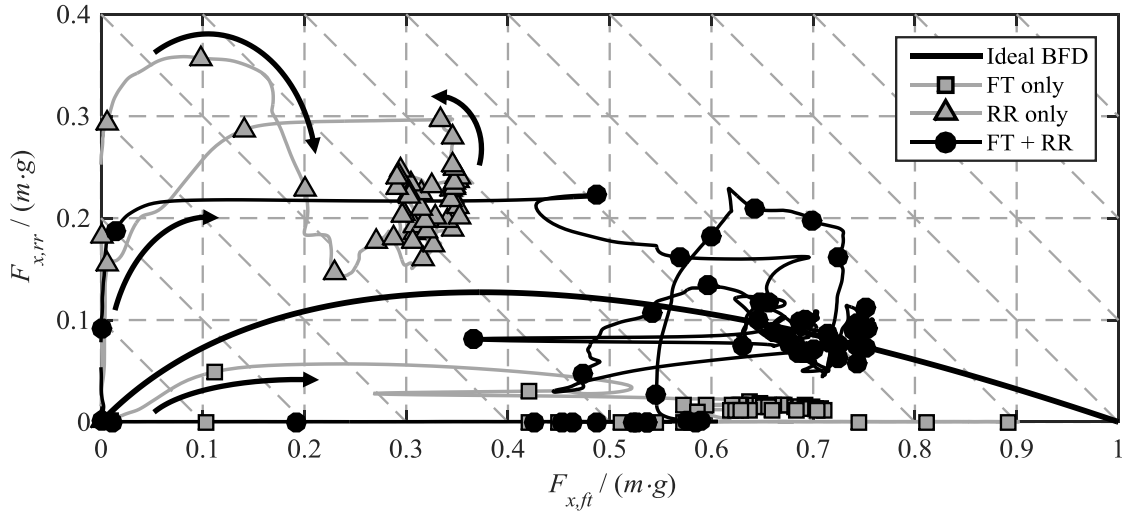

Figure 3.19: Comparison of ideal and maximal (ABS controlled) real BFD of the Honda CBR 600 RR test motorcycle in three subsequent straight braking maneuvers from $v_0 \approx 28$ m/s ≈ 100 km/h to standstill using front, rear or both brakes (achieving deceleration levels of $a_x \approx 0.75g$, $0.59g$, and $0.81g$, respectively, on a test track with 0.7% downward slope). Data points are marked every 0.1 s of the measurement, starting in the origin of the diagram and following the direction of the curved arrows.

Finally, for the combined actuation of both brakes, also the advanced rise in rear brake force is to be observed, with a sharp increase of the front brake force between 0.2 and 0.3 s of braking. After less than 0.5 s, the BFD has settled. With only two exceptions for ABS respectively pitch control, it remains nicely on the ideal BFD curve, delivering an average deceleration of 0.81*g* in the presented example. It has to be noted, that the experiment was conducted on a slight downward slope of 0.7% and that higher decelerations are achieved with the unmodified base vehicle with a curb mass of only 197 kg compared to 29 kg more of the BSTAM prototype vehicle.

Real Brake Force Distributions in Maximal and Partial Corner Braking

Figure 3.20 illustrates the real BFD achieved for two corner braking experiments on a constant radius of $R = 50$ m. The first is a maximal braking maneuver, using both brakes. Its BFD exhibits great similarities to that for maximal straight braking (cf. Figure 3.19), especially in the initial phase of brake force build-up. However, an imaginary hull curve is resembling the simulated ideal BFD for the maximal corner braking experiment presented in Figure 3.18 (case 1), however, staying below in both brake forces and hence also deceleration level (7.6 m/s² in the experiment vs. simulated 9.5 m/s²).

[153] cf. Präckel (1999): Die Motorradbremsung im System, Chapter 6.1, p. 83 ff, e.g. Bild 35, p. 103

Besides the more challenging initial conditions of the experiment, this is mostly due to the fact that the real brake system needs to keep a certain safety margin to the absolute physical limits in order to maintain stability as well as the idealizing simplifications of the model calculation. This BFD was chosen as the reference for "state of the art corner braking" experiments with the standard chassis.

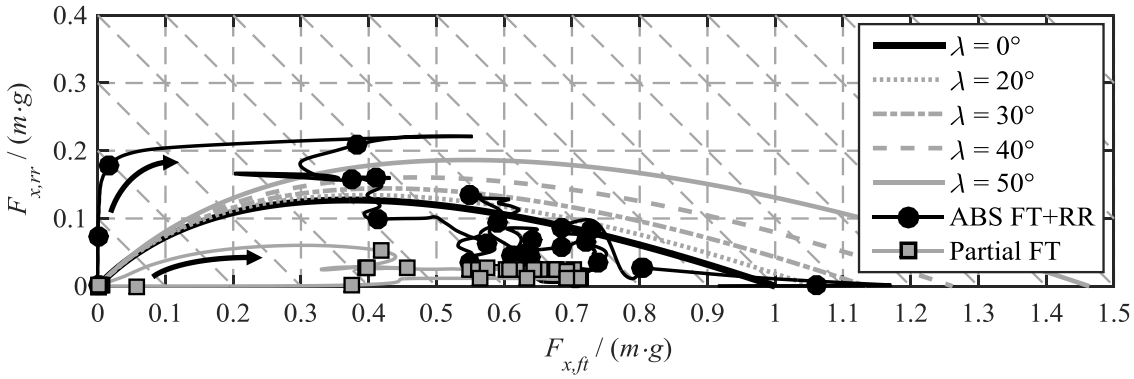

Figure 3.20: Comparison of ideal BFD curves with two real BFD of the Honda CBR 600 RR test motorcycle in corner braking experiments on a constant radius turn with $R = 50$ m. The first experiment is maximal braking with both brakes ($v_0 \approx 18.6$ m/s ≈ 67 km/h, $a_{y,0} \approx 6.9$ m/s², $\lambda_0 \approx 35°$, $a_x \approx 7.6$ m/s² $\approx 0.77g$) and the second is partial front braking ($v_0 \approx 18.3$ m/s ≈ 66 km/h, $a_{y,0} \approx 6.7$ m/s², $\lambda_0 \approx 30°$, achieving a mean deceleration of $a_x \approx 6.1$ m/s² $\approx 0.62g$). Data points are marked every 0.1 s of the measurement, starting in the origin of the diagram and following the direction of the curved arrows.

The second is a partial front braking experiment. Also the BFD achieved in this case resembles strongly to that in straight running (cf. Figure 3.19). After the initial phase with a quick rise in rear brake force, it also settles towards a clearly front wheel oriented BFD with almost constant rear wheel contribute. A mean deceleration of 6.1 m/s² is achieved at slightly milder initial conditions than for the simulations, aiming at just $0.5g \approx 4.91$ $^{m}/_{s^2}$ of deceleration. A qualitative comparison to the simulated BFD (cf. Figure 3.18, cases 5 and 7) suggests a transferability of the conclusions from the simulations towards the experiment, since the real BFD still comes close to the "front only" simulated one (case 7). However, improvements on the BST effect are to be expected through combined application with the rear brake in the sense of a tendency towards a more "ideal" BFD (case 5). – Since this BFD was easy to reproduce with high repeatability and before the background, that the BST effect and improvements thereon are most relevant for partial braking, this BFD was chosen the reference for experiments to compare BSTAM with the standard chassis.

3.7 Hypotheses for Riding Experiments and Concluding Remarks

3.7.1 Hypotheses on the Expected Performance of Standard Chassis and BSTAM in Riding Tests

Concerning the performance gap between standard steering and BSTAM, the simulations with the refined model under variation of the BFD support the prior findings of the simpler model, and hypotheses for practical testing are derived as follows.

Hypotheses on Riding Style with Standard Chassis ($H_{RidingStyle}$)

Compared to the riding style "lean with", the riding style "lean in" ("lean out") generates:

- lower (higher) stationary steering torque demand (STD).
- similar or lower (higher) steering torque deviations upon brake activation and hence less (more) deviations in steering angle, roll angle, and course.
- a lower (higher) level of total STD during the braking process and hence easier (more difficult) control for the rider.

Hypotheses on the Performance of BSTAM (H_{BSTAM})

Compared to the baseline reference in a given corner braking situation, the BSTAM realized in the prototype motorcycle (PMC), as addressed in more detail in chapter 4, will exhibit the following characteristics concerning the steering torque demand:

- A significant increase in stationary steering torque demand (STD).
- A significant reduction in steering torque deviations upon brake activation and hence less deviations in steering angle, roll angle, and course.
- A similar level of total STD as a combination of both prior values, with potential benefits for narrowing radius turns, experiments with clutch engaged, or higher decelerations, and downsides (i.e. a higher total STD) for lower decelerations.

Moreover, before the background of increased caster angle and trail, the BSTAM realized in the PMC features a more indirect steering transmission ratio (cf. chapter 2.1.5) and is therefore expected to yield poorer performance regarding handling in the tested "long trail" setup (cf. chapter 2.3.4, Figure 2.21, and chapter 5.2).

Hypotheses on the Performance of an OPT BSTAM ($H_{OPT\ BSTAM}$)

Even though these cannot be tested within the scope of this research, in contrast to the prototype, an OPT BSTAM is expected to perform even better.

Compared to the baseline reference in a given corner braking situation, an OPT BSTAM will exhibit the following characteristics concerning the steering torque demand:

- An approximately similar stationary steering torque demand (a potential small increase through partial loss in transfer of rolling resistance force superimposed with a decrease through more indirect transfer of other torque components).
- A significant reduction in steering torque deviations upon brake activation and hence less deviations in steering angle, roll angle, and course.
- A significant reduction in total STD as a combination of both prior values, with further benefits for narrowing radius turns or experiments with clutch engaged.

While the highest benefits are expected from an "ideal" implementation of the mathematical description of OPT BSTAM, a mechanically simpler and more practical "non ideal" implementation will also fulfill the qualitative hypotheses, however, at a slightly reduced performance level (cf. chapter 3.3.3).

3.7.2 Concluding Remarks

In completion of research aim 1.3 of the first field, the effectiveness of Cornering Adaptive Brake Force Distribution (CA-BFD) as well as multi-lever steering has been investigated. While the first brings great benefits in terms of steering torque deviations and steering torque demand level, especially for partial decelerations, the latter shows downsides in steering torque demand, both for free cornering and corner braking.

Regarding the second research field, the first three aims have been addressed and completed. The main influence factors of BSTAM on the driving dynamics compared to the baseline have been identified (cf. aim 2.1) and criteria for an optimized kinematic layout have been derived (cf. aim 2.2). Finally, refined hypotheses on the expected effectiveness of BSTAM compared to the standard chassis have been formulated (cf. aim 2.3).

4 Implementing BSTAM in a Motorcycle

This chapter addresses aims 2.4 through 2.6 in research field two on the practical feasibility of BSTAM.

Chapter 4.1 deals with the mechanical setup of a real BSTAM. Prior to the construction of the prototype motorcycle (PMC), the field of possible arrangements of adjustable steering bearings is generated by using methods of product development and investigated along with their pros and cons in combination with different chassis designs (see chapters 4.1.1 through 4.1.4).

A target motorcycle and a corresponding BSTAM concept are chosen (see chapter 4.2.1) and criteria for its layout under the given geometric boundary conditions as well as a simple geometric control algorithm are derived (chapters 4.2.2 and 4.2.3).

Along with the control algorithm, an equation set is presented that expresses the effective lever arms $l_{x/y/z}$ of the front tire contact forces already utilized for the computation of the steering torque demand in chapter 3 (cf. chapters 3.3.4 and 3.6). Concluding the considerations on the mechanical setup, chassis geometry changes through BSTAM are discussed in chapter 4.2.4.

An overview of the prototype motorcycle setup is given in 4.3, while its measurement and control setup is discussed along with its performance characteristics and limitations in chapter 4.4. The achievement of the set aims is briefly addressed in chapter 4.5.

4.1 General Considerations on Mechanical Setup

The optimized (OPT) BSTAM design derived for neutral free cornering in chapter 3.3.2 requires purely lateral displacement of the steering bearings in order to keep the kinematic steering axis in its original plane. Moreover, the instantaneous center of steering axis inclination should be located below the front wheel hub.

Despite its elegance for retro-fitment on the steering head of a conventional chassis with telescopic fork, the excentric adjustment of Weidele's original BSTAM design (cf. Figure 2.21 and Figure 4.7) comes along with downsides regarding the realization of an OPT BSTAM. First, the desired lateral steering axis displacement is inherently linked to undesired changes in caster angle and trail, and second, the increase in tire sprung mass might exceed driving dynamic constraints, when mounted close to the wheel hub of alternative front suspension / steering systems.

Hence, alternative solutions were sought for, to incorporate an OPT BSTAM into a real vehicle. As a starting point, the analysis of engineering constraints encountered for the integration of a BSTAM into a real motorcycle revealed four key features that define the basic mechanical layout. These are the kinematic concept, the chassis type, the implemented trajectory of manipulating the steering bearing position, and the utilized actuation concept. The four aspects are summarized in form of a morphological box in Table 4.1 and are individually discussed in the following chapters. In conclusion of the process, alternative concepts for the incorporation of an (OPT) BSTAM were developed, and are exemplarily addressed in chapter 4.1.4 and appendix A.4.1 (without claim to be exhaustive or complete).

Table 4.1: Morphological box for the meachanical integration of a BSTAM into a motorcycle (yielding 315 theoretical combinations)

Kinematic Concept	KC 1	KC 2	KC 3	KC 4	KC 5	KC 6	KC 7
Chassis Type	Telescopic Fork	Telelever	Duolever	King-Pin-Steering	Hub-Center Steering		
Bearing Trajectory	Axially Circular (Excenter)	Radially Circular (Inclinable Steering Head)	Laterally Linear (Linear Sliders)				
Actuation Concept	Coupled (Single Actuator)	Mixed Form (Single or Double Actuator)	Individual (Double Actuator)				

4.1.1 Basic Kinematic Concepts of a BSTAM

Table 4.2: Theoretical field of kinematic BSTAM concepts

KC 1	KC 2	KC 3	KC 4	KC 5	KC 6	KC 7
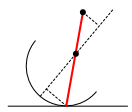	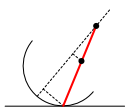	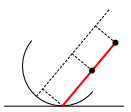	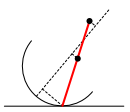	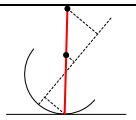	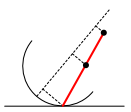	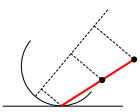
1 adjustable bearing	2 adjustable bearings					
simple (combined) actuation				more complex (separate) actuation		

The theoretical field of kinematic BSTAM concepts as derived from the product development process is shown in Table 4.2. Before the background of the diverse possibilities of actuation concepts and bearing trajectories as addressed in chapters 4.1.3 and 4.1.4, the applicability of all seven theoretical arrangements is discussed in the following.

KC 1 and 2 feature the adjustment of only one bearing, which makes them kinematically simple. However, since the major part of load is (typically) transferred via the lower bearing, it is reasonable to keep it fixed and adjust the upper one, thus preferring KC 1 over KC 2. KC 3 and KC 4 feature two adjustable bearings, but are still easily feasible with combined actuation of both bearings[154]. Moreover, no special spherical bearings are needed. Setups KC 5 through KC 7 require more demanding actuation concepts. While KC 7 is directly disqualified by steering axis inclination to the wrong side in terms of "neutral" steering balance (see chapter 3), KC 5 and 6 are theoretically also feasible on the basis of the same combined actuation concept as KC 4. For given vertical distances between tire contact patch and bearing points (in vehicle coordinates, along the z'-direction), the instantaneous center of steering axis rotation is then preferably lower for KC 5 in conjunction with desirably higher steering axis inclinations, however at the cost of greater lateral displacement and construction space requirements compared to KC 6. In case both concepts are realized on the basis of independent adjustment of both bearings, the kinematic center point is variable at the cost of higher system complexity (and presumably also mass). In case the kinematic center is adjusted to ideally match the optimal location (as defined in chapters 3.3.2 and 3.3.3), both KC 5 and 6 are congruent for given vertical distances.

As a side note for the sake of completeness, the product development process also yields solutions with the kinematic inversion of the presented principle, i.e. to keep the steering bearings fixed in the symmetry plane of the vehicle and compensate the tire scrub radius through movement of either the whole wheel carrier (cf. Figure 2.22) or the front wheel relative to the latter. However, in accordance with former research on the subject[155], such solutions were not further pursued due to various engineering constraints. Just to name a few examples, these range from chassis geometry variations (i.e. height of the center of gravity and angular offset of tire contact patch line) that influence the roll equilibrium, through higher moving masses (cf. Table A.6 for tire and wheel parameters) and correlated required actuation power, to the lateral construction space needed within the wheel carrier (i.e. the space between the fork legs).

Staying with the classical BSTAM principle of adjustable steering bearings, in sum of their positive characteristics, the kinematic concepts KC 1, KC 3, and KC 4 are considered preferable for the practical implementation of BSTAM in a motorcycle.

---

[154] E.g. KC 3 can be achieved through coupling of both bearings in a conventional steering head by repetition of Weidele's double excentric layout (producing a parallel BSTAM, however with variable fork offset), while KC 4 can be realized on the basis of an inclinable steering head, cf. Figure 4.5.

[155] Cf. Biermann (1990): Entwurf zur Verhinderung des Bremslenkmoments, and Homann (1992): Konstruktion und Analyse des BLMV, both historical student research projects.

4.1.2 Combining BSTAM with Different Chassis Designs

The bearing configurations of different front suspension / steering systems are exemplarily shown and approximately drawn to scale in Figure 4.1. Their pros and cons regarding the implementation of BSTAM are briefly discussed in the following.

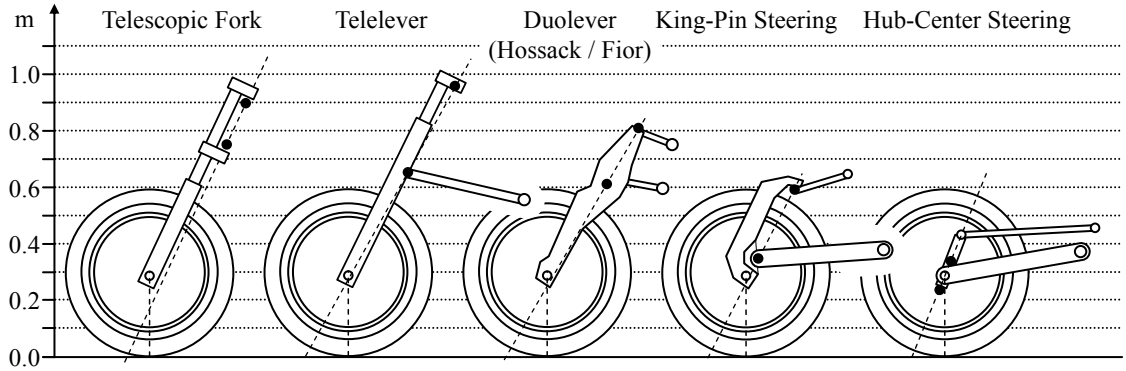

Figure 4.1: Bearing configurations of different front suspension / steering systems (approximately drawn to scale)[156]

Telescopic Fork

The telescopic fork – in either classical or upside-down configuration – is undoubtedly the most common front suspension / steering system contemporarily found on motorcycles. When mounted at the steering head, the additional mass of a BSTAM will not increase the tire sprung masses, but fully belong to the sprung mass of the vehicle. While the bearing distance remains constant, the distance between the tire contact patch and bearings in the steering head varies with suspension travel. Fork compression reduces the effective compensation ratio, while extension increases it for a given bearing displacement (see chapter 4.2.2). The bearing distance is typically small compared to the distance between contact patch and lower bearing which allows relatively small displacements in combination with KC 1, KC 2, or KC 4, while larger displacements are required for a combination with KC 3. Finally, this setup is prone to huge pitch motions and fork dive under strong braking, resulting in considerable changes in chassis geometry, especially a decrease in caster angle and consequently trail. Besides the provision of more direct steering and brake force transmission ratio (cf. chapters 2.1.5 and 3.2), especially the loss in trail may be a concern for a BSTAM design (cf. chapter 4.2.4 for the prototype BSTAM with the excenter turned forward to “short trail” setups, i.e. to 180° in Figure 4.12).

[156] More alternative front suspension / steering systems can be found in: Foale (2002): Motorcycle Handling and Chassis Design. Further information and a collection of pictures is available on the corresponding website. Foale – virtual: www.tonyfoale.com, last access: 2014-11-30.

Telelever[157]

Telelever setups are combining telescopic elements with a lower triangular wishbone, typically using ball joints as steering bearings. Besides the improved longitudinal bending stiffness, the main benefit over a conventional telescopic fork is the positioning of the kinematic brake pitch center on a level close to the center of gravity height. It is typically adjusted to yield about 70% of mechanical brake pitch compensation, delivering superior load transfer qualities and reduced risk of dynamic over-braking (cf. chapter 2.1.8). Concerning BSTAM implementation, the bearing distance is shrinking for front suspension compression. For BSTAM designs with laterally inclined steering axis, this is leading to a rising effective compensation ratio (*ecr*), if no special measures are taken. For typical chassis dimensions, these changes in *ecr* may easily reach a factor in the order of 3 and lead to unexpected changes of sign in steering torque demand. Even though it cannot generally be excluded, that a favorable design can be found, where these changes are beneficial, it is more likely that they are compromising the riding behavior through rather challenging fluctuations in steering torque demand when negotiating curves on bumpy roads. Hence, a Telelever suspension should either be only utilized in combination with kinematic concept KC 3, a parallel BSTAM design, where changes in bearing distance do not alter the effective compensation ratio, or, suspension travel needs to be taken into account for other kinematic setups. Especially for KC 1 and KC 2, this may be possible through mechanical superimposition gears or by choosing a suspension travel adaptive compensation ratio. While the first of both suggestions will lead to a sophisticated mechanism, at least with downsides in maintenance, the latter may suffer downsides in control-delays and will presumably cause a higher energy consumption than other solutions, due to the permanent adjustments required to compensate for road irregularities. In sum total, a Telelever suspension is not regarded as beneficial for the combination with BSTAM.

---

[157] "Telelever" is a registered brand name of BMW that introduced this alternative front suspension / steering system in series production in 1993. However, the original design principle was already found in custom built chassis by Saxon / Motodd prior to that date. Cf. Foale – virtual: www.tonyfoale.com → Gallery → Alternative Front Ends, last access: 2014-11-30.

Double Wishbone Suspensions (Duolever[158], King-Pin and Hub-Center Steering)

The last three suspension types depicted in Figure 4.1 may be summarized to the category of double wishbone suspensions that kinematically are four-bar linkages – but not to be confused with a four-bar linkage multi-lever steering as treated in chapters 2.3.4 and 3.4.2. – All of the three suspension systems consist of a "steered upright" or "wheel carrier" that picks up the front wheel, two wishbones to transfer the wheel loads towards the frame, being the fourth element of the linkage system. Of cause also a spring / damper element needs to be present and is typically mounted on the lower wishbone. Usually, ball bearings or kinematically similar cross-plane arrangements of conventional bearings are used as steering bearings. While the Duolever has both steering bearings outside the wheel circumference, the lower bearing point is located inside for the king-pin steering, and both for the hub-center steering. The latter is often making use of a configuration of conventional bearings like in the steering head of a telescopic fork, however, located inside the wheel hub, with the lower wishbone carrying the main loads and the upper one taking care of the angular orientation of the upright and thus the caster angle. All three types allow advanced brake pitch compensation as already discussed for the Telelever suspension.

Concerning the implementation of an OPT BSTAM, this chassis category comes along with several benefits. Firstly, except for very small changes in the frontal projection values, both the bearing distance and the distance between tire contact patch and bearing points are not (or only marginally) subject to suspension travel. Hence, also the compensation ratio will remain favorably constant. Finally, especially the latter two suspension types are favorable in terms of the low positioning of the steering bearings. Based on KC 1 or KC 4, the realization of the optimized instantaneous center of steering axis inclination (according to chapters 3.3.2 and 3.3.3) can be obtained with reasonable lateral bearing offsets (cf. chapter 4.1.4 and appendix A.4.1).

Overview on the Suitability of Different Chassis Designs for OPT BSTAM

While a parallel BSTAM according to KC 3 may require larger lateral displacements as a BSTAM with lateral steering axis inclination and is only suited for certain (radical) chassis parameter sets in terms of steering torque demand levels (cf. chapter 3.4), it

[158] "Duolever" is a registered brand name of BMW that introduced this alternative front suspension / steering system in series production in 2004. However, the original design principle with double wishbone configuration originates from Norman Hossack and was successfully applied in racing (e.g. by Claude Fior and John Britten) two decades earlier. Cf. Hossack – virtual: www.hossack-design.com, last access: 2014-11-30.

keeps constant the effective compensation ratio, regardless of suspension type and travel. However, for typical chassis geometries of contemporary motorcycles for on-road use, the implementation of an OPT BSTAM seems more favorable on the basis of kinematic concepts KC 1 and KC 4, when combined with a double wishbone suspension. The results of the presented considerations are summarized in Table 4.3.

Table 4.3: Overview of the suitability of different chassis designs for BSTAM implementation

Characteristic	**Telescopic Fork**	**Telelever**	**Double Wishbone**
Opt. kinematic center and steering axis inclination w/ reasonable bearing displ.	No (-)	No (-)	Yes (+)
Dependency of compensation ratio (*ecr*) on suspension travel	Yes, but reducing (safe side) for compression (o)	Yes, increasing (over-compensating) for compression (-)	(Almost) invariant (+)
Constancy of bearing distance (simplifies actuation)	Yes (+)	No (-/o)	Yes (+)
Contribute to tire sprung mass	No (+)	Yes / No, depending on concept (o)	Yes (-)
Rank (sum of judgments)	**2 (-,o,+,+)**	**3 (-,-,-/o,o)**	**1 (+,+,+,-)**
Favored kin. concepts	KC 1, (3), 4	(KC 3)	KC 1, (3), 4
Legend of judgments	+ = positive | o = neutral | - = negative		

As a side note, the considerations on the telescopic fork are also addressing all other forms of front suspensions mounted on a steering head, such as classical Girder, Springer, Push- or Pull-Rod Forks, just to mention a few common examples.

4.1.3 Bearing Trajectory and Actuation Concept

Since the last two aspects of the morphological box in Table 4.1 are closely interlinked, they are as well discussed in context.

General Considerations on the Bearing Trajectory

The BSTAM concept is based on the idea of moving the kinematic steering axis, which is typically defined by the interconnection line of two steering bearing center points in three dimensional space. In order to move the kinematic center point of a bearing, also

the physical bearing needs to be displaced[159]. Since each bearing has two sides (e.g. ball and socket of a ball joint, or inner and outer ring of a roller bearing), that are mounted on either side of the steering system (e.g. fork and frame side), both parts have to be moved synchronously together, in order to avoid undesired movements of the wheel carrier system upon bearing adjustment. Theoretically it is also possible, to combine circular and linear displacement trajectories for the adjustment of each individual steering bearing side, delivering $3^4 = 81$ possible combinations. However, since these lead to the said movements of the wheel carrier system, they also will lead to higher energy consumption and interferences in riding dynamics. Therefore, just 3 possibilities were considered in the morphological box under the assumption that the chosen bearing trajectory will be the same for all adjusted bearing sides.

Besides the already addressed double excentric layout with axially circular displacements of a steering bearing (cf. Figure 2.21 and Figure 4.7), Weidele also suggested a radially circular displacement in terms of an inclinable steering head[160], however without specifying the required kinematics. Pursuing the aim of keeping the steering axis in its original plane in terms of an OPT BSTAM, an exemplary solution for such an arrangement was developed along with options for linear lateral adjustments and is addressed in more detail along the discussion of the actuation concept in chapter 4.1.4.

As a concluding side note, movements of the wheel carrier system also occur for synchronous adjustments with the same bearing trajectory, when the steering angle is not zero, especially, when large steering angles and lateral steering axis inclinations are superimposed. However, firstly, large steering angles only occur for low speeds and low roll angles, while steering angles at higher speeds and larger roll angles are typically rather small (cf. chapter 2.1.5), so such a situation is practically not occurring in ordinary riding or pushing the vehicle. Secondly, the activation energy to move the steering system around the displaced kinematic steering axis comes from the rider's arms, while it must only be delivered by the actuator, when a displacement shall be superimposed to already present large steering angles, which is again a practically irrelevant situation.

General Considerations on the Actuation Concept

The lateral steering axis inclination of an OPT BSTAM in its original plane (y'_{st}-z'_{st}) introduces the rotation around the x'_{st}-axis as an additional degree of freedom between

[159] This holds also true for the virtual instantaneous center of a multi-lever steering that moves in dependency of the steering angle. I.e. when steering with a four-bar linkage, two physical bearings are moving their position in three dimensional space in relation to the other two of the four bearings that define the setup. Also cf. chapter 6.2 on the transferability of the BSTAM concept to multi-lever steering.

[160] Weidele (1990): Compensated Steering for Motorcycle. Patent Application DE3933058A1

the front wheel carrier system and the frame (note: this axis is exact only for zero steering angle, $\delta = 0$). Any actuation concept must therefore be able to couple torques around this axis back to the frame. Of cause, steerability must be possible through an appropriate mechanism, while suspension characteristics should not be compromised.

As addressed in the previous section, in order to move a steering bearing, both sides of it need to be displaced. Hence, Weidele suggested either a coupled or individual actuation of each bearing side through only one or two separate actuators[160].

While a concept with separate actuators as illustrated in Figure 4.2 is kinematically simple and offers great design freedom, special care needs to be taken for their control, to synchronize the adjustments of both bearings. Moreover, each actuator needs to carry and operate against the full loads on the bearing (in terms of reaction forces and / or torques). On one hand, this means, that the required operation power and energy consumption of the system are estimated to be rather high. On the other, compact actuator concepts with zero backlash, high transmission ratios, and low friction are required, as might exemplarily be incorporated using electric motors with ball screws or strain wave gears[161]. Furthermore, even self-locking characteristics may be favorable, to unload the actuators from passive reactions. Finally, typically at least one of the separate actuators contributes to the mass and inertia of the steering system and is therefore relevant from a stability point of view (cf. chapter 2.1.6).

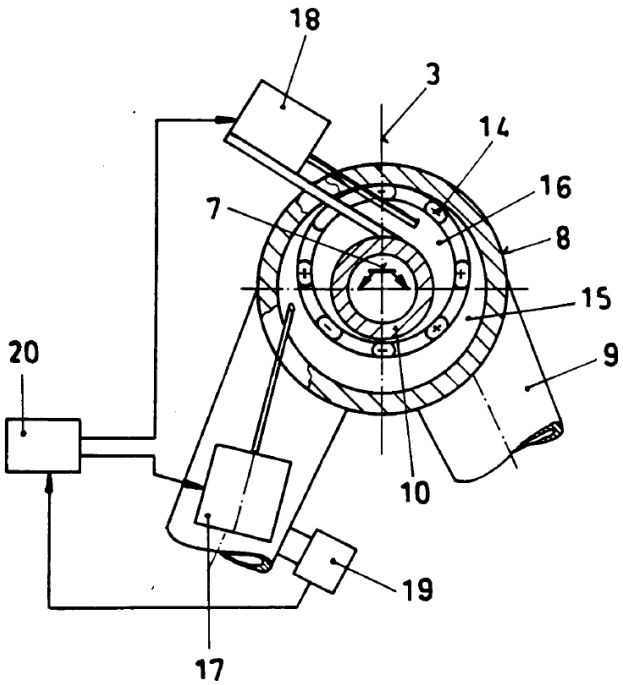

Figure 4.2: Individual actuation of bearing sides using a double actuator concept (No. 17/18)[160]

[161] Harmonic Drive – virtual: www.harmonicdrive.de, last access: 2014-12-01

In contrast, a mechanically coupled actuation with a single actuator keeps the movement of both bearing sides inherently synchronous and the base loads on the adjusted bearing can be compensated (i.e. by appropriate gearing, cf. Figure 4.7 and Figure A.1 for the force flow of Weidele's original setup, as well as chapter 4.1.4 and appendix A.4.1 for alternatives). Hence, only the friction forces inside the mechanism and the (typically low) inertia of the actuated parts need to be overcome by the actuator, possibly superimposed by small movements of the steering system when a significant steering angle is present upon actuation. Therefore, the actuation power and energy consumption of such an arrangement are seen in favor, when compared to the double actuator concept. As a downside, the mechanical coupling typically requires sophisticated kinematics that go along with elevated requirements in keeping the necessary stiffness of the steering-system-to-frame connection as well as zero backlash in the drive chain. Moreover, a great number of movable parts not only goes along with increased maintenance efforts, it also leads to mass increase. This is especially relevant from a riding dynamic point of view in terms of tire sprung mass increase, if the mechanism is located near the optimal kinematic center close to the front wheel hub. Yet another downside shall be illustrated using Weidele's original setup (cf. Figure 4.7) as an example. While it is really beneficial for retro-fitting on a conventional steering head, the fact that its housing is floating with the inclined steering axis for steering movements makes it hard to integrate into a new frame design.

4.1.4 Alternative BSTAM Actuation Concepts

While an OPT BSTAM concept with separate actuators (cf. Figure 4.2) is kinematically simple to realize, the product development process focused on minimizing the aforementioned downsides of solutions with mechanical coupling of the steering bearing adjustments (cf. last section in previous chapter). It yielded four different classes of alternative actuation concepts (AC 1-4), that are subsequently discussed in detail on the basis of exemplary kinematic sketches. Moreover, further variants of the first three classes are provided in appendix A.4.1 for combinations with diverse chassis setups.

Class AC 1: Drive Shaft through Fixed Spherical Bearing

As exemplarily illustrated in Figure 4.3 for a double wishbone suspension, actuation concepts of the first class AC 1 apply to kinematic concepts KC 1 and 2, for which either the upper or lower steering bearing is adjustable. In order to achieve the coupling of a linear (or excentric) lateral adjustment of both bearing sides, drive shafts with constant velocity (or universal) joints are used that run through a spherical bearing arrangement of the fixed steering bearing (the lower one in the example). While the transfer of reaction torques along the x'_{st}-axis from the front wheel to the main frame

system through reaction forces in the bearings of the vertical drive shafts and the coupling through the central drive shaft underline the challenge of obtaining the necessary stiffness, the replacement of the simple spur gear with rack combinations by self-inhibiting or even self-locking linear adjustments would presumably solve this issue.

As a peculiarity, the presented example features an upper wishbone that laterally floats together with the bearing adjustment. Such a setup may be practicable for king-pin or hub-center steering systems, where the upper wishbone is a relatively lightweight push-pull-rod that mainly transfers the brake torques towards the frame and controls the caster angle. However, not only in that case, the available construction space may set limiting constraints for a floating wishbone. Therefore, also a solution with a fixed upper wishbone has been developed, that only features a moving ball joint at its tip, thanks to incorporation of another drive shaft (cf. Figure A.3). Such a setup is seen favorable for the use with Duolever suspensions. A much simpler derivative of the system (cf. Figure A.4) not only allows BSTAM adjustment of a steering head arrangement, but also can be mounted on the double wishbones of a hub-center steering with its side that faces the main frame system. In the latter case, it has to be considered, that either the actuator is contributing to the tire sprung mass, or that the mechanism needs to be driven from an actuator on the frame via a drive shaft running through one of the wishbones in analogy to Figure 4.3.

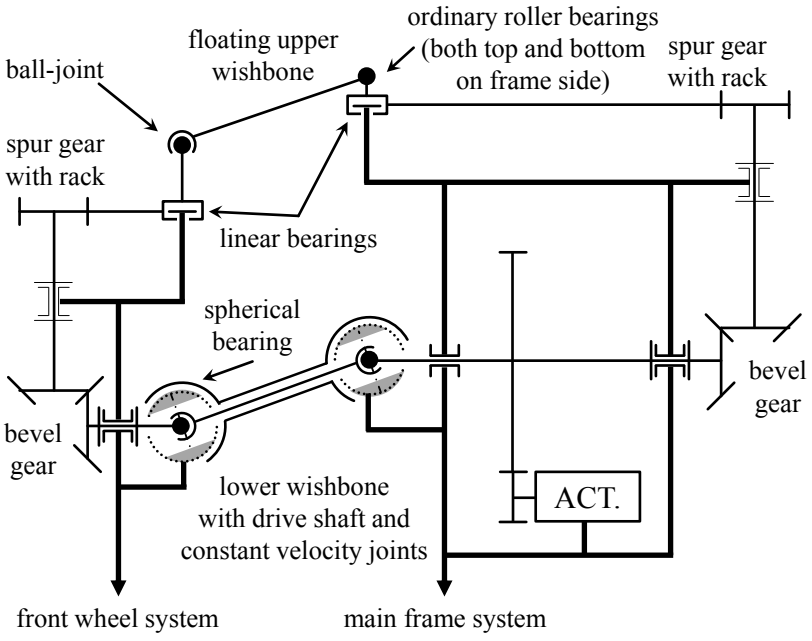

Figure 4.3: Kinematics of an OPT BSTAM on the basis of a double wishbone suspension, using a drive shaft with constant velocity joints running through a spherical bearing arrangement

In these regards, the presented example illustrates well, how the greater part of additional components – and especially the actuator - can be mounted in a fixed position on the sprung frame side to keep increases in tire-sprung mass reasonably low.

Class AC 2: Floating Drive Shaft through (or along) Adjusted Bearing

As exemplarily illustrated in Figure 4.4 for a double wishbone suspension, the actuation concepts of class AC 2 operate with a drive shaft that floats laterally with the adjustable steering bearing and are therefore suitable to incorporate all kinematic concepts KC 1-7. While KC 1-3 are simple to realize with a single actuator, it is still feasible for KC 4, but hardly practicable. Hence, two separate actuators are favorable to realize KC 4-7.

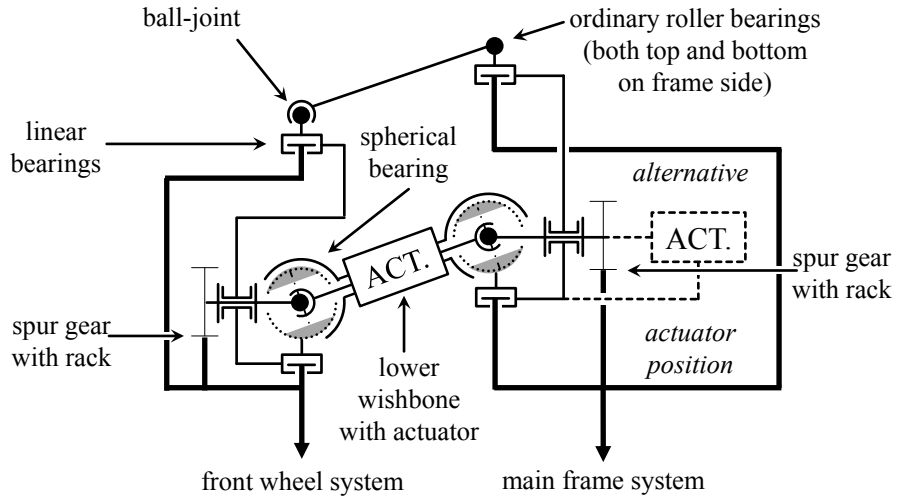

Figure 4.4: Kinematics of a parallel BSTAM on the basis of a double wishbone suspension, using floating wishbones, drive shaft, and actuator

The presented example shows a parallel BSTAM arrangement (KC 3) with the peculiarity of two floating wishbones as well as a floating actuator. It can either be part of the lower wishbone where it contributes to the tire sprung mass, or favorably stay on the fully sprung frame side, however, always requiring sufficient construction space. Leaving out the parallel coupling of the upper wishbone creates an OPT BSTAM according to KC 2 with adjustment of the lower bearing, while flipping the same upside-down leads to KC 1. The coupling of reaction torques along the x'_{st}-axis is realized through its decomposition in a pair of lateral forces in the upper and lower steering bearing, the drive shaft having to cope with a proportional torque that is lower for smaller diameters of the spur gears. As for AC 1, leaving out the wishbones creates simpler derivatives that are suitable for steering head solutions (cf. Figure A.5). These allow the realization of parallel BSTAM setups with conventional (i.e. non-spherical) steering bearings[162] and can again be mounted on the double wishbones of a hub-center steering on the side that points to the main frame. Finally, by using prismatic drive shafts with sliders, it is also possible to transfer the actuation concepts of this class AC 2 from floating to fixed

[162] Such a solution has already been proposed for the use with a telescopic fork on a movable steering head in conventional position by Biermann (1990): Entwurf zur Verhinderung des Bremslenkmoments, Bild 13a and 14a, in a historical student research project.

wishbones and actuators (cf. Figure A.6). This significantly lowers the required construction space, the moving and tire sprung mass, and therefore also the necessary actuation power, which practically eliminates many potential downsides of this class.

Class AC 3: Inclinable Steering Head

The need to couple reaction torques around the x'_{st}-axis from the front wheel system to the frame becomes directly apparent, when a rotary degree of freedom is introduced in the sense of an inclinable steering head, as illustrated in Figure 4.5. While the synchronous motion coupling of both steering head sides is inherently given through the steering bearings, the coupling of reaction torques can favorably be achieved in two ways. Firstly, by a central shaft that runs through the steering head (left sketch), and secondly, by an external torsion frame (right sketch), that is kinematically equal to a decomposed universal joint and can cope with higher torque levels.

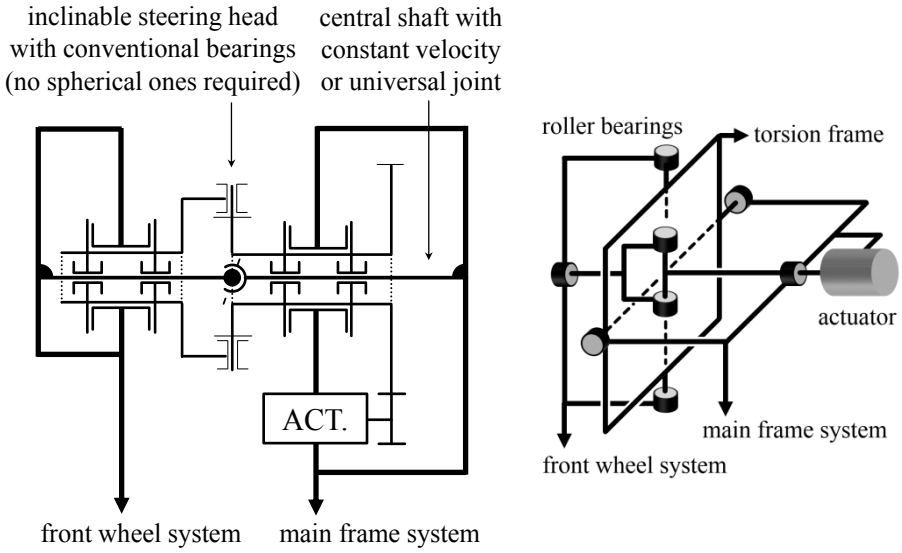

Figure 4.5: Kinematics of an inclinable steering head with central coupling shaft or external torsion frame (i.e. a decomposed universal joint)[163]

Even though this class of actuation concepts AC 3 is pre-destined to incorporate the kinematic concept KC 4 with symmetric, radially circular adjustment of both steering bearings in its inclinable steering head, also asymmetric layouts in the sense of KC 1, 2, 5, and 6 are feasible. The only pre-requisite to keep is, that the kinematic steering axis needs to intersect with the center point of the coupling shaft or torsion frame, or in other words, that the axis of steering head inclination coincides with this shaft or the center-line of the torsion frame.

[163] Cf. Biermann (1990): Entwurf zur Verhinderung des Bremslenkmoments, Bild 13b, 14b, and 16, in a historical student research project, as well as Figure A.7 as an intermediate step to the same solution.

Compared to the previous two classes of actuation concepts, the inclinable steering head is mechanically simpler and can be realized with standard bearings (i.e. 10 tapered roller bearings for the solution with torsion frame) instead of necessitating spherical ones. This will presumably not only keep the costs down, but also the stiffness sufficiently high, the dimensions compact, and the system mass relatively low. Therefore, the construction is not only suitable for front suspension systems that are mounted on a classical steering head (i.e. a telescopic fork), but its main frame oriented side could as well be mounted on the double wishbones of a hub-center steering in the sense of an OPT BSTAM. In that case, the actuator would contribute to the tire sprung mass. Since it is also possible to move it to the main frame and drive the BSTAM through a drive shaft incorporated in one of the wishbones, the better solution must be evaluated case by case with real component data. While a self-inhibiting worm gear or strain wave gear set are seen as practicable solutions to incorporate a compact electrical actuator directly within the wheel hub, a single-sided layout of the front suspension system may offer advantages in construction space, accessibility, and wheel change, without necessitating oversized wheel bearings as would typically be the case for double sided constructions. In sum total, the described system is currently regarded as the most promising solution to incorporate an OPT BSTAM into a new chassis design.

Class AC 4: Hydraulic Coupling

In order to combine the low power requirement of coupled actuation with the flexibility of separate actuation, functional analysis and synthesis have been used. The process yielded the fourth class of hydraulic BSTAM concepts, AC 4, that is suitable for all kinematic concepts KC 1-7. As illustrated in Figure 4.6, the function is subdivided into the actuation task and carrying the base load through hydraulic coupling.

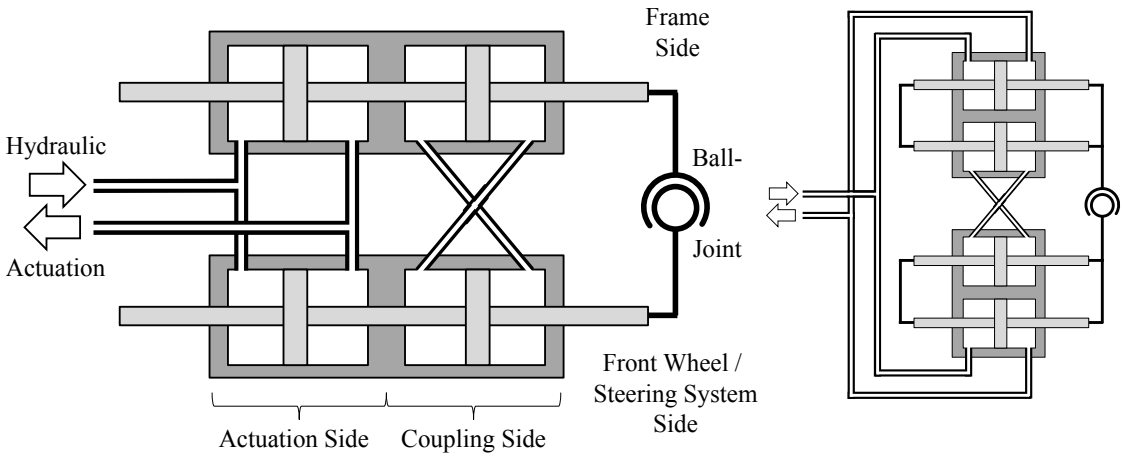

Figure 4.6: Hydraulic coupling of both sides of a single ball-joint

The cross-coupling of the coupling side allows lateral adjustment of the ball-joint position through the actuation side and is withstanding the “actio = reactio” forces at either side of the joint at the same time. While the concept presented in Figure 4.6, left, requires additional prismatic guidance elements to keep both sides of the ball joint from rotating around the axes of the hydraulic cylinders, a parallel arrangement as in the drawing on the right can directly integrate this function.

Besides these two examples, the concept is transferrable to all thinkable bearing types and trajectories as well as diverse hydraulic actuators, respectively coupling devices. While the hydraulic principle allows simple coupling also for arrangements with both bearings adjusted, the actuation side does neither have to be hydraulic, nor coupled. It may for instance as well be electric, using two separate actuators for each bearing to adjust. Moreover, high-pressure hydraulics as used in fork lift trucks might even allow to eliminate the coupling side and withstand the reaction forces directly.

Summing up, this concept theoretically offers the highest design freedom at lowest mechanical complexity. However, before the background of the compressibility of fluids, flow and throttle losses, as well as “blow-by” effects that might practically occur, it remains to be investigated, in how far such a hydraulic arrangement can at all provide the required stiffness, positioning quality, and dynamics.

4.2 Mechanical Setup of the BSTAM Prototype

4.2.1 Definition of Prototype Motorcycle and Choice of BSTAM Concept

In order to investigate the benefit of a BSTAM system against the state of the art of motorcycle corner braking and provide a safe conduct of tests, different vehicles and brake systems were test ridden and finally a Honda CBR 600 RR was chosen for the following reasons:

- State of the art brake system (C-ABS in brake-by-wire architecture with smooth brake control, pitch control and combined function).
- State of the art chassis design with easy handling and sensible steering feedback.
- State of the art semi-active steering damper (HESD).
- Construction space within and near the steering head of the frame.

Since the realization of an OPT BSTAM would have required massive changes either in the front suspension / steering system or even frame, a direct comparison and quick transition from baseline to BSTAM setup would not have been possible.

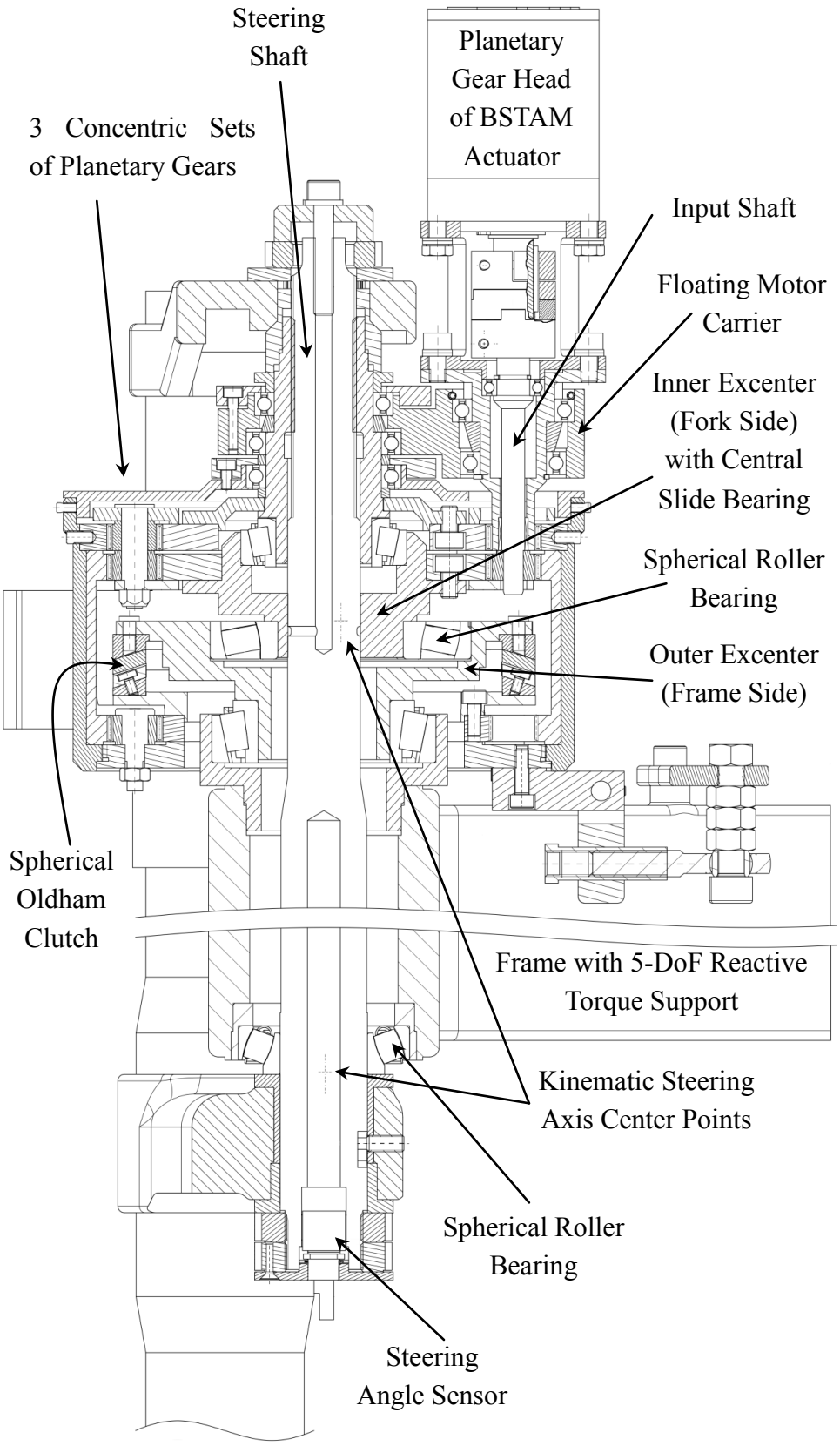

Figure 4.7: Weidele's original double excentric BSTAM design as incorporated into the Prototype Motorcycle Honda CBR 600 RR (cf. Figure A.1 for an illustration of the force flow)

Despite the downsides given through varying compensation ratios with a telescopic fork (cf. chapter 4.1.2), it has been maintained, and the classical double excentric BSTAM design with mechanical coupling according to Weidele has been chosen and incorporated into the baseline vehicle (see Figure 4.7).

Its function can be briefly described as providing a second torque path between steering system and frame in parallel to the rider (cf. appendix A.2, Figure A.1), which is either diminishing the steering torque demand at handlebar level (as desired in corner braking) or superimposing additional components, such as in free cornering.

The last mentioned downside concerning the elevated steering torque demand as well as the compromised handling (cf. chapters 3.3.4 and 3.6), which arise from changes in fork offset, caster angle and trail, are accepted before the background of its relatively easy retro-fitment on the conventional steering head without significant modifications. Hence it was easily possible, to switch from a centered steering axis to BSTAM setup and vice versa, keeping many of the mechanical components identical.

As another benefit for the progress of the project, the majority of parts of an already existing lab prototype constructed in the 1990s for retro-fitment on a BMW K100 test motorcycle could be modified to fit the requirements on the new target vehicle (cf. the historical student research work on BSTAM that is cited at the end of this thesis).

The layout of the system is addressed in detail in the following chapters.

4.2.2 Excentricity Layout

The choice of BSTAM excentricity is subject to diverse engineering constraints. Among others, the available construction space around the steering head and between the fork legs is limiting the overall size of the BSTAM housing and thus indirectly also the excentricity (cf. Figure 4.7). In the example of the prototype motorcycle (PMC), it is limited to $e = 8$ mm. In the following section, it is illustrated, how a desired excentricity is computed and discussed, which consequences arise from the limited excentricity.

Influence of Suspension Travel and Pitch on Compensation Ratio

The size of excentricity firstly depends on the necessary lateral displacement of the steering bearing to achieve a desired compensation ratio. For a given suspension travel, tire and chassis parameters, in can be computed using the theorem on intersecting lines with the frontal projection provided in Figure 4.8 as follows.

Under the simplified assumption, that the projected vertical distance of bearing points (H and G) is not significantly affected by the excentricity of BSTAM (i.e. that $\Delta h_1 \ll h_1$, in Figure 4.8, right, which holds true in the order of less than 1.4% for the PMC), the projected distances h_1 through h_3 are:

$$h_1 = bd \cdot \cos\tau \tag{4.1}$$

$$h_2 = fl \cdot \cos\tau - fo \cdot \sin\tau \tag{4.2}$$

$$h_3 = r_{r,ft} = r_{ft} - (1 - \cos\lambda) \cdot r_{c,ft} \tag{4.3}$$

Together with the tire scrub radius:

$$sr_{tir} = r_{c,ft} \cdot \sin\lambda \tag{4.4}$$

the required lateral displacement at the BSTAM bearing amounts to:

$$\Delta y_{target} = sr_{tir} \cdot \frac{h_1}{h_2 + h_3} \cdot tcr \tag{4.5}$$

with $0 < tcr < 1$ being the desired geometrical target compensation ratio.

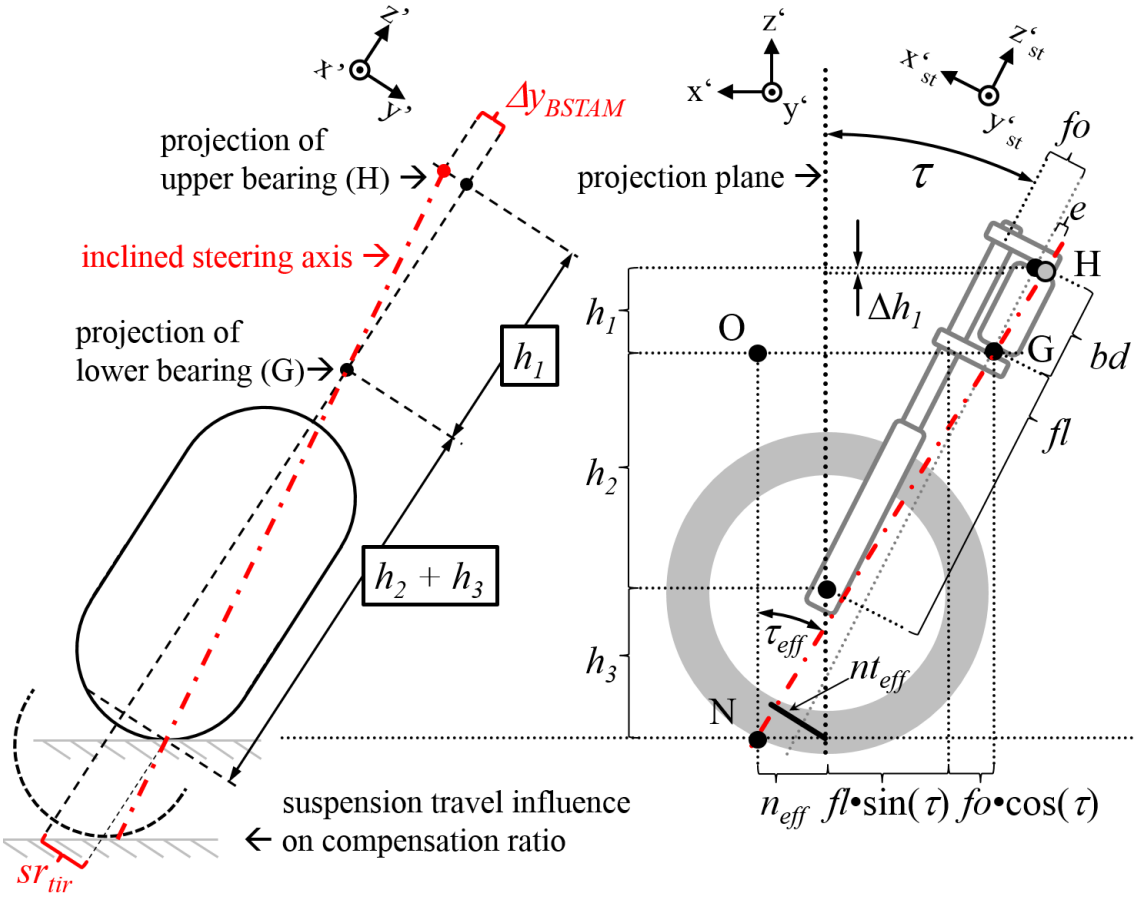

Figure 4.8: Chassis parameters and compensation scheme of the BSTAM prototype

As already addressed in chapter 4.1.2, the projection and hence the target offset depend on suspension travel of the telescopic fork, that is often attributed to brake pitch, leading to a reduction in caster angle by the pitch angle.

Figure 4.9 illustrates both influences for the parameters of the PMC and full compensation target (*tcr* = 1) for the fork being fully extended, in static trim, or fully compressed (*fl* = 494 mm, 465 mm, or 386 mm, respectively) with standard caster angle (black lines) or a generic reduction of the same by 10° to account for pitch (grey lines).

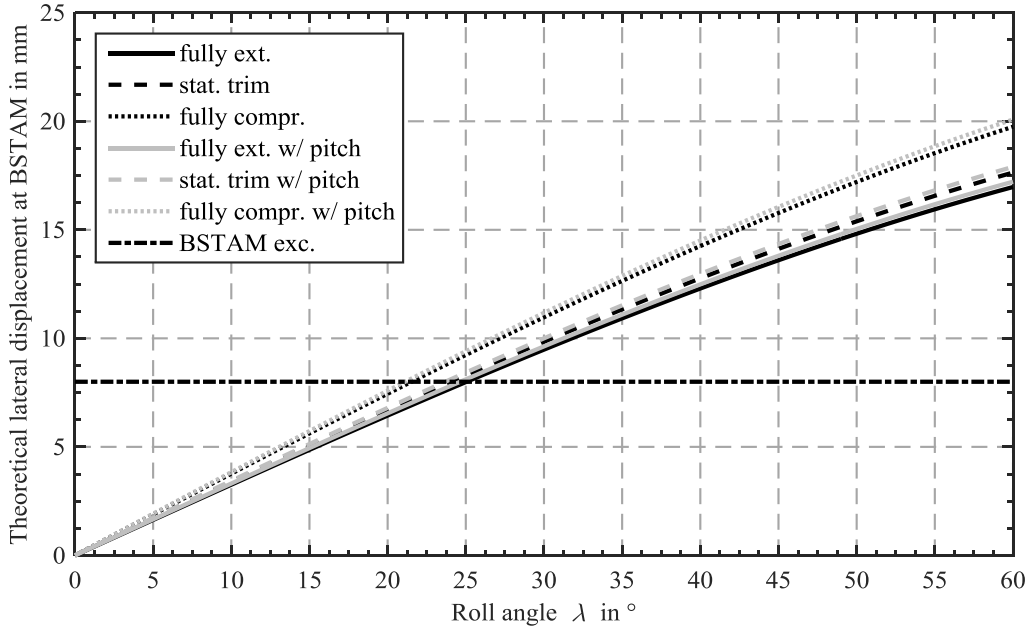

Figure 4.9: Definition of required lateral steering bearing displacement

As can be seen from the figure, the required lateral displacements at large roll angles are in the order of more than twice the excentricity available in the PMC. This will limit the maximal possible compensation ratio for a given roll angle (cf. Figure 3.14) or the maximal roll angle at which full compensation can be achieved, ranging between 22° and 25° in the example.

Excentricity Enlargement Factor and Displacement Sensitivity

Another influence factor on the layout of excentricity is the circular motion. At full lateral displacement of the excenter, no lateral displacement of the bearing is achieved for a given change in excenter rotation. In order to account for that characteristic, excenter angles close to $\varepsilon = 90°$ should be avoided, hence requiring a still enlarged excentricity.

This circumstance is expressed by the Excentricity Enlargement Factor (*EEF*) and the Displacement Sensitivity (*DS*) as illustrated in Figure 4.10 and defined by the following equations[164]:

[164] Homann (1992): Konstruktion und Analyse des BLMV, historical student research project

$$EEF = \frac{1}{\sin \varepsilon} = \frac{e}{\Delta y_{BSTAM}} \tag{4.6}$$

$$DS = EEF \cdot \cos \varepsilon = \frac{1}{\tan \varepsilon} = \frac{\partial y_{BSTAM}}{\partial \varepsilon_{BSTAM}} \tag{4.7}$$

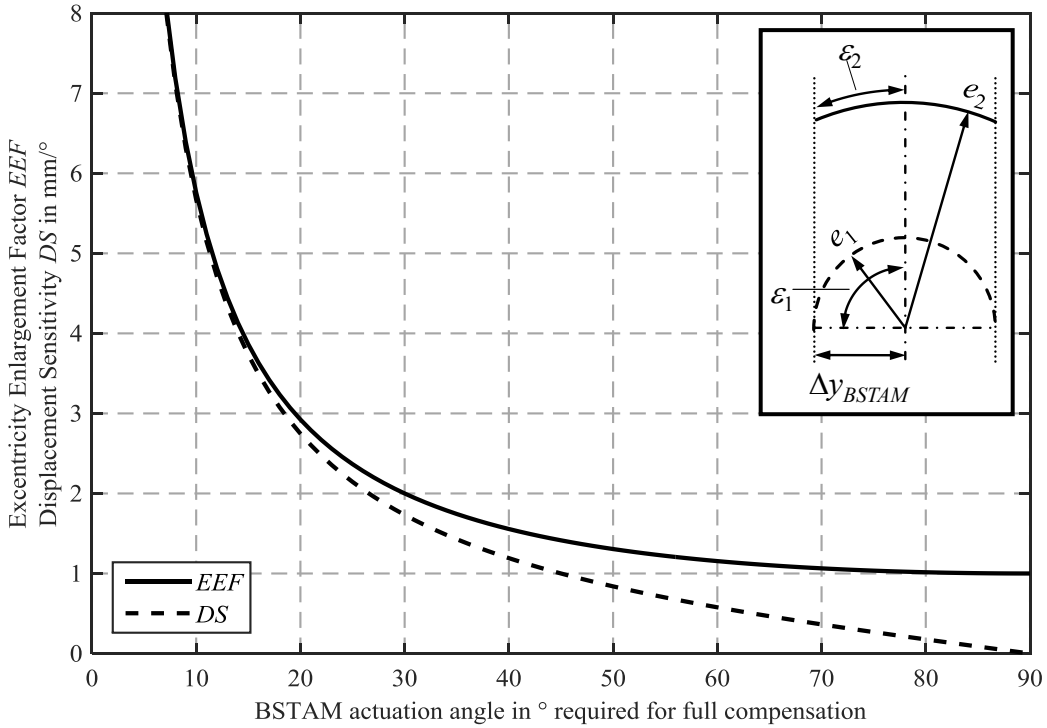

Figure 4.10: Excentricity Enlargement Factor (*EEF*) and Displacement Sensitivity (*DS*)[164]

In order to achieve a good *DS* in the order of 1 mm/°, the chosen excentricity should be about 50% larger, than the theoretically determined value, which of cause collides with the available construction space. Due to the very limited excentricity in case of the prototype motorcycle (PMC), the excenter actuation angle has been limited to 80° as a compromise to guarantee a small remaining displacement sensitivity while allowing as much compensation as possible for a given roll angle.

4.2.3 Simple Geometric Control Algorithm and Computation of Lever Arms

The prior considerations directly yield the basis for a simple, roll angle based control algorithm incorporated in the PMC. While the target lateral offset Δy_{target} of BSTAM was defined in eq. (4.5), its limitations are defined as:

$$\Delta y_{limit} = e \cdot \sin(80°) \tag{4.8}$$

yielding the effective lateral displacement as:

$$\Delta y_{BSTAM} = \min\left(\Delta y_{target}, \Delta y_{limit}\right) \tag{4.9}$$

From that, the BSTAM actuation angle can be computed as:

$$\varepsilon = \arcsin\left(\Delta y_{BSTAM}\right) \tag{4.10}$$

and the according longitudinal offset of the BSTAM is then given by:

$$\Delta x_{BSTAM} = e \cdot \cos\varepsilon \tag{4.11}$$

This variation in upper fork yoke offset is affecting caster angle and trail as follows:

$$\Delta\tau = \arctan\left(\frac{\Delta x_{BSTAM}}{bd}\right) \tag{4.12}$$

with *bd* being the bearing distance along z'$_{st}$-coordinates, yielding the effective caster angle, as illustrated in Figure 4.8, right:

$$\tau_{eff} = \tau + \Delta\tau \tag{4.13}$$

Again neglecting small changes Δh_1 in the vertical distance h_1, the frontally projected king-pin and steering axis inclination angles σ and γ as introduced in Figure 3.1 are:

$$\sigma = \cos\tau \cdot \arctan\left(\frac{\Delta y_{BSTAM}}{bd}\right) \tag{4.14}$$

$$\gamma = \lambda - \sigma \tag{4.15}$$

The compensated portion of the tire scrub radius sr_{cmp} and the resulting effective compensation ratio *ecr* according to the same figure are then given by:

$$sr_{cmp} = \frac{h_2 + h_3}{h_1} \cdot \Delta y_{BSTAM} \tag{4.16}$$

$$ecr = \frac{sr_{cmp}}{sr_{tir}} \tag{4.17}$$

using sr_{tir} from eq. (4.4) and Δy_{BSTAM} from eq. (4.9).

The effective scrub radius towards the inclined BSTAM steering axis is then:

$$sr_{eff} = (1 - ecr) \cdot sr_{tir} \cdot \cos(\sigma) \tag{4.18}$$

while the effective trail n_{eff} can be computed within triangle (N-G-O) in Figure 4.8:

$$n_{eff} = (h_2 + h_3) \cdot \tan\left(\tau_{eff}\right) - (fl \cdot \sin\tau + fo \cdot \cos\tau) \tag{4.19}$$

yielding the effective normal trail nt_{eff}:

$$nt_{eff} = \cos\left(\tau_{eff}\right) \cdot\ n_{eff} \tag{4.20}$$

Finally, the effective lever arms of front tire forces towards the inclined steering axis (as already used for simulations in chapter 3) are computed in analogy to eq. (3.8) to (3.10):

$$l_x = + \cos\tau_{eff} \cdot sr_{eff} \tag{4.21}$$

$$l_y = -\cos\gamma \cdot nt_{eff} - \sin\gamma \cdot \sin\tau_{eff} \cdot sr_{eff} \tag{4.22}$$

$$l_z = +\sin\gamma \cdot nt_{eff} - \cos\gamma \cdot \sin\tau_{eff} \cdot sr_{eff} \tag{4.23}$$

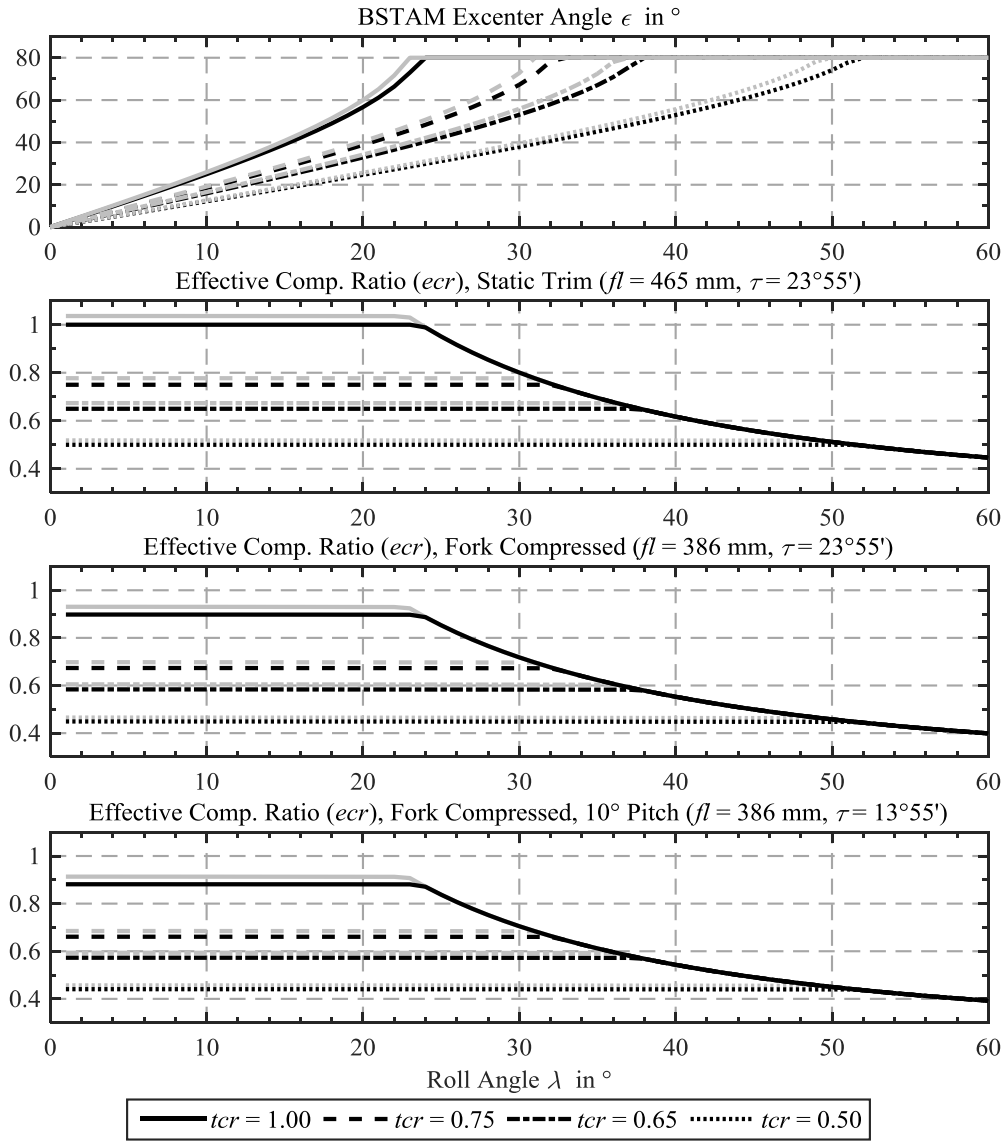

Figure 4.11: BSTAM excenter angle and effective compensation ratio as a function of roll angle, target compensation ratio, fork travel and pitch. Black lines for correct chassis parameters, grey lines as erroneously incorporated into the control algorithm of the prototype.

The BSTAM actuation angle obtained from the presented control algorithm as well as the achievable effective compensation ratio are illustrated as a function of roll angle, target compensation ratio, fork travel and pitch in Figure 4.11.

While the black lines indicate the use of correct chassis parameters ($bd = 233$ mm, $fo = 30$ mm, $r_{ft} = 295$ mm, and $\cos(\tau) \approx 0.914$), a preliminary version of the control algorithm was kept in the prototype motorcycle due to a programming error, yielding the grey curves. It uses different projection parameters ($bd = 233.5$ mm, $fo = 0$, $r_{ft} = 282$ mm, and $\cos(\tau) \approx 0.999$, the latter as a mismatch between computation in radian and degree), resulting in slightly higher actuation angles and compensation ratios.

The example shows the limit roll angles, at which a certain compensation target can still be achieved. E.g. for $\lambda = 35°$ in the last diagram, the maximal achievable *ecr* is about 0.6, no matter how high the target compensation ratio *tcr* is chosen.

4.2.4 Chassis Geometry Changes through BSTAM

Finally, a parameter variation of BSTAM actuation angle, roll angle, fork travel and pitch reveals the maximal possible chassis parameter variations through BSTAM as presented in Figure 4.12 as well as Figure 2.21.

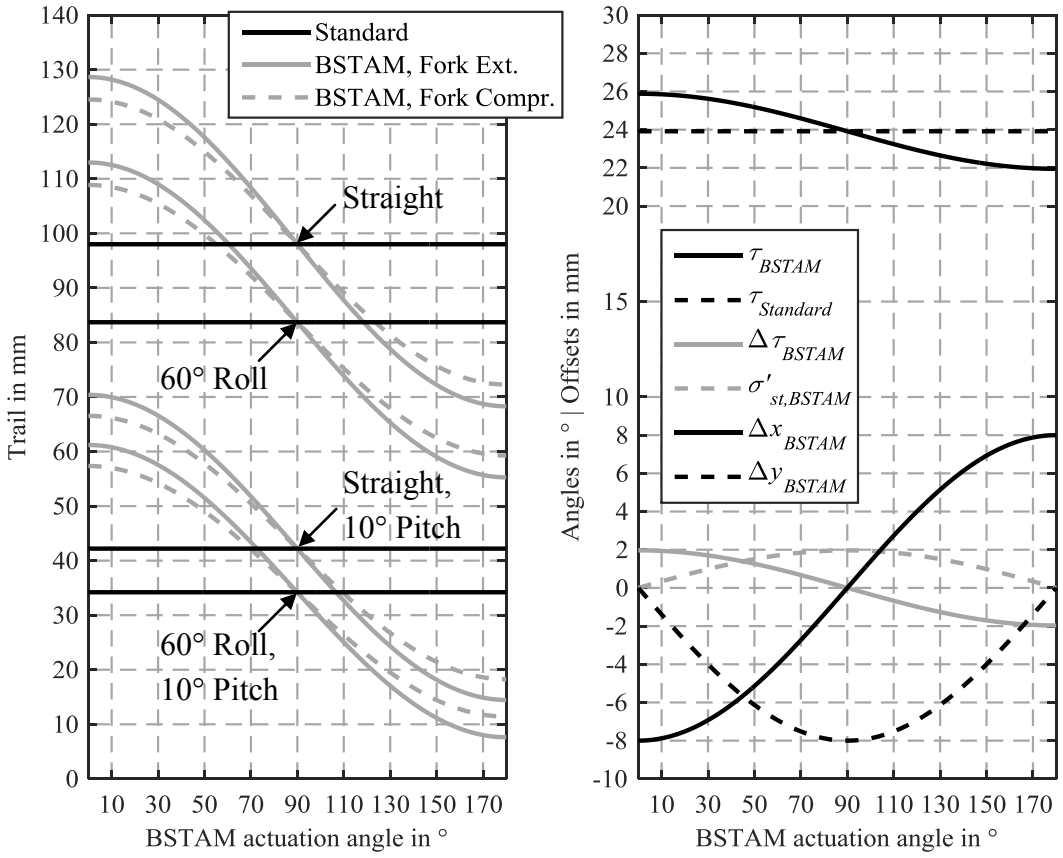

Figure 4.12: Chassis parameter variations due to BSTAM actuation, roll, fork travel, and pitch. (Each annotation in the left diagram applies to one horizontal black Standard and two curved grey BSTAM graph lines, marked with an arrow at their respective intersection.)

The reference position of the BSTAM actuation angle is $\varepsilon = 0$, when the kinematic center point is located aft of the original steering shaft, leading to an increase in caster

angle and trail (cf. Figure 4.7, Figure 4.8, and Figure 2.21), hence called a "long trail" setup. Consequently, $\varepsilon = 90°$ is equal to full lateral displacement, putting the steering axis back to its original plane (y'_{st}-z'_{st}) and yielding the same trail values as for the baseline chassis (cf. Figure 4.12, left). Finally, $\varepsilon = 180°$ represents a "short trail" setup, with the kinematic center in front of the steering shaft. While steering transmission and ease of handling are compromised for the long trail setup along with an increasing stability (cf. chapters 2.1.5 and 2.1.6), the opposite is the case for the short trail setup.

The left illustration in Figure 4.12 shows, how the trail in straight running increases from 98 mm of the reference towards 128 mm for the long trail setup and decreases to only 68 mm for the short trail setup. While fork compression decreases the trail value in long trail setups, it is increasing them for the short trail ones, which is favorable in both cases. Following the diagram from top to bottom shows, how the trail is already decreasing for the standard setup with increasing roll and pitch (of cause with an exaggerated racing style roll angle of $\lambda = 60°$ to highlight the effect) to a value as low as 34 mm. Given a BSTAM with its steering axis passively centered in a short trail setup, trail is decreasing to only 7 mm, which is theoretically critical from a stability point of view. However, during orienting tests with short trail setups, this was practically not an issue. Firstly, roll and pitch angels stayed below these example values. Secondly, the pneumatic trail of tires is actually increasing the effective trail, yielding higher stability. And thirdly, when BSTAM is used in active mode, the excenter assumes turn angles close to the pre-set 80° limit for large roll angles. It is hence favorably increasing (decreasing) the trail of a short (long) trail setup to be relatively close to the value of the standard steering geometry, especially at the beginning of a corner braking maneuver. Despite the possibility to actually ride with short trail setups, the riding tests presented in chapter 5 were completely focused on the "safer" long trail setup, in face of the impending winter.

The right side of Figure 4.12 shows the lateral and longitudinal displacements of the BSTAM's kinematic center point as well as its lateral steering axis inclination in the fork coordinate system and the variations in caster angle.

While the general steering axis inclination with regards to the steering shaft is equal to the maximal changes in caster angle:

$$\sigma'_{st} = \Delta\tau_{max} = \arctan\frac{e}{bd} \approx 1.966° \tag{4.24}$$

the frontal projection of the same at maximal lateral displacement is:

$$\sigma = \arctan\frac{e}{bd \cdot \cos\tau} \approx 2.137° \tag{4.25}$$

When limited to 80° actuation angle, these values are only marginally reduced in the order of 1% and become:

$$\sigma'_{st,red} = \arctan\frac{e \cdot \sin 80°}{bd} \approx 1.937° \tag{4.26}$$

$$\sigma_{red} = \arctan\frac{e \cdot \sin 80°}{bd \cdot \cos\tau} \approx 2.118° \tag{4.27}$$

Which underlines the assumption of negligible changes in the transfer ratio of secondary effects on steering torque demand as discussed in chapter 3.3.5.

4.3 Overview of the BSTAM Prototype

Figure 4.13: Overview of the ready BSTAM Prototype Motorcycle (PMC) Setup with different center of gravity locations

Figure 4.13 gives an overview of the BSTAM Prototype Motorcycle (PMC) ready for testing. The numbers indicate the center of gravity location in different vehicle setups, that can be read from Table 4.4 along with the respective mass increase that was plus 29 kg compared to the baseline vehicle for the full BSTAM setup and plus 16 kg for the

setup using centered steering axis. However, as in the latter case not only the BSTAM is missing at the front but also the accumulators for additional power supply in the top case, the overall center of gravity location for all setups remains very close together.

The flexible thin metal sheet yielding from the bottom of the top case towards the rider's back is loosely strapped to the belt of the action camera mounted on the rider's chest. It can slide freely, allowing full rider movement also in longitudinal direction, providing rider lean angle measurement and "free escape" in case of an emergency.

Table 4.4: Mass and center of gravity locations of the PMC in different configurations according to own measurements respectively estimate calculations, based on the assumption of a constant wheelbase l = 1375 mm. Results rounded on full 5 mm.

Vehicle configuration		Curb mass (full tank)	Center of gravity location in static trim		
		m in kg	l_{rr} in mm	l_{ft} in mm	h_{cg} in mm
Vehicle alone without rider					
1	Baseline	197	700	675	530
2	PMC with centered steering axis	213	660	715	595
3	PMC with BSTAM	226	670	705	615
Rider alone, body height: 1.92 m, with protective gear, helmet, and camera					
4	In usual riding posture	79	580	795	1060
Vehicle with rider					
5	Baseline	276	665	710	680
6	PMC with centered steering axis	292	640	735	720
7	PMC with BSTAM	305	645	730	730
Vehicle with rider – Unified reference values for quasi-stationary simulation					
8	All setups	300	675	700	700
9	Aerodynamic pressure point in the center of the projected frontal area with rider in typical riding position, coinciding with the center of the ram air intake.				

A list of further vehicle parameters is provided in appendix A.4.2.

4.4 Measurement and Control Setup

4.4.1 Overview of Main Components

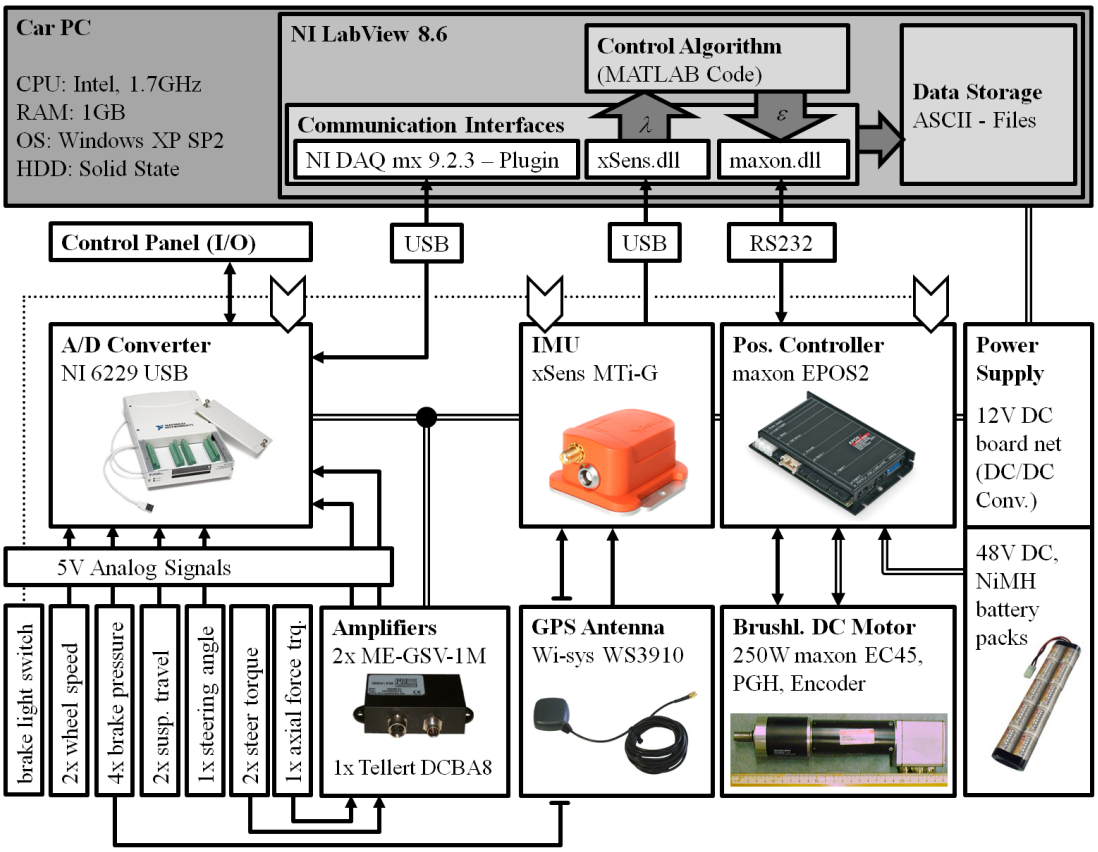

Figure 4.14: Overview of the Measurement and Control Setup of the BSTAM PMC

The main measurement and control components as illustrated in Figure 4.14 are:

- A Car PC, running National Instruments LabView on a Windows XP (SP2) operating system, as the central controller and unit for data storage (top).
- Analogue measurements and a control panel linked to a National Instruments A/D Converter, captured at 500 Hz sampling rate.
- Inertial Measurements supported by GPS provided by a xSens MTi-G inertial measurement unit (IMU) with internal Kalman Filtering and 100 Hz update rate.
- BSTAM Positioning Controller, using a maxon EPOS2 positioning controller (with cascaded PI(D) control for position, motor speed and current as well as auto tuning of control parameters) in conjunction with a 250 W maxon EC45 brushless DC motor, a planetary gear head with 1:19 transmission ratio and an encoder with a position resolution of 2000 / turn.
- Power Supply via 12V on board net and DC/DC converter for the first three components, and NiMH battery packs delivering 48V to the positioning control.

4.4.2 Accuracy of Relevant Measurements

The most relevant measurements and their accuracy are listed in Table 4.5, including the sensor type.

Table 4.5: Accuracy of relevant measurements

Signal	Symbol	Sensor type	Accuracy
Steering Torque	T	strain gauges with amplifiers	1 Nm[165] (resolution < 0.05 Nm)
Steering Angle	δ	hall sensor	0.01°
Rider Lean Angle	χ	hall sensor	2°
Front Wheel Circumferential Speed	v	induction sensor with 6 signal donators	0.3 m/s towards GPS reference for higher speeds, inaccurate for $v < 2.5$ m/s or $v > 33$ m/s
Front Brake Pressure	p_{ft}	pressure transducer	0.05 bar
Front Suspension Travel	Δfl	linear potentiometer	0.5 mm
Roll Angle	λ	IMU	1° (RMS)[166]
Roll Rate	$\dot{\lambda}$		0.3°/s
BSTAM Angle	ε	motor controller with encoder	< 0.5°
BSTAM Angular Velocity	$\dot{\varepsilon}$		< 1.5°/s

4.4.3 Data Sampling and Post Processing

Since a Windows PC has deficiencies as a real time controller, a deterministic loop structure was created within NI LabView, allowing a mean update rate of 10 Hz for the complete system (cf. Figure 4.15). While the data of the analogue measurements captured at 500 Hz is read out in data blocks of 50 samples and composed to a continuous data set of 500 Hz sampling rate when saving the data, the inertial measurement and motor controller channels only deliver one sample per read out phase (in average, at

[165] Refer to appendix A.4.3 for considerations on steering torque measurement.

[166] Refer to appendix A.4.4 for considerations on roll angle measurement.

10 Hz). All data is time-stamped and a trigger signal from the brake light switch is sent to all devices, in order to provide consistent offline synchronization of the data. Analogue data channels are low pass filtered using a filter of first order[167] with a cut-off frequency of 20 Hz, except for the rider lean angle, where a 3 Hz cut-off is used[168]. Data from the inertial measurement and motor controller have already undergone internal signal treatment and are taken as is.

4.4.4 System Performance

The system performance in terms of update rate, motor current and excenter angular velocity are exemplarily shown in Figure 4.15 for a series of four corner braking experiments and three turn maneuvers conducted during 175 s total experiment time.

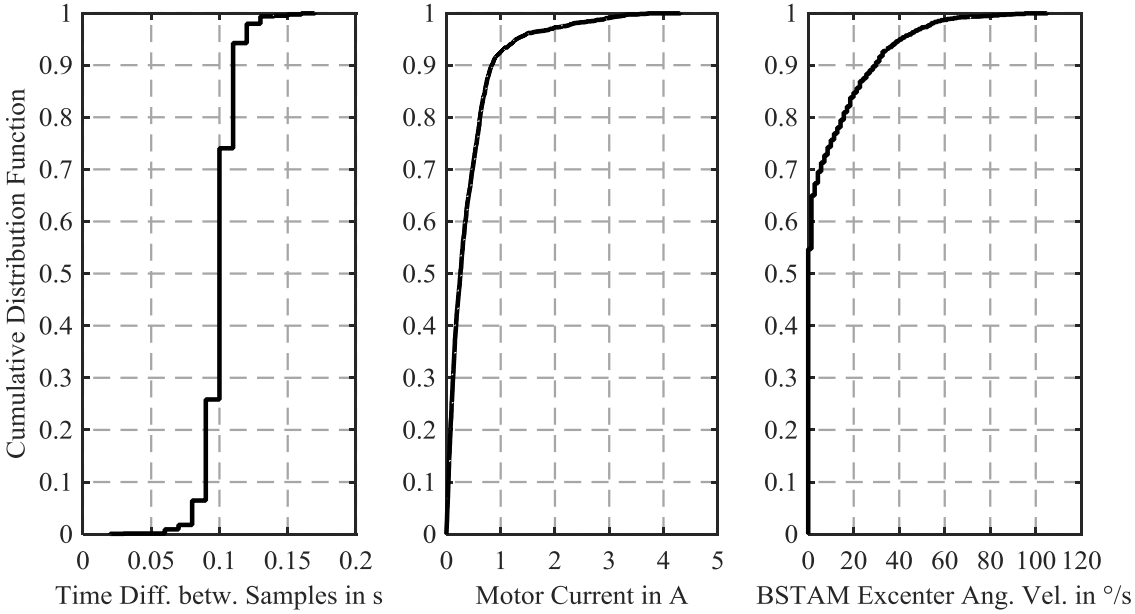

Figure 4.15: System Performance in terms of update rate, motor current and excenter angular velocity for a series of four cornerbraking experiments and three turn maneuvers conducted with BSTAM active at *tcr* = 0.75 on *R* = 50 m test track within 175 seconds.

As can be seen from the first graph, the mean time difference between samples is 0.1 seconds, only rarely deviating to 0.09 s or 0.11 s with extreme values of 0.06 s and 0.15 seconds. The motor current is an indicator for the power consumption of and the input torque to the system. At an operating voltage of 48 V, typical values for these three measures are listed in Table 4.6.

[167] Using the "filtfilt"-command of MATLAB ® Software.

[168] Cf. appendix A.4.5 on the definition of filter parameters.

Table 4.6: Typical motor current, power consumption and input torques (Motor torque constant: 70.4 mNm/A, gear ratio 1:19, operating voltage 48 V)

Situation	Current i_{BSTAM} in A	Power in W	Input Torque in Nm
Straight Running	0.2-0.3	10-15	0.27-0.40
Free Cornering	0.8-1.4	38-67	1.07-1.87
Peak in Corner Braking	4.3	207	5.75
Average	0.4	19.9	0.56

Even when adding the power consumption of the inertial measurement unit, which is below 1 W, the average power consumption of the BSTAM system stays below half the value of a typical headlight (featuring 55 W).

The average time lag of positioning control from the capturing of the roll angle, the computation of the target position and feedback of the achieved position was two samples (≈ 0.2 s), with maximal deviations of up to 4 samples (≈ 0.4 s) only encountered at points of very sudden changes in roll angle or for "jump algorithms" (cf. chapter 4.4.5). Figure 4.16 illustrates the time lag between BSTAM target and actual excenter position angles ε, offline computed and online fed back from the motor controller for the same corner braking maneuver with BSTAM active ($tcr = 0.75$) as later discussed in context of Figure 5.3. Despite reaching the excenter adjustment limits of $\varepsilon = 80°$ and a low displacement sensitivity for $\lambda_0 = 37.3°$, the time lag only very shortly exceeds 0.2 s when the excenter starts turning at $t \approx 0.8$ s.

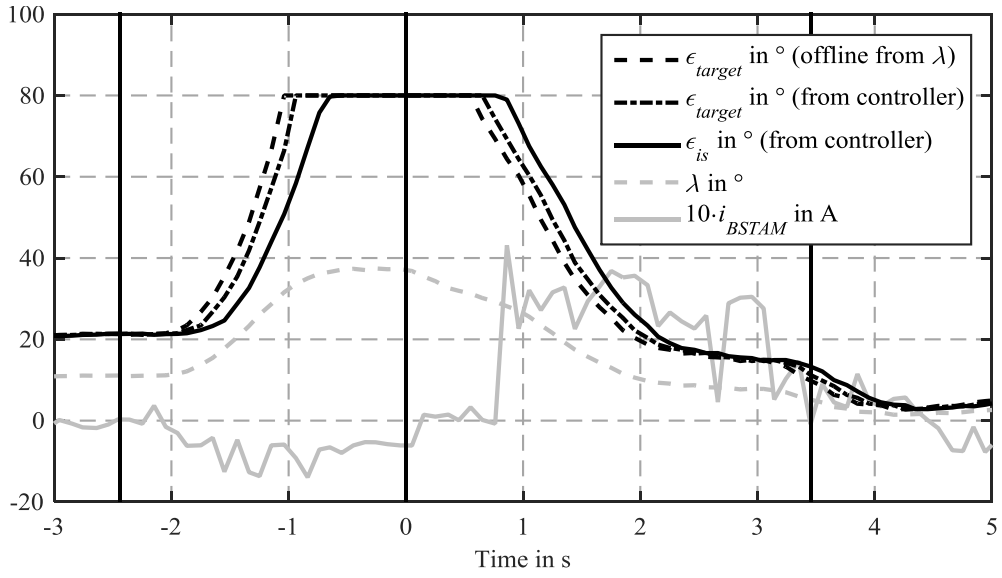

Figure 4.16: Positioning control performance for partial front corner braking maneuver on $R = 50$ m turn radius from $v_0 = 18.6$ m/s and $\lambda_0 = 37.3°$, $a_x = 5.3$ m/s² with BSTAM active, $tcr = 0.75$. Cf. Figure 5.3 for other measurements of this experiment and a detailed discussion of deviations arising from an overload situation from t ≈ 2 s onwards.

4.4.5 Extended Control Algorithms

Jump Algorithms

As illustrated in chapters 3.3.4 and 3.6, the presented BSTAM layout with roll angle dependent control algorithm has the downside of an elevated stationary steering torque demand in free cornering. Given the fact that the actuator only needs to accelerate the low inertia ($I_{BSTAM} \approx 4.14 \cdot 10^{-3}$ kgm² at input pivot) of the movable BSTAM parts and overcome the internal friction forces, a theoretical relief lies in "jump algorithms" that operate with lower or even zero compensation ratio during free cornering and jump or gradually increase the compensation ratio only when needed during braking.

To keep the implementation simple, the following three jump algorithms just modify the target compensation ratio of the standard control algorithm, which has been set to $tcr = 0.75$ for all driving experiments with jump algorithms.

Jump Algorithm A (ja)

The first jump algorithm halves the target compensation ratio for free riding and lets it jump to the full value when the brake light switch (*trigger*) indicates brake actuation:

$$tcr_{ja} = \begin{cases} \frac{tcr}{2} & \text{for } trigger = 0 \\ tcr & \text{for } trigger = 1 \end{cases} \tag{4.28}$$

Jump Algorithm B (jb)

Starting from a lower pressure threshold for the front brake pressure p_{lower}, the second jump algorithm operates with a brake pressure proportional target compensation ratio with a cut-off at the pre-set target compensation ratio when reaching the upper brake pressure threshold p_{upper}:

$$tcr_{jb} = \begin{cases} 0 & \text{for } p_{ft} \leq p_{lower} \\ tcr \cdot \frac{p_{ft}}{p_{upper}} & \text{for } p_{lower} < p_{ft} \leq p_{upper} \\ tcr & \text{for } p_{ft} > p_{upper} \end{cases} \tag{4.29}$$

The lower threshold was introduced to exclude malfunctions due to sensor noise and has been set to $p_{lower} = 1$ bar for the driving experiments (cf. chapter 5.4.3), while the upper threshold has been set to $p_{upper} = 10$ bar. This is about two thirds of the ABS threshold pressure in straight braking and corresponds to decelerations of 6-7 m/s². Since these are already among the maximal values achieved during the partial braking experiments, the effective target compensation ratio typically remains below the pre-set value of 0.75.

Jump Algorithm C (jc)

Finally, the third jump algorithm delivers a real jump from zero to full compensation ratio upon brake activation:

$$tcr_{jc} = \begin{cases} 0 & \text{for } trigger = 0 \\ tcr & \text{for } trigger = 1 \end{cases} \tag{4.30}$$

However, during the test campaign it was implemented as a derivative of "jb" by choosing the thresholds p_{lower} = 1.0 bar and p_{upper} = 1.1 bar very close together, which practically delivers the same results for the given experiment type.

4.4.6 Relevance of Elevated Curve Detection

For a series application, BSTAM control is strongly recommended to feature a detection of elevated curves. Otherwise, the steering axis is also laterally displaced during quasi-straight running conditions. On one hand, this leads to misaligning (inward) steering torque components resulting from the super-elevated front tire normal force, that can intuitively be outbalanced by the rider in free running conditions by applying an outward steering torque. While the forward shift in wheel load through rear braking is amplifying this effect, strong front braking can on the other hand overcompensate it with aligning (outward) steering torque components that suddenly require an inward steering torque of the rider. This change of sign may become critical, if occurring repeatedly in quick sequence as may be a result of "rough" ABS control. Full braking tests with maximal lateral BSTAM deflection in straight running conditions on the prototype motorcycle were however always controllable (with lateral path deviations of about 1 m) thanks to the smooth control of the Honda C-ABS. Finally, also front wheel load fluctuations as they result from strong acceleration, change of gears, or running over unevenness will analogously cause fluctuations in steering torque demand, that could foster the occurrence of kick-back (cf. chapter 2.1.6).

4.5 Concluding Remarks

All three set aims 2.4 through 2.6 from research field two have been successfully addressed. The main aspects of incorporating BSTAM into a real vehicle were analyzed in chapter 4.1 (cf. aim 2.4), including exemplary solutions for the implementation of an OPT BSTAM concept (cf. aim 2.5), while the key aspects of the incorporation of an exemplary BSTAM into the prototype motorcycle were addressed in detail in chapters 4.2 through 4.4 (cf. aim 2.6).

5 Driving Tests

The driving tests address the third research field, aiming to evaluate the effectiveness of BSTAM in comparison to the baseline with centered steering axis through experimental testing of the working hypotheses and their refinements (cf. chapters 1.2 and 3.7).

An appropriate test design and evaluation criteria are defined and the prototype motorcycle (cf. chapter 4), is comparatively tested with baseline and BSTAM steering geometry. Measurements and subjective impressions on the riding behavior and feel are evaluated and conclusions on BSTAM's effectiveness and benefit for the rider are drawn.

5.1 Test Design

5.1.1 General Requirements

The test track and maneuvers for a corner braking experiment should:

- Be realistic for typical BST relevant situations on rural roads (cf. chapter 2.3.1, turn radii $R < 100$ m, opening angles $\alpha > 30°$, better $\alpha > 72°$).
- Clearly show the desired effects:
  - Stationary steering torque demand in a free cornering phase.
  - Steering torque deviations ("kick-in") at the beginning of braking.
  - Level of STD during the brake maneuver (providing enough time to capture the BST effect without interferences through impending standstill, like balancing and taking the feet from the footrests).
- Be safe and easy to perform (with high reproducibility and repeatability).
- Match the facilities of the university's proving ground, August Euler Airfield.

5.1.2 Test Track Definition

As indicated in the top drawing in Figure 5.1, two favorable test locations have been identified on the target proving ground, the first with turn radius $R = 50$ m at an opening angle of $\alpha = 86°$ and the other with $R = 70$ m and $\alpha = 72°$, respectively.

Lanes have been marked with pylons, choosing the reference radii as the outer boundary and lane and widths of 3.5 m on R50 and 3.75 m on R70, respectively. These values are oriented at standard cross-section profiles RQ9.5 (3 m lane width + 0.25 m shoulder) and RQ10.5 (3.5 m lane width + 0.25 m shoulder) of the former RAS-Q standard, add-

ing 0.25 m extra width on the smaller R50 turn radius to allow other proving ground users to pass more easily. Figure 5.1, bottom, gives an impression of the lane width with a VW Crafter transporter (of 1.99 m body width) as a reference and illustrates the typical positioning of the test motorcycle within the lane during a test maneuver.

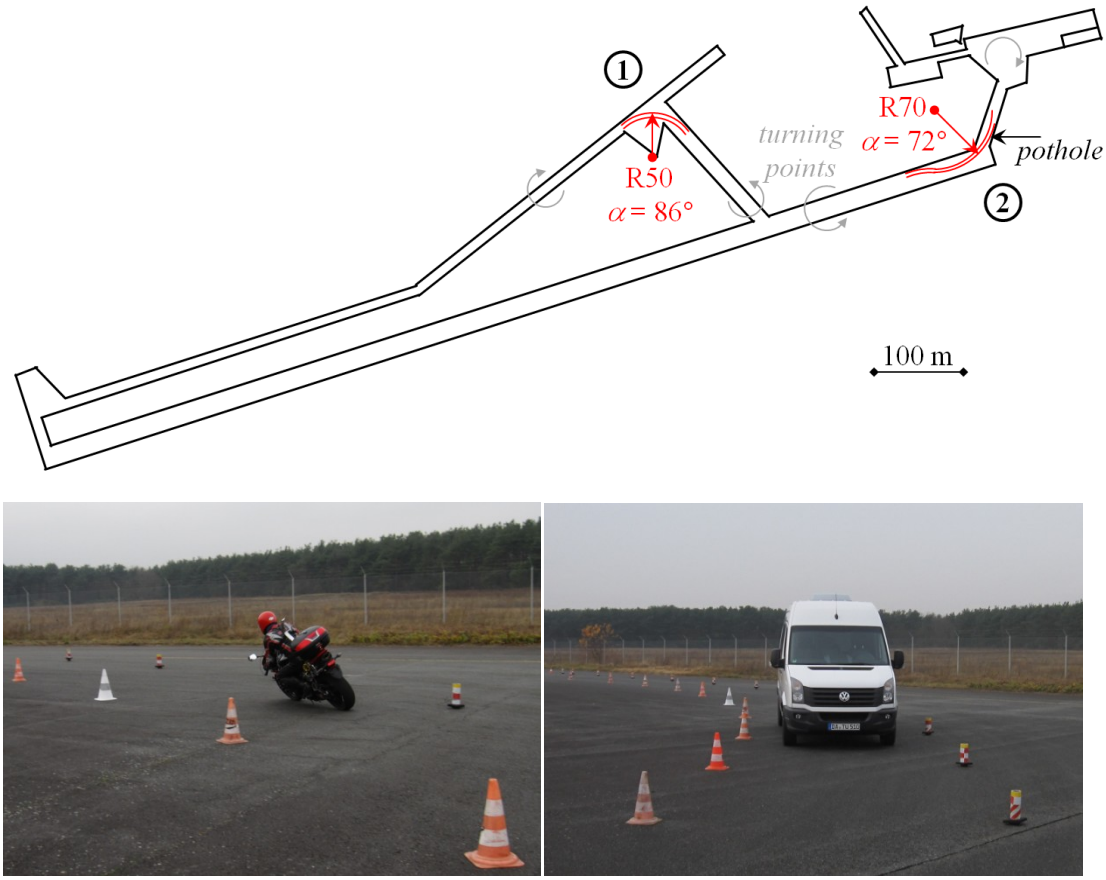

Figure 5.1: Top: Overview of August Euler Airfield proving ground with two different test locations (1: R50, 2: R70). Bottom: Typical positioning of the test motorcycle and a transporter (as a reference for lane width) within the lane at location (1, R50)

The cornering line was defined in preliminary experiments with three students and the author as test riders on the unmodified test motorcycle. Given the task to negotiate the turn as if it were a well known real rural road delivered very similar personal "ideal lines" and curve speeds. Generally, the orientation was along the outer boundary with slight corner-cutting (outside-inside-outside), keeping the tire contact patches within $^1/_3$ of the lane width at entrance and exit while typically not crossing over the center even in the middle of the track. After a little practice and with increasing speeds, this delivered very reproducible cornering radii, which are estimated to be between 48 and 52 m for the R50 track, while the deviations cannot clearly be defined but might be bigger on R70, because a swerving maneuver was required on one side while a pothole needed to be evaded on the other, see Figure 5.1, top (location 2, R70).

5.1.3 Test Maneuver and Riding Task

The test maneuver to be performed is a combination of the following three elements:

- Entering the turn from straight (used for evaluation of handling):
  - Accelerate from straight, a little higher than speed target for braking: Speedometer 65-70 km/h in 3rd gear on R50, 85-90 km/h in 4th on R70.
  - Disengage the clutch before, or latest upon entering the turn (giving 0.5 s to 1 s settling time to roll angle measurement, suspension, and steering torque demand, without negative influences by drive-train reactions).
- Free rolling cornering maneuver:
  - Choose a cornering line as you would on a rural road you know well.
- Corner braking maneuver:
  - After reaching steady state, apply the brakes until a full stop and try to maintain the intended cornering line as good as possible.

5.1.4 Test Setups and Maneuver Variations

As a background for the interpretation of results in chapters 5.3 and 5.4, an overview of parameter variations during riding experiments is given in Table 5.1.

Table 5.1: Parameter variations in conducted riding tests according to chassis setup

	Standard Steering	**BSTAM**
Riding Style	• Lean In / With / Out	• Lean With
Brake Actuation	• Front • Both brakes	• Front (mostly) • Both brakes
Deceleration	• Maximal (mostly) • Partial	• Partial
Chassis Setup	• Without and • With steering damper (HESD)	• Passive centered steering axis • Three compensation ratios
Orienting tests (low number)	• Rider Coupling (Loose / Tight)	• Narrowing Radius Turn • Braking with clutch engaged • Combination of both • “Jump Algorithms”

Orienting Tests

Preliminary tests showed, that the **coupling of the rider** has a certain influence on the stand-up triggered by the BST effect. In order to get an impression about the test riders' typical coupling, a few experiments were conducted, where the task was to be as tightly or loosely coupled as possible.

In order to facilitate **narrowing radius turn experiments** in both directions, the pylon road was not closed with further cones. Rather, from the moment of starting to brake, a specific cone on the inside of the test track was focused (in a distance of 5 to 7 cones away), aiming to leave the lane just next to this cone but still stopping within its limits. The result was an estimated change in turn radius from 50 m to approximately 30 m, which is in the range of "critical" radius ratios with $R_1 > 1.5 \cdot R_2$ (cf. chapter 2.3.1). The same parameters were also used for the simulation study (cf. chapter 3.6.4).

Corner braking while **keeping the clutch engaged**, follows the same pattern as the experiments with disengaged clutch, however, without disengaging the clutch and keeping the throttle opened a little by jamming it with the right hand when activating the front brake lever. Since the engine should not be stalled completely, the brakes are released before reaching full stop.

5.1.5 Comments on the Conduct of Tests

For reasons of reproducibility and comparability, all presented experiments have been conducted by the author as test rider (who had approximately 70.000 km of motorcycling experience and was well trained on the test vehicle at that time).

The tests have been conducted at dry conditions, however at rather low ambient temperatures of typically 8° to 9°C (min: 3°, max: 13°C) from Oct., 18th to Nov., 13th, 2012.

A warm-up phase of 15 minutes or more was kept, for engine, tires, dampers and brakes to reach operating temperature, and for the Kalman-Filter of the inertial measurement.

Interim free cornering experiments were conducted when changing from one chassis setup to another, to get a better feel for the free cornering behavior and enhance the performance in keeping a constant cornering line.

Reference maneuvers with passive steering (centered steering axis) were conducted every day to account for tire wear and personal shape of the test rider.

All experiments have been conducted with the same set of Bridgestone S20 tires, first with standard steering, than with BSTAM, in slight excess of the wear indicators.

The fuel tank was refilled every test day, resulting in a maximal mass difference of about 7.5 kg on one of the last test days. However, since the tank is located very close to the overall center of gravity, effects thereon remain small.

5.2 Criteria for Evaluation

5.2.1 Definition of Characteristic Values

Following the course of the experiment and the BST chain of effects, a set of 20 characteristic values has been determined from each riding experiment for comparative analysis. In the following, these values are defined in corresponding groups, before their computation is exemplarily illustrated for two partial front braking maneuvers, one with standard chassis and one with BSTAM. Moreover an illustration scheme of 18 among the 20 values is introduced, that will be utilized throughout the chapter.

Entering the Turn: Koch's Handling Index

A well known characteristic value to quantify the handling qualities of a motorcycle is **Koch's handling index**[169]. For the time between the first steering impulse and reaching the maximal roll angle of entering into a turn from straight conditions, it is defined by the maximal steering torque divided by the maximal achieved roll rate multiplied by the (mean) vehicle speed during that time span:

$$K = \frac{\max(T)}{\max(\dot{\lambda}) \cdot \mathrm{mean}(v)} \text{ in } {}^{\mathrm{Ncm}}/_{(\mathrm{m}°/\mathrm{s}^2)} \tag{5.1}$$

Typical values for well handling motorcycles stay below 5 ${}^{\mathrm{Ncm}}/_{(\mathrm{m}°/\mathrm{s}^2)}$. It is expected, that the passive BSTAM will produce only slightly higher values than the baseline standard chassis, due to its increased caster angle and more indirect steering transmission, while active BSTAM setups will produce higher values due to the increase in steering torque demand that goes along with the reduction in scrub radius for increasing roll angles.

Reference Values for Corner Braking Experiment

Most of the following groups of characteristic values also contain an initial reference value that is captured at the **beginning of the braking process** $t = t_0 = 0$, which is determined by the instant, when the rear brake pressure rises above $p_{rr} > 0.2$ bar:

$$t_0 = \min(p_{rr} > 0.2 \text{ bar}) \tag{5.2}$$

Other values depend on the **end time** t_{end} **of the braking process**, which is determined when either the front wheel circumferential speed drops below 0.3 m/s, the front suspension extends beyond its initial compression at t_0, or both brake pressures drop below 0.1 bar, whatever comes first:

[169] Koch (1980): Untersuchungen des Motorrad-Fahrer-Systems, p. 147

$$t_{end} = \min \begin{cases} t(v < 0.3\ \mathrm{m/s}) \\ t(fl > fl(t_0)) \\ t(p_{rr} < 0.1\ \mathrm{bar}\ \&\ p_{ft} < 0.1\ \mathrm{bar}) \end{cases} \tag{5.3}$$

The **initial velocity** is defined as:

$$v_0 = v(t_0)\ \text{in m/s} \tag{5.4}$$

using the front wheel circumferential speed as a reference. As a side note, this speed reference is offline-corrected of roll angle dependent tire rolling radius variations.

As a reference value for the harshness of the brake kick-in, the **mean front brake pressure increase rate** is defined as the front brake pressure difference between the last local minimum below 0.2 bar and the first local maximum greater than 1 bar, divided by the time span needed for that increase:

$$\dot{p}_{ft,mean} = \frac{p_{ft,first,max} - p_{ft,last,min}}{t(p_{ft,first,max}) - t(p_{ft,last,min})}\ \text{in bar/s} \tag{5.5}$$

The chosen algorithm is ignoring intermediate drops during the increase phase of up to 0.1 bar. As a side note, the captured values strongly depend on the definition of the beginning of pressure increase. They are much higher, when the initial phase of low increase rates is ignored. The qualitative results and correlation to other values remains however basically the same.

As further reference value to describe the intensity of the brake maneuver throughout its duration, the **mean deceleration** is defined on the basis of the speed difference from the beginning of the brake maneuver to its end. A case distinction is made for experiments with clutch disengaged or engaged:

$$a_{x,mean} = \begin{cases} \frac{v_0}{t_{end} - t_0}\ \text{for braking until stop, clutch disengaged} \\ \frac{v_0 - v(t_{end})}{t_{end} - t_0}\ \text{for braking with clutch engaged} \end{cases} \text{in m/s²} \tag{5.6}$$

Finally, as a reference for the intensity of stand-up motion, a **reference roll angle** is computed on the basis of the front wheel circumferential speed v under the assumption of a constant cornering radius R, with the gravity constant g (cf. eq. (2.2) and (2.9)):

$$\lambda_{ref} = 1.115 \cdot \arctan\left(\frac{v^2}{R \cdot g}\right)\ \text{in °} \tag{5.7}$$

Steering Torque

Concerning the steering torque, three values are captured.

The **stationary free cornering steering toque** at the moment of applying the brakes, which is determined by the rear brake pressure rising beyond 0.2 bar:

$$T_0 = T(t_0) \text{ in Nm} \tag{5.8}$$

While the passive BSTAM is only expected to show slight increases toward the baseline, according to the model calculations from chapters 3.3 and 3.6, the active setups will produce significantly higher values in the order of 10 to 20 Nm.

The **maximal steering torque deviation** is sought for in the first 0.6 s of the brake maneuver and defined by:

$$\Delta T_{max} = \max(T) - T_0 \text{ in Nm} \tag{5.9}$$

The **relative steering torque deviation** is defined as:

$$\Delta T_{rel} = \frac{\Delta T_{max}}{a_{x,mean}} \text{ in Nm/(m/s²)} \tag{5.10}$$

Finally, the **mean steering torque gradient** is defined as a measure for the rate of change in steering torque demand upon brake kick in:

$$\dot{T}_{mean} = \frac{\Delta T_{max}}{t(\Delta T_{max}) - t_0} \text{ in Nm} \tag{5.11}$$

In case ΔT_{max} arises at t_0, the result is not a number because of the division by zero. However, this happened only for one single experiment out of 119 with BSTAM active and 283 in total.

Given the same boundary conditions of the experiment, the latter three values are expected to be always lower for BSTAM active than for the standard reference. However, due to its increased stationary steering torque, the **absolute steering torque demand level** of BSTAM may as well be higher than for the reference. This value can be read from the presented results by adding T_0 and ΔT_{max}.

Steering Angle

In the same way, as for the steering torque, the initial conditions, maximal change, and rate of change are also captured for the steering angle.

In combination with the initial speed and roll angle, the **initial steering angle** gives an idea about the cornering state when beginning to brake:

$$\delta_0 = \delta(t_0) \text{ in } ^\circ \tag{5.12}$$

As an indicator for the similarity of initial conditions, it should be kept close together between single experiment groups.

The **maximal (inward) steering angle deviation** is sought for in the first 0.3 seconds of the brake maneuver and defined by:

$$\Delta\delta_{max} = \max(\delta - \delta_0) \text{ in } ° \tag{5.13}$$

Finally, the **maximal (inward) steering rate** is defined from the time derivative of the steering angle signal, before reaching the first inward maximum in steering angle:

$$\dot{\delta}_{max} = \max\left(\dot{\delta}\right) \text{ in } °/s \tag{5.14}$$

While the initial steering angle is expected to remain in the same order for BSTAM as for the baseline with only marginal increases, the two latter indicators of disturbance are expected to be generally lower with BSTAM active than for the standard chassis under identical conditions.

Roll Angle: Stand-Up Tendency

As an indicator on the chosen cornering line (and indirect measure for riding style) the **initial roll angle** is defined by:

$$\lambda_0 = \lambda(t_0) \text{ in } ° \tag{5.15}$$

As an indicator for the stand-up tendency, the **maximal roll angle deviation** is defined towards the reference roll angle (cf. eq. (5.7)). This definition helps to account for roll angle deviations that were already present at the beginning of braking:

$$\Delta\lambda_{max} = \max\Big(\left(\lambda_{ref} - \lambda\right) - \left(\lambda_{ref,0} - \lambda_0\right)\Big) \text{ in } ° \tag{5.16}$$

In order to allow comparisons between corner braking experiments on different turn radii, the **dimensionless relative roll angle deviation** has been defined as follows:

$$\Delta\lambda_{rel} = \left(\frac{\lambda_0}{\lambda_{ref,0}} - \frac{\Delta\lambda_{max}}{\lambda_{ref}}\right) \tag{5.17}$$

However, the value is highly correlating to the previous one (correlation coefficient $R > 0.85$ for all experiments, and $R > 0.94$ for experiments with centered steering axis). Since the initial roll angles on both turn radii of the experiments were very similar, and values in degree are more intuitive to envision and understand, the first definition is chosen for further discussions.

Finally, the **maximal (upward) roll rate** is captured:

$$\dot{\lambda}_{max} = \max\left(\dot{\lambda}\right) \text{ in } °/s \tag{5.18}$$

Again, BSTAM is expected to mitigate the deviation values when compared to the baseline for a given situation.

Rider Lean Angle

The **initial rider lean angle** gives an information on the chosen riding style. It is more positive for lean in and more negative for lean out:

$$\chi_0 = \chi(t_0) \text{ in } ^\circ \tag{5.19}$$

The **maximal (inward) rider lean angle deviation** gives an indirect hint on the looseness of rider coupling and – in context with the roll angle deviation – his perception of stand-up motion. It is sought for in the first second of the experiment and defined as:

$$\Delta\chi_{max} = \max(\chi - \chi_0) \text{ in } ^\circ \tag{5.20}$$

Finally, also the **maximal (inward) rider lean angle velocity** is captured as a maximal value of the time derivative of the rider lean angle signal, again sought for in the first second of the experiment:

$$\dot{\chi}_{max} = \max(\dot{\chi}) \text{ in } ^\circ \tag{5.21}$$

Under the assumption of similar rider coupling, the deviations for experiments with BSTAM active should be smaller than for the baseline, since also the stand-up in terms of roll angle deviation is expected to be lower.

Path Deviations

Due to the relatively loose definition of the target cornering line within the pylon tracks, absolute path deviations can only be estimated from the video footage. Typically, they stayed below ½ m and below ½ of the track width in maximum. However, also the rider's subjective impression can be taken into account for evaluation of apparent differences for active BSTAM setups that are expected to bring improvements with regards to the baseline.

(Dynamic) Steering Unsteadiness

Weidele[170] suggested two integral characteristic values for the assessment of the quality of a corner braking experiment. The first is the **steering unsteadiness** and defined as:

$$W = \text{mean}|T| \cdot \text{mean}|\delta| \text{ in Nm}^\circ \tag{5.22}$$

[170] Weidele (1994): Bremsverhalten von Motorrädern, p. 149ff

Due to the elevated stationary steering torque demand of active BSTAM setups that also causes an elevated absolute steering torque demand during the braking process, it is expected to yield similar values, as for baseline setups with centered steering axis.

The second one is the **dynamic steering unsteadiness**, that accounts better for the dynamic nature of steering fluctuations, as they were common with the rather "rough" control of the first ABS generation:

$$W_{dyn} = \text{mean}|T| \cdot \text{mean}\left|\dot{\delta}\right| \text{ in Nm°/s} \tag{5.23}$$

Before that background, it is estimated to be lower for active BSTAM than for baseline setups. As a side note, the main effect of the experiments is to be observed during the first two seconds of the experiment, while the end of the experiments is superimposed by balancing inputs of the rider, both in terms of steering torque and angle. Therefore, only the first two seconds of the experiment have been taken into account for the determination of both values. For an initial velocity of 50 km/h and initial lateral accelerations $4 < a_y < 5$ m/s² (corresponding to roll angles of up to $\lambda \approx 30°$, which is comparable to the tests conducted in the framework of this study), Weidele determined maximal steering unsteadiness values of 20 Nm° for a standard brake and up to 30 Nm° for ABS regulated braking. The dynamic steering unsteadiness captured by Weidele ranges from the order of 100 Nm°/s for the unregulated standard brake to about 550 Nm°/s for the ABS regulated case, while all experiments were conducted by a very experienced test rider at that time. Before the background of the smooth operation of the Honda C-ABS compared to the ABS utilized by Weidele, it is expected, that this level can be reduced for both characteristic values. Finally, in order to simultaneously capture the main effects and avoid undesired interferences with the rider's steering corrections to balance the vehicle when taking the feet off prior to standstill, both characteristic values are determined in the first two seconds of the experiment.

Video Footage with Audio Comments

With only a few exceptions, the majority of riding experiments were captured by an on board camera mounted on the rider's chest. The videos are synchronized with measured data through display of measurement number and a brake light indicator in the cockpit of the vehicle. Subjective judgments of the rider were typically given on handling upon entering the turn, steering torque demand in terms of initial level, kick-in, and total level during the maneuver in terms of steerability, as well as on disturbances in steering, roll and rider lean angles, and finally course deviations or lane keeping. Moreover, diverse comments were captured, e.g. on brake actuation, deceleration level, rider coupling, the occurrence of dynamic over-braking, or the general "feel" of a specific setup. This additional information is also taken into account for the interpretation of the measured test results in later passages.

5.2.2 Exemplary Comparison of Characteristic Values in Corner Braking Experiments with Standard Chassis vs. BSTAM

In order to illustrate how the previously defined characteristic values are derived from measurements, the time history of measured data is displayed and exemplarily compared for two similar corner braking experiments conducted with the standard chassis (HESD steering damper disconnected) and the BSTAM prototype setup ($tcr = 0.75$). Both experiments were done with partial front braking, using riding style lean with. A detailed list for direct comparison of the characteristic values is provided in Table 5.2.

The measurements for the standard setup are shown in Figure 5.2. The maneuver is starting with a straight acceleration phase. As a side note, a deviation of about 10° in the roll angle measurement (4th diagram) during acceleration is induced by engine vibrations. However, since turn maneuvers before each experiment were conducted in the same turn direction, the deviation is always towards the inside of the following experiment curve and eliminated, when roll dynamics occur during the experiment. Crossing the first solid vertical line in time indicates the initiation of the turn and start of the time span for handling evaluation. Around that time, also the clutch is disengaged for both experiments. However, despite the roll angle correction of the front wheel circumferential speed under assumption of undeformable tires, a slight increase in the signal is still to be observed due to the diminution of effective rolling radius for increasing roll angles (cf. 1st diagram). An outward steering torque impulse of 28.5 Nm at $t \approx -1.47$ s is causing a downward roll rate of 43.0°/s at $t \approx -1.35$ s (cf. 2nd and 4th diagram), the peak values of which are combined with the speed to Koch's handling index. In that case, an impressively low value of $K \approx 3.3$ $^{Ncm}/_{(m°/s²)}$ is highlighting the excellent handling of the baseline vehicle, compared to a reference value of $K \approx 5$ $^{Ncm}/_{(m°/s²)}$ for a "well handling" machine (cf. chapter 5.2.1). Reaching the next vertical line (at $t = 0$) indicates the end of the time for handling evaluation and the start of the brake maneuver. Until then, the roll angle of $\lambda \approx 35°$ matches well with the reference computed from speed (4th diagram) and the steering torque (2nd diagram) has settled to its really low free cornering value of only 5.3 Nm, directly followed by a sharp rise of $\Delta T_0 = 27.4$ Nm to its peak value of 32.7 Nm during just 0.2 s after brake kick-in. This is in the order of the expectations from the model prediction, i.e. ΔT_0 between the 25.7 Nm for the "ideal" brake force distribution (BFD) and 39.5 Nm for pure front braking (cf. cases 5 and 7 in Table 3.4). However, since only the front brake was activated, also the Combined-ABS will create a front oriented BFD that tends to create a steering torque demand (STD) that is closer to the higher value. The remaining part of total STD increase, that also arises from other steering torque components such as the tire twisting torque, is simply not balanced by the rider and therefore not measured. It creates disturbances along the BST chain of effects as follows. Regarding the steering angular disturbances (3rd diagram), the maximal steering rate of 23.7°/s is reached about 0.1 s after brake kick-in, causing the maximal

steering angle deviation of 1.6° just 0.05 s later, at $t \approx 0.15$ s. This is subsequently leading to the maximal upward roll rate of 58.2°/s at $t \approx 0.35$ s and roll angle deviation of 11.4° at $t \approx 0.65$ s (4th diagram).

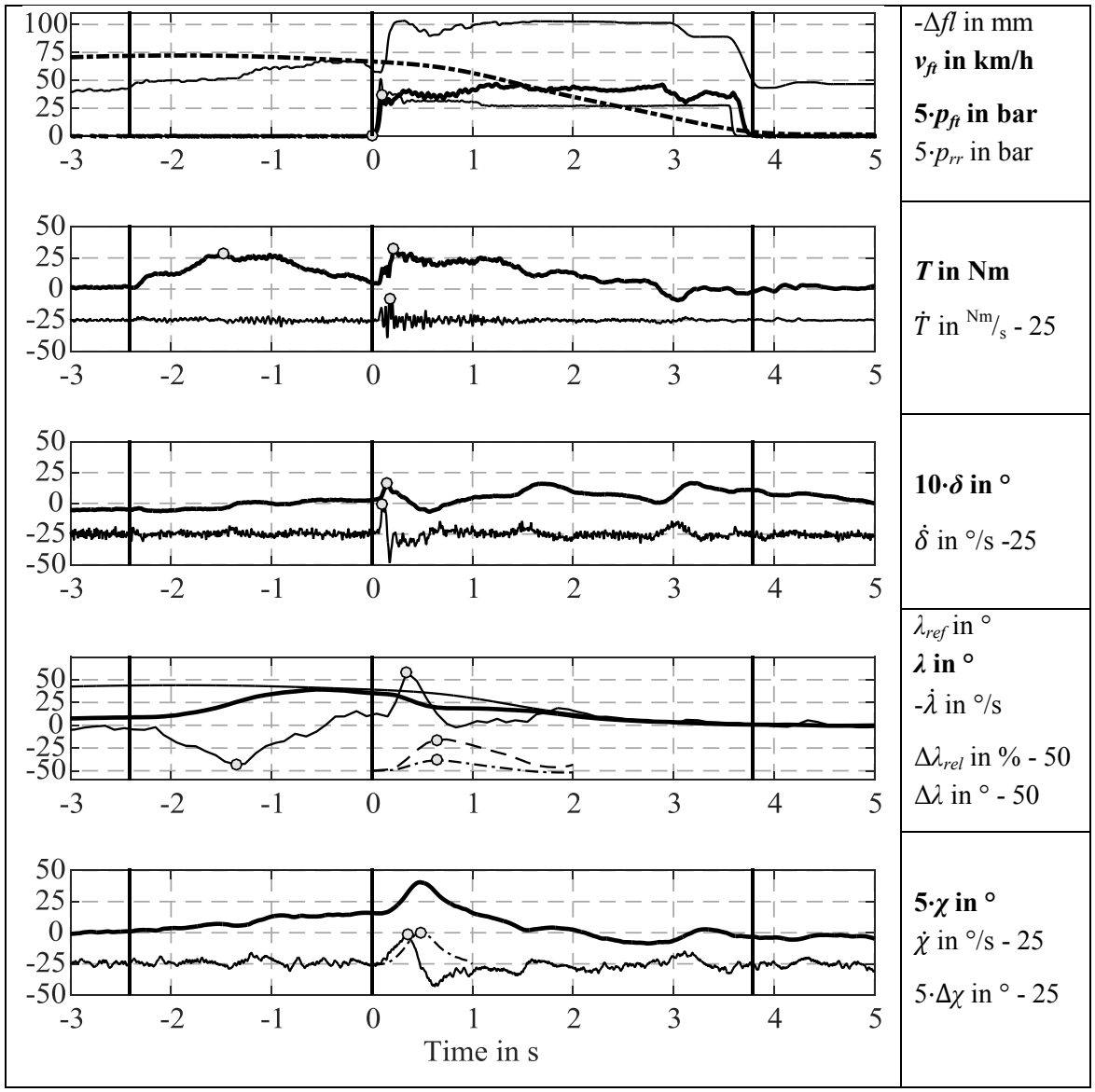

Figure 5.2: Time history of characteristic measurements for a partial front braking maneuver with standard chassis, riding style lean with, and steering damper (HESD) disconnected on $R = 50$ m cornering radius. Three solid vertical lines characterize the phase relevant for handling evaluation and brake maneuver. Circular markers indicate data points used for the derivation of characteristic values, except those that can be read from the intersection with the vertical line at $t = 0$. All derived characteristic values are listed in detail in Table 5.2.

The maximal rider lean angle velocity of 4.7°/s (5th diagram) is captured simultaneously with the maximal vehicle roll rate, delivering a peak rider lean angle deviation of about 5° inward at $t \approx 0.48$ s, prior to the peak deviation in vehicle roll angle at $t \approx 0.65$ s.

In global view of the experiment, an interplay between steering torque, angle, and roll fluctuations is to be observed up to $t \approx 2$ s, before the background of the bi-directional

coupling of steer and roll motion (cf. chapter 2.1.6). Finally, only a few tenth of a second later, the rider increasingly starts to superimpose balancing inputs to the steering and takes off his feet at about $t \approx 3$ s to hold the vehicle upright after standstill.

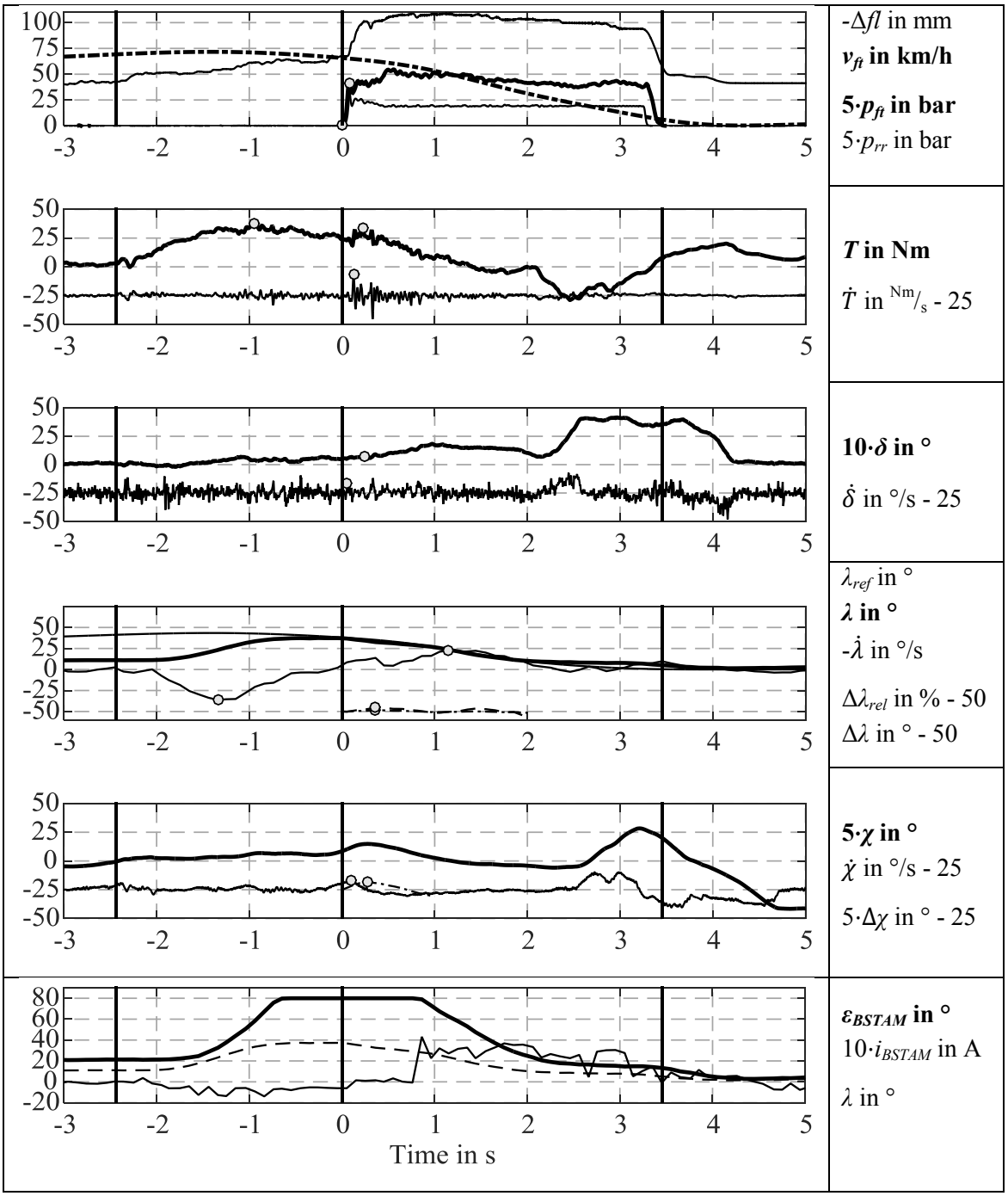

Figure 5.3: Time history of characteristic measurements for a partial front braking maneuver with BSTAM active (*tcr* = 0.75), and riding style lean with on $R = 50$ m cornering radius. Three solid vertical lines characterize the phase relevant for handling evaluation and brake maneuver. Circular markers indicate data points used for the derivation of characteristic values, except those that can be read from the intersection with the vertical line at $t = 0$. All derived characteristic values are listed in detail in Table 5.2.

As a side note, if the maximal rate in steering torque changes (2nd diagram in Figure 5.2) is directly derived from the steering torque signal, it strongly depends on minimal local fluctuations and the filter cutoff frequency. Hence, the mean increase rate (eq. (5.11)) is proposed as an indicator to better represent the character of the experiment and subjective impression of the rider.

Table 5.2: Characteristic values for partial front corner braking experiments on R = 50 m with the standard chassis (HESD steering damper disconnected) and active BSTAM, both for riding style lean with. Values with downsides for BSTAM have been highlighted in **bold**.

Characteristic Value	Unit	Standard Setup	BSTAM (*tcr* = 0.75)
v_0	m/s	18.6	18.6
K	Ncm/(m°/s²)	**3.3**	**5.3**
$\dot{p}_{ft,mean}$	bar/s	68.4	96.5
$a_{x,mean}$	m/s²	4.9	5.3
T_0	Nm	**5.3**	**24.0**
ΔT_{max}	Nm	27.4	10.3
T_{max}	Nm	**32.7**	**34.3**
ΔT_{rel}	Nm/(m/s²)	5.6	2.0
$\dot{T}_{mean}$	Nm/s	128.0	46.9
δ_0	°	0.26	0.48
$\Delta\delta_{max}$	°	1.33	0.27
$\dot{\delta}_{max}$	°/s	23.74	7.95
λ_0	°	35.0	37.3
$\Delta\lambda_{max}$	°	11.4	0.0
$\Delta\lambda_{rel}$	%	34.0	0.0
$\dot{\lambda}_{max}$	°/s	58.2	22.9
χ_0	°	3.2	1.7
$\Delta\chi_{max}$	°	4.9	1.3
$\dot{\chi}_{max}$	°/s	23.1	15.3
W	Nm°	**13.8**	**14.7**
W_{dyn}	Nm°/s	69.3	31.7

The measurements for the BSTAM setup to be compared to the baseline reference are shown in Figure 5.3. The presented example was chosen, because it combines typical aspects during the approach and main braking phase (-2.4 s ≤ t ≤ 2 s) with peculiarities at the beginning (0 s ≤ t ≤ 0.15 s) and at the end of the braking phase (t > 2 s). Starting with the typical aspects, the prior comments on the initial straight acceleration phase and speed measurement are equally applicable in that case. The turn is initiated by an outward steering impulse and Koch's handling index computed in the same way. However, as the steering torque demand is rising with increasing roll angle due to growing lateral steering axis displacement and loss of aligning steering torque components from the front tire lateral and normal forces $F_{y/z,ft}$ (cf. chapter 3), the handling index is growing considerably, in that case to $K \approx 5.3$ $^{Ncm}/_{(m°/s²)}$, which is still a relatively good absolute value, but 60% worse than the excellent baseline. Until the start of the braking maneuver at $t = 0$, the roll angle of $\lambda \approx 37°$(cf. 4th diagram) matches well with the reference and the stationary steering torque settles to 24 Nm. This is a difference of 18.7 Nm compared to the baseline of 5.3 Nm, and even higher than the model predictions (i.e. $T_{0,rel}$ = 12.9 Nm for B75 in Table 3.4). Transferred to driving on a rural road, such a high stationary STD would be very exhaustive for the rider and therefore unacceptable.

The picture is changing completely when the design situation of BSTAM, corner braking, comes into play. Despite slightly more challenging initial conditions in the BSTAM experiment in terms of front pressure gradient, deceleration level and initial roll angle, all captured disturbances in steering torque and angle, roll and rider lean angles as well as their change rates stay significantly below the baseline reference (cf. Table 5.2 for a complete list of direct comparison). The increase in steering torque (2nd diagram) after brake activation is only ΔT_0 = 10.3 Nm and in line with the model predictions (cf. 8.8 Nm ≤ ΔT_0 ≤ 13.1 Nm for a BFD between cases 5 and 7 in Table 3.4 for B75). Despite this reduction of 17.1 Nm in comparison to ΔT_0 = 27.4 Nm of the baseline, the absolute STD of 34.3 Nm with BSTAM is still a little higher than the 32.7 Nm of the baseline. This is mainly due to the elevated stationary STD of BSTAM, but to a certain degree as well due to the elevated average deceleration in the BSTAM experiment, with 5.3 vs. 4.9 m/s². While neither the peak values in steering angle or angular velocity are distinct (3rd diagram), the initial "stand-up" roll rate at $t \approx 0.36$ s is only 13.8°/s, compared to 58.2°/s of the baseline, and the maximal roll rate of 22.9°/s at $t \approx 1.15$ s is encountered as a natural consequence of keeping the roll equilibrium for decreasing speed (4th diagram). Moreover, the roll angle deviation towards the reference roll angle stays almost zero, underlining the desired and expected effectiveness of BSTAM compared to the deviations with the baseline. While the steering unsteadiness is again slightly elevated due to the higher stationary STD level of BSTAM, with 14.7 vs. 13.8 Nm°, the dynamic steering unsteadiness of BSTAM is ranging clearly below the baseline, with 31.7 vs. 69.3 Nm°/s.

Taking a digression to the first peculiarity at the beginning of the braking procedure ($t \geq 0$), the combination of a relatively new set of tires (i.e. high front wheel inertia) and sharp increase in brake pressure of 96.5 bar/s compared to only 68.4 bar/s in the baseline experiment, led to the only time, the "inertia effect" (cf. chapter 3.3.6) was actually captured and clearly felt by the test rider during all experiments. Hence, the measured steering torque (2nd diagram) is first dropping, before it increases due to the BST.

However, the absolute numbers in the signal that was low-pass filtered with 20 Hz cutoff frequency may be misleading. Starting from $t \approx 0.07$ s, this signal is dropping by 6.6 Nm until $t \approx 0.11$ s and then rising again by 14 Nm within only 0.03 s until $t \approx 0.14$ s. In contrast to this seemingly immense fluctuation, the drop in steering torque demand in a 3 Hz low-pass filtered signal is only 1.3 Nm (not displayed in the figure). This is exactly in the order of the model predictions (of 0.5 to 1 Nm) and in line with the rider's report on a "small but distinctive disturbance" that was different from ordinary dynamic over-braking and fluctuations encountered more regularly through transient slip conditions at the front wheel. Even though the latter effect may also have played a role to contribute to the large differences in the 20 Hz signal, a bandwidth of 3 Hz seems more applicable for the rider's feel[171].

Following the time course of the STD (2nd diagram) after this initial peculiarity, the STD is continuously dropping with decreasing speed and roll angle in qualitative accordance with the model predictions (cf. chapter 3.6.3) and quicker than for the baseline (cf. Figure 5.2). Also typical for experiments with a target compensation ratio of $tcr = 0.75$ is a tendency to over-compensation, that leads to a change of sign in steering torque demand, at around $t \approx 1.4$ s in the example. This means, that the rider needs to switch from applying an outward steering torque towards an inward steering torque to keep the intended cornering line. If this is not done, the vehicle tends to increase the roll angle (in analogy to a very gentle outward steering impulse). Due to the smooth transition and low absolute values (cf. $1.4 \text{ s} \leq t \leq 2.0$ s and a peak of -4 Nm), this is however done intuitively. Moreover, this characteristic is a great help to negotiate narrowing radius turns under braking with a very low STD (cf. chapter 5.4.3).

At the beginning of the brake maneuver, the position of the BSTAM excenter (cf. last diagram in Figure 5.3) stays at its pre-set limits of 80° until it starts turning at $t = 0.8$ s and $\lambda \approx 28°$. Concerning the circular markers of the characteristic values, except for the maximal roll rate, they all lie well within this period of no excenter movement.

This is the key-word for the transition to the final peculiarity of the presented example from $t = 2$ s and onwards, a reaction of the BSTAM mechanics (cf. Figure 4.7 and Figure A.1) to an overload situation and its driving dynamic consequences. During normal

[171] cf. Koch (1980): Untersuchungen des Motorrad-Fahrer-Systems, Chapter 1.2, p. 29ff

operation, the "actio = reactio" torques on both excenters balance each other out through the coupling with planetary gears. However, while the outer excenter is pivoting in two roller bearings (a tapered one towards the frame and a spherical one towards the inner excenter), the inner excenter centrally only features a slide bearing towards the steering shaft. Especially under higher loads when braking, increased friction torques and stick-slip effects in that bearing lead to deviations in the said balance, in a sense that the excenter assembly would turn back towards higher excenter angles and higher effective geometrical compensation ratios. Therefore, the BSTAM actuator is providing extra torque to restore the balance without any notice of the rider. To protect the planetary gears inside the BSTAM from damage, this is however only possible up to a certain level of input torque. As a safety mechanism, the clamping at the input shaft is designed to slip for input torques in excess of approximately 6 Nm. However, in the presented example, the shrink fit of the driving gear in the second planetary gear set was a weaker point and starting to slide from just after $t = 2$ s (it was reinforced for later experiments). In consequence, the excenter was sliding back by approximately 35° to positions of up to 45° during the rest of the brake maneuver, which would be fit for roll angles in the order of $\lambda \approx 20°$. – Even though not indicated by the position measurement that is placed at the actuator, this can be concluded from a controlled excenter movement of 10° when putting the vehicle upright after standstill and the necessity of a manual re-adjustment of 35° after the experiment.

Since the roll angle has already dropped to $\lambda \approx 10°$ at $t = 2$ s, the driving dynamic consequence is a strong over-compensation. Since the rider was already operating on the edge of applying inward steering torques, he reacted intuitively and promptly with a peak inward steering torque of almost 29 Nm at $t = 2.46$ s. Still, a drop in steering angle δ from about 1° to just 0.7° at $t = 2.1$ s (cf. 3rd diagram) marks a distinct outward steering impulse that is slowing down the desired upward roll movement (cf. 4th diagram). Until the end of the experiment, the roll angle stays higher than the reference, with a maximal deviation of up to 6.5° at $t = 3.05$ s and about 5° at standstill, trying to force the vehicle to a narrowing radius. To stay as good as possible on a constant radius and to balance the vehicle towards a more upright position upon standstill, the rider is increasing the steering angle to values slightly beyond 4° which are reached shortly after the peak in inward steering torque, at $t = 2.57$ s, which remain until the end of the experiment. The video footage documents impressively, how the rider's inward steering effort is supported in a self-stabilizing way by the friction torque that arises in the central slide bearing at the steering shaft when the inner excenter is sliding from its target position to higher values. As another measure to keep the balance, the rider is also increasing his body lean angle (cf. 5th diagram), from around 1° lean out at $t = 2.5$ s up to almost 6° of lean in at $t = 3.2$ s. Finally, also the steering torque demand (cf. 2nd diagram) tends back to slight outward steering with the rider's pre-stop control actions, taking off his feet and supporting his upper body against the handlebars.

5.2.3 Arrangement and Display of Results

As a basis for the analysis and presentation of results for all riding tests, 18 of the presented characteristic values have been selected, grouped and arranged in a matrix form along the BST chain of effects as illustrated in Table 5.3. The same arrangement is subsequently used for different types of analysis and display formats as discussed in context of the respective chapter where first used.

Table 5.3: Matrix arrangement of 18 characteristic values, following the BST chain of effects.

Initial Conditions for reference	Handling	Deceleration for reference	Characteristic Value Group along the chain of Effects
v_0	K	$a_{x,mean}$	
T_0	ΔT_{max}	$\dot{T}_{mean}$	Steering Torque
δ_0	$\Delta\delta_{max}$	$\dot{\delta}_{max}$	Steering Angle
λ_0	$\Delta\lambda_{max}$	$\dot{\lambda}_{max}$	Roll Angle
χ_0	$\Delta\chi_{max}$	$\dot{\chi}_{max}$	Rider Lean Angle
$\dot{p}_{ft,mean}$	W	W_{dyn}	Integral Measures
	Deviation	Rate of change	
	Results Corner Braking		

5.3 Global Analysis of All Test Results

The matrix arrangement of characteristic values as presented in Table 5.3 was chosen under two assumptions. Firstly, that the characteristic disturbance values in one group along the horizontal direction (e.g. steering torque deviation and rate of change) are correlated and may be interpreted together. And secondly, that there are also correlations to be found between the different groups in vertical direction, following the chain of effects. In case this assumption proves justified, it supports the validity of the hypothesis that smaller disturbances in steering torque, respectively steering angle values, also lead to smaller disturbances concerning the “stand-up” in roll motion as well as subsequent course deviations. On that basis, it is furthermore also justified, to compare experiments with centered steering axis chassis setups with those with active BSTAM on a global level. Hence, a global analysis of results is conducted in two steps, starting with a correlation analysis (cf. chapter 5.3.1.) to check the preconditions for the second step. Table 5.4 gives an overview of all evaluated experiments, clustered in setup groups.

Table 5.4: Nomenclature of global setup groups and number of evaluated tests[172]

<table>
<tr><th>Setup Groups</th><th>R70</th><th>R50</th><th>Sum per Setup Group</th><th>Sum CTR LOW</th><th>Sum CTR ALL</th></tr>
<tr><td>STA ABS</td><td>57</td><td>52</td><td>109</td><td colspan="2" rowspan="3">164</td></tr>
<tr><td>STA (LOW)</td><td>10</td><td>3</td><td>13</td><td rowspan="2">55</td></tr>
<tr><td>BPC (LOW)</td><td>0</td><td>42</td><td>42</td></tr>
<tr><td>BSTAM (LOW)</td><td>21</td><td>98</td><td>119</td><td colspan="2" rowspan="5">STA: Standard Steering Axis
BPC: BSTAM passive center
CTR: Centered Steering Axis (STA + BPC)
BSTAM: BSTAM active
ABS: High / Max. Deceleration
LOW: Partial Deceleration</td></tr>
<tr><td>Sum per Radius</td><td>88</td><td>195</td><td></td></tr>
<tr><td>Total Sum ALL EXP</td><td colspan="2">283</td><td></td></tr>
</table>

5.3.1 Correlation Analysis of Characteristic Values

The correlation analysis is done for three groups: All experiments (ALL EXP) and its two sub-groups of all experiments with centered steering axis (CTR ALL = STA + BPC), and finally all experiments with BSTAM in active mode (BSTAM).

Within these three groups, all characteristic values are correlated with one another[173], obtaining correlation coefficients R and probability values p for the probability of getting a correlation R as large as the observed value by random chance, when the true correlation is zero. In case p is small ($p < 0.05$) the correlation R is assumed to be significant. In a next step, scatter plots are generated and linear regression lines are introduced[174], as exemplarily illustrated in Figure 5.4.

[172] Note that a much higher number of tests was conducted especially for the standard reference (STA LOW). However, the captured data files were physically corrupted and could not be evaluated. Moreover, many more tests were done during the development phase of the prototype motorcycle with different tires and only partially functional measurement setup. While these are consequently also not taken into account for numerical evaluation, the gained subjective impressions of the test rider are however a valuable help for the interpretation of the remaining small number of complete data sets.

[173] Using the "corrcoef"-command in MATLAB ® Software.

[174] Using the "polyfit"-command in MATLAB ® Software.

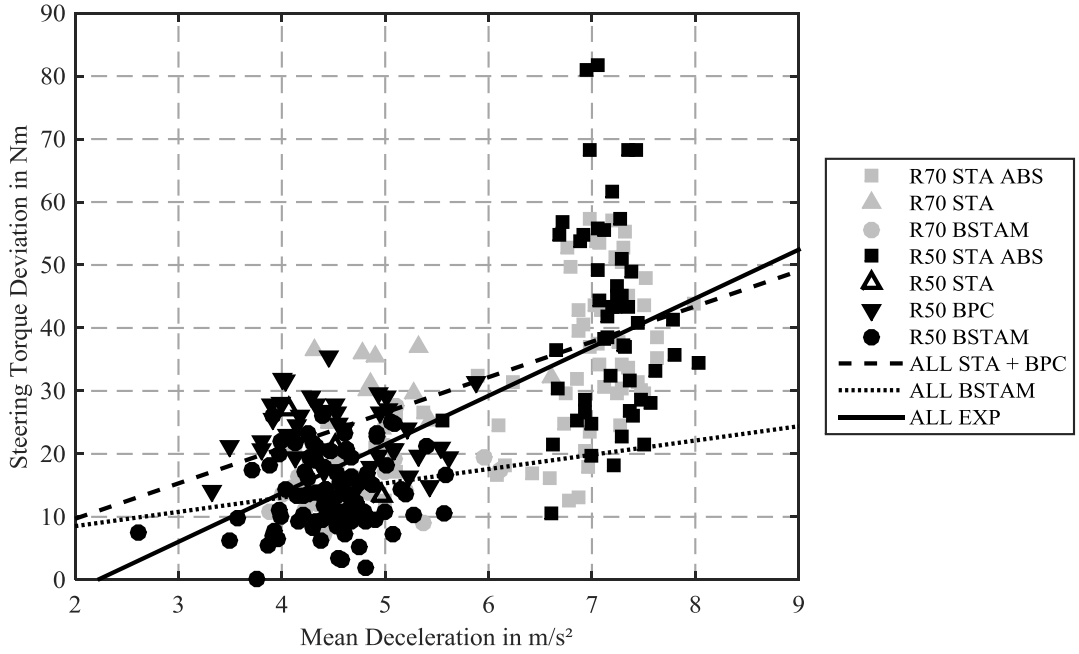

Setup	*R*	*p*	g_1 in $^{Nm}/_{(m/s^2)}$	g_2 in Nm
ALL EXP	0.691	$1.52 \cdot 10^{-41}$	7.73	-17.2
CTR ALL (STA + BPC)	0.512	$2.53 \cdot 10^{-12}$	5.62	-1.55
ALL BSTAM	0.197	0.0319	2.27	3.99

Figure 5.4: Example of a scatter plot between two characteristic values

Along with the correlation coefficients R and probabilities p, also the slope and axis intercept parameters g_1 and g_2 of the regression lines have been computed for all possible correlations. If x is the first characteristic value and y the second that is correlated to the first (in the example x is the mean deceleration and y the steering torque deviation), the regression line is defined by the following equation:

$$y = g_1 \cdot x + g_2 \tag{5.24}$$

The unit of the slope parameter is $[g_1] = [y]/[x]$ and that of the axis intercept $[g_2] = [y]$, which can be read for the example from the table in Figure 5.4. As a side note, the full correlation results are listed in tables (for R, p, g_1, and g_2 parameters) in appendix A.5.

Regarding the example scatter plot with the correlation of steering torque deviation and mean deceleration in Figure 5.4, it is apparent, that BSTAM experiments have typically been conducted at partial decelerations, while $^2/_3$ of experiments with centered steering axis have been done at high decelerations (ABS). A high correlation of $R = 0.691$ has been found for all experiments, while the decomposition into the two subgroups reveals a stronger correlation and steeper slope parameter ($R = 0.512$, $g_1 = 5.62$ $^{Nm}/_{(m/s^2)}$) for

setups with centered steering than for BSTAM ($R = 0.197$, $g_1 = 2.27\ ^{Nm}/_{(m/s^2)}$), which hints at a certain decoupling of the correlation through BSTAM.

Results of Correlation Analysis

Finally, all combinations of characteristic values, where a correlation of $R \geq 0.35$ is obtained at least within one of the three experiment groups (ALL EXP, CTR ALL, ALL BSTAM) are analyzed in detail and entered into global correlation charts (cf. Figure 5.5) that follow the arrangement scheme presented in Table 5.3.

Only correlations with a correlation coefficient of $R \geq 0.3$ are entered into the scheme, following the illustration patterns as shown in the legend of Figure 5.5. For reasons of a better overview, dominating correlations (towards deceleration, pressure increase rate, stationary steering torque demand and dynamic steering unsteadiness) have not been illustrated using arrows, but rather letters (a, p, T, W) in either of the four corners of each characteristic value field correlated to it.

The correlation charts in Figure 5.5 (a through c) are to be regarded differentially. First, the chart (a) for ALL experiments confirms both the expected horizontal and vertical coupling among the characteristic disturbance values along the chain of effects. Moreover, a strong coupling of the majority of variables is given towards the mean pressure increase rate, the mean deceleration and the stationary steering torque. Before the background, that the experiments with active BSTAM exhibit a distinctively higher stationary steering torque and were moreover conducted as partial braking experiments, while the experiments with centered steering axis comprise $^2/_3$ of maximal braking maneuvers, it lies at hand, that the picture will change, if the correlations are regarded separately for the two subgroups of experiments.

Regarding correlation chart (b) for the experiments with centered steering in Figure 5.5, the strong horizontal coupling of disturbance values remains approximately at the same level, while the vertical coupling along the chain of effects appears partially weaker, especially between the steering and roll disturbances. It is however still present with correlation factors $R > 0.4$. While the coupling of many variables towards the pressure increase rate and mean deceleration remains, the coupling towards the initial steering torque is lessening, however still present. This can be explained by the fact of variations in riding style (lean in, lean with, and lean out), which will be addressed in more detail for the analysis of individual experiment groups in chapter 5.4.

Regarding the correlation chart (c) for the BSTAM experiments in Figure 5.5, the horizontal coupling remains at a lower level and the vertical coupling along the chain of effects is greatly weakened, especially between the disturbances in steering torque and steering angle values. Most of all, the coupling of all result variables towards the brake pressure increase rate and the mean deceleration level are completely nullified, under-

lining the effectiveness of BSTAM in this respect. A relatively strong coupling of some variables remains however towards the stationary steering torque. The reason is, that the higher the compensation ratio is chosen, the higher is the stationary steering torque demand, while at the same time reducing the disturbance values to a greater extend. Hence, the resulting negative correlations (marked "-T") are arising.

As a side note on negative couplings that are valid for all three experiment groups, the higher the initial speed, the lower the initial steering angle in accordance with chapter 2.1.5. And, the more the rider starts off with a lean in riding style, the less will he be moved further inward for a stand up of the vehicle.

In conclusion of the correlation analysis it can be stated, that both the horizontal and vertical coupling are there, as expected, so that the variables in each group may be discussed together, as well as along the chain of effects. This finding is also in line with the subjective impression of the test rider.

5.3.2 Performance of Centered Steering Axis vs. BSTAM

Comments on the Display Format: Notched Box-Plots

In the following sections, the characteristic values obtained in riding experiments with different setup groups are displayed, compared, and discussed using notched box-plots. Each experiment yields a single data point and multiple experiments within one group form a vector that can be displayed using a box-plot. This display format is briefly discussed in the following[175] (for a visual impression, refer to Figure 5.6).

On each box, the central mark is the median and the edges of the box are the 25th and 75th percentiles (Q_1 and Q_3) of the displayed data. Whiskers extend like antennas with dashed lines from the box to the most extreme data points not considered outliers. As a standard value, the maximum whisker length L is set to 1.5 times the inter-quartile range, which corresponds to approximately ± 2.7-σ and 99.3% coverage of the data, if they are normally distributed[176]. Hence, data points are defined as outliers and plotted individually using "+"-markers if they are larger than $Q_3 + L \cdot (Q_3 - Q_1)$ or smaller than $Q_1 - L \cdot (Q_3 - Q_1)$. In order to allow direct comparison between test setups, comparison intervals are displayed using notches. Two medians are significantly different at the 5% level if their intervals do not overlap. The interval endpoints are the extremes of the notches, which may extend beyond the end of the box when the sample size is small.

[175] The explanation is based on the MATLAB ® help on the "boxplot"-command and contains some similar phrases that were not indicated as quotes for better readability.

[176] In that context, the Greek letter σ stands for the standard deviation, not to be confused with the king-pin inclination angle in the previous chapters.

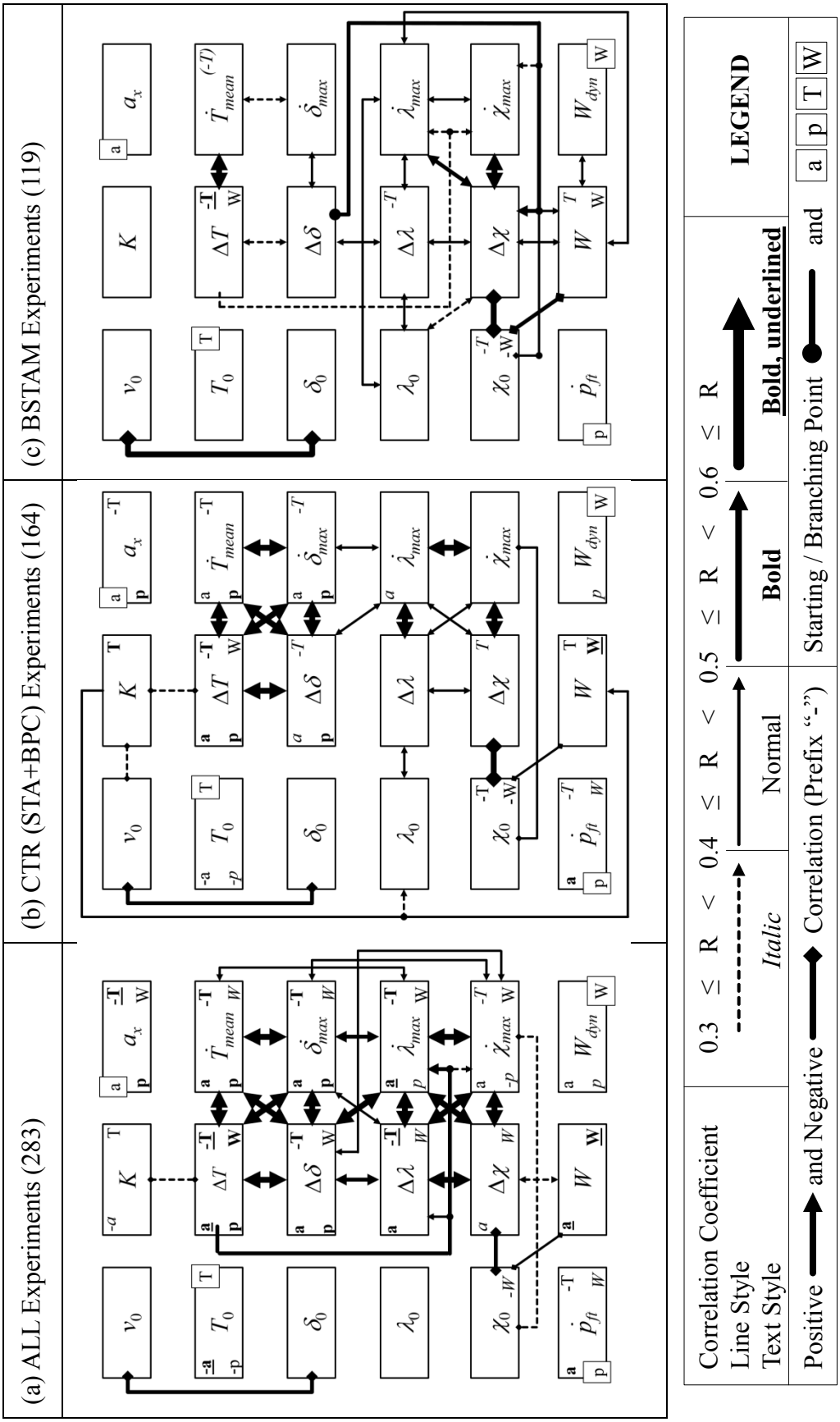

Figure 5.5: Correlation charts for global experiment groups (Note that the figure belongs to the previous chapter)

Results of Global Comparison

Based on the findings from the correlation analysis, the obtained characteristic values for active BSTAM setups (annotation: BSTAM) are compared to those of centered steering axis setups (CTR ALL). The latter group is further subdivided in experiments with high deceleration, which were solely conducted with baseline steering geometry (STA ABS), and those that were performed as partial braking experiments, mostly with BSTAM in passive centered position (CTR LOW). The results of the global comparison are summarized in Figure 5.6, using notched box-plots in the matrix arrangement from Table 5.3, and including the results of all experiments (ALL EXP) for reference.

Starting with the initial conditions in the first column in Figure 5.6, the experiments with centered steering axis comprise more experiments on the R70 test track and hence feature higher initial velocities. Most of the partial braking maneuvers were conducted on the R50 test track and show no significant differences in the median of initial speeds.

Compared to the STA setups, the initial steering torque demand is already significantly higher for the group CTR LOW, with three exceptions all conducted with BSTAM in passive centered mode. While a small difference was expected on the basis of model calculations, two contributing factors may be seen in the presence of more R70 experiments for the STA setups as well as in increasing tire wear throughout the experiments. As expected, the stationary steering torque demand is again significantly higher for the active BSTAM setups.

The medians of the initial steering, roll and rider lean angles do not significantly differ between the five groups. The initial rider lean angle shows a slight tendency towards a lean in riding style of 3° to 4° body lean. The outliers for the standard setups included in ALL EXP, STA ABS and CTR ALL groups, result from the use of different riding styles and the swerve maneuver required at the entry of the R70 test track.

The mean front brake pressure increase rate (bottom left) and deceleration level (top right) are naturally highest for the ABS experiments. Among the partial deceleration experiments, the median of the pressure increase rate is approximately 14% (but not significantly) lower for the active BSTAM setups, while the deceleration level only differs by less than 2%, with 4.61 $^{m}/_{s^2}$ compared to 4.52 $^{m}/_{s^2}$, respectively.

Concerning the steering torque deviation, it is significantly lower for the low deceleration experiments (CTR LOW) than for those with high decelerations (STA ABS) and again significantly lower for the active BSTAM setups. Even the total steering torque demand combined from the initial and deviation value remain slightly below for the active BSTAM setups compared to CTR LOW (with medians of 34 Nm vs. 37 Nm). A similar picture repeats for the steering torque gradient, however without significant improvements for BSTAM compared to other partial braking experiments. Especially high values are encountered for ABS regulated braking and riding style lean out.

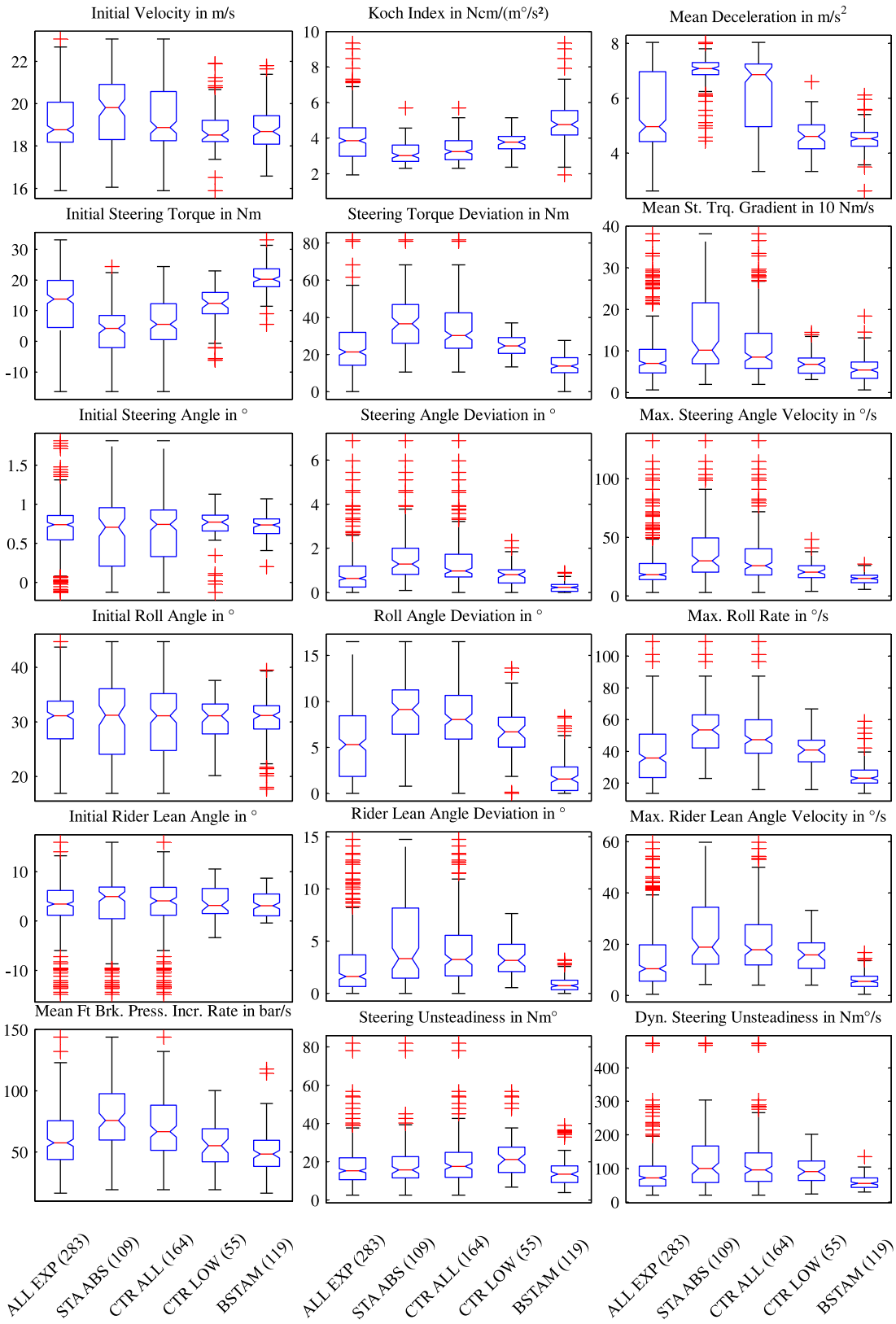

Figure 5.6: Results of global performance comparison between active BSTAM and centered steering axis. Note, that three outliers between 10 and 28 Ncm/(m°/s²) are omitted for the Koch Index (center diagram in the top row), both in the BSTAM and ALL EXP groups. The value in brackets behind the annotation is the number of tests in each setup group.

Following the chain of effects, the disturbances in steering, roll, and rider lean angles as well as their change rates are always significantly lower for active BSTAM setups compared to partial braking with centered steering axis, CTR LOW. Again, ABS brake maneuvers or lean out foster higher values in the first three regarded experiment groups.

Finally, also the steering unsteadiness and dynamic steering unsteadiness are significantly lower for BSTAM compared to the other partial braking experiments. It is worth noting, that the obtained medians of both values for ABS braking stay below the reference values found by Weidele (W: 15.8 vs. 20 to 30 Nm°, W_{dyn}: 99.5 vs. 100 to 550 Nm°/s), while also the absolute peaks for the dynamic value are lower. Despite the more severe boundary conditions in terms of initial speeds and lateral acceleration, this underlines the past 20 years' improvements is brake technology, especially ABS control quality (in terms of "smoothness").

As a side note, the diagram is also provided using cumulative distribution functions ("CDF-plots") as display format in appendix A.5.1, along with single diagrams on the omitted relative steering torque deviation as well as relative roll angle deviation values.

5.3.3 Interim Conclusions from Global Analysis

The results of the global analysis are in line with the exemplary analysis (cf. chapter 5.2.2) and confirm the proposed hypotheses on the performance of BSTAM (cf. H_{BSTAM} in chapter 3.7.1) as follows.

Concerning the handling characteristics, already the passive BSTAM with centered steering axis is performing slightly poorer, than the baseline reference, due to the increased caster angle, trail, and more indirect steering transfer ratio (cf. chapter 2.1.5).

Except for the significantly increased stationary steering torque demand (of 20.3 Nm compared to 5.6 Nm for baseline and 12.4 Nm in median for BSTAM in passive mode), the active BSTAM performs generally better in all disturbance values than the baseline, under similar boundary conditions.

However, as expected, the benefits in absolute steering torque level are marginal (34 Nm vs. 37 Nm for the partial braking maneuvers), and those for the steering unsteadiness small (13.6 Nm° vs. 21.2 Nm°), which is also a consequence of the high stationary steering torque demand of the active BSTAM setups.

Even though the median of initial brake pressure gradient is by approximately 14% lower in the active BSTAM experiments than in the other partial braking ones, the significance of BSTAM's benefit in all other analyzed criteria cannot be turned down, even when linear scaling would be applied for these values.

5.4 Detailed Analysis of Individual Test Results

In this section, the already known box-plot display format in matrix arrangement is used to compare the test results of six individual experiment groups. The first two are, maximal (ABS) braking on both 50 m and 70 m turn radii with standard chassis setup under variation of riding style, rider coupling, brake force distribution, and connection of steering damper (HESD). The second two are partial braking with both standard reference chassis and BSTAM in different setups on both turn radii, and the latter two are special tests, comprising experiments on narrowing radius turn, with clutch engaged, and with BSTAM "jump algorithms" on the 50 m radius (cf. chapters 3.6.4 and 4.4.5).

5.4.1 Test Setup Nomenclature of Abbreviations

In order to allow brief annotation of the box-plot result figures, the different test setups are described in short form by a concatenation of the symbols explained in Table 5.5.

Table 5.5 (part 1): Test setup nomenclature of abbreviations (continued on the next page)

Symbol	Explanation
Steering Axis Geometry	
S	Standard (centered) steering axis without HESD
H	Standard (centered) steering axis with HESD
B(L)	BSTAM in long trail mode. If not indicated, this is the default.
(BS)	(BSTAM in short trail mode, not presented)
BSTAM Actuation Mode (applies to BSTAM setups only)	
pc	Passive center, with upper steering bearing and consequently also the steering axis fixed in centered position
50 / 65 / 75	Active control with target compensation ratio *tcr* = 0.5 / 0.65 / 0.75
ja / jb / jc	Jump algorithm a / b / c (according to definition in chapter 4.4.5)
Riding Style	
LW / LI / LO	Lean With / In / Out. If not indicated, the default is LW.
Brake Application	
ft / rr / bb	Application of front brake only / rear brake only / both brakes. If not indicated, the default is ft with partial deceleration.

Table 5.5 (part 2): Test setup nomenclature of abbreviations (continued from prev. page)

Symbol	Explanation
Miscellaneous Suffixes	
N	Narrowing curve radius. If not indicated, the default is constant radius.
E	Clutch engaged with throttle jammed in different positions. If not indicated, the default is clutch disengaged and engine at idle speed.
tc / lc	Explicitly tight / loose coupling of the rider, in terms of body and esp. arm pre-tensioning. If not indicated, the default is normal coupling.

As an example “HLIbblc” describes a constant radius corner braking maneuver with standard steering axis, HESD active, riding style lean in, partial application of both brakes with the rider explicitly loosely coupled to the vehicle.

5.4.2 ABS Braking with Standard Steering under Variation of Brake Application, Riding Style, and Steering Damper

ABS Braking with Standard Steering – Results R70 (Figure 5.7)

As a general remark on the experiments conducted on the $R = 70$ m test course, it needs to be reminded, that the entrance into the pylon lane required a right-left swerve maneuver from one side and that a pothole needed to be evaded on the other. In combination with the relatively high initial speeds and lane width, the initial conditions of individual experiments are much harder to keep constant for the test rider, as they are on the test track with $R = 50$ m turn radius.

Starting in the top row of Figure 5.7, the initial speeds at brake activation do not significantly differ and reach a median of 20.8 m/s. The median of Koch’s handling index is 2.8 $^{Nm}/_{(m°/s²)}$, underlining the excellent handling qualities of the baseline motorcycle, with a small benefit and less scatter for lean in riding style. The median of achieved decelerations is just below 7 m/s² with a tendency towards higher possible decelerations when using both brakes, but only with a non-significant distance to sole front braking.

Following the first column on the initial conditions further downwards, the median of initial steering torque is only 2.7 Nm, with significant increases for lean out (8.7 Nm) and significant decreases for lean in (-6.9 Nm) riding style. The medians of both initial steering and roll angles show no significant differences among the test setups and their medians are 0.67° and 31.2°, respectively. It has to be noted, that the median of initial roll was much (however not significantly) lower for the latter two setup groups.

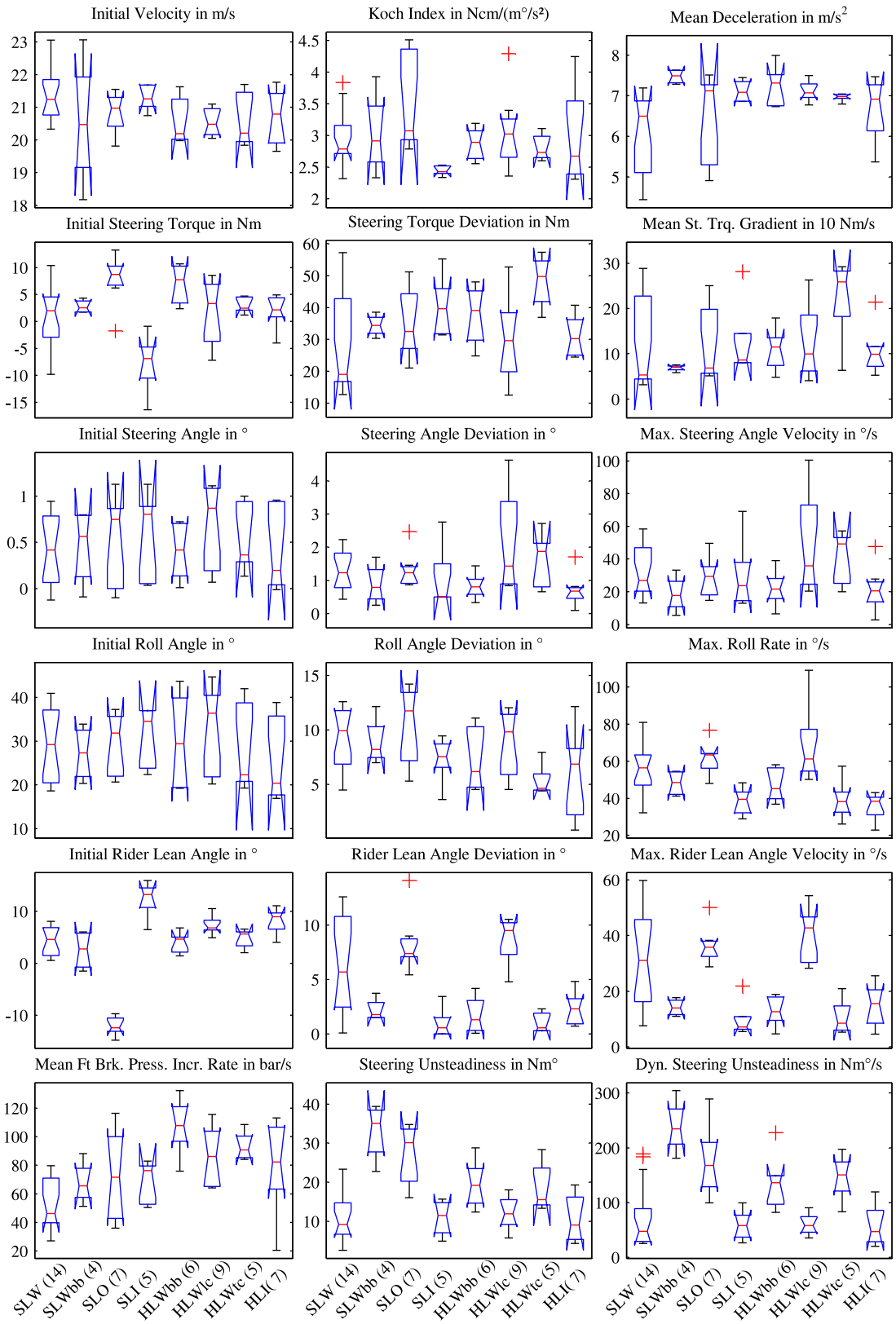

Figure 5.7: Results for ABS braking experiments with standard steering under variation of brake application, riding style, and steering damper on $R = 70$ m turn radius. The value in brackets behind the annotation is the number of tests in each setup group.

The initial rider lean angle's median is 5.9° towards lean in, showing significant differences towards both riding styles lean in (13.2°) and out (-12.4°), with an exception for the last setup, that does not significantly differ from the prior lean with setups due to the said limitations in repeatability on the R70 track. Finally, the mean front brake pressure increase rate shows a median of 74 bar/s, but varies quite distinctively between the setups, i.e. being generally higher with the activated steering damper, than without.

Tracing down the results in the second and third column together from the second row, the medians of steering torque deviations range between 20 and 50 Nm with an overall median of 32.5 Nm. The only significant differences occur between loose and tight rider coupling, with the higher value achieved for tight coupling. The same holds true for the steering torque gradient, with a median of 89.5 Nm/s (note the scaling factor 10), where significant differences are to be found analogously between the same two groups.

The steering angular disturbances (in the third row) display no significant differences between setups, with medians of 0.93° and 26.7°/s, respectively. Despite the elevated brake pressure increase rates for experiments with steering damper active, this experiment group shows a tendency towards lower disturbances.

Regarding roll angle deviations (see fourth row), this picture is repeated, with a median of just below 8° and lower values for the tight coupling experiments, which typically already started at lower initial roll angles. The roll rate shows a median of 52.1°/s, and has a tendency to higher values for lean out riding style. It reaches its peak values around 100°/s for loose rider coupling, while lowest values are achieved for tight rider coupling or lean in riding style, with the steering damper active.

The rider lean angle deviation (see fifth row) with a median of about only 3° shows significant increases for experiments with lean out and lose coupling (in the order of 10°). Again, this picture is repeated for the maximal rider lean angle velocity with a median of just below 19°/s and lean out, respectively lose coupling experiments reaching significantly higher levels in the order of 40°/s and more.

Finally, regarding both the steering unsteadiness parameters (in the sixth row of the figure), the medians are 14.6 Nm° and 87.5 Nm°/s, respectively. The highest values are achieved when using both brakes or lean out riding style. Concerning the rider coupling, higher values occur for tight coupling in comparison to lose coupling, with significant differences for the dynamic steering unsteadiness. The lowest values occur for light coupling and lean in riding style, both with steering damper active.

ABS Braking with Standard Steering – Results R50 (Figure 5.8)

Figure 5.8 presents the results for the same experiment type on the $R = 50$ m test track. Starting again in the top row of the figure, it is worth noting, that the results of the first setup SLW were captured during the test definition phase with still lower entry speeds

and variations in rider coupling as documented in the video footage, while all other experiments were conducted on a single test day. Hence the other initial speeds at brake activation do not significantly differ and reach a median of 18.3 m/s. The median of Koch's handling index is 3.0 $^{Nm}/_{(m°/s²)}$, with a tendency to higher values for experiments with both brakes and especially lean out riding style, which results from the elevated steering torque demand using lean out on the one hand and may be fostered by the rider's anticipation of high decelerations for tests with both brakes on the other.

The median of achieved decelerations is just below 7.2 m/s² with a tendency towards higher possible decelerations when using both brakes, but only with non-significant distance towards sole front braking.

Following down the first column of initial conditions, the median of initial steering torque is 5.3 Nm, with significant increases for lean out riding style. While values for lean in differ significantly from lean out, the gaps towards lean with are non-significant. Moreover, due to the lower speeds of the first experiment group, the initial steering torque is even inward the turn, which is in line with literature (cf. Figure 3.8[177]).

Apart from the naturally higher steering angle and lower roll angle at the lower speed of the SLW setup group (cf. chapters 2.1.2, and 2.1.5), the medians of both initial steering and roll angles show no significant differences among the test setups and their medians are 0.75° and 31.1°, respectively. The initial rider lean angle's median is 2.6° towards lean in. Provided the better boundary conditions, clearly distinct and significant differences towards both riding styles lean in and out were obtained. Finally, the mean front brake pressure increase rate shows a median of 83.2 bar/s, with a tendency to higher values when using both brakes. Again, a deviation has to be marked for the SLW setup, where the scatter in brake activation rates was biggest, reaching peak values in the order of 140 bar/s. As documented on video, this involved a few experiments with beginning dynamic over-braking of the front wheel, being quickly resolved by C-ABS control.

Jumping to the inner field of results (in the second row), the medians of steering torque deviations range between 25 and 55 Nm with an average of 39.7 Nm and the lowest median for lean out, which already featured a high stationary steering torque demand. Due to the high pressure increase rates, the highest medians are achieved for the SLW experiments, directly followed by those of SLI. This picture is repeated also for the steering torque gradient with a median of 116.7 Nm/s (note the scaling factor 10).

The steering angular disturbances (see third row) display the same behavior, with the highest values for SLW and SLI, which for the SLW experiments can likely be attributed to short slides of the front wheel under dynamic over-braking. Other than that, differences between setups remain non-significant, with medians of 1.6° respectively 38.2°/s.

[177] According to Cossalter (2006): Motorcycle Dynamics, p. 134, Fig. 4-30

Regarding roll angle deviations with a median of 9.9° (in the fourth row), the highest values are encountered for lean out riding style. In case both brakes are used, this results in significant differences towards lean in riding style. The significantly lowest values are to be observed for lean in riding style, with no significant changes within this group when using both brakes or engaging the steering damper. This picture is repeated, with a median of 57.8°/s for the maximal roll rate, however, with significant differences only between the lean out and lean in groups and lower values for the latter.

Rider lean angle deviations with a median of 3.6° are significantly highest for lean out (around 12°) and lowest for lean in riding style (below 2°), while the latter only benefits slightly over lean with (ca. 3.5°), since also these experiments are conducted with lean in tendency. The same holds true for the maximal rider lean angular velocity, with an overall median of 19.4°/s, around 36°/s for lean out and just around 10°/s for lean with.

Finally, regarding the two steering unsteadiness parameters (in the sixth row), the medians are 17.0 Nm° and 120.5 Nm°/s, respectively. The highest values are achieved when using both brakes, especially when in combination with lean out riding style, while the lowest values are attributed again to lean in riding style, regardless of using just the front brake, both brakes or activating the steering damper.

ABS Braking with Standard Steering – Conclusions

In conclusion of the maximal ABS regulated corner braking experiments, it has to be stated that the BST effect was not an issue under the controlled test conditions when the rider was always anticipating the impending brake maneuver.

Especially for the lean in riding style, subjective improvements were clearly to be felt, as expected from the hypotheses ($H_{RidingStyle}$) derived in chapter 3.7, while lean out went along with downsides and a perception of greater steering and roll oscillations that were however neither regarded as critical nor reflected in the box-plot format of evaluated data. In this respect, the hypothesis on lean out riding style cannot be fully confirmed for the captured steering torque and angle deviations, while they hold true for the other disturbance values and the subjective impression of the rider. The achieved upward roll motion in the experiments matched generally well with the provided deceleration level, requiring an upright position at standstill. Even for very harsh brake actuation, partially involving slight dynamic over-braking, it feels like the front wheel is taking itself the necessary sideslip angle, leading to a self-stabilization of the braking process. While the roll-moment generated through the different tire contour radii in front and rear is mitigating the stand-up tendency upon brake activation (cf. chapter 2.1.7, i.e. Figure 2.13 and eq. (2.30)), the vehicle performs its initial stand-up motion below the rider, leading to a more “lean in” riding position, which is additionally lowering the STD and improving its balance to the rider’s steering effort (cf. chapters 2.1.2, 2.1.3, 2.2.3, and 3.2).

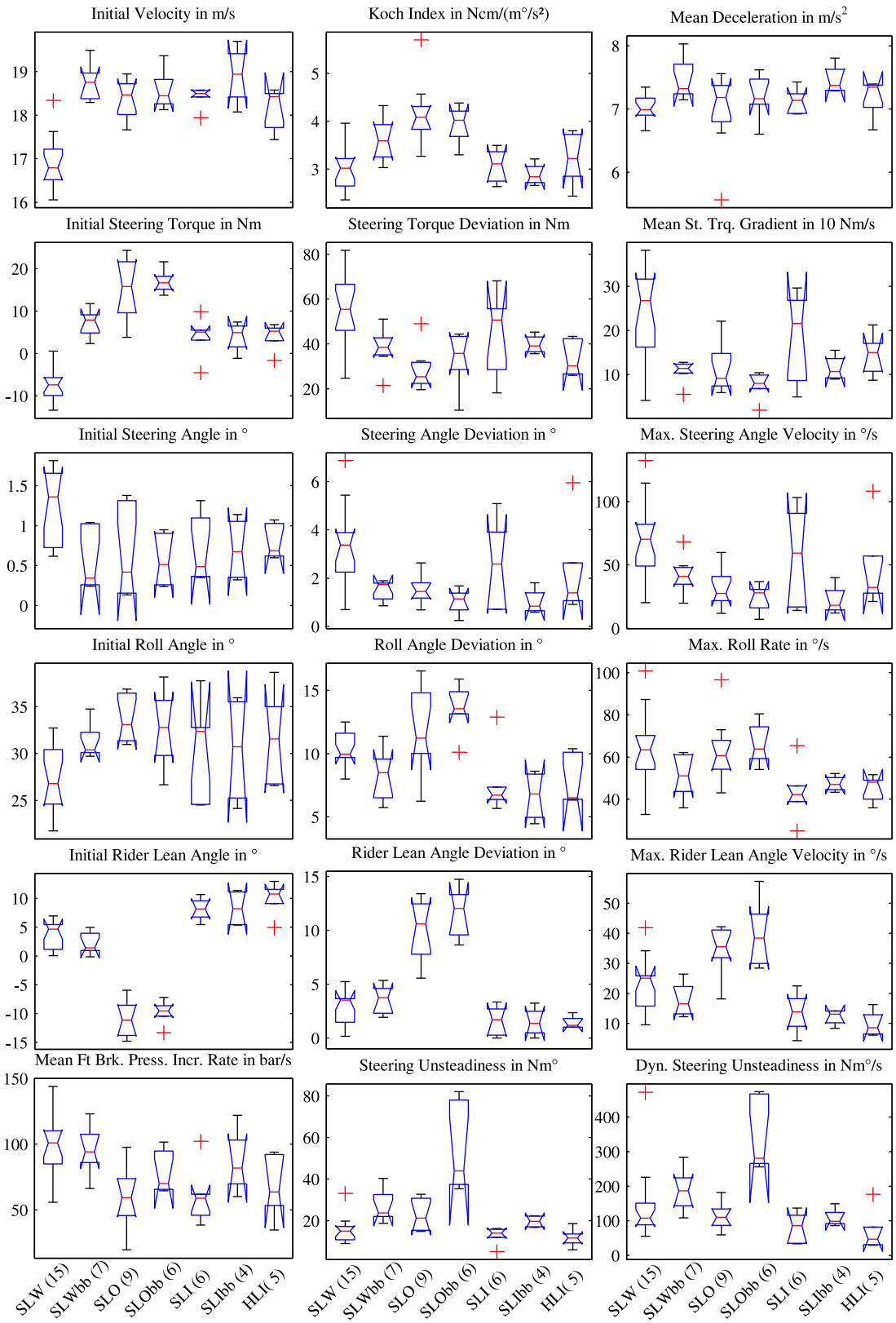

Figure 5.8: Results for ABS braking experiments with standard steering under variation of brake application, riding style, and steering damper on $R = 50$ m turn radius. The value in brackets behind the annotation is the number of tests in each setup group.

However, this does by no means reduce the relevance of the BST effect in real life that typically occurs for a non-prepared rider and far below ABS thresholds. In any case this result underlines the opportunity for rider training to dare to slam the brakes more in case of an emergency, as far as ABS control is present.

As a side note on orienting tests, the influence of rider coupling (tight or loose) was clearly to be observed, however, no real conclusions can be drawn on the small data basis with even slightly different initial conditions for both experiment groups. As a first tendency, it can however be stated, that the force transfer of the tightly coupled rider towards the motorcycle was more direct, giving higher peaks in steering torque deviation values while at the same time keeping roll angular disturbances as well as relative movements of the rider to the motorcycle lower than for a loose coupling. Despite similar initial speeds, brake pressure increase rates, and deceleration levels, as well as a lower median of the initial roll angle, the tight coupling caused slightly higher steering angular deviations and correlated (dynamic) steering unsteadiness values than the experiments with light coupling. Since the opposite would be expected from theory, and one possible explanation lies in the boundary conditions of the R70 test track (swerve maneuver and pothole), more experiments on another track would be required for a clarification. In any case, a focused and pre-tensioned test rider in anticipation of a defined experiment on the test track is likely to react differently as a frightened, tensed-up rider in a sudden, surprising BST critical situation in real traffic.

Also for experiments with steering damper, the number of experiments was rather small. However, in that case, steering oscillations after brake kick-in in the order of the wobble (or “shimmy”) eigenfrequency of the front wheel system were much lower, delivering a subjective improvement in smoothness of the initial phase of the brake maneuver. An advanced semi-active steering damper control that is sensing a BST relevant situation (e.g. by measuring the roll angle and rider brake demand) is therefore definitively recommended to be analyzed in the future.

5.4.3 Partial Front Braking with Standard Steering vs. BSTAM

Partial (Front) Braking Standard vs. BSTAM – Results R70 (Figure 5.9)

The partial braking experiments of BSTAM compared to the baseline chassis setup as presented in Figure 5.9 are almost completely in line with the proposed hypothesis (cf. chapter 3.7.1, H_{BSTAM}). With one exception in the last test group with only 4 experiments, the handling characteristics are typically compromised for active BSTAM and the stationary steering torque demand is significantly increasing for active BSTAM and higher compensation ratios, delivering similar total steering torque demand levels.

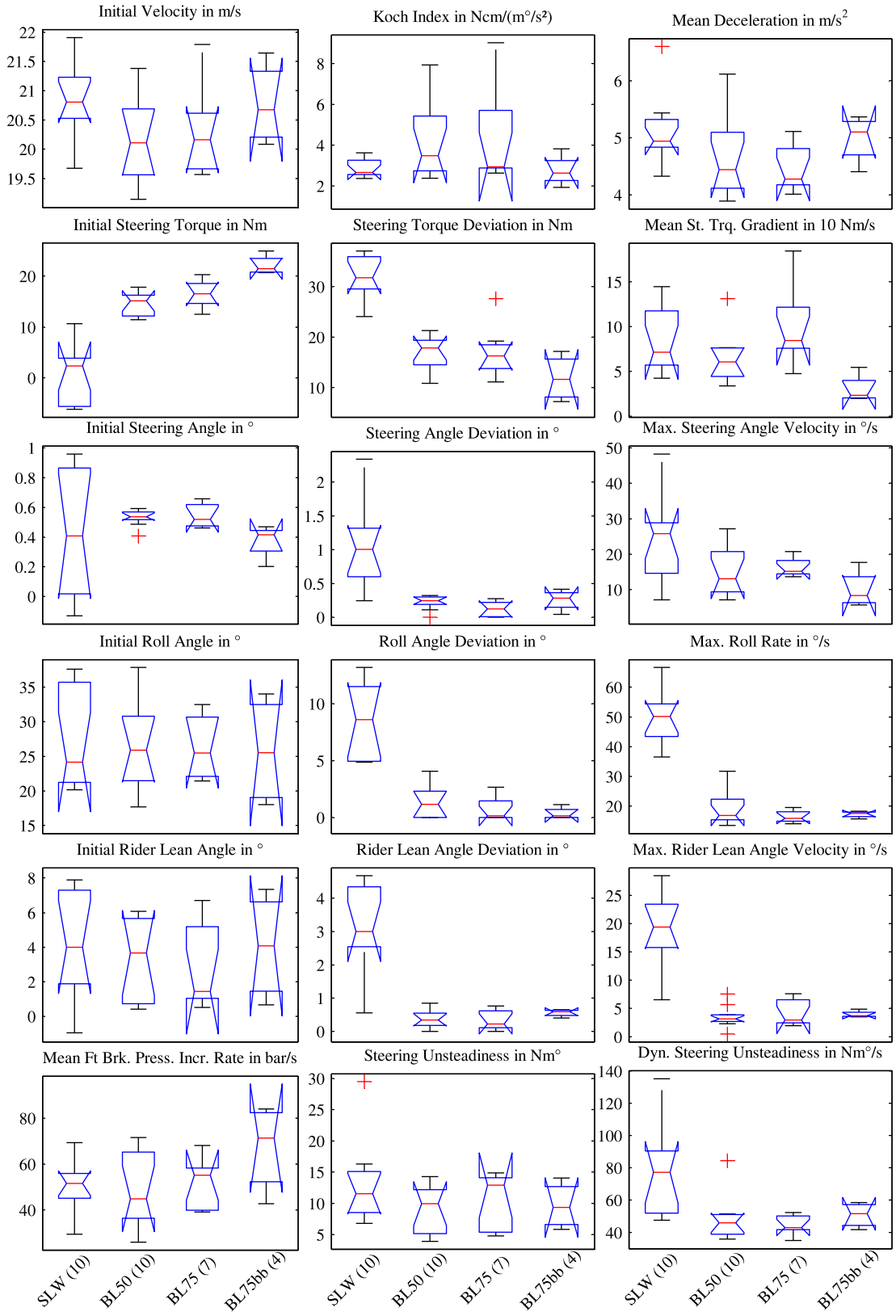

Figure 5.9: Results for partial front braking experiments with standard steering vs. BSTAM under variation of compensation ratio and brake application on $R = 70$ m turn radius. The value in brackets behind the annotation is the number of tests in each setup group.

In contrast, the majority of deviation values stays significantly below the reference, with only a few exceptions in the steering torque gradient, steering angle velocity, and steering unsteadiness values.

Starting in the first row of plots in Figure 5.9 for a closer look on the results, the initial speed of all presented experiments stays in close boundaries with medians ranging between 20.1 and 20.8 m/s. The medians obtained for Koch's handling index are an excellent 2.7 $^{Ncm}/_{(m°/s²)}$ for the standard chassis and increase to approximately 3.5 and 2.9 $^{Ncm}/_{(m°/s²)}$ for the active BSTAM setups BL50 and BL75. On one hand, this is in line with the changes in effective caster angle (that is lower for BL75 compared to BL50) and increased stationary steering torque demand (which is slightly higher for BL75). On the other, it is already surprisingly low compared to the global result of active BSTAM setups with a median of 4.77 $^{Ncm}/_{(m°/s²)}$. Even more surprisingly, the last presented setup BL75bb achieves a median of merely 2.6 $^{Ncm}/_{(m°/s²)}$, outperforming the SLW reference. The explanation lies in the time lag of the prototype BSTAM controller in combination with the special boundary conditions of the R70 test track, that require a swerve maneuver when entering the track from one side and the avoidance of a pothole on the other. In consequence, the steering axis position of BSTAM is still on the "wrong" side, creating (outward) steering torque components that assist the rider to enter into the following turn. Hence also the steering torque demand and handling index are lower, than when entering the turn from straight running (cf. results on R50 in the following section).

Following down the first column of the figure for the initial conditions, the medians of the initial steering torque are significantly higher for the active BSTAM setups compared to the standard reference SLW. While the latter only needs around 2.3 Nm, BL50 requires more than 15 Nm, BL75 still a bit more with 16.5 Nm, and the last experiment group BL75bb just below 21.5 Nm, since the BSTAM controller was given a little bit more time to settle positions before starting to brake after the swerve maneuver. The medians of all other initial conditions show no significant differences between setups. The medians of initial steering angles range between 0.4° and 0.53° and show a larger spread for the SLW experiments. The medians of initial roll angles range from 24° to 26°, while the initial rider lean angles display medians between 1.4° and 4.1° lean in tendency, with the lowest value for BL75. While the medians of brake pressure increase rates lie around 50 bar/s for the first three experiment groups, with the lowest value for BL50, BL75bb achieves the highest median above 71 bar/s for the use of both brakes. Finally, the top right diagram shows mean deceleration levels with medians of 4.9 and 5.1 m/s² for SLW and BL75bb, while BL50 and BL75 only reach lower but similar values of 4.4 and 4.3 m/s².

Jumping to the inner field of result values (in the second row of the figure), the medians of steering torque deviations show significant improvements of the active BSTAM setups compared to the baseline SLW. While the latter shows a median of 31.7 Nm,

BL50 operates with 17.8 Nm, BL75 with 16.3 Nm, and – despite the higher deceleration level – BL75bb with only 11.6 Nm, thanks to utilization of a more rear-oriented brake force distribution (BFD). However, before the background of the increased stationary steering torque demands with BSTAM, only similar levels of total steering torque demand in the order of 33 to 34 Nm are achieved. With values of 60 and 84 Nm/s, the medians of mean steering torque gradients of BL50 and BL75, play in a similar range as the 70 Nm of the baseline SLW, in accordance with their respective differences in brake pressure increase rates. BL75bb again profits from its more rear-oriented BFD, achieving a significantly lower level of just 23 Nm/s.

The disturbance values in steering, roll, and rider lean angle and their respective velocities (in rows 3 to 5 of the figure) show significant improvements for all active BSTAM setups compared to the baseline, with only one exception of the steering angle velocity of BL50, that is on the numerical edge of being significant as well. The median values of steering angle disturbances are cut down from 1° to a range of 0.1 to 0.3°, while steering angle velocities shrink from almost 26°/s to levels in the order of 13 to 15 °/s with front braking and even further to around 8°/s for using both brakes. Roll angle deviations drop from 8.6° to around 1° or even lower, while roll rate deviations come down from 50°/s to below 20°/s with BSTAM. Rider lean angle deviations drop from 3° to values between 0.2 and 0.6°, while their velocity drops from 20°/s to around just 3°/s.

Finally, and in accordance with the respective increased stationary steering torque demand as well as the brake pressure increase rates, the steering unsteadiness values do not significantly differ. The medians range between 10 and 12.9 Nm° for the first three setup groups and the lowest value of 9.3 Nm° is obtained for BL75bb. The dynamic steering unsteadiness shows significant improvements of BL50 and BL75, cutting the more than 77 Nm°/s of the baseline SLW down to levels between 43 and 46 Nm°/s, while BL57bb is on the numerical edge of a significant difference with its median of 51.5 Nm°/s.

Partial Front Braking Standard vs. BSTAM – Results R50 (Figure 5.10)

Concerning the main group of experiments as presented in Figure 5.10, it has to be stated, that the SLW baseline only contains three experiments at a rather low entry speed and may only give a rough orientation. Rather, the BLpc setup is to be regarded as reference for the other experiments. A difference in initial steering torque demand, and handling index is clearly to be observed in terms of increasing downsides for increasing compensation ratio. However, regarding the disturbance values of the central three groups of experiments compared to the first two, mostly significant benefits arise, with a slight tendency of BL75 towards over-compensation and exceptions in steering torque gradient, steering angle velocity and steering unsteadiness values. The last two experiment types were conducted with throttle jammed and clutch engaged, stalling the en-

gine. However, compared to their references BLpc and BL65, the tests showed no significant differences in measured disturbance values, while a subjective benefit was reported by the rider (cf. comments thereon in the conclusions).

Starting in the first row of Figure 5.10 for a closer look on the results, the initial velocities of all experiments (except SLW) range around 18 to 19 m/s, with the biggest gap between BL65 and BL75 setups with a slightly higher, respectively lower entry speed within their comparison group. The handling index of SLW is naturally lowest and around 3.0-3.3 $^{Ncm}/_{(m°/s²)}$ (cf. also Figure 5.8). It already increases to 3.8 $^{Ncm}/_{(m°/s²)}$ for BLpc and rises further with increasing compensation ratio of BL50, 65, and 75 to 5.5 $^{Ncm}/_{(m°/s²)}$ (cf. the much lower values on R70 in Figure 5.9). Slight but non-significant increases in the order of just 0.1 to 0.2 $^{Ncm}/_{(m°/s²)}$ are to be observed when transitioning from experiments with clutch disengaged (BLpc and BL65) to those with clutch engaged (BLpcE and BL65E).

Following down the first column of initial conditions, the picture of the handling index repeats. While the initial steering torque demand is just around 0 Nm for SLW, already BLpc significantly increases to 13.8 Nm with further increases with increasing compensation ratio. The highest median of 23.9 Nm is however achieved for BL65 and not for BL75, since the initial velocity of the latter setup was a bit lower. Compared to the respective experiments with clutch disengaged, similar levels are achieved for the experiments with clutch engaged. Medians of the initial steering angle show no significant differences among setups and range between 0.7° and 0.9°. The medians of the initial roll angles are very well in line of about 32°, with an exception of almost 34° for BL65. The initial rider lean angles show medians with the already known tendency of 3° to 4° lean in, with an exceptional increase of 5.6° for BLpc. While the medians of the front brake pressure increase rate range between 40 and just below 62 bar/s, the biggest gap for direct comparison groups appears between a relatively low value of BL65 compared to a relatively high one for BL75. The experiments with clutch engaged reach similar levels to those with clutch disengaged. Finally jumping to the achieved deceleration level (top right diagram), medians range between 4 and 4.9 m/s², where BL50 and 65 slightly drop below BLpc and BL75 in their comparative group and the lowest values are obtained for the experiments with clutch engaged, featuring similar brake activation that however needs to counteract the driving torque at the rear wheel.

Moving on to the central results field of disturbance values (in the second row), the steering torque deviation of SLW would surely have been higher than the presented value of just around 21 Nm, had the initial speed and roll angle been higher as well. However, in that case, BLpc keeps approximately the same level, while the values drop significantly for active BSTAM setups with increasing compensation ratio, reaching similar values of around 10.7 Nm for BL65 and 75. The difference would have been clearer for keeping the initial conditions more constant.

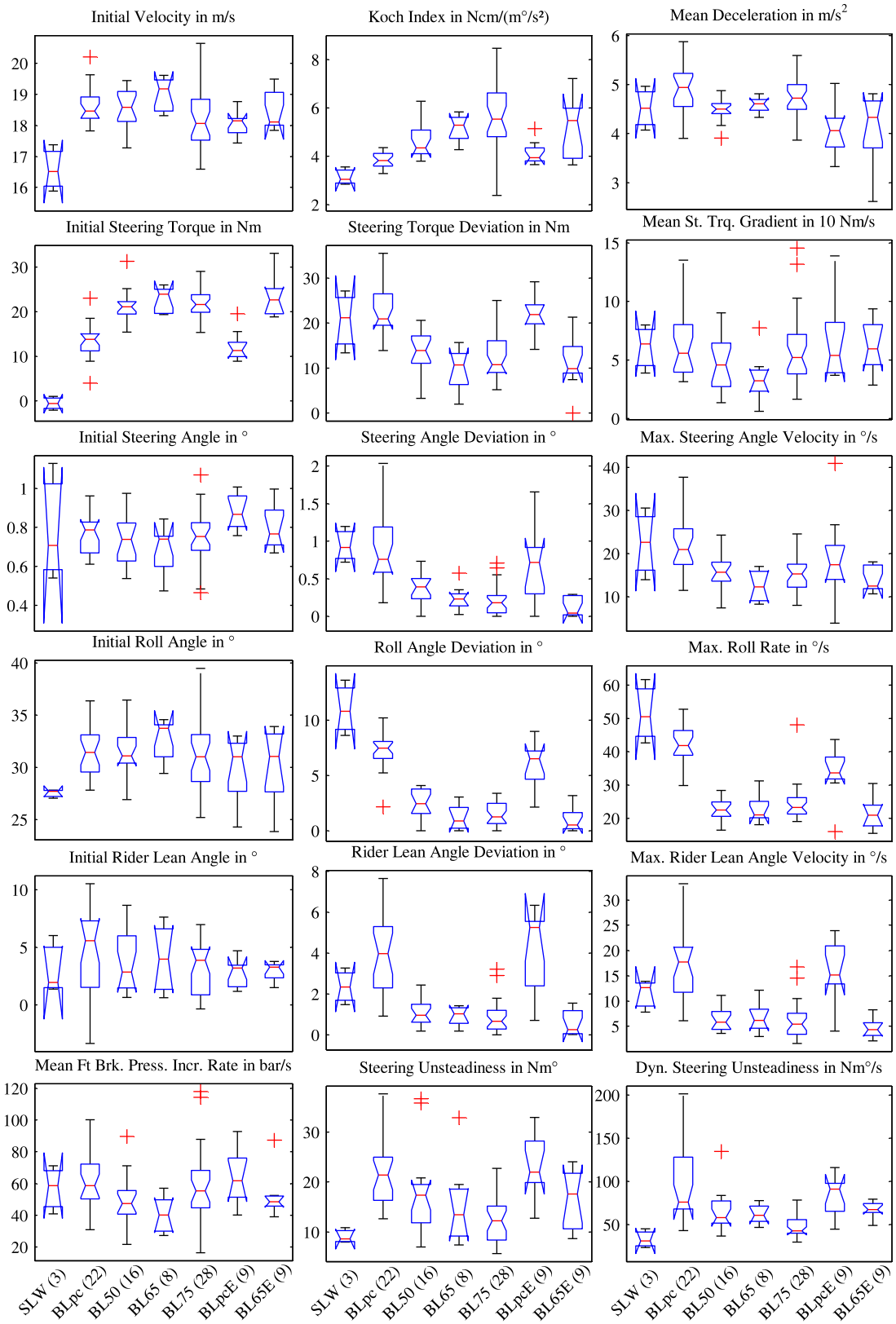

Figure 5.10: Results for partial front braking experiments with standard steering vs. BSTAM under variation of compensation ratio and clutch mode on $R = 50$ m turn radius. The value in brackets behind the annotation is the number of tests in each setup group.

Finally, the active setup BL65E delivers a significant benefit over BLpcE in a similar way to the experiments with clutch disengaged. Concerning the steering torque increase rate, clear benefits for BL50 and 65 occur compared to BLpc, while BL75 loses this benefit because of its high brake pressure increase rate and deceleration level. BLpcE and BL65E show no significant differences compared against BLpc – the median is even slightly higher for the active setup with clutch engaged.

The medians of steering angle disturbances (third row) of SLW and BLpc range in a similar order between 0.9° and 0.76°, while significant reductions are obtained with active BSTAM, down to 0.18° for BL75. The same holds true for experiments with clutch engaged, with hardly any disturbance for BL65E. Concerning the steering angle velocities, SLW and BLpc similarly keep between 21°/s and 23°/s, with the most significant reductions for BL65 below 12.3°/s, while BL75 suffers from the higher pressure increase and deceleration level. The reduction from 17.4°/s of BLpcE to 12.5°/s for BL65E is clear, but not significant.

A similar picture repeats for the roll and rider lean angular disturbances (fourth and fifth row). The roll angle deviation ranges from medians of almost 11° for SLW and 7.5° for BLpc to a significant reduction of the active BSTAM setups, the lowest being again BL65 with just 0.9°. The reduction from BLpcE to BL65E is also significant, from 6.5° to 0.5°. The same holds true for the comparison of roll rates. Starting from 50.5°/s for SLW and 41.9°/s for BLpc, significant reductions are obtained with active BSTAM, down to 21°/s for BL65. The reduction from BLpcE to BL65E is also significant, from 33.7°/s to 20.9°/s.

Rider lean angle disturbances (fifth row) range between medians of 2.3° and 5.3° for SLW and BLpc(E) setups, with significant reductions for active BSTAM of down to 0.2° for BL65E. This repeats for the rider lean angle velocity, ranging between 12.7°/s and 17.7°/s for SLW and BLpc(E) setups, significantly reduced to 4.3°/s for BL65E.

Finally, while both steering unsteadiness values (last row) are not comparable for SLW because of the lower initial velocities and roll angles, the steering unsteadiness improves with increasing compensation ratio of the active setups. While BLpc yields 21.4 Nm°, a significant reduction is achieved for BL75 with a median of just 12.2 Nm°. Also for the experiments with clutch engaged the active setup brings a benefit and the value drops from 22 Nm° of BLpcE to 17.6 Nm° of BL65E. All in all, it looks similar for the dynamic steering unsteadiness, yielding a median of 76 Nm°/s for BLpc, significantly cut down to 42.6 Nm°/s for BL75. The value drops from 91 Nm°/s for BLpcE to 67.3 Nm°/s for BL65E, yielding an improvement on the edge of numerical significance.

Partial Front Braking – Results on Narrowing Radius Turn (Figure 5.11)

The results presented in Figure 5.11 are subdivided into three groups of test setups. While the first group of three setups is repeated for reference from the constant radius experiments (cf. Figure 5.10), the three setups in the second group are on the narrowing radius turn with clutch disengaged, while the third group with just two setups combines the narrowing radius with an engaged clutch. Before the background of only very few repetitions of the experiments, it is worth noting that only tendencies can be derived and matched with the subjective impression of the test rider.

Starting in the first row of Figure 5.11, the initial velocities of all experiments range between 18.5 and 19 m/s. While the handling index only increases marginally when changing from BLpc to BLpcN from 3.8 to 3.9 $^{Ncm}/_{(m°/s²)}$, an increased value of 4.2 $^{Ncm}/_{(m°/s²)}$ is achieved for BLpcNE. For the active BSTAM setups the handling index grows with increasing compensation ratio, reaching 5.0 $^{Ncm}/_{(m°/s²)}$ for BL75N and 4.8 $^{Ncm}/_{(m°/s²)}$ for BL65NE compared to 5.5 $^{Ncm}/_{(m°/s²)}$ for BL65E.

Following down the first column of initial conditions, the initial steering torque increases on the narrowing radius from 13.8 Nm for BLpc to 17.2 Nm for BLpcN and a similar 17.4 Nm for BLpcNE compared to 13.2 Nm for BLpcE. Again, the steering torque demand rises, sometimes significantly, for the active BSTAM setups, yielding 22.6 Nm for BL65E, 21.8 Nm for BL75N, and 24.9 Nm for BL65NE. The initial steering angles show no significant differences and range between 0.7° and 0.87°. Also the initial roll angles stay without significant differences, ranging between 30.6° and just below 33°. However, in the middle test setup group, BLpcN is slightly elevated and BL75N slightly lower than BL65N, the center point of this group. Initial rider lean angles show a tendency of 1° to 5.6° of lean in, again with no significant differences, but with relatively low values for BLpcN and BL75N compared to a relatively high one of BL50N in the middle experiment group. Even though the differences in brake pressure increase rates are also non-significant, the spread is between 39.7 bar/s to 61.7 bar/s, again with peculiarities in the middle group, having an increasing tendency from BLpcN to BL75N that is opposite of the tendency in initial roll angles. Completing the picture with the achieved deceleration levels (top right), all setups stay within a range of non-significant differences with medians between 4.0 and 4.5 m/s², with the only exception of BLpc featuring 4.9 m/s².

Moving on to the central results field of disturbance values (in the second row), the steering torque deviation is increasing on the narrowing radius. Compared to 20.9 and 21.9 Nm of BLpc and BLpcE, BLpcN reaches 28.1 Nm and BLpcNE 25.7 Nm. Significant reductions are always achieved with active BSTAM, cutting down to 9.8 Nm for BL65E, 17.8 and 17.3 Nm for BL50N and BL75N, as well as 13.5 Nm for BL65NE. Combined with the initial steering torque demands, the active setups also lead to lower

absolute steering torques for experiments with clutch engaged. BL65E is lowering the 33.2 Nm of BLpcE to 32.4 Nm, and BL65NE is even delivering a greater benefit, cutting the 43.1 Nm of BLpcNE to 38.4 Nm. However, in analogy to the experiments with clutch disengaged on the constant radius, the active setups also have a higher total steering torque demand on the narrowing one. Compared to 35.3 Nm of BLpcN, BL50N yields 38.0 Nm and BL75N 39.1 Nm. Steering torque gradients range between 51 and 87 Nm/s for BL50N and BL75N with significant differences only in the middle group of experiments, dropping from BLpcN to BL50N and rising again for BL75N, which is a result of the respective combination of initial conditions (cf. initial roll angles and brake pressure increase rates). Otherwise, a further drop for BL75N would be expected. Tests with clutch engaged in the first and last group stay rather similar to the reference BLpc.

While the active BSTAM generates significant benefits in the steering angle deviations (third row) for the experiments with clutch engaged – compare 0.72° of BLpcE with 0.04° of BL65E as well as 0.56° of BLpcNE with 0.04° of BL65NE – the benefits in the middle group are clearly present, but non-significant – reducing from 0.83° of BLpcN to 0.2° and 0.33° for BL50N and BL75N. Differences in steering angle velocity range between 20.9°/s for BLpc and 12.4°/s for BL65E, but remain generally non-significant. However, besides BL75N, the active setups typically go along with desirable reductions compared to their passive reference cases.

Roll angle deviations (fourth row) sink significantly from 6.5° of BLpcE to 0.5° of BL65E as well as with increasing compensation ratio in the middle group, from 4.6° of BLpcN to 0° of BL75N. The benefit from nearly 2.0° of BLpcNE to a little more than 0.2° of BL65NE remains however non-significant. Roll rates range between 20.9°/s of BL65E to 41.9°/s of BLpc. While BL65E achieves a significant benefit towards BLpcE, BL50N only achieves a non-significant benefit over BLpcN, while BL75N again stays at a similar level. Surprisingly, BL65NE shows higher roll rates, than BLpcNE, which may be attributed to the very low number of conducted experiments in conjunction with the relatively loose test track definition.

Also the rider lean angle deviations (fifth row) follow the same tendencies with medians between 0.2° for BL65E and 5.3° for BLpcE. A significant benefit is achieved for BL65E compared to BLpcE, while benefits of the other active setups are clear, but non-significant towards their respective passive references. This repeats for the rider lean angle velocity, with extreme values between 4.3°/s and 17.7°/s for BL65E and BLpc.

Finally, the active BSTAM setups always ameliorate both steering unsteadiness values. The steering unsteadiness level rises in conjunction with the total steering torque demand from roundabout 20 Nm° on the constant radius to an approximate average of 30 Nm° for experiments on the narrowing radius. The benefit is greatest for the combination with the clutch engaged, comparing the 39.7 Nm° of BLpcNE with just below 23 Nm° of BL65NE.

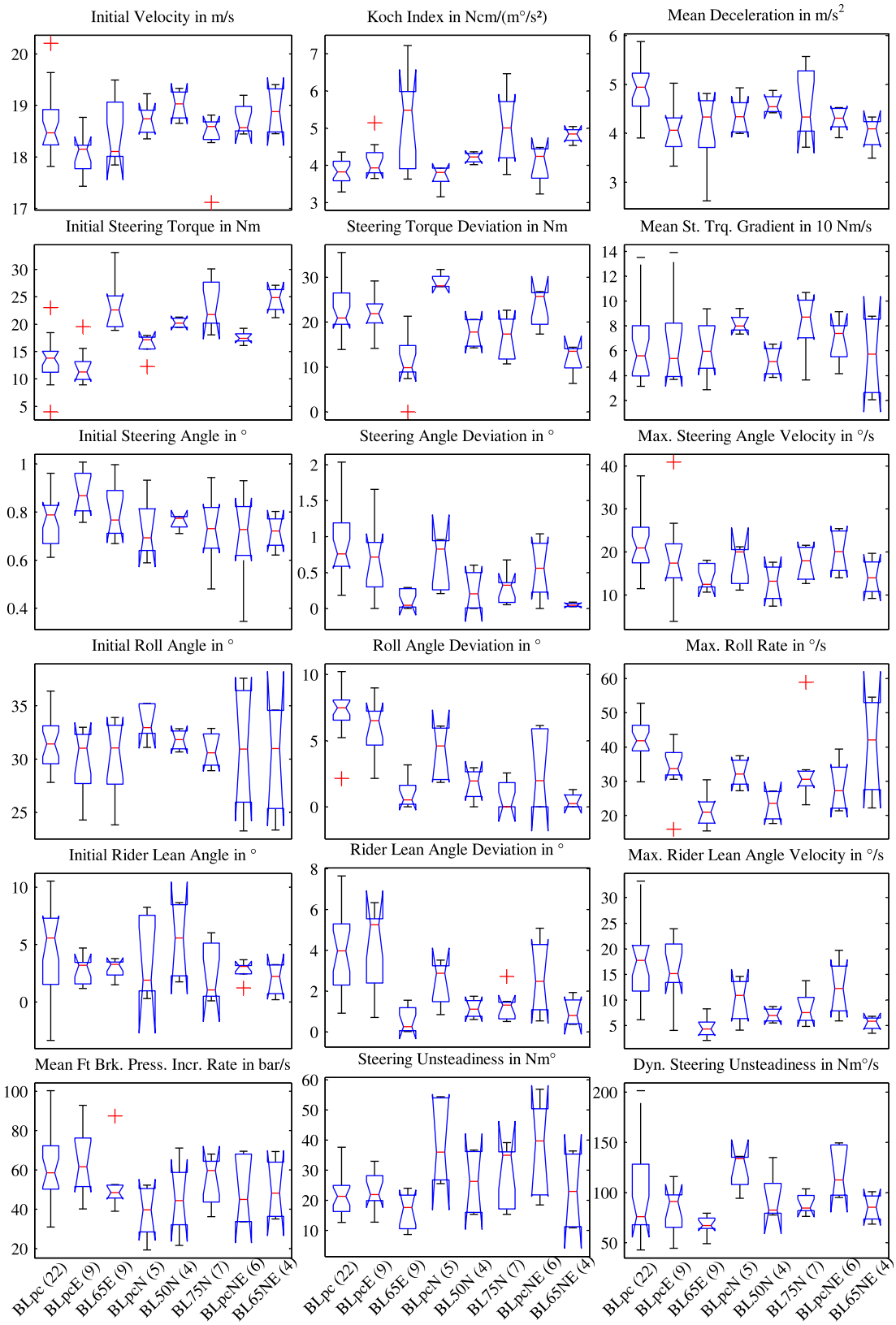

Figure 5.11: Results for partial front braking experiments with BSTAM under variation of compensation ratio, clutch mode, on $R_1 = 50$ m and narrowing turn radius, $R_2 \approx 30$ m. The value in brackets behind the annotation is the number of tests in each setup group.

However, all benefits remain non-significant. The picture changes for the dynamic steering unsteadiness, where the reduction in the middle group are the greatest and even become significant, comparing 133.8 Nm°/s of BLpcN with 82.5 and 84.7 Nm°/s of BL50N and BL75N. The benefits in the first and last group are present, but remain numerically non-significant.

Partial Front Braking – Results R50 with "Jump Algorithms" (Figure 5.12)

The jump algorithms as proposed in chapter 4.4.5 aim at the reduction of stationary steering torque demand through keeping the BSTAM steering axis closer to centered position, until a brake maneuver is detected. Only then will the controller quickly "jump" to the desired compensation position. The base compensation ratio in all cases is *tcr* = 0.75, and BLpc and BL75 setups have been repeated for reference from Figure 5.10. The key results of interest are the stationary steering torque and its deviations, that are briefly discussed along with roll angular disturbances and handling index.

The initial conditions of the experiments with jump algorithms are generally well in line with those of the reference experiments and are not repeatedly treated in detail. However, both the level of brake pressure increase rates (bottom left diagram) and deceleration (top right) stay below the reference (37 to 46 bar/s vs. 55 to 58 bar/s and only 4.0 to 4.6 m/s² vs. 4.7 to 4.9 m/s², meaning a significantly lower level for BLjb and BLjc).

Setup BLja was operating with half a continuous base compensation, keeping the required jump small and leading to non-significant differences compared to BL75. While the reference BLpc features a stationary steering torque demand with a median of 13.8 Nm, BL75 and BLja lie significantly higher, at 21.6 and 22.3 Nm. The inverse picture is found for the steering torque deviations, cutting down significantly from 20.9 Nm of BLpc to 10.8 and 10.9 Nm of BL75 and BLja. The result are similar total steering torque demand levels from 34.7 Nm of BLpc down to 32.4 Nm of BL75.

Other than BLja, BLjb and BLjc setups operated with real jumps, creating a perceptible reduction in stationary steering torque of only 17.5 and 17.6 Nm compared to 21.6 and 22.3 Nm of BL75 and BLja. However, this is achieved at the cost of steering torque deviations of 19.7 to 22.6 Nm that are in the order of the passive system BLpc with 20.9 Nm and significantly higher than for BL75 and BLja. Consequently, the total steering torque demand levels of 37.2 and 40.2 Nm of BLjb and BLjc even exceed the reference of 34.7 Nm of BLpc – despite the lower deceleration levels.

The picture of steering torque demand levels and disturbances is directly reflected in the handling characteristics and subsequent disturbance values, such as those of the roll angle. While the Koch indices are 3.8 and 5.5 $^{Ncm}/_{(m°/s²)}$ for BLpc and BL75, all jump setups stay below the latter value with around 4.7 $^{Ncm}/_{(m°/s²)}$ for both BLja and BLjb, and 4.3 $^{Ncm}/_{(m°/s²)}$ for BLjc.

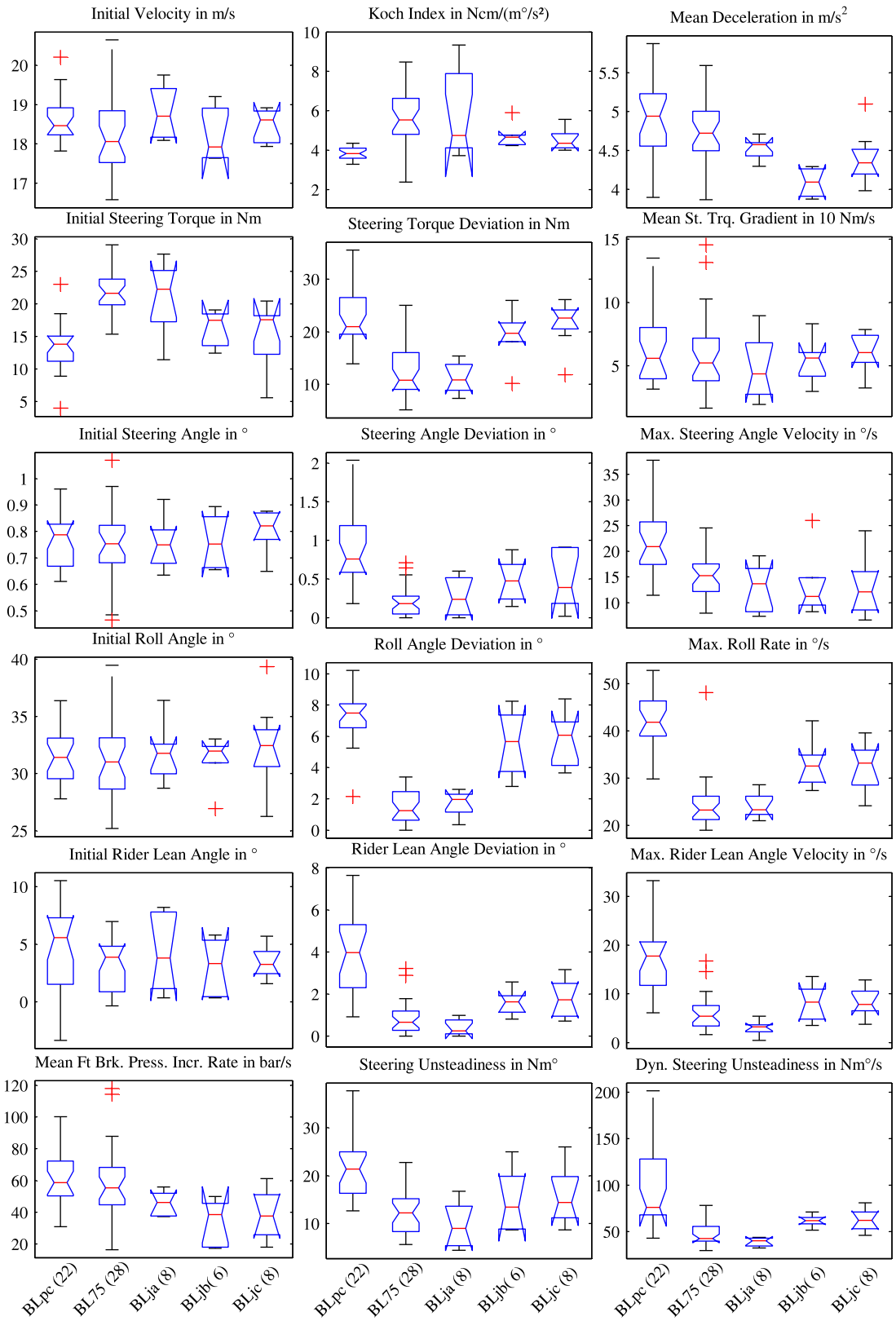

Figure 5.12: Results for partial front braking experiments with BSTAM under variation of compensation ratio and "jump" control algorithms on $R = 50$ m turn radius. The value in brackets behind the annotation is the number of tests in each setup group.

This is in line with the lower initial effective compensation ratio and stationary steering torque demand. The medians of roll angle deviations sink significantly from 7.5° of BLpc to 1.3° and just below 2.0° for BL75 and BLja and increase again significantly to 5.7° and 6.7° of BLjb an BLjc – a non-significant reduction compared to BLpc. Finally, also the medians of roll rates sink significantly from 41.9°/s of BLpc to 23.2° and 23.3°/s for BL75 and BLja and increase again significantly to 32.6 and 33.2°/s of BLjb an BLjc – in this case, still a significant reduction compared to BLpc.

Even though a tendency in the right direction can be derived from the measurements, especially from the initial steering torques of BLjb and BLjc, the obtained high steering torque deviations unfortunately overcompensate this benefit. The reason for the ineffectiveness of this experiment is found in the limited capabilities of the utilized control hardware (cf. chapter 4.4), that yielded time delays concerning the jump algorithms of up to 0.4 seconds. Compared against the duration of the whole experiment that rarely exceeds 2.5 seconds, this is of cause unbearable and comes much too late in the chain of effects to be of true assistance. Consequently, also the test rider expressed his disproof of the discontinuous steering feel through the delayed jump algorithms.

Partial Front Braking Standard vs. BSTAM – Conclusions

With only a few exceptions that are attributed to deviations in the (initial) boundary conditions of the experiments (especially on R70), the following general statements can be derived for the performance of the prototype BSTAM in accordance with the hypotheses (H_{BSTAM}) from chapter 3.7.1.

The transition from the standard steering to the passive BSTAM with centered steering axis already goes along with increases in stationary steering torque demand and handling index, while other disturbance values stay at a similar level. Starting from the passive BSTAM as a reference for the active setups, both the stationary steering torque demand and handling index increase with increasing compensation ratio, while the steering torque deviations and all other disturbance values along the chain of effects decrease with increasing compensation ratio. In the main group of experiments on the R50 test track (setups BLpc, BL50, 65, and 75 in Figure 5.10) these reductions are mathematically significant for the steering torque deviation, steering angle deviation and velocity, roll angle deviation and rate, as well as the rider lean angle deviation and velocity, meaning all disturbance values except for the steering torque gradient and the two steering unsteadiness parameters. For these three values, a tendency to increasing but non-significant benefits with increasing compensation ratio is to be observed.

Before that background, the prototype BSTAM can be rated effective in the sense of the initial hypotheses H_{Wa} and hence also H_{0a} (cf. chapter 1.2).

Regarding the mathematical definition of the steering unsteadiness parameters, the obtained values suffer from the fact, that the achieved reductions in steering torque deviation are often overcompensated by the elevated stationary steering torque of the active BSTAM setups. Hence, also their total steering torque demand level does not significantly differ from the baseline SLW or BLpc reference.

However, the subsequent disturbance values along the chain of effects, for instance the "stand-up tendency" in terms of roll angle deviations and rates, are undoubtedly (and often significantly) improved. This is also underlined by the subjective impression of easier lane keeping and directional control, especially on narrowing radius turns.

In extension of the initial hypotheses (cf. chapter 1.2), this leads to the formulation of a new hypothesis with its subsequent explanation:

H_{0c}: Given the same total steering torque demand level during corner braking maneuvers with two different chassis setups, a higher stationary steering torque demand and small steering torque deviation ("kick-in") are preferable over a lower stationary steering torque demand and larger "kick-in".

The first combination is easier to compensate for the rider, who is already pre-tensioned trough application of the higher stationary steering torque demand, resulting in lower disturbance values along the chain of effects. – Despite this conclusion, the ultimate aim is of cause to have both a low stationary steering torque demand and "kick-in" at the same time, as it would be possible with an optimized BSTAM.

Moreover, while the measured increases in stationary steering torque demand are relatively well in line with the model predictions from chapter 3.6 (i.e. the figures from Table 3.4 in chapter 3.6.3), the steering torque deviations (ΔT_0) are rather lower than predicted for sole front braking on the standard chassis. In turn, also the measured reductions through BSTAM are not as high as would be expected. Despite natural differences in the (initial) boundary conditions of simulation and experiment (i.e. v_0, a_{y0}, λ_0, a_x), this can be explained by two major influence factors. The first one is the C-ABS of the test motorcycle, that is also applying the rear brake for sole activation of the front brake lever and consequently taking a certain amount of brake load from the front wheel. Hence, the measured results are much more in line with the predictions for an ideal brake force distribution (bb-eq in Table 3.4), underlining the benefits of combined brake systems. The second reason for remaining differences can be seen in the fact, that a human rider is not a rigid body and cannot instantaneously compensate the "kick-in" in steering torque demand. Its temporary difference to the rider's steering effort is then accelerating the steering system, leading to the steering angle fluctuations and other disturbances along the BST chain of effects.

In contrast to the model predictions regarding experiments with clutch engaged (i.e. stalling the engine with a jammed throttle, cf. chapter 3.6.4) on a constant radius, the measured disturbance values showed no significant differences compared to the reference experiments with disengaged clutch (cf. BLpc/E and BL65/E in Figure 5.10). One reason for this is again found in the C-ABS of the test motorcycle, that is already compensating a part of the driving force at the rear wheel. And a second reason is the presence of the driving force itself, that is leading to lower deceleration levels – despite similar gradients of front brake activation. Aggravating the boundary conditions with corner braking experiments on a narrowing radius turn is increasing both the initial steering torque demand and disturbance for both the centered steering axis and active BSTAM setups (cf. Figure 5.11). Even though it is not reflected in the presented measurements, the elevated steering torque demand remains active for a longer time period on the narrowing radius turn (cf. Figure 3.17).

Before the background of H_{0c} and its explanation, the subjective impression of much easier directional control of the test rider confirms the effectiveness of BSTAM in the sense of the initial hypotheses H_{Wb} and hence H_{0b}.

As a final side note, the time lag of the BSTAM controller on one hand thwarted a successful test with “jump algorithms”. And on the other, its temporary “wrong side compensation” led to reduced handling indices after the swerve maneuver on the R70 test track, which even outperform the baseline handling characteristics slightly.

5.5 Concluding Remarks

In chapter 5, the three first aims of research field 3 have been successfully addressed. A driving test design and performance criteria for the evaluation have been defined in chapters 5.1 and 5.2 (cf. aim 3.1), while the performance of BSTAM has been compared to the baseline motorcycle in real driving tests (cf. aim 3.2). The obtained measurements and subjective impressions are analyzed through a global correlation analysis in chapter 5.3 and evaluated in detail against the hypothesis on their expected behavior (from chapter 3.7) in chapter 5.4 (cf. aim 3.3).

While the hypotheses on the behavior of the standard chassis with different riding styles ($H_{RidingStyle}$) hold principally true for the riding style lean in compared to lean with during experiments with high decelerations (i.e. ABS regulated braking), the steering torque deviations captured for lean out were not higher as expected, but even lower than for lean with. This can be explained before the background of the influence of rider coupling and the new hypotheses H_{0c} derived in the previous chapter, but should be rechecked also for partial decelerations and a higher number of experiments.

The hypotheses on the performance of the prototype BSTAM (H_{BSTAM}) hold fully true and suggest that a transferability of results is valid also for the hypotheses set up for the optimized BSTAM ($H_{OPT\ BSTAM}$, cf. chapter 3.7.1). As another result and in line with the model predictions (cf. chapter 3.6.3), the corner braking experiments with the C-ABS of the test motorcycle underlined a significant positive influence of a combined brake system on the steering torque demand level and hence the BST effect.

In sum total, the initial Hypotheses $H_{Wa,b}$, respectively $H_{0a,b}$ (cf. chapter 1.2), are approved (i.e. were not falsified) by the obtained results and even extended by a third hypothesis, H_{0c} (cf. chapter 5.4.3), that should be considered in further research.

The last aim, that has not yet been addressed, is to draw a conclusion, whether BST countermeasures beyond the state of the art technology are necessary at all or at least recommendable (aim 3.4). This question is discussed in detail in the following chapter.

6 Discussion and Outlook

6.1 Results

In this thesis, the Brake Steer Torque (BST) induced stand-up tendency of Powered Two Wheelers (PTW) and measures to lower the associated risk to run off track or into oncoming traffic during sudden, unforeseen corner braking situations has been investigated. The focus was set on the BST Avoidance Mechanism (BSTAM), using a Honda CBR 600 RR (C-ABS, 2010 model) as reference vehicle for analytical and experimental analysis. The main results are the following[178]:

Field 1: BST Effect and Countermeasures

- Based on the underlying fundamentals of vehicle dynamics, the main influence factors on the BST chain of effects are identified and brought into a unified picture (cf. chapters 2.1 and 2.2, especially Figure 2.17).
- Potential countermeasures range from rider training and road design to technical measures on the vehicle (cf. chapter 2.3).
- Besides BSTAM, a counter steering actuator, Cornering Adaptive Brake Force Distribution (CA-BFD), semi-active steering dampers, and multi-lever steering are identified as theoretically promising (cf. chapter 2.4).
- Multi-track tilting vehicles with two front wheels (such as the Piaggio MP3) can directly benefit from the use of slimmer front tires. Moreover, they theoretically offer three potential ways of using left / right asymmetries – in normal and brake forces as well as scrub radii – to influence the BST effect (cf. chapter 2.3.9).

Field 2: Feasibility and Layout of BSTAM

- The main influence of a BSTAM on the steering torque demand (STD) of a PTW is caused by changes in the transmission ratios of front tire contact forces towards the steering axis.

[178] The presentation of results uses the headlines of the three original research fields (cf. chapter 1.3), but does not strictly follow their sub-structure with detailed aims. Many results derive from more than one of the interdependent fields, but are mentioned only once, in context where they fit best.

- The balance between misaligning and aligning steering torque components arising from normal and lateral force is crucial for a "neutral" steering, especially in free cornering.
- For a generic BSTAM (for instance Weidele's original design implemented in the test motorcycle), the compensation of the tire scrub radius not only eliminates the disturbing influence of the brake force (BST), but also diminishes helpful aligning steering torque components generated by the normal and lateral force, leading to an undesired increase in STD.
- As a basis for analytical kinematic optimization and BSTAM control algorithm design, a geometric compensation ratio (*gcr*) is defined (cf. target compensation ratio *tcr* in the control algorithm vs. the effective compensation ratio *ecr* achieved during a real driving test, e.g. under the influence of suspension travel).
- An optimized BSTAM layout is proposed to restore the desired steering balance (cf. chapter 3.3.2 and following). It uses king-pin inclination angles in the order of 10° and an instantaneous center of steering axis inclination located at the intersection of the baseline steering axis with the vertical connection from front tire contact point to wheel hub in upright position. Small steering disturbances arising from the deceleration of wheel spin inertia ("inertia effect", cf. chapter 3.3.6) and inertial forces on the steering system can be accounted for through limitation of front brake pressure gradients and by keeping the instantaneous center of steering axis inclination close to the steering system's center of gravity.
- The optimized BSTAM concept is universal for all front suspension / steering systems with two steering bearings. Its mathematical definition inherently maintains the transfer ratios of front tire contact forces towards the steering axis, even if the baseline uses a telescopic fork that is prone to brake pitch and correlated changes in caster angle and trail. However, this means that the instantaneous center of steering axis inclination is not fixed but moving positions. On one hand, this is practically feasible with independent adjustment of both steering bearings and the consideration of pitch angle in the control algorithm to compute the king-pin inclination angle. On the other hand, a mechanically simpler "non ideal" layout of the optimized BSTAM, with a fixed instantaneous center of steering axis inclination that coincides with the lower steering bearing and a king-pin inclination angle computed on the basis of an invariant caster angle, is proven to yield very similar results and therefore preferred over the theoretically ideal but practically more complex solution (cf. chapter 3.3.3).
- Four classes of alternative actuation concepts are proposed for the practical implementation of the optimized BSTAM concept, that may be favorably incorporated basing on a king-pin or hub-center steering (cf. chapter 4.1.4).
- BSTAM concepts with parallel lateral displacement of the steering axis appeal through the simplicity of certain mechanical incorporations. However, it is

mathematically proven, that a "neutral" steering balance cannot be obtained for full compensation of the tire scrub radius. Acceptable steering balance can only be obtained with partial compensation for unusually large caster angles and fork offsets (around 50° and 140 mm). Moreover, such setups suffer considerable disturbances through longitudinal accelerations on the steering system (in the order of 10 Nm). While these can be accounted for through increasing the compensation ratio in the braking case, they might pose problems in the acceleration case.

- As an example for a multi-lever steering, a four-bar linkage can be regarded as a special form of parallel BSTAM with steering angle dependent compensation ratio. The choice of a perpendicular caster angle ($\tau = 0$) allows to keep the balance between steering torque contributes of the lateral and normal front tire forces independent of the steering angle, but at the same time creates unacceptable downsides. Firstly, it leads to extreme increases in stationary steering torque demand (in the order of 20-30 Nm), and secondly to a more direct transmission of the brake force, which is even increasing the BST effect compared to the baseline.
- A simple roll angle dependent BSTAM control algorithm is proposed. Despite considerable time lag in the prototypical control loop (in the order of 0.1-0.2 s), it yields predictable and intuitive control for the rider in free cornering and corner braking experiments. Also if more sensory inputs (like brake pressure or deceleration) are considered, a BSTAM control should ideally have no time lag (i.e. be "real time") and always be transparent to the rider. Exemplary tests of discontinuous "jump algorithms" (cf. chapters 4.4.5 and 5.4.3) suggest, that a continuous behavior is more favorable. Finally, BSTAM control for a series application is strongly recommended to have a detection of elevated curves to avoid unnecessary steering axis adjustments. These may otherwise cause potentially dangerous steering torque fluctuations, especially when ABS-regulated braking with "rough" control is involved (cf. chapter 4.4.6).

Field 3: Effectiveness and Benefit of BSTAM for the Rider

- For the first time ever, a motorcycle (Honda CBR 600 RR with Combined-ABS) is prototypically equipped with a BSTAM (following Weidele's original design with double excentric adjustment of the upper steering head bearing). It is compared to the baseline with centered steering axis in analytical investigations and riding experiments.
- Correlation analysis of all conducted riding tests confirms the BST chain of effects, interconnecting disturbances in steering torque, steering angle, roll angle, and also rider body lean angle relative to the vehicle (cf. chapter 5.3).

- Moreover, it shows a strong dependency of the disturbance values on the initial brake pressure increase rate and mean deceleration for centered steering axis, while BSTAM eliminates this correlation to a great extend (cf. Figure 5.5).
- Model prediction and riding tests with the baseline chassis show a positive influence of "lean in" riding style (cf. chapter 5.4).
- For maximal braking under controlled test track conditions, the "stand-up" of the baseline vehicle matches well with the required reductions in roll angle towards lower speeds (cf. chapter 5.4.2).
- Comparison of baseline and prototype BSTAM in partial front braking maneuvers fully confirms the behavior expected from model calculations. The handling is compromised due to increases in caster angle and trail (handling index 3.0-3.3 vs. 4.9 $^{Ncm}/_{(m°/s²)}$, these and following figures are global median values for the main experiments on R50). The stationary steering torque is significantly increased (from 5.3 to 20.9 Nm). Significant reductions in steering torque deviations upon brake kick-in (21.2 and higher vs. 13.4 Nm) are followed by (mostly significant) improvements in all other measured disturbance values in steering angle, roll angle, and rider body lean angle. Moreover, the subjective impression of test riders certifies the BSTAM prototype to allow easier directional control in corner braking situations than the baseline, especially on narrowing radius turns.
- The results obtained with the prototype BSTAM suggest that they can be extrapolated to the improved performance of an optimized BSTAM (cf. H_{BSTAM} and $H_{OPT\ BSTAM}$ in chapter 3.7.1). Hence, the BSTAM technology is rated an effective BST countermeasure in the sense of the original hypotheses ($H_{Wa,b}$ and therefore also $H_{0a,b}$, cf. chapter 1.2), that are furthermore extended by a third hypothesis H_{0c} (cf. chapter 5.4.3), which should be considered in further research.
- Quasi-stationary corner braking simulations with different brake force distributions (BFD) show, that BSTAM setups (i.e. the optimized and prototypical one) can always deliver lower steering torque disturbances than the baseline for a given BFD and deceleration level. For partial braking it is however shown, that a Cornering Adaptive BFD on a standard chassis already reduces the steering torque disturbances to such low absolute levels, that this measure alone bears the potential to address a great deal of BST relevant situations in real traffic. This analytical result is supported by the measurements with sole activation of the front brake lever of the test motorcycle's combined brake system C-ABS, that already cut down disturbance values through involving the rear brake.
- Orienting driving tests with Honda's series Electronic Steering Damper (HESD) showed slight improvements in disturbance values and subjective rider impression compared to the baseline setup with disconnected steering damper. Therefore, advanced semi-active steering damper control (as suggested in chapter 2.3.7) could be an easy to realize compliment to Cornering Adaptive BFD.

6.2 Transferability of Results

The presented results were obtained using a Honda CBR 600 RR super-sport motorcycle for reference that is characterized by:

- A precise and neutral handling.
- A high center of gravity and short wheelbase.
- A typical front tire dimension for on-road motorcycles (120/70ZR17).
- A set of tires with little stand-up tendency in corner braking (Bridgestone S20).
- A telescopic fork as front suspension / steering system.
- A Combined-ABS (in brake-by-wire architecture).

As further boundary conditions:

- All analytical considerations were conducted based on simplifying assumptions.
- BSTAM was implemented in Weidele's original double-excentric layout.
- Only one test driver was doing all presented driving experiments.

Before that background, the obtained results are discussed in the following sections.

Other Vehicle Categories

The research approach can analogously be applied to all other types of powered two wheelers for road use, be it motorcycles of different categories, cabin motorcycles, scooters, and – to a certain extend – even multi-track tilting vehicles with centered steering axes. All these vehicles typically feature mass, inertia, and geometry properties that differ (sometimes greatly) from those of the reference motorcycle (cf. chapter 4.3 and appendix A.4.2). In consequence, they will also react differently to the BST effect. This is exemplarily visual for scooters with small but wide tires[179] and rear swingarm mounted engine or for heavy cruiser motorcycles[180] with high mass, low center of gravity, long wheelbase, an often "flat" caster angle with huge trail, and even wider tires but typically also extra wide handlebars that assist the rider to counterbalance the BST.

The presented equation set can be used to obtain a first estimate for the steering torque demand of the regarded baseline vehicle, as well as the expected improvements through an optimized BSTAM or Cornering Adaptive BFD. Special attention should however be paid to the magnitude of the "inertia effect" and the neglected effects (cf. chapters 3.3.5

[179] E.g. MKB Booster 50 Track: Vehicle mass $m \approx 77$ kg, wheelbase $l = 1170$ mm, front and rear tire dimension: 130/90R10.

[180] E.g. Kawasaki VN 2000: Vehicle mass $m = 371$ kg, wheelbase $l = 1735$ mm, caster angle $\tau = 32°$, trail $n = 182$ mm, front and rear tire dimensions: 150/80R16 and 200/60R16.

and 3.3.6) in relation to the steering torque components arising from the tire contact forces, since these might need to be separately considered on another vehicle. As an example, the influence of tire characteristics is briefly discussed in chapter 6.3.

For experimental investigations on the said vehicle categories, qualitatively similar results in the sense of the working hypotheses (cf. chapters 1.2, 3.7, and 5.4) and correlation study (cf. chapter 5.3 ff) are to be expected.

BSTAM with Alternative Front Suspension / Steering Systems

Besides the telescopic fork and other steering head fitted fork types, the mathematical definition of the optimal instantaneous center of steering axis inclination for a BSTAM (at the intersection of the baseline steering axis with the vertical connection from front tire contact point to wheel hub in upright vehicle position) holds universally true for all typical front suspension / steering systems with two steering bearings (cf. Figure 4.1).

The original transfer ratios of front tire contact forces towards the steering axis are inherently maintained – in ideal case exactly, in a more practicable “non ideal” case approximately – even for changes in caster angle and trail due to suspension travel or brake pitch, if these properties are kept the same as for the baseline when doing the conversion to a BSTAM chassis (cf. chapter 3.3.3).

If the practical implementation of a BSTAM is however going along with a change of the front suspension / steering system, there will be further deviations that need to be separately analyzed. As a practical example, it is for instance mechanically possible, to implement the optimized BSTAM concept (i.e. a non ideal one) for the prototype motorcycle with a linear (i.e. telescopic) front suspension, but mechanically it makes much more sense to utilize hub-center steering or king-pin steering with a more traditional leading swingarm or double wishbone suspension. These will however not keep the original transfer ratios due to differences in brake pitch compensation and correlated caster angle and trail variations under braking.

In any case, the presented equation set can be used to estimate the expected differences when doing the system layout. Again, attention should be paid concerning the transfer ratios of the neglected effects and the “inertia effect” (cf. chapters 3.3.5 and 3.3.6), especially if vehicle properties deviate extremely from those of the baseline reference.

Alternative BSTAM Actuation Concepts

A huge field of alternative BSTAM actuation concepts for the application with various front suspension / steering systems has been elaborated, without claim to be exhaustive or complete (cf. chapter 4.1, i.e. 4.1.4, and appendix A.4.1).

These represent idealized kinematic concepts that require further concretization and study on the basis of real components and vehicle properties. Some concepts (i.e. the inclinable steering head in Figure A.7) only work for specific geometric setups and gear ratios. The majority of concepts with mechanical coupling involves relatively long drive trains with several gear sets and it stands to question, whether these can be realized in a play-free manner and yield the required chassis stiffness. On one hand, this issue could be overcome by replacing the simple spur gear and rack combinations from the concept sketches by self-inhibiting or even self-locking linear adjustments, and on the other the question of achieving sufficient stiffness with a hydraulic coupling remains to be answered. While purely lateral steering axis adjustment inherently keeps steering reaction torques upon BSTAM activation (close to) zero for (close to) zero steering angles, the occurrence of undesired reactions should also be evaluated case by case, when basic properties of the practical setup are already known.

With these limitations in mind, the presented concepts may be a starting point and inspiration for motorcycle manufacturers and custom bike builders that delight in the unique BSTAM mechanics or want to realize extreme front tire widths without compromising corner braking safety.

Brake Systems

The Combined-ABS of the reference motorcycle always activates both brakes, no matter which lever is applied by the rider and activates the rear brake in slight advance of the front brake (cf. chapters 2.3.3 and 3.6.6). Compared to a conventional brake system with two separate brake circuits, both characteristics are mitigating the BST effect to a certain extent, especially when only the front brake is applied. When both brakes are applied, the C-ABS is helping the rider to approach the “ideal” brake force distribution, with equally large reserves in friction potential at both wheels. For sole application of the rear brake, relatively high decelerations can be achieved with a well controllable increase in steering torque demand thanks to gradually increasing involvement of the front brake. Moreover, its by-wire architecture allows “smooth” ABS control.

To a certain degree, these characteristics approach those of a Cornering Adaptive Brake Force Distribution (cf. chapter 3.6). Therefore, the measured performance gap between baseline and BSTAM setup in the majority of driving experiments with sole front brake actuation would have been larger with conventional separate brakes than with the C-ABS, and expectedly smaller with a fully Cornering Adaptive BFD. Depending on the rider capability, the same is likely for activation of both brakes. Orienting driving tests with sole (maximal) rear brake actuation showed that the C-ABS already operates in the sense of a rear wheel oriented Cornering Adaptive BFD. In contrast to the analytically derived idealized case (cf. chapter 3.6), any practical implementation will be slightly less beneficial concerning BST mitigation, because it needs to keep a safety margin

from the friction limits in order to avoid destabilizing effects through pre-mature ABS activation at the rear wheel. Finally, concerning ABS controlled experiments with high deceleration levels, larger disturbance values would be expected from brake systems with conventionally "pulsating" ABS control than those obtained with C-ABS.

Multi-Lever Steering

Multi-lever steering systems benefit from virtual instantaneous centers of rotation to allow lateral displacement and / or inclination of the kinematic steering axis – and hence geometric compensation of the tire scrub radius – as a function of steering angle. Their exemplarily analysis on the basis of a simple four-bar linkage with perpendicular caster angle ($\tau = 0$) revealed significant downsides in form of an elevated stationary steering torque demand and a more direct transmission of the BST (cf. chapters 3.4.2 and 6.1).

Despite these findings, it can however not be excluded that a practical implementation of the setup with favorably fine tuned parameters (such as suspension characteristics and front wheel inertia) will perform considerably well in practical driving thanks to other benefits. Especially the direct steering transmission is expected to yield benefits in handling characteristics and transparency of feedback from the front wheel.

While the achievable effective compensation ratio of the analyzed four-bar linkage remained in a nearly negligible order, it cannot be excluded, that it is possible to find a three-dimensional setup of a multi-lever front suspension / steering system that can effectively ameliorate the BST effect and at the same time keep stationary steering torque demand desirably low. The presented basic kinematic concepts of steering axis displacement (cf. chapter 4.1.1) may serve as a starting point to answer this question.

Finally, it is technically also feasible – however not recommended – to implement the idea of displacing a virtual bearing point of a multi-lever steering in the original sense of a BSTAM. Firstly, it is not expected to bring additional performance benefits compared to a BSTAM that is based on a conventional steering system. And secondly, it is increasing mechanical complexity: Since each virtual bearing point is constituted of multiple physical bearings and interconnecting joints, moving the same synchronously on wheel carrier and frame side (and in independence of the steering angle) means to move a whole set of physical parts instead of just one or two physical bearings for the conventional BSTAM. Lastly, and provided that sufficient stiffness can be achieved, a hydraulic coupling (cf. Figure 4.6) with separate actuators should be the simplest way to implement such a setup, if at all desired.

Multi-Track Tilting Vehicles

The BSTAM concept can also be transferred to multi-track tilting vehicles. On one hand, for all concepts known to the author, favorable roll angle measurement relative to

the road surface is easily possible from moving parts of the tilting mechanism with a simple angular sensor or can even directly be used as a mechanical input for the BSTAM. On the other hand, a twin-fold steering bearing adjustment is required on left and right side. It has hitherto not been analyzed, in how far a favorable mechanical design can be found, since this will ultimately depend on the chassis layout of the base vehicle. Again provided that sufficient stiffness can be achieved, a hydraulic coupling (cf. Figure 4.6) with separate actuators should be the simplest way to implement a BSTAM on a multi-track tilting vehicle. In an ideal case, the hydraulic actuation could be achieved by direct roll angle input from the tilting mechanism.

Finally, further research needs to be done to evaluate, in how far the theoretical potential to mitigate the BST effect through left / right asymmetries (in normal and brake forces as well as scrub radii) can be transferred into practice.

6.3 Relevance of Results for other Systems and Stakeholders

BST Countermeasures in Racing

Racing applications typically involve corner braking with high deceleration levels close to the friction limits as well as lean in (i.e. hanging-off) riding style that displaces the rider body's center of gravity significantly towards the inside of the curve. As confirmed by the presented research, the "stand-up" tendency is therefore well in line with the required reduction of roll angle. Also balancing of the BST is no problem, because corner braking is done intentionally under controlled conditions. BST countermeasures like a BSTAM or a counter steering torque actuator could however relief the rider to a certain extent from the physical work required to counterbalance the steering torque demand during corner braking and thus help to keep up concentration over the whole racing distance. In order to investigate the potential effectiveness of such measures, it is necessary to analyze the way riders are supporting their body to counteract inertial forces when braking. While aerodynamic drag plays a significant role especially at high speeds, a certain amount of force surely needs to be balanced against the vehicle. If this is done on a direct path from the rider body's center of gravity through the inner arm to the inner handlebar, this is already automatically balancing a great deal of the BST and a reduction of the same would rather cause problems than be a benefit. In any case, steering transparency and clear feedback are of utmost importance for the system layout.

PTW with All-Wheel Drive

Every now and then, prototypes or small series productions of All-Wheel Drive (AWD) motorcycles are making headlines in the press, with new possibilities through hybrid technology with electrical front wheel drive[181].

The presented considerations and equation sets on the optimized BSTAM layout may easily be modified for the traction case to make use of the system for mitigation of steering reaction torques that result from drive forces at the front wheel.

While the benefit is estimated to be rather marginal on motorcycles with short wheelbase and high center of gravity, because the front wheel cannot contribute much for traction under strong acceleration, a beneficial steering axis adjustment is hardly possible to achieve for the continuously varying ground contact positions in off-road use.

Therefore, the ideal target vehicle would for instance be an on-road "all-weather" cabin motorcycle with long wheelbase, low center of gravity, and high front wheel loads to provide enough traction potential to realize a powerful front wheel drive.

Rider Education and Training

Even experienced riders often lack essential knowledge that might save their lives in a hazardous situation[182]. Therefore, the fundamentals of motorcycle dynamics, the physical potential and limits of corner braking (including those of modern tires and brake systems), as well as the BST chain of effects (including startle reactions and the mental roll angle limit), are strongly recommended to be part of rider education. In ideal case, practical riding exercises such as corner braking should be part of the training. Finally, a simple information that must not be missed, is that almost everyone can do something to ameliorate the "stand-up" tendency of the own vehicle through the choice of tires.

PTW and Tire Manufacturers

In the same way as the handling characteristics of a motorcycle, also its "stand-up" tendency in a corner braking situation is the result of an intricately interwoven interplay of chassis layout and tire characteristics. Even though it may not be the main development aim, it should neither be forgotten when designing a chassis or tire.

Especially tire design is typically a compromise (for instance concerning handling characteristics, mileage, wet-grip, stand-up tendency, etc.), that should additionally fit to

---

[181] Wunderlich – virtual: BMW R1200GS LC Hybrid, www.wunderlich.de/action/... ...konzeptfahrzeuge/r/wunderlich-r-1200-gs-lc-hybrid/, last access: 2016-09-08

[182] cf. Hämel (2010): Survey on Corner Braking Behavior, Bachelor-Thesis

several different motorcycles and work well with dynamic control systems. Consequently, not every tire of the desired dimension works well on every motorcycle concerning the BST effect. While the research motorcycle benefitted greatly of changing from one tire generation to the second next of the same tire manufacturer, a different tire brand performed very poor in tests with a non instrumented motorcycle of the same type. Therefore, it is recommended that motorcycle manufacturers take that aspect more into account during their tire approval process.

Moreover, the possibilities of BST countermeasures such as BSTAM or a counter steering torque actuator could open new perspectives both for chassis layout and tire design. I.e., if less care needs to be taken about the occurrence of the BST related stand-up tendency, because this is covered by the control system, other desirable tire characteristics might be further improved.

Finally, any BST countermeasure that involves electronic control will need to interact with other control systems and should ideally be an integral part of the whole control environment[183]. This setup will naturally have to consider aspects of functional safety and may consist of an interaction of various sensory inputs (inertial measurement, brake pressures, and others), brake and traction control systems, engine control (i.e. engine braking control), gearbox management (e.g. automatic disengagement of the clutch in automated gearboxes such as Dual Clutch Transmission, DCT), semi-active electronic steering and chassis dampers. This is an exemplary list, without claim to be exhaustive or complete (cf. outlook in the next chapter).

6.4 Outlook

Parameter Variations

The first step that is directly possible with the presented analytical equation set is to conduct parameter variations to investigate geometric properties and effectiveness of an optimized BSTAM and Cornering Adaptive Brake Force Distributions (CA-BFD) for different vehicle categories (cf. chapter 6.2).

[183] Among other terms, such integrated systems are often referred to as Integrated Chassis Management (ICM) or Global Chassis Control (GCC) for passenger cars. For motorcycles, Bosch is promoting its Motorcycle Stability Control (MSC) as an integrated control architecture.

Further Driving Experiments with existing Prototype Motorcycle

With slight improvements on the existing BSTAM prototype, the following driving experiments would be of further interest:

- Corner braking experiments under variation of tire manufacturer and study of tire wear. Different tires showed a huge discrepancy in stand-up tendency that could be quantified through further tests. Moreover, the tire contour and also the mass and inertia of the front wheel are significantly changing through tire wear (in the order of 16%, cf. Table A.6). The impact of this influence on driving characteristics ought to be systematically investigated.
- Corner braking experiments with different brake force distributions, especially rear oriented ones, to evaluate their effectiveness concerning the BST effect (cf. chapter 6.2).
- Corner braking over friction steps (i.e. in form of small sheet metal strips). Thanks to lower steering torque deviations upon ABS brake release and subsequent ramp up, BSTAM is expected to yield easier control and stability than setups with passively centered steering axis.
- Corner braking experiments with "short trail" setups. Orienting tests showed, that these can also be safely conducted. On one side, significantly better handling characteristics are expected due to reduced caster angle and trail, on the other, the downside of increased stationary steering torque demand should prevail in similar magnitudes.
- Parameter variations to study the influence of controller time lag in slalom and handling experiments. In the transition phase between two curves of a slalom, the time lag of BSTAM control causes the steering axis to be inclined to the "wrong" side. This creates (outward) steering torque components that support the steering impulse to enter the next turn. Orienting tests showed, that the prototype motorcycle would therefore do the slalom "almost all by itself" for a given cone distance and speed that match with the controller time lag and chosen target compensation ratio. Moreover, before entering into the left turn of the test track on the 70 m radius, a swerve maneuver trough a right curve was necessary. Thanks to the time lag effect, the median of obtained handling indices for BSTAM is very close to those of the unmodified chassis and sometimes even slightly better (2.67 $^{Nm}/_{(m°/s^2)}$ of the baseline vs. 2.64-3.49 for BSTAM), whereas handling performance was much worse on the 50 m radius, that was always entered from straight conditions (3.0-3.3 vs. 4.9 $^{Nm}/_{(m°/s^2)}$). This could therefore be used to ameliorate handling characteristics by assisting the counter steering impulse, if the rider intention can be reliably detected or predicted, as would be the case in a racetrack situation with no impending overtaking maneuvers.

- Finally, also tests with a larger number of riders with different experience levels are of interest, as well as tests on rural roads or a race track with professional test riders to investigate high speed stability, handling, and rider coupling. However, due to the limitations of the BSTAM prototype, all this makes more sense at later development stages with an optimized BSTAM (see next section).

Stiffness, Stability & Handling of Optimized BSTAM

As already addressed in chapter 6.2, it stands to question, whether the proposed concepts for practical implementation of an optimized BSTAM layout can yield the required chassis stiffness. It should be investigated case by case on the basis of real mechanical components and a concretized chassis setup.

Before the background of steering axis inclinations in the order of 10°, that represent much greater deviations from a centered steering axis than the approximately 2° of the current BSTAM prototype, an analysis of stability (i.e. wobble, weave, and kick-back) as well as handling characteristics should be conducted before construction of a prototype with optimized BSTAM. This can favorably be done using multi body simulation.

Experimental Investigations with Optimized BSTAM

In case the prior questions can be answered in favor of an optimized BSTAM, it could be implemented into a new research motorcycle to conduct further riding experiments to evaluate its practical performance and feel. In ideal case, such a prototype would at the same time combine several BST relevant measures to evaluate their respective effectiveness. An exemplary setup could consist of the following:

- An optimized BSTAM chassis (that will directly allow to test the centered steering axis setup with no interference in caster angle or trail as on the prototype).
- An advanced semi active steering damper.
- A brake system to allow any (Cornering Adaptive) Brake Force Distribution (e.g. through a programmable controller for the brake-by-wire C-ABS).
- A counter steering torque actuator. – In contrast to BSTAM, this allows separate analysis of the initial and extended working hypotheses ($H_{Wa,b}$, respectively $H_{0a,b,c}$, cf. chapters 1.2 and 5.4.3), thanks to free combinations of high and low stationary steering torque demand, steering torque deviation upon brake activation, and steering torque level during the experiment.

As further options, the following could as well be included:

- A semi-active suspension system (to study dynamic influences on BST kick-in).
- A multi-lever steering system (for comparative study, which would however need to be a replacement for the BSTAM front suspension / steering system).

Predictive Brake Assist (PBA) and Autonomous Emergency Braking (AEB)

Effective BST countermeasures as discussed in this thesis are a necessary pre-requisite for the realization of future brake systems that can autonomously activate the brakes in cornering situations. However, as a sufficient condition to evaluate their theoretical potential and practical limitations, fundamental research needs to be conducted to understand the dynamic rider coupling to the vehicle and active rider reactions (i.e. steering compensation capabilities). General thresholds for the system layout could for instance safely be derived with test riders using a realistic motorcycle riding simulator[184] under variation of roll angles, deceleration levels, brake pressure increase rates, steering torque demand levels, and other relevant parameters.

Based on these thresholds and the results from the performance study of different BST countermeasures as described in the previous section, an appropriate BST countermeasure could be chosen for a favorable realization of PBA or AEB.

From a current point of view, rider retention systems such as seat belts are regarded as beneficial to allow high autonomously triggered decelerations. While seat belts are still under investigation for conventional motorcycles[185], they typically belong to the standard equipment of cabin motorcycles that moreover feature an additional safety cell (such as the MonoTracer[186] or the discontinued BMW C1[187]) Since some sort of environmental recognition or at least vehicular communication would need to be present for an autonomous brake system, the choice of a counter steering torque actuator as BST countermeasure is promising the highest functional flexibility, because it might also allow to manipulate the vehicle trajectory in the sense of an anti-collision avoidance maneuver.

Real World Information on the BST Effect

In order to be able to evaluate, which performance level is required from BST countermeasures in series applications, a twin-fold approach is suggested. Firstly, the BST chain of effects should more precisely be considered in the framework of in-depth accident studies. And secondly, BST critical situations (near accidents and accidents) from real traffic should be analyzed. This is ideally done with a huge pool of instrumented motorcycles in the framework of a naturalistic driving study, that could not only provide

[184] Will et al. (2016): Bringing single track vehicle dynamics to motorcycle riding simulators

[185] Cf. Murri et al. (2008): Sicherheitsgurt für Motorradfahrer, proceedings pp. 418-429, and Unger (2010): Sicherheitskonzept, proceedings pp. 2-48

[186] MonoTracer – virtual: https://peraves.wordpress.com/, last access: 2016-11-11

[187] Kompass et al (1998): The Safety Concept of BMW C1, proceedings pp. 223-241

the time history of relevant measured data (such as GPS and inertial data, i.e. the roll angle, steering torque and angle, brake activation, wheel speeds and deceleration, rider position, suspension travel, etc.), but also a video footage for environmental reference. Since many riders already film their rides with action cameras and sometimes even record GPS-tracks with their smart phones, which could easily provide complimentary inertial measurements if attached to the vehicle in a defined manner, a simple way to conduct such a study would be a public campaign to hand in relevant data deliberately. Moreover, it would be of interest to capture data from first series vehicles incorporating dedicated BST countermeasures. All this information will not only help to improve the design of PTW concerning the BST effect, but – depending on the outcome - might also inspire insurances to lower their fees for vehicles with additional safety technology, or lawmakers to take such measures onto their roadmap. However, from today's point of view and status of development, this is to be regarded in a long term perspective.

Concluding Comment

Closing the bracket from the initially set research aims, the answer to the last aim 3.4 is still open that requires to draw a conclusion, whether BST countermeasures beyond the state of the art technology are necessary at all or at least recommendable.

From a current perspective, the answer is: It depends - on the desired application and target vehicle type. On one hand, a combination and further optimization of networked state-of-the-art systems (i.e. combined anti-lock brake systems with Cornering Adaptive BFD, advanced semi-active steering damper control, and potentially also semi-active chassis suspension) along with appropriate tire design might already sufficiently address a huge number of BST relevant situations in real traffic. On the other hand, more powerful measures like BSTAM and the counter steering actuator are seen as a necessary prerequisite to obtain the best accident avoidance performance with autonomous braking systems. Moreover, they also offer new design possibilities for both chassis and tire development.

In final conclusion of this thesis and as an argument for further research on BST countermeasures, especially on BSTAM, the unique feel of opening and closing the brakes with hardly any disturbance when cornering on the current BSTAM prototype cannot be put into better words than those of one occasional test rider:

"It feels so natural, like it should always be this way. – Why is it not always this way?"

A Appendix

A.1 Appendix to Chapter 1

Survey on Corner Braking Behavior – Main Results

In summer 2010, a "Survey on the Corner Braking Behavior of Motorcycle Riders" was conducted in form of a student research project[188] in the context of the presented research.

In total 311 complete data sets could be generated. While 122 questionnaires were filled in at 7 local motorcyclists' meeting points (in the Odenwald, Spessart and Vogelsberg area), 189 valid data sets were generated during an internet survey that was linked to in various motorcyclists' user forums, in university forums and on the homepage of the Institute of Automotive Engineering Darmstadt (*FZD*).

The riders' personal experience that is reflected in the results of the survey confirm the impression about the BST effect derived from accident figures already described in the introduction (cf. chapter 1.1). In brief, the survey's main results are the following:

- More than 20% of all participants were repeatedly surprised when confronted with the BST effect (stand-up tendency).
- It was listed by about 67% of the participants as No. 1 reason for near accidents (No. 2: reaching mental roll angle limit, listed by 61%, No. 3: Over-braking, listed by 50%).
- In 82% of the participants' near accidents, a startle reaction was involved (53% with marginal, 29% with significant influence).
- In 58% of the participants' accidents, a startle reaction was involved (32% with marginal, 26% with significant influence).
- From a subjective point of view, the BST effect was ranked the 3rd most dangerous situation (1st: Being overseen by other road users, especially passenger car drivers, 2nd: Over-braking and falling when cornering).
- When given seven options on what extra feature to buy with a new motorcycle based on a limited budget, together with TCS and suspension / chassis tuning, a BSTAM system was ranked right after protective clothing and ABS / CBS. Thus, it was clearly preferred before an airbag or engine tuning.

[188] Hämel (2010): Survey on Corner Braking Behavior, Bachelor-Thesis

A.2 Appendix to Chapter 2

Force Flow of BSTAM as incorporated in the Prototype Motorcycle

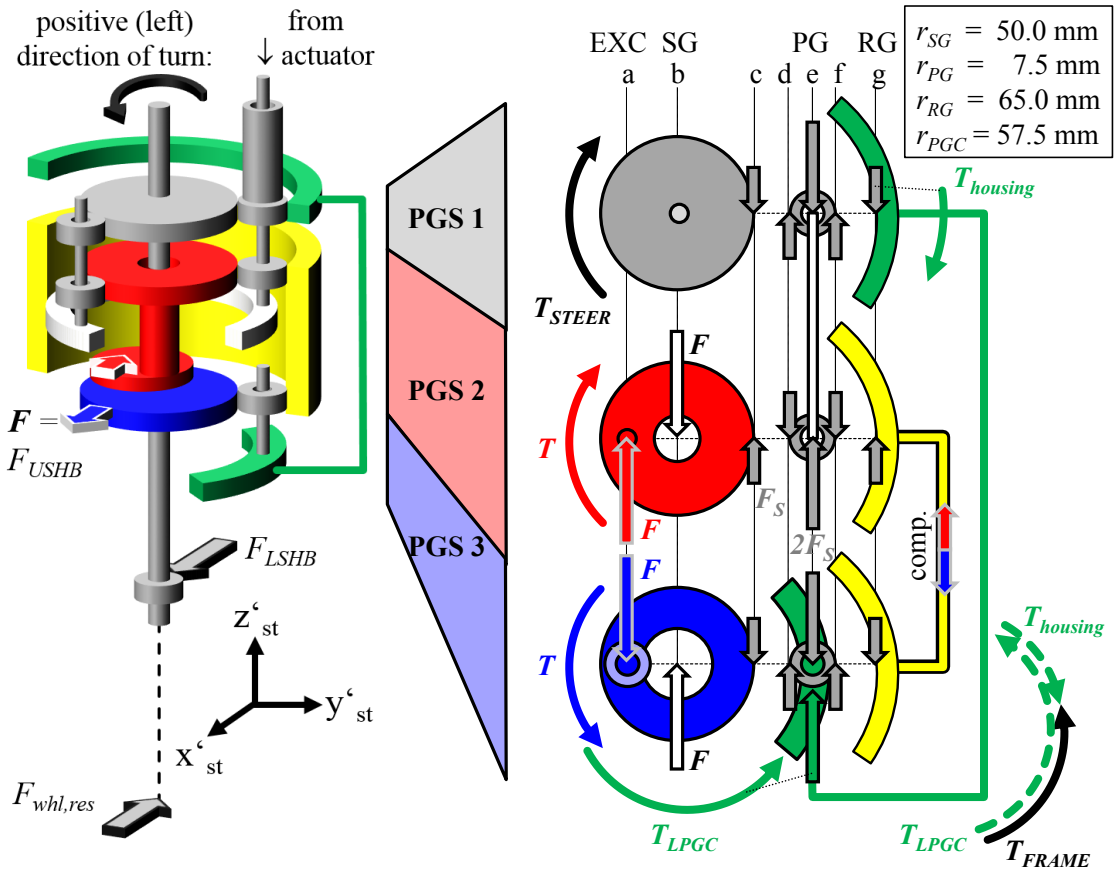

Legend of Variables, Indices, and Abbreviations (if not self-explanatory)	
F, T	Force in N, Torque in Nm
$F_{whl,res}$	Resulting front wheel force in (i.e. against) x'$_{st}$-direction
T_{STEER}, T_{FRAME}	Torque of same magnitude imposed by BSTAM in opposing directions on the steering system and vehicle frame
r	Radius (equal to half the number of teeth) of the respective gears
USHB, LSHB	Upper and Lower Steering Head Bearing
PGS, LPGC	Planetary Gear Set, Lower Planetary Gear Carrier
EXC, SG, PG, RG	Excenter, Sun Gear, Planetary Gear, Ring Gear

Figure A.1: Force flow of BSTAM, illustrating the coupling of excenter forces towards steering shaft and frame for straight braking with maximal lateral excenter offset (cf. Figure 3.1 for the generation of $F_{whl,res}$ as vector composition of F_x and F_z and Figure 4.7 for a technical drawing).

A.3 Appendix to Chapter 3

A.3.1 Equation Set for the Derivation of the Optimized Instantaneous Center of Steering Axis Inclination of OPT BSTAM

This section shows a step-by-step solution for the transition from eq. (3.21) to (3.22) in chapter 3.3.2. for the definition of the optimal position of the instantaneous center of steering axis inclination (point G in Figure 3.1). Taking over eq. (3.21) as a starting point, the height of the instantaneous center (G) is expressed as:

$$h_G = \left(1 + \frac{\sin\gamma_{opt}}{\sin(\lambda - \gamma_{opt})}\right) \cdot r_{c,ft} \tag{A.1}$$

The term in the denominator can be replaced as follows by making use of a trigonometric addition theorem[189]:

$$h_G = \left(1 + \frac{\sin\gamma_{opt}}{\sin(\lambda)\cdot\cos(\gamma_{opt}) - \cos(\lambda)\cdot\sin(\gamma_{opt})}\right) \cdot r_{c,ft} \tag{A.2}$$

Division of both numerator and denominator of the fraction by $\sin(\gamma_{opt})$ leads to:

$$h_G = \left(1 + \frac{1}{\sin(\lambda)\cdot\frac{1}{\tan(\gamma_{opt})} - \cos(\lambda)}\right) \cdot r_{c,ft} \tag{A.3}$$

This equation only contains γ_{opt} in a favorable way in the form of a singular tangent expression. Recalling eq. (3.19), γ_{opt} is defined by the following arc-tangent expression:

$$\gamma_{opt}(\lambda) = \arctan\left(\frac{\sin\lambda\cdot nt_{sta} - \cos\lambda\cdot\sin\tau\cdot sr_{sta}}{\cos\lambda\cdot nt_{sta} + \sin\lambda\cdot\sin\tau\cdot sr_{sta}}\right) = \arctan(A) \tag{A.4}$$

With A being a substitute for the fraction in brackets. Composing nt_{sta} and sr_{sta} in their expanded forms based on eq. (3.4) and (3.7) yields:

$$nt_{sta} = r_{r,ft}\cdot\sin\tau - fo \tag{A.5}$$

$$sr_{sta} = \sin\lambda\cdot r_{c,ft} \tag{A.6}$$

and both expressions inserted into eq. (A.4) deliver:

$$A = \frac{\sin\lambda\cdot r_{r,ft}\cdot\sin\tau - \sin\lambda\cdot fo - \cos\lambda\cdot\sin\tau\cdot\sin\lambda\cdot r_{c,ft}}{\cos\lambda\cdot r_{r,ft}\cdot\sin\tau - \cos\lambda\cdot fo + \sin\lambda\cdot\sin\tau\cdot\sin\lambda\cdot r_{c,ft}} \tag{A.7}$$

[189] Merziger et al. (2001): Formeln + Hilfen. Chapter 3 Elementare Funktionen / Additionstheoreme, p. 38

Division of both numerator and denominator by sin(λ) and sin(τ) leads to:

$$A = \frac{r_{r,ft} - \frac{fo}{\sin\tau} - \cos\lambda \cdot r_{c,ft}}{\frac{1}{\tan\lambda} \cdot r_{r,ft} - \frac{1}{\tan\lambda} \cdot \frac{fo}{\sin\tau} + \sin\lambda \cdot r_{c,ft}} \tag{A.8}$$

Inserting $r_{r,ft}$ from eq (3.3) in its expanded form:

$$r_{r,ft} = r_{ft} - (1 - \cos\lambda) \cdot r_{c,ft} \tag{A.9}$$

leads to:

$$A = \frac{r_{ft} - (1 - \cos\lambda) \cdot r_{c,ft} - \frac{fo}{\sin\tau} - \cos\lambda \cdot r_{c,ft}}{\frac{1}{\tan\lambda} \cdot \left(r_{ft} - (1 - \cos\lambda) \cdot r_{c,ft}\right) - \frac{1}{\tan\lambda} \cdot \frac{fo}{\sin\tau} + \sin\lambda \cdot r_{c,ft}} \tag{A.10}$$

Rearranging and cancelling equal terms of opposite sign in the numerator leads to:

$$A = \frac{r_{ft} - r_{c,ft} - \frac{fo}{\sin\tau}}{\frac{1}{\tan\lambda} \cdot \left(r_{ft} - r_{c,ft} + r_{c,ft} \cdot \cos\lambda\right) - \frac{1}{\tan\lambda} \cdot \frac{fo}{\sin\tau} + \sin\lambda \cdot r_{c,ft}} \tag{A.11}$$

Multiplication of both numerator and denominator with tan(λ) leads to:

$$A = \frac{\left(r_{ft} - r_{c,ft} - \frac{fo}{\sin\tau}\right) \cdot \tan\lambda}{r_{ft} - r_{c,ft} + r_{c,ft} \cdot \cos\lambda - \frac{fo}{\sin\tau} + \sin\lambda \cdot \tan\lambda \cdot r_{c,ft}} \tag{A.12}$$

Rearranging yields:

$$A = \frac{\left(r_{ft} - r_{c,ft} - \frac{fo}{\sin\tau}\right) \cdot \tan\lambda}{\left(r_{ft} - r_{c,ft} - \frac{fo}{\sin\tau}\right) + r_{c,ft} \cdot (\cos\lambda + \sin\lambda \cdot \tan\lambda)} \tag{A.13}$$

Substitution of the equal expressions in brackets in numerator and denominator of the fraction with *B* as follows:

$$\left(r_{ft} - r_{c,ft} - \frac{fo}{\sin\tau}\right) = B \tag{A.14}$$

as well as reducing the fraction in expression *A* by dividing both numerator and denominator by *B* delivers:

$$A = \frac{\tan\lambda}{1 + \frac{r_{c,ft} \cdot (\cos\lambda + \sin\lambda \cdot \tan\lambda)}{B}} \tag{A.15}$$

Re-substituting *A* into eq. (A.4) yields:

$$\gamma_{opt} = \arctan\left(\frac{\tan\lambda}{1+\frac{r_{c,ft}\cdot(\cos\lambda+\sin\lambda\cdot\tan\lambda)}{B}}\right) \tag{A.16}$$

Since the γ_{opt}-dependent expression required for the insertion into equation (A.3) is a tangent function, it cancels the arc-tangent in the prior equation (A.16) to obtain:

$$\frac{1}{\tan\gamma_{opt}} = \frac{1+\frac{r_{c,ft}\cdot(\cos\lambda+\sin\lambda\cdot\tan\lambda)}{B}}{\tan\lambda} \tag{A.17}$$

Rearranging yields:

$$\frac{1}{\tan\gamma_{opt}} = \frac{1}{\tan\lambda}+\frac{r_{c,ft}}{B}\cdot\left(\frac{\cos^2\lambda}{\sin\lambda}+\sin\lambda\right) \tag{A.18}$$

Bringing the expressions in brackets on the common denominator sin(λ) allows to apply the addition theorem $\cos^2(\lambda) + \sin^2(\lambda) = 1$ as follows:

$$\frac{1}{\tan\gamma_{opt}} = \frac{1}{\tan\lambda}+\frac{r_{c,ft}}{B}\cdot\left(\frac{\cos^2\lambda+\sin^2\lambda}{\sin\lambda}\right) = \frac{1}{\tan\lambda}+\frac{r_{c,ft}}{B\cdot\sin\lambda} \tag{A.19}$$

Reformulation yields:

$$\frac{1}{\tan\gamma_{opt}} = \frac{1}{\sin\lambda}\cdot\left(\cos\lambda+\frac{r_{c,ft}}{B}\right) \tag{A.20}$$

And the re-substitution of B from equation (A.14) delivers:

$$\frac{1}{\tan\gamma_{opt}} = \frac{1}{\sin\lambda}\cdot\left(\cos\lambda+\frac{r_{c,ft}}{r_{ft}-r_{c,ft}-\frac{fo}{\sin\tau}}\right) \tag{A.21}$$

Inserting this expression into equation (A.3) leads to:

$$h_G = \left(1+\frac{1}{\sin\lambda\cdot\left(\frac{1}{\sin\lambda}\cdot\left(\cos\lambda+\frac{r_{c,ft}}{r_{ft}-r_{c,ft}-\frac{fo}{\sin\tau}}\right)\right)-\cos\lambda}\right)\cdot r_{c,ft} \tag{A.22}$$

The roll angle dependent sine and subsequently also the cosine expressions cancel themselves out and lead to the final formulation that is only dependent on the three geometrical chassis parameters front tire radius r_{ft}, fork offset fo and caster angle τ:

$$h_G = \left(1 + \frac{r_{ft} - r_{c,ft} - \frac{fo}{\sin\tau}}{r_{c,ft}}\right) \cdot r_{c,ft} = r_{ft} - \frac{fo}{\sin\tau} \tag{A.23}$$

This is the final formulation as taken up again in eq. (3.22) for the argumentation in chapter 3.3.2.

A.3.2 Equation Set for the Computation of Tire Contact Forces with different Brake Force Distributions (BFD)

This appendix provides the equation set of the extended quasi-stationary corner braking simulation model utilized for the analysis in chapter 3.6 for the comparison of the effectiveness of BSTAM and a standard chassis with varying brake force distributions.

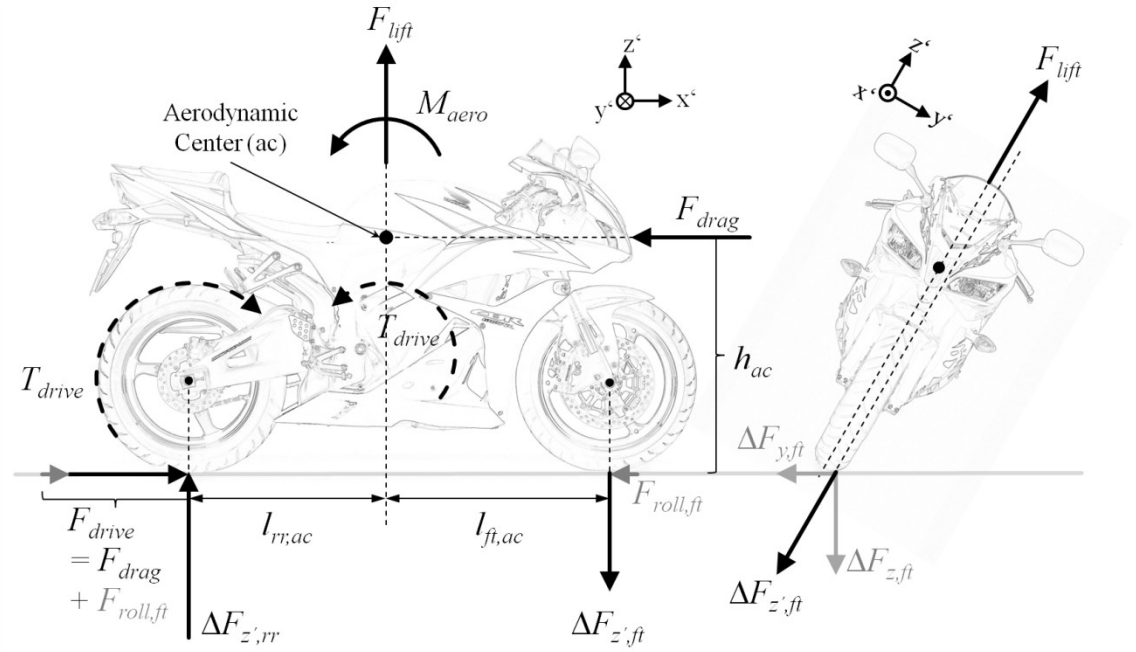

Figure A.2: Influences of aerodynamic effects, rolling resistance, and driving torque on the tire forces [Motorcycle Pictures (c) Honda]

Figure A.2 schematically illustrates how aerodynamic drag, lift and pitch moment, rolling resistance, and rear wheel driving torque affect the tire forces and are subsequently addressed in the model calculations.

Adding Aerodynamic Influences

In analogy to eq. (2.3) in chapter 2.1.2, also a mean tire contour radius can be defined for the location of the aerodynamic center:

$$r_{c,ac} = \frac{r_{c,ft} \cdot l_{rr,ac} + r_{c,rr} \cdot l_{ft,ac}}{l} \tag{A.24}$$

delivering the roll angle dependent vertical lever arm of the drag force:

$$h_{ac} = h_{ac,0} - r_{c,ac} \cdot (1 - \cos\lambda) \tag{A.25}$$

with $h_{ac,0}$ being the aerodynamic center's height over ground in upright vehicle position. The aerodynamic drag and lift forces as well as the aerodynamic pitch moment are defined positive in direction of the arrows in Figure A.2 as follows:

$$F_{drag} = c_w \cdot A \cdot \frac{\rho}{2} \cdot v^2 \tag{A.26}$$

$$F_{lift} = c_l \cdot A \cdot \frac{\rho}{2} \cdot v^2 \tag{A.27}$$

$$M_{aero} = c_p \cdot A \cdot l \cdot \frac{\rho}{2} \cdot v^2 \tag{A.28}$$

with c_w, c_l, and c_p being the dimensionless aerodynamic drag, lift and pitch coefficients, A the frontal projection area of the motorcycle (including the rider in typical half-erect riding position) in m², l the wheelbase of the motorcycle in m, $\rho = 1.2$ kg/m³ the air density and v the forward velocity of the vehicle in m/s.

While both the aerodynamic drag force and pitch moment cause wheel load differences of equal amplitudes but opposite sign in the sense of an increase at the rear and decrease at the front, the lift force is unloading both wheels. As illustrated in Figure A.2, it has a lateral offset towards the tire contact patch line, causing a roll moment that tends to increase the roll angle. However, for the initial conditions of the analyzed reference maneuver and the parameters of the test motorcycle, it can be neglected: $r_{c,ac} = 78.95$ mm, multiplied by the sine of the roll angle $\lambda = 35°$ it delivers an effective lever arm of 45.3 mm that combines with a maximal lift force of $F_{lift} = 9.72$ N to a disturbing roll moment of only $M_{x,lift} \approx 0.44$ Nm. Hence the quasi-stationary roll equilibrium from eq. (2.8) in chapter 2.1.2 is also utilized for the extended model.

Adding Driving Reaction Torque

In case the clutch is not disengaged and only the front brake is applied during a brake maneuver, a driving torque remains at the rear wheel and a corresponding reaction torque on the vehicle body that leads to a rearward wheel load shift. Summarizing all these effects yields the wheel load differences in the z'-direction of the vehicle coordinate system:

$$\Delta F_{z',ft/rr} = \frac{1}{l} \cdot \left(\mp F_{drag} \cdot h_{ac} - F_{lift} \cdot l_{rr/ft,ac} \mp M_{aero} \mp T_{drive} \right) \tag{A.29}$$

Wheel Load Differences and Rolling Resistance

The vectorial decomposition of the wheel load differences in the vehicle coordinate system as presented in Figure A.2 allows to express them in the leveled coordinate system as follows:

$$\Delta F_{z,ft/rr} = \Delta F_{z\prime,ft/rr} \cdot \cos\lambda \tag{A.30}$$

$$\Delta F_{y,ft/rr} = \Delta F_{z\prime,ft/rr} \cdot \sin\lambda \tag{A.31}$$

Superimposition with the basic definition of wheel loads from eq. (2.26) and (2.27) in chapter 2.1.7 delivers:

$$F_{z,ft/rr} = m \cdot g \cdot \frac{l_{rr/ft}}{l} \pm m \cdot a_x \cdot \frac{h_{cg}}{l} + \Delta F_{z,ft/rr} \tag{A.32}$$

$$F_{y,ft/rr} = \frac{a_y}{g} \cdot \left(m \cdot g \cdot \frac{l_{rr/ft}}{l} \pm m \cdot a_x \cdot \frac{h_{cg}}{l} \right) + \Delta F_{y,ft/rr} \tag{A.33}$$

With the knowledge of the individual vertical wheel loads $F_{z,ft/rr}$ and the assumption of a constant dimensionless rolling resistance coefficient $c_{roll} = 0.02$ it is possible to define the rolling resistance at each wheel:

$$F_{x,ft/rr,roll} = c_{roll} \cdot F_{z,ft/rr} \tag{A.34}$$

and also globally, either as a sum of the individual parts or based on the diminution of the overall weight force $F_{z,cg} = m \cdot g$ by the lift effect:

$$F_{roll} = c_{roll} \cdot \left(m \cdot g - F_{lift} \cdot \cos\lambda \right) = c_{roll} \cdot (F_{z,ft} + F_{z,rr}) \tag{A.35}$$

With this information it is now furthermore possible, to define the amount of driving reaction torque in case the clutch is not disengaged when using the front brake only. Under the assumption that the driving torque needed to overcome the aerodynamic and rolling resistances prior to braking (at time $t = t_0$, initial velocity v_0, and roll angle λ_0) remains constant after brake initiation, it becomes:

$$T_{drive} = T_{drive}(t_0) = \left(F_{drag}(t_0) + F_{roll}(t_0) \right) \cdot r_{r,rr}(t_0) \tag{A.36}$$

with $r_{r,rr}(t_0)$ being the effective rear tire rolling radius at the initial roll angle $\lambda(t_0) = \lambda_0$ that can be expressed by the free rolling radius r_{rr} and the contour radius $r_{c,rr}$ as follows, in analogy to eq. (3.3):

$$r_{r,rr}(\lambda_0) = r_{rr} - r_{c,rr} \cdot (1 - \cos\lambda_0) \tag{A.37}$$

Definition of Deceleration Limits

In order to complete the equation set, the front and rear braking forces remain to be defined for different BFD in accordance with the desired deceleration level.

For maximal braking maneuvers, this is limited by the maximal available friction potential or reaching the brake flip-over point and remains to be determined as a necessary input to compute the lateral and normal forces and subsequently the brake forces.

Table A.1 gives an overview of the different BFD to be simulated.

Table A.1: Overview of different Brake Force Distributions

Case No.	Deceleration Level	Brake Force Distribution (BFD)		Clutch
1	maximal (limited by friction potential or brake flip-over)	bb-eq	Use of both brakes, with equal use of friction potential ("ideal" BFD)	disengaged
2		ft	Front braking only	
3				engaged
4		rr	Rear braking only	disengaged
5	partial	bb-eq	Use of both brakes, with equal use of friction potential ("ideal" BFD)	
6	$a_{x,target} = 0.5g$	bb-rr	Use of both brakes, with maximal use of friction potential at the rear	disengaged
7		ft	Front braking only	
8	(same limits as above)			engaged
9		rr	Rear braking only	disengaged

Defining a rear wheel lift-off as the instant when the rear wheel reaches the friction limit, the computation of both limitations in maximal possible deceleration a_x, due to brake flip-over or friction limits, can be formulated as reaching the friction limit according to Kamm's friction circle (cf. chapter 2.1.4) as follows:

$$F_x^2 + F_y^2 = (\mu \cdot F_z)^2 \tag{A.38}$$

Replacing each tire force in this equation by a generic expression that consists of a deceleration dependent and a second independent coefficient yields the following general quadratic problem:

$$(e + \mathscr{f} \cdot a_x)^2 + (c + d \cdot a_x)^2 = (a + \mathscr{b} \cdot a_x)^2 \tag{A.39}$$

and its general resolution:

$$a_x = \frac{\sqrt{(-2a\mathscr{b} + 2cd + 2e\mathscr{f})^2 - 4(-a^2 + c^2 + e^2)(-\mathscr{b}^2 + d^2 + \mathscr{f}^2)} + 2a\mathscr{b} - 2cd - 2e\mathscr{f}}{2(-\mathscr{b}^2 + d^2 + \mathscr{f}^2)} \tag{A.40}$$

In the following, the individual coefficients are defined in accordance with the different brake force distribution cases in order to determine the two limitations of the maximal possible deceleration through rear wheel "lift-off" or reaching the friction limits. Table A.2 starts with the deceleration limits set by rear wheel "lift-off".

Deceleration Limits set by Rear Wheel "Lift-Off" ($a_{x,max,rlp}$)

Table A.2: Coefficients for the determination of the deceleration limit given by rear wheel "lift-off", $a_{x,max,rlp}$

Case	Comments on longitudinal forces at the rear wheel	Substitutes of rear wheel forces					
		$\mu \cdot F_{z,rr} = (a + \mathscr{b} \cdot a_x)$		$F_{y,rr} = (c + d \cdot a_x)$		$F_{x,rr} = (e + \mathscr{f} \cdot a_x)$	
		a	$\mathscr{b}$	c	d	e	$\mathscr{f}$
1	rolling resist. depending on current wheel load	$\mu \cdot \left(\frac{l_{ft}}{l} \cdot m \cdot g + \Delta F_{z,rr}\right)$	$\mu \cdot \left(-\frac{h_{cg}}{l} \cdot m\right)$	$\frac{a_y}{g} \cdot \left(\frac{l_{ft}}{l} \cdot m \cdot g\right) + \Delta F_{y,rr}$	$\frac{a_y}{g} \cdot \left(-\frac{h_{cg}}{l} \cdot m\right)$	$c_{roll} \cdot \left(\frac{l_{ft}}{l} \cdot m \cdot g + \Delta F_{z,rr}\right)$	$c_{roll} \cdot \left(-\frac{h_{cg}}{l} \cdot m\right)$
2							
3	driv. torque less current rolling resist. (note sign convention!)					$-\frac{T_{drive,0}}{r_{r,rr}} + c_{roll} \cdot \left(\frac{l_{ft}}{l} \cdot m \cdot g + \Delta F_{z,rr}\right)$	
4	see separate notes					$-c_{roll} \cdot \left(\frac{l_{rr}}{l} \cdot m \cdot g + \Delta F_{z,ft}\right) + F_{drag}$	$m - c_{roll} \cdot \left(\frac{h_{cg}}{l} \cdot m\right)$
5,6,7	see case 1					see case 1	
8	see case 3					see case 3	
9	see separate notes on c. 4					see case 4	

Note: In both **cases 4 and 9** for rear braking with clutch disengaged (which for an unsprung chassis is the same as overcompensating a still present driving torque with the rear brake) it is actually impossible for the rear wheel to lift-off, since the maximum transferrable forces are limited by the rear wheel load that diminishes with increasing

deceleration. Hence, in these cases the "lift-off" condition is given when reaching the friction limits at the rear wheel ($a_{x,max,rlp} = a_{x,max,friction}$) for the transfer of the necessary lateral force in conjunction with the maximum possible brake force, while the front wheel only transfers its lateral and rolling resistance force.

The overall deceleration is then given by:

$$m \cdot a_x = F_{x,rr} + F_{x,roll,ft} + F_{drag} = F_{x,rr} + c_{roll} \cdot F_{z,ft} + F_{drag} \,. \quad \text{(A.41)}$$

Insertion of $F_{z,ft}$ from eq. (A.32) and rearranging for $F_{x,rr}$ delivers the substitute components e and f as listed in Table A.2.

Deceleration Limits set by Rear Friction Forces ($a_{x,max,friction}$)

While cases 4 and 9 for rear wheel braking have already been addressed within the prior definition of the friction limits set by rear wheel "lift-off", the remaining 7 cases still need to be addressed.

Using both Brakes (cases 1, 5, and 6)

Using both brakes, the maximum possible deceleration is achieved for reaching the friction limits at both wheels simultaneously. Therefore, Kamm's friction circle can be applied as for a single wheel mass point model:

$$F_x^2 + F_y^2 = (\mu \cdot F_z)^2 \quad \text{(A.42)}$$

with

$$F_y = m \cdot a_y - F_{lift} \cdot \sin\lambda \quad \text{(A.43)}$$

$$F_z = m \cdot g - F_{lift} \cdot \cos\lambda \quad \text{(A.44)}$$

and

$$m \cdot a_x = F_x + F_{drag} \quad \text{(A.45)}$$

Insertion of eq. (A.42) through (A.44) in eq. (A.45) and resolution for a_x yields:

$$a_x = \frac{1}{m}\left(\sqrt{\left(\mu\left(m \cdot g - F_{lift} \cdot \cos\lambda\right)\right)^2 - \left(m \cdot a_y - F_{lift} \cdot \sin\lambda\right)^2} + F_{drag}\right). \quad \text{(A.46)}$$

Cases 5 and 6 address partial braking maneuvers with a pre-defined deceleration a_x. In case maximal deceleration is required, they are identical to case 1 with $a_x = a_{x,max,friction}$.

In **cases 2, 3, 7, and 8** for **using the front brake only**, with either clutch engaged or disengaged, the deceleration can generally be written as:

$$m \cdot a_x = F_{x,ft} + F_{x,rr} + F_{drag} \tag{A.47}$$

with the rear wheel contribute possibly being a driving force.

In all four cases, the friction limit is first reached at the front wheel. Hence, the mathematical problem can be solved by using the general quadratic solution from eq. (A.40) with the substitutes presented in Table A.3.

Table A.3: Coefficients for the determination of the deceleration limit given by friction limits for front braking only, $a_{x,max,friction}$

Case	Comments on longitudinal forces at the front wheel	Substitutes of front wheel forces					
		$\mu \cdot F_{z,ft} = (a + b \cdot a_x)$		$F_{y,ft} = (c + d \cdot a_x)$		$F_{x,ft} = (e + f \cdot a_x)$	
		a	b	c	d	e	f
2, 7	Besides the drag force, also the rear wheel rolling resistance contributes to overall deceleration, relieving the front brake effort.	$\mu \cdot \left(\frac{l_{rr}}{l} \cdot m \cdot g + \Delta F_{z,ft}\right)$	$\mu \cdot \left(\frac{h_{cg}}{l} \cdot m\right)$	$\frac{a_y}{g} \cdot \left(\frac{l_{rr}}{l} \cdot m \cdot g\right) + \Delta F_{y,ft}$	$\frac{a_y}{g} \cdot \left(\frac{h_{cg}}{l} \cdot m\right)$	$-c_{roll} \cdot \left(\frac{l_{ft}}{l} \cdot m \cdot g + \Delta F_{z,rr}\right) - F_{drag}$	$m + c_{roll} \cdot \left(\frac{h_{cg}}{l} \cdot m\right)$
3, 8	While the drag force relieves the front brake effort, the persisting driving torque diminished by the rear wheel rolling resistance is burdening it additionally.					$\frac{T_{drive,0}}{r_{r,rr}} - c_{roll} \cdot \left(\frac{l_{ft}}{l} \cdot m \cdot g + \Delta F_{z,rr}\right) - F_{drag}$	

Based on the achieved results, the appropriate deceleration level can be defined for the different phases of the experiment, starting with a steady state cornering phase, a free rolling phase, decelerated by the resistances, and finally, the braking phase:

Steady state cornering $$a_x = 0 \tag{A.48}$$

Free Rolling (clutch disengaged) $$a_x = \frac{1}{m}\left(F_{roll} + F_{drag}\right) \tag{A.49}$$

Corner braking $$a_x = \min\left(a_{x,partial}, a_{x,rlp}, a_{x,friction}\right) \tag{A.50}$$

Note, that $a_{x,partial}$ is only included in eq. (A.50) if separately pre-defined in cases 5 through 9 for partial decelerations.

Tire Forces

With the known deceleration levels for each case, the front and rear normal and lateral forces $F_{z,ft/rr}$ and $F_{y,ft/rr}$ can be determined according to eq. (A.32) and (A.33) and subsequently also the longitudinal forces $F_{x,ft/rr}$, depending on the current experiment phase.

Longitudinal Forces in the Pre-Braking Phase

Steady state cornering and free rolling (clutch disengaged)

$$F_{x,ft} = c_{roll} \cdot F_{z,ft} \tag{A.51}$$

Steady state cornering (overcoming driving resistances)

$$F_{x,rr} = -(F_{x,ft} + F_{drag}) \tag{A.52}$$

Free Rolling (clutch disengaged)

$$F_{x,rr} = c_{roll} \cdot F_{z,rr} \tag{A.53}$$

Longitudinal Forces in the Braking Phase

The computation of longitudinal forces in the braking phase depends of cause on the selected case.

For the **ideal brake force distributions** with equal use of friction potential (μ_{used}), at both wheels (**cases 1 and 5**), they can be computed on the basis of the normal and lateral forces at each wheel (cf. eq. (A.32) and (A.33)) and under the assumption of an ideal Kamm friction circle for the tire-road interaction as follows:

$$F_{x,ft}^2 + F_{y,ft}^2 = \mu_{used}^2 \cdot F_{z,ft}^2 \tag{A.54}$$

$$F_{x,rr}^2 + F_{y,rr}^2 = \mu_{used}^2 \cdot F_{z,rr}^2 \tag{A.55}$$

Both brake forces together with the aerodynamic drag force must deliver the desired overall deceleration:

$$F_{x,tot} = F_{x,ft} + F_{x,rr} + F_{drag} = m \cdot a_x \tag{A.56}$$

Reformulating equations (A.54) and (A.56) leads to:

$$\mu_{used} = \sqrt{\frac{F_{x,ft}^2 + F_{y,ft}^2}{F_{z,ft}^2}} \tag{A.57}$$

$$F_{x,rr} = m \cdot a_x - F_{x,ft} - F_{drag} \tag{A.58}$$

With equations (A.57) and (A.58) set into eq. (A.55) leads to the quadratic equation:

$$(m \cdot a_x - F_{x,ft} - F_{drag})^2 + F_{y,rr}^2 = \frac{F_{x,ft}^2 + F_{y,ft}^2}{F_{z,ft}^2} \cdot F_{z,rr}^2 \tag{A.59}$$

Which can be resolved to deliver the front brake force $F_{x,ft}$. In an analogous way, these reformulations can be done to obtain the rear brake force $F_{x,rr}$ and after some arithmetic[190], both can be expressed as follows:

$$F_{x,ft/rr} = \frac{1}{\pm\left(F_{z,rr}^2 - F_{z,ft}^2\right)} \cdot \left(\sqrt{\begin{pmatrix} \left(m \cdot a_x \cdot F_{z,ft} \cdot F_{z,rr}\right)^2 - 2 \cdot m \cdot a_x \cdot F_{drag} \cdot F_{z,ft}^2 \cdot F_{z,rr}^2 + \\ +F_{drag}^2 \cdot F_{z,ft}^2 \cdot F_{z,rr}^2 + \left(F_{y,ft}^2 \cdot F_{z,rr}^2 - F_{y,rr}^2 \cdot F_{z,ft}^2\right) \cdot \left(F_{z,ft}^2 - F_{z,rr}^2\right) \end{pmatrix}} - \right) \cdot \left(-(m \cdot a_x - F_{drag}) \cdot F_{z,ft/rr}^2 \right) \tag{A.60}$$

Elimination of the drag force from the equation yields the following form that was already presented with the simpler quasi-stationary model in chapter 2.1.7, eq. (2.29):

$$F_{x,ft/rr} = = \frac{\sqrt{\left(m \cdot a_x \cdot F_{z,ft} \cdot F_{z,rr}\right)^2 + \left(F_{y,ft}^2 \cdot F_{z,rr}^2 - F_{y,rr}^2 \cdot F_{z,ft}^2\right) \cdot \left(F_{z,ft}^2 - F_{z,rr}^2\right)} - m \cdot a_x \cdot F_{z,ft/rr}^2}{\pm\left(F_{z,rr}^2 - F_{z,ft}^2\right)} \tag{A.61}$$

In order to minimize the BST in partial braking situations, **the rear wheel oriented Cornering Adaptive BFD in case 6** reduces the front brake force by applying the maximum possible rear brake force for a given available friction potential ($\mu_{used,ft} < \mu_{used,rr} = \mu_{available}$):

$$F_{x,rr} = \sqrt{(\mu \cdot F_{z,rr})^2 - F_{y,rr}^2} \tag{A.62}$$

Given the rearward shift in BFD, the front is just contributing the remaining longitudinal force according to eq. (A.56), in order to achieve the target deceleration a_x.

For maximal or partial **front braking with clutch disengaged (cases 2 and 7)**, the rear wheel is only transferring its rolling resistance force in longitudinal direction:

$$F_{x,rr} = c_{roll} \cdot F_{z,rr} \tag{A.63}$$

And again, the front brake is doing the rest according to eq. (A.56). However, it has to be noted that the prior definition of a_x is different for the different cases.

For maximal or partial **front braking with clutch engaged (cases 3 and 8, stalling the engine)**, the rear wheel is transferring the initial driving torque divided by the current

[190] The quadratic equation has been solved using a Texas Instruments TI-92 calculator and checked against the solution derived with www.WolframAlpha.com.

rear wheel rolling radius reduced by its rolling resistance. (Note the sign convention of the driving force as a negative braking force.)

$$F_{x,rr} = -\frac{T_{drive,0}}{r_{r,rr}} + c_{roll} \cdot F_{z,rr} \tag{A.64}$$

And again, the front brake force is doing the rest according to eq. (A.56) on the basis of the prior definition of a_x. However, for partial braking (case 8) the front wheel is transferring more brake load than with clutch disengaged (case 7), increasing the BST.

In case of maximal or partial **rear wheel braking (cases 4 and 9) with clutch disengaged**, the front wheel is only transferring its rolling resistance force in longitudinal direction:

$$F_{x,ft} = c_{roll} \cdot F_{z,ft} \tag{A.65}$$

while the rear is doing the rest, according to eq. (A.56) and the prior definition of a_x, that is, as much as possible in case 4 and 9 but no more than the pre-defined $a_{x,partial}$ in the latter case, should this be lower than the deceleration limit set by available friction potential. Herewith, the equation set for the proposed extended quasi-stationary corner braking model used for the simulations in chapter 3.6 is completely defined. The parameter values of the prototype motorcycle that were used for the simulations are listed in appendix A.4.2.

A.3.3 Equation Set for the Computation of Measured Brake Force Distributions for the Entry in the BFD Diagram

The following considerations show, how data points for the entry in the brake force distribution (BFD) diagram (cf. chapter 3.6.6) are computed from measurements of the brake pressures p_{brk} and roll angle λ. In order to obtain consistent signals, the roll angle with an average sample rate of 10 Hz is linearly interpolated[191] to match the brake pressure measurements with 500 Hz sample rate. The following equation set holds equally true for both brakes, the respective indices (*ft* and *rr*) have however been omitted for easier readability. As a last side note, care needs to be taken with unit conversions. It is easiest to enter all parameters into the presented equations using plain SI-units (i.e. pressures in N/m² instead of bar, lengths in m instead of mm, and surfaces in m² instead of mm²).

[191] Using the "interp1"-command of MATLAB ® Software.

Table A.4: Brake system parameters of the test motorcycle (Honda CBR 600 RR)

Brake	No. (z_{brk}) and type of calipers	Piston diameters $d_{1,2}$	Eff. friction surface A_{brk}	Disk diameter D	Eff. friction radius r_{brk}	Friction coefficient μ_{brk}
Front	2 x four-piston, fixed	30 mm, 32 mm	6044,4 mm²	310 mm	138.5 mm	0.49
Rear	1 x single-piston, floating	30 mm	1413.7 mm²	220 mm	93.0 mm	0.46

Since every caliper has brake pads on two friction sides, the effective friction surface A_{brk} of each brake is computed as follows from the brake piston diameters $d_{1,2}$ and number of calipers z_{brk}:

$$A_{brk} = (d_1^2 + d_2^2) \cdot \frac{\pi}{4} \cdot 2 \cdot z_{brk} \text{ (with } d_2 = 0 \text{ for the rear brake)} \tag{A.66}$$

The brake torque T_{brk} can then be computed on the basis of the measured brake pressure p_{brk} along with the effective friction surface, radius, and coefficient A_{brk}, r_{brk}, and μ_{brk}:

$$T_{brk} = p_{brk} \cdot A_{brk} \cdot r_{brk} \cdot \mu_{brk} \tag{A.67}$$

The brake force in the respective tire contact patch F_x can then be computed with the roll angle dependent current rolling radius r_r of each tire (cf. eq. (3.3)) as:

$$F_x = \frac{T_{brk}}{r_r} = \frac{T_{brk}}{r - r_c \cdot (1 - \cos\lambda)} \tag{A.68}$$

For the entry of data points into the brake force distribution diagram, this result needs finally to be divided by the vehicle mass m (cf. Table A.5) and the gravity constant g.

A.4 Appendix to Chapter 4

A.4.1 Alternative Actuation Concepts

The alternative actuation concepts presented in this appendix compliment the general considerations from chapter 4.1 and the concrete examples from chapter 4.1.4. While some are already discussed in context of this latter chapter, the appendix only comprises additional explanations, if applicable. The suggested field of solutions stays without claim to be exhaustive or complete. The examples are regarded as principal ideas and an inspiration to develop further derivatives or completely new concepts. In any case, a

thorough analysis on the basis of real component properties is recommended to ensure the functionality, before putting any of the concepts into practice.

Class AC 1: Drive Shaft through Fixed Spherical Bearing

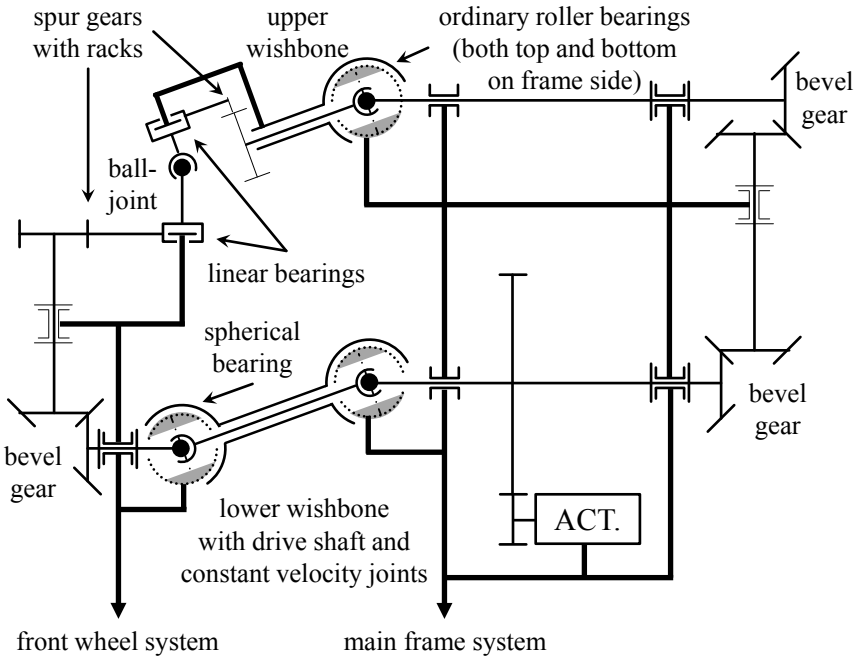

Figure A.3: BSTAM on a double wishbone suspension, using drive shafts with constant velocity joints running through both wishbones to adjust the upper bearing without the need of a floating wishbone (KC 1, AC 1), cf. Figure 4.3

Flipping the setups presented in Figure A.3 and Figure A.4 upside-down transfers KC°1 to KC 2, with sole adjustment of the lower instead of the upper steering bearing.

Even though the implementation on a Telelever suspension goes along with certain downsides and is therefore not recommended (cf. chapter 4.1.2), the functional principle of class AC 1 can also be transferred to this suspension type. However, for adjustment of either bearing, the vertical drive shaft on the front wheel system side needs to be equipped with a prismatic drive shaft with a slider (in analogy to Figure A.6) in parallel to the fork tubes. Finally, since the spring / damper element of a Telelever suspension is typically mounted on the wishbone, a laterally fixed wishbone (in the sense of Figure A.3 flipped upside-down for KC 2) is preferable over a floating one (cf. Figure 4.3).

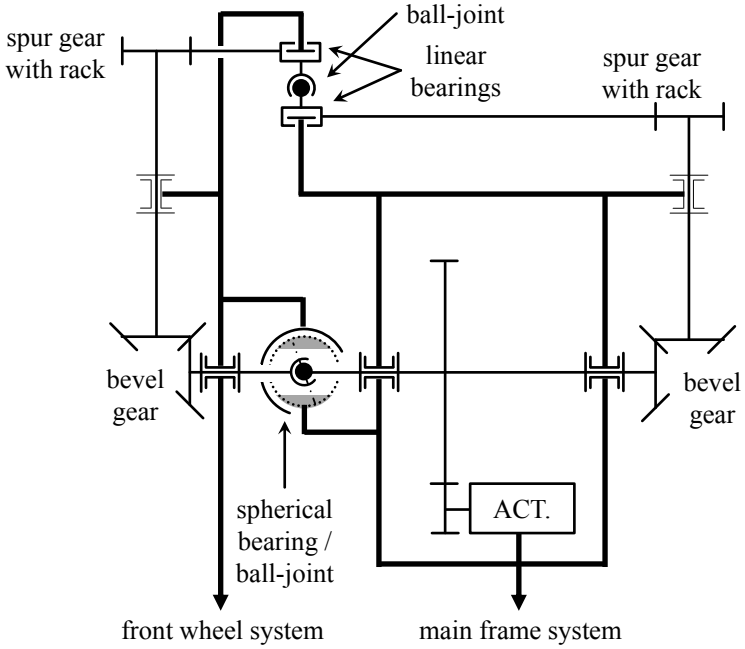

Figure A.4: BSTAM with adjustment of the upper ball-joint, driven by a shaft with constant velocity joint that runs through the lower spherical bearing arrangement (KC°1, AC 1). As a derivative of the double wishbone setup from Figure 4.3, the layout is suitable for the use in a steering head or the attachment to the double wishbones of a hub-center steering.

Class AC 2: Floating Drive Shaft through (or along) Adjusted Bearing

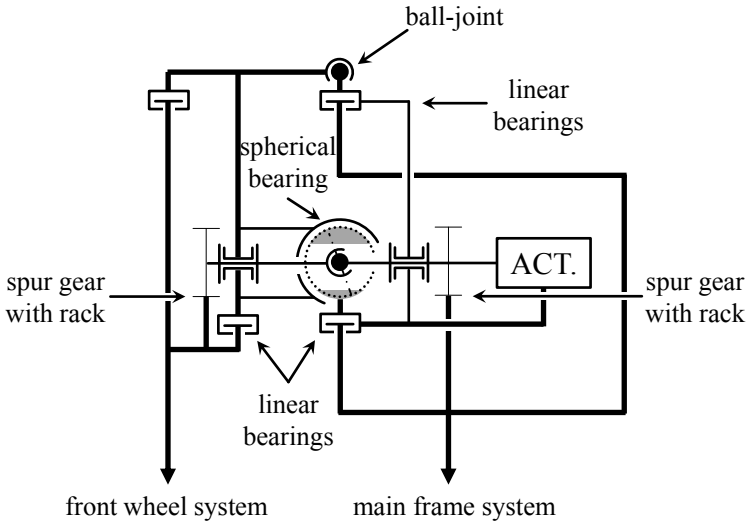

Figure A.5: Parallel BSTAM with floating drive shaft and actuator, derived from Figure 4.4 for the use in a steering head or attachment to the double wishbones of a hub-center steering (KC 3, AC 2). In this case, also conventional steering bearings can be used instead of the ball joints[192].

[192] Cf. Biermann (1990): Entwurf zur Verhinderung des Bremslenkmoments, Bild 13a and 14a, in a historical student research project.

Leaving away the parallel coupling for the adjustment of the upper ball joint in Figure A.5 leads to KC 2, while flipping the same arrangement upside-down yields KC 1. Moreover, there are various alternatives to incorporate the actuator, that does not necessarily have to be floating (cf. Figure 4.4 and Figure A.6).

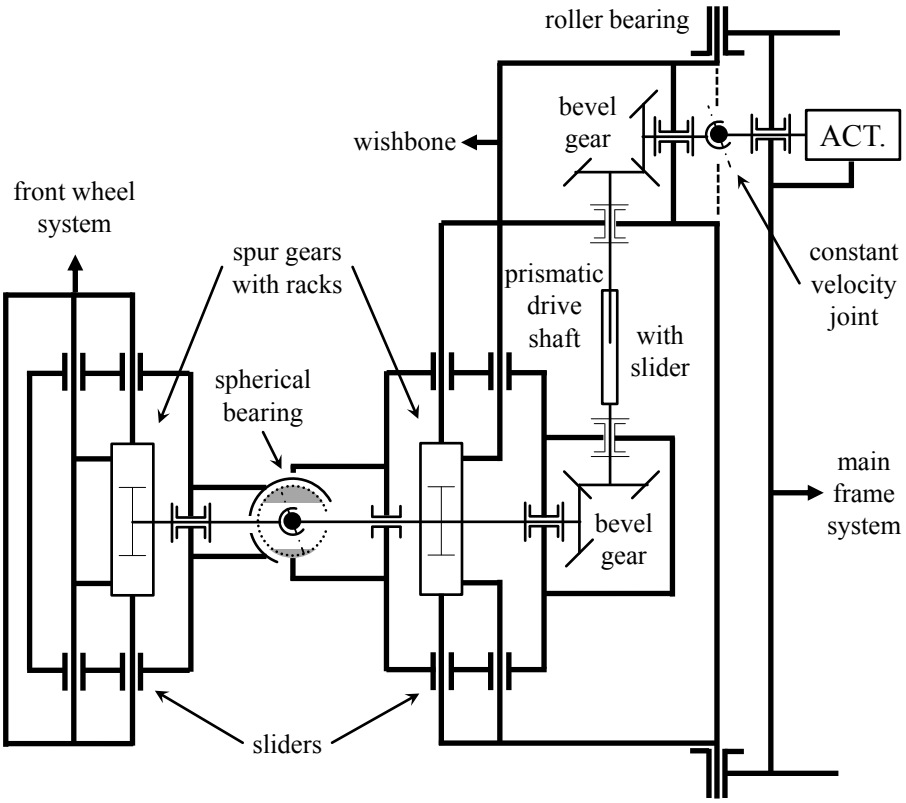

Figure A.6: Adjustment of a single spherical bearing on a wishbone with a floating drive shaft and a prismatic drive shaft with slider that allows to place the actuator fixedly on the main frame side (suitable for all KC 1-7, AC 2)

The principle presented in Figure A.6 can analogously be transferred to any incorporation of this actuation concept class with its adjustable bearings directly driven trough (or in parallel to) themselves. Especially the arrangement of components allows almost countless variations. As two examples, the actuator in the figure could for instance as well be placed inside the wishbone, while the prismatic drive shaft with slider assembly could also be located on the sprung frame side.

Even though not recommended (cf. chapter 4.1.2), this design flexibility also allows to transfer concepts of class AC 2 to Telelever suspensions. While the upper ball joint can easily be adjusted in analogy to the lower bearing of in Figure A.5 in the sense of KC 1, the principle from Figure A.6 is directly applicable to the adjustment of the lower bearing in the sense of KC 2. If this principle of fixed positioning of the actuator in the frame is repeated for the adjustment of the upper ball joint, a coupling of both adjustments with just one actuator is possible, allowing generally all kinematic concepts KC 1-7. Moreover, a mechanical superimposition gearing could use the movement of

the wishbone as input to compensate suspension travel related fluctuations in compensation ratio. However, such a system is conceivably complex with no functional benefits compared to simpler solutions with other suspension types. For the sake of completeness, a parallel BSTAM (KC 3) on a Telelever can alternatively be realized in analogy to Figure 4.4, using linear sliders in parallel to the fork tubes to couple the adjustment of a floating wishbone with the upper ball joint. Of cause, all aforementioned permutations of locating the actuator and driving the adjustment mechanism apply analogously.

Class AC 3: Inclinable Steering Head

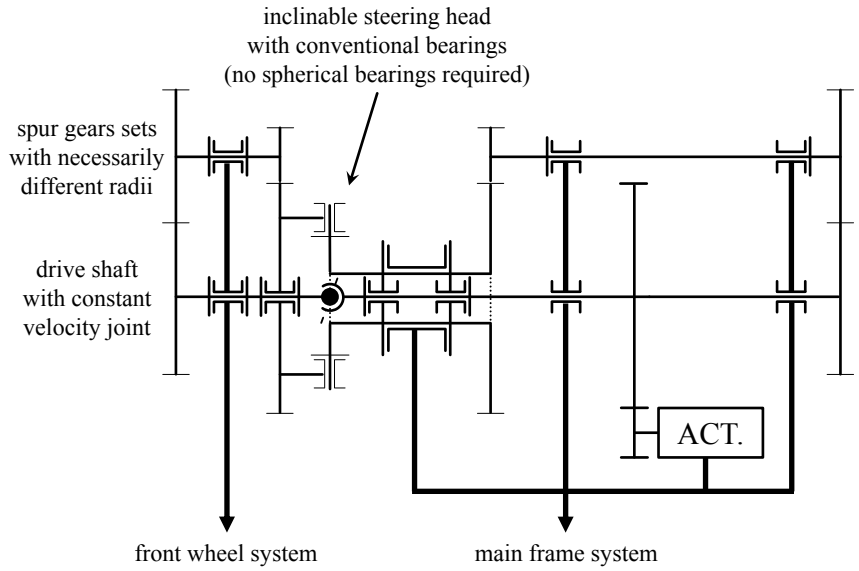

Figure A.7: BSTAM with inclinable steering head (KC 4, AC 3)

The BSTAM with inclinable steering head as shown in Figure A.7 has been developed as a derivative of class AC 1 (e.g. cf. Figure A.4). In order to be able to take up the reaction torques along the x'_{st}-axis, the spur gear sets necessarily have to have different radii and of cause be backlash-free. Alternatively, the spur gear sets can be replaced by vertical drive shafts with bevel gearing. Moreover, self-inhibiting or self-locking transmissions on both sides of the inclinable steering head would help to unload the central drive shaft from bearing the full reaction torque. However, taking the instantaneous force flow of such a solution one step further, leads to the much simpler and therefore preferable solution presented in Figure 4.5, in accordance with prior research[193].

[193] Cf. Biermann (1990): Entwurf zur Verhinderung des Bremslenkmoments, Bild 13b, 14b, and 16, in a historical student research project

A.4.2 Technical Data of the Prototype Motorcycle

The test motorcycle utilized for this study is a Honda CBR 600 RR super-sport machine of the model year 2010 with Combined-ABS (C-ABS, "Brake-by-Wire").

Table A.5 Technical data used for simulations

Parameter	Meaning	Value	Unit
A	frontal projection area	0.75	m²
I_{yy}	front wheel (spinning) mass moment of inertia	0.48	kgm²
bd	bearing distance	233	mm
c_w	aerodynamic drag coefficient	0.6	-
c_l	aerodynamic lift coefficient	0.072	-
c_p	aerodynamic pitch coefficient	0	-
c_{roll}	rolling resistance parameter	0.02	-
e	BSTAM excentricity	8	mm
fo	fork offset	30	mm
fl	fork length (compressed, static trim, extended)	386, 465, 494	mm
l	wheelbase	1375	mm
l_{ft}	x-distance front tire contact patch to CoG	700	mm
l_{rr}	x-distance rear tire contact patch to CoG	675	mm
h_{cg}	height of CoG in static trim	700	mm
$l_{ft,ac}$	x-distance front tire contact patch to aero center	l/2	mm
$l_{rr,ac}$	x-distance rear tire contact patch to aero center	l/2	mm
h_{ac}	height of aero center in static trim	700	mm
m	mass vehicle + rider	300	kg
n	trail	98	mm
τ	caster angle	23°55'	°
r_{ft}	front tire rolling radius	295	mm
r_{rr}	rear tire rolling radius	305	mm
$r_{c,ft}$	front tire contour radius	64.6	mm
$r_{c,rr}$	rear tire contour radius	93.3	mm

Table A.6: Mass and inertia properties of front and rear tires and wheels, the latter including the rims and all rotating parts such as brake disks and chain sprocket of the Honda CBR 600 RR test motorcycle. - Own measurements on the basis of two different sets of tires of the same type. Front tire flanks worn in excess of the tire wear index (TWI) at 1 mm remaining profile depth.

	Wheel			**Tire**			**Profile Depth**	
Parameter [unit]	m_{whl} [kg]	$I_{yy,whl}$ [kgm²]	$I_{zz,whl}$ [kgm²]	m_{tir} [kg]	$I_{yy,tir}$ [kgm²]	$I_{zz,tir}$ [kgm²]	*center* [mm]	*flanks* [mm]
Front Wheel / Tire - Bridgestone Battlax S20F, 120/70ZR17 M/C (58W)								
New	10.850	0.526	0.294	4.275	0.335	0.178	4.0	3.2
Worn	10.075	0.438	0.255	3.500	0.275	0.143	3.0	0.3
Difference	*0.775*	*0.088*	*0.039*	*0.775*	*0.060*	*0.035*	*1.0*	*2.9*
Rel. Diff. in %	*7.1*	*16.7*	*13.3*	*18.0*	*17.9*	*19.7*	*25.0*	*90.6*
Rear Wheel / Tire - Bridgestone Battlax S20R, 180/55ZR17 M/C (73W)								
New	14.370	0.728	0.447	6.225	0.539	0.293	5.9	4.8
Worn	13.700	0.616	0.385	5.160	0.437	0.241	1.8	2.0
Difference	*0.670*	*0.112*	*0.062*	*1.065*	*0.102*	*0.052*	*4.1*	*2.8*
Rel. Diff. in %	*4.7*	*15.4*	*13.9*	*17.1*	*18.9*	*17.7*	*69.5*	*58.3*

Parameters of the brake system are listed in appendix A.3.3, Table A.4.

A.4.3 Considerations on Steering Torque Measurement

The steering torque measurement is the most essential for the presented study and was based on specially manufactured handlebars that act as bending beams with strain gauges in full bridge on either side. However, this setup is ignoring steering torque components in axial direction of the handlebars. For a rough estimate of their influence, axial measurement has been added on the left handlebar, yielding maximal contributions of 5-8 Nm. These are however mostly cancelled out by opposing components on the other side, as concluded from left and right turn experiments. Hence, the maximal deviation is estimated to be in the order of only 1 Nm. Moreover, also the definition of filter parameters has an influence in the observed peak values. It is discussed in appendix A.4.5.

A.4.4 Considerations on Roll Angle Measurement

For some experiments, the roll angle shows an offset of up to about 10° during the more or less straight acceleration phase before the curve for the actual experiment is entered.

Depending on the riding style (lean in or lean out), this may be a result of a pre-positioning of the rider for the subsequent experiment. However, when such an offset occurs for the standard lean with riding style, it is kept from the last turning maneuver. This is basically a result of the low temperatures towards the end of the study that changed the desired transfer behavior of engine vibrations through the rubber elements of the mechanical low-pass to the inertial measurement unit. However, as can be seen from the well match with reference roll angles in time history data (for instance refer to Figure 5.2 and Figure 5.3), correct roll angle measurement is re-obtained when significant roll dynamics occur upon entering the curve of interest. Moreover, in order to keep tire wear symmetric as well as to minimize free play in the BSTAM mechanics upon brake kick-in during the experiment, almost all turn maneuvers during the study were performed in the same direction as the subsequent curve of interest. Therefore, the roll angle dependent steering axis displacement of BSTAM before entering the turn is kept both low (cf. chapter 4.2) and symmetric with regards to left and right turns. Anyway, despite the consistency of this effect, it might have contributed in a slightly elevated steering torque demand upon entering the turn and thus also led to an increase in Koch's handling index achieved for active BSTAM setups.

A.4.5 Definition of Filter Parameters

Correct measurement of steering torque and angle are of utmost importance for the computation of characteristic values to describe the maneuver performance of different setups (cf. chapter 5.2). While rider activity is supposed to have a bandwidth of about 2-3 Hz[194], chassis reactions to corner braking experiments are expected in a frequency range of 2-4 Hz for the bi-directional coupling of steer and roll motion (just as for the "weave" instability, see chapter 2.1.6) as well as in the range of the steering system's eigenfrequency between 8-10 Hz (just as for the "wobble" instability, see chapter 2.1.6).

However, besides this desired information, the measured raw signals are subject to noise and external disturbances, especially engine vibrations of first and second order. Most experiments were conducted in free rolling, with clutch disengaged (see chapter 5.1). So after the acceleration phase with higher rpm, the engine usually dropped to a still slightly increased idle speed before the braking maneuver was initiated. The idle speed is 1400 ± 100 rpm[195], which leads to an expected disturbance at 25 Hz. However, due to the elevated idle speed after accelerating, the measured first order disturbance was typically around 27 Hz. Finally dropping to very low idle speeds, the transfer of

[194] cf. Koch (1980): Untersuchungen des Motorrad-Fahrer-Systems, Chapter 1.2, p. 29ff

[195] Honda CBR 600 RR (MY2010), Workshop Manual

second order vibrations around 43-46 Hz becomes important for steering angle measurement, as will be addressed later.

The layout of an appropriate filter should at the same time allow to capture the desired rider action and oscillatory phenomena as well as to exclude the said noise and engine disturbances efficiently. Due to Nyquist's Theorem, the minimal sampling frequency to capture an oscillation should be at least twice the frequency of interest. Therefore, a first order low pass filter with a cutoff frequency of 20 Hz has been chosen as a compromise between the two layout targets. Besides the steering torque and steering angle measurement, this filter has also been applied to brake pressure measurement.

However, since the subjective feel of steering torque and movements reported by the test riders goes very well in line with signals obtained from a low pass filter with only 3 Hz cutoff frequency[194], its results are often used as auxiliary indicator for the interpretation of time domain data. Moreover, the 3 Hz cutoff has been used as well for filtering the rider body lean angle signal, since no higher frequency content was expected and its system immanent free play made it prone to higher frequency disturbances by wind and road unevenness.

The performance of the derived filters is exemplarily discussed on the basis of three different corner braking maneuvers in Figure A.8 through Figure A.11.

Figure A.8 shows the time history data of a typical strong corner braking maneuver in a right turn (R = 50 m) with actuation of the front brake only. While the first diagram in the figure presents roll angle[196], front wheel speed and front brake pressure for reference, diagrams 2, 3, and 4 address the filter layout for steering torque measurement, as do the final two diagrams for steering angle and steering angle velocity.

Looking at the second diagram in the figure, the curve is initiated by a steering impulse about 1.8 s prior to the brake actuation, with the clutch still engaged. Peak-to-peak noise in the steering torque raw signal during the acceleration phase is between 12-15 Nm. After the clutch is disengaged, engine speed and vibration disturbances drop to a minimum for one second before brake actuation. Peak-to-peak values are then as low as 3-5 Nm. When the brakes are finally actuated, noise is increasing again due to the more direct vibration transfer via the stronger loaded steering head bearings as well as contributes from brake friction, with peak-to-peak values in the same order, as before the clutch was disengaged. As illustrated by the following two diagrams that also show the signal content cut off by the respective 3 and 20 Hz filter, the latter approaches the first steering torque peak after brake kick-in very well. Taken away 2 Nm offset for half the peak-to-peak range of noise at that time, the absolute difference is less than 5 Nm which ranges just around 10% of the captured peak value.

[196] See section A.4.4 for considerations on roll angle deviations during the straight acceleration phase.

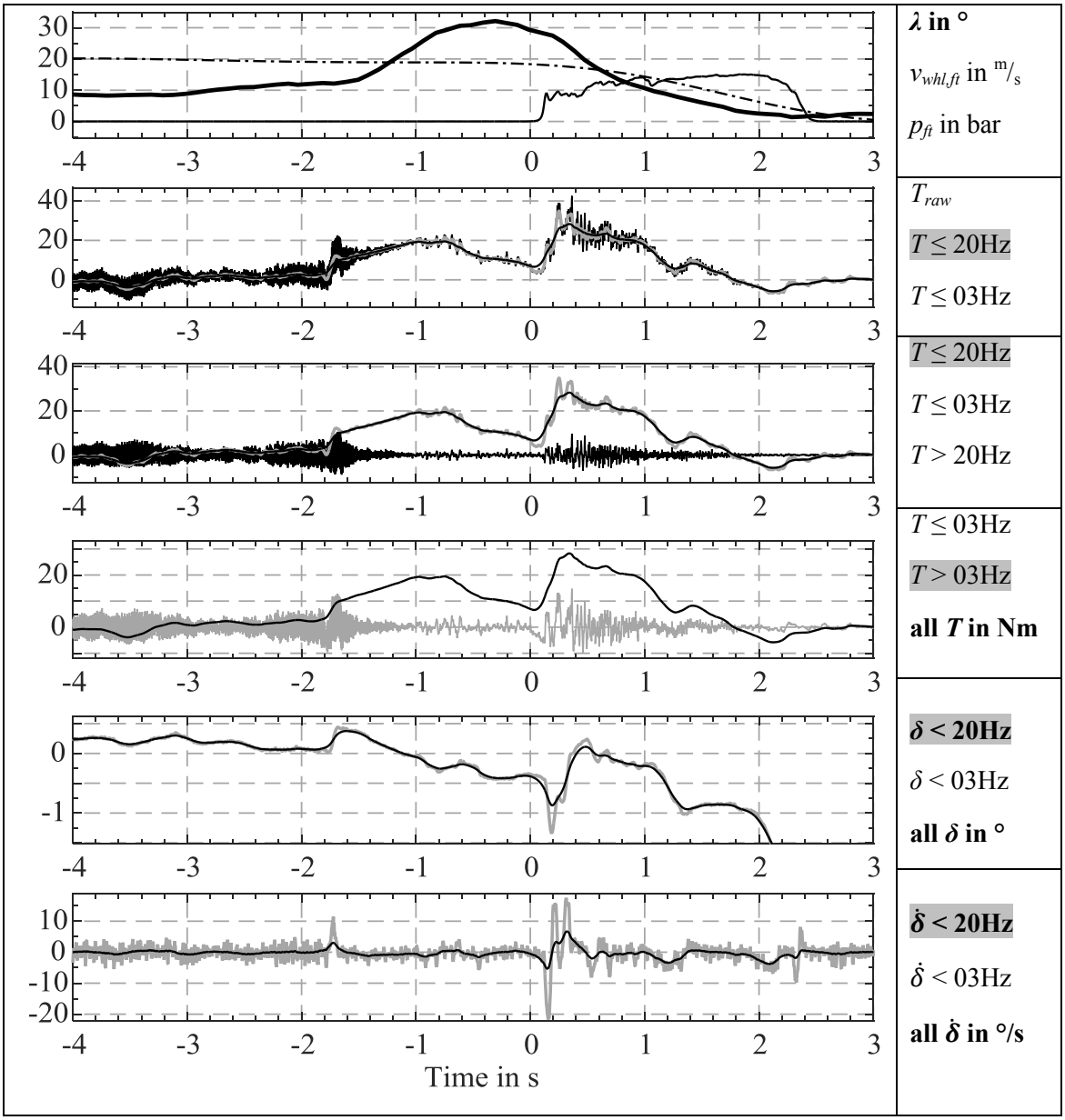

Figure A.8: Layout case: Typical strong corner braking maneuver with standard steering, $R = 50$ m, $a_x \approx 7.6$ m/s²

Regarding the last two diagrams in Figure A.8, the raw signals for both steering angle and its velocity are omitted, because engine vibration is directly fed from the frame to the sensor mount at the bottom of the lower fork yoke, generating considerable noise. The signals obtained from the 20 Hz filter show significantly larger absolute values in both measurands and especially the steering velocity fluctuations at the beginning of the brake process display the wobble eigenmode at about 9 Hz much better than the signal obtained from the 3 Hz filter. The frequency content of the steering angle velocity in the reference brake maneuver is exemplarily displayed for the raw and 20 Hz filtered signal in Figure A.9.

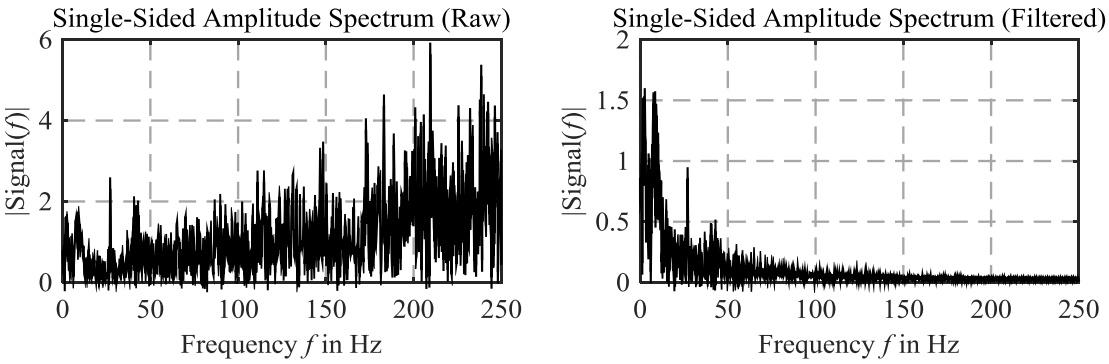

Figure A.9: Amplitude spectrum of steering angle velocity during the reference brake maneuver. Left: raw signal, right: first order low pass filtered with 20 Hz cutoff frequency

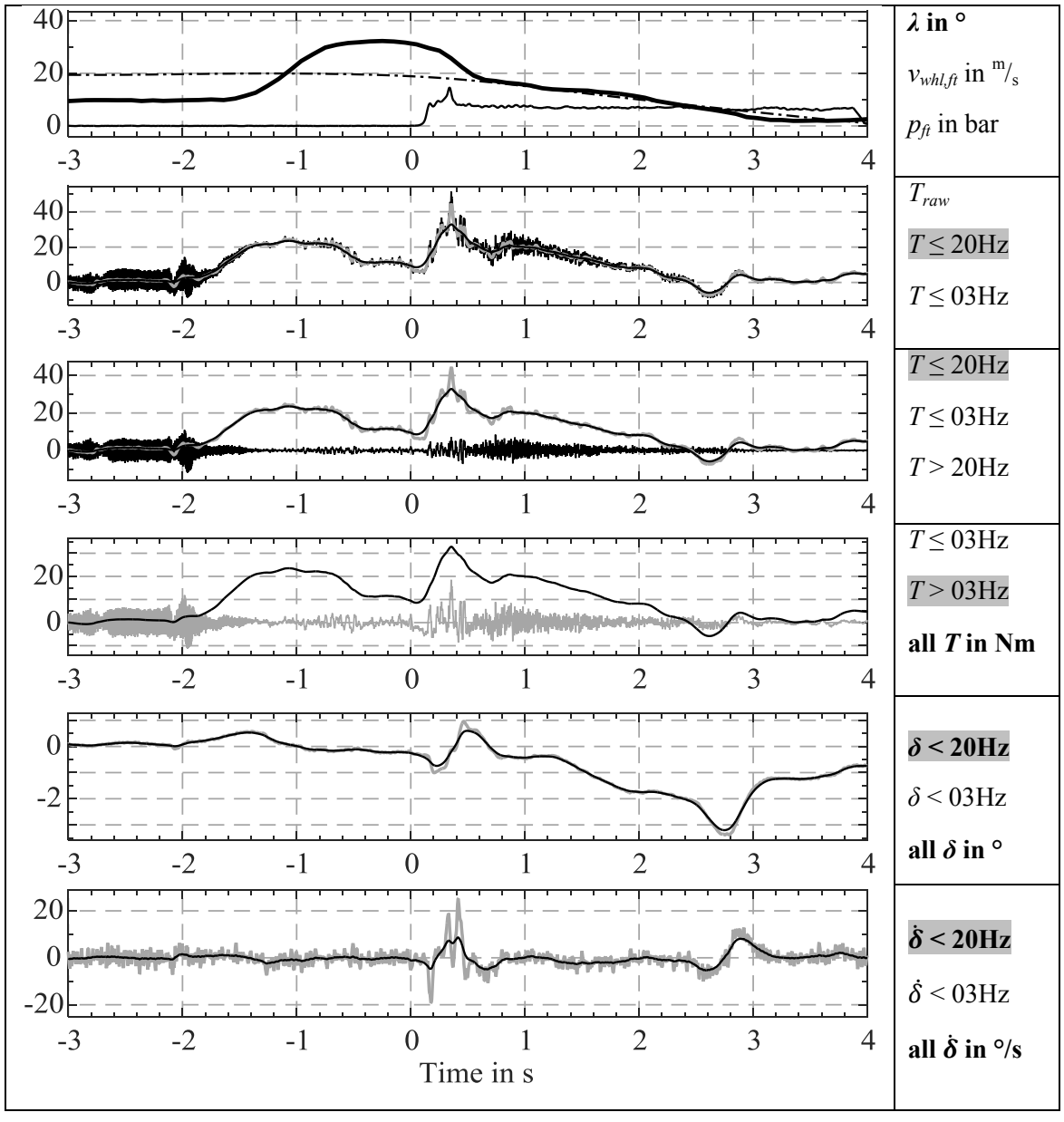

Figure A.10: Control case 1: Partial braking with dynamic over-braking and standard steering, $R = 50$ m, $a_x \approx 4.7$ m/s²

While the desired frequency content of up to 10 Hz is well covered, higher frequency noise and engine vibrations of first and second order (at about 27 Hz and 43-46 Hz, respectively) are efficiently filtered out, despite a tolerable small rest.

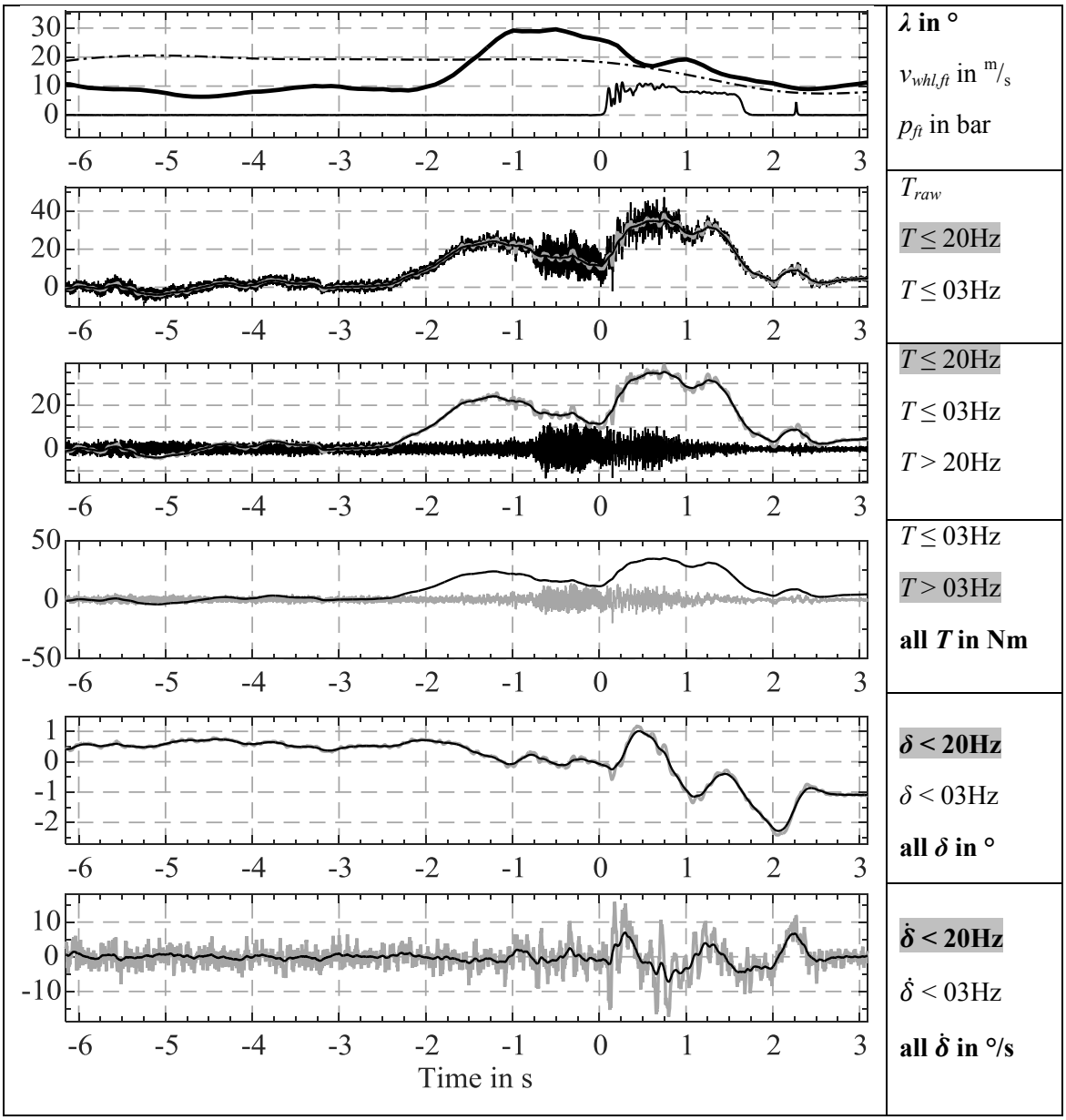

Figure A.11: Control case 2: Partial braking while stalling the engine with BSTAM in long trail passive centered position (BLpc), R = 50 m, $a_x \approx 5.0$ m/s²

The same signals as for the reference case in Figure A.8 are shown for two extreme control cases in Figure A.10 and Figure A.11. The partial braking experiment with dynamic over-braking of the front wheel in Figure A.10 shows a good correlation with the results of the 20 Hz filter in the layout case in terms of less than 10% difference to the steering torque peak value as well as good display of the steering system's eigenmode in the steering angle and angular velocity signals. However, for the special case of braking with clutch engaged, throttle jammed and thus stalling the engine pre-

sented in Figure A.11, engine vibration transfer generates disturbances in steering torque measurement greater than 22 Nm in peak-to-peak values. With less than 10 Nm the absolute difference between the raw and 20 Hz filtered signals at the essential first peak in steering torque after brake kick-in is even less than half the disturbance value. Even if not accounted for this fact, the absolute measured difference in peak-value is in the order of 20%. Otherwise, a similar performance as for the other two cases can be expected also for experiments with clutch engaged.

A.5 Appendix to Chapter 5

A.5.1 Results of Global Analysis in CDF-Plot Format

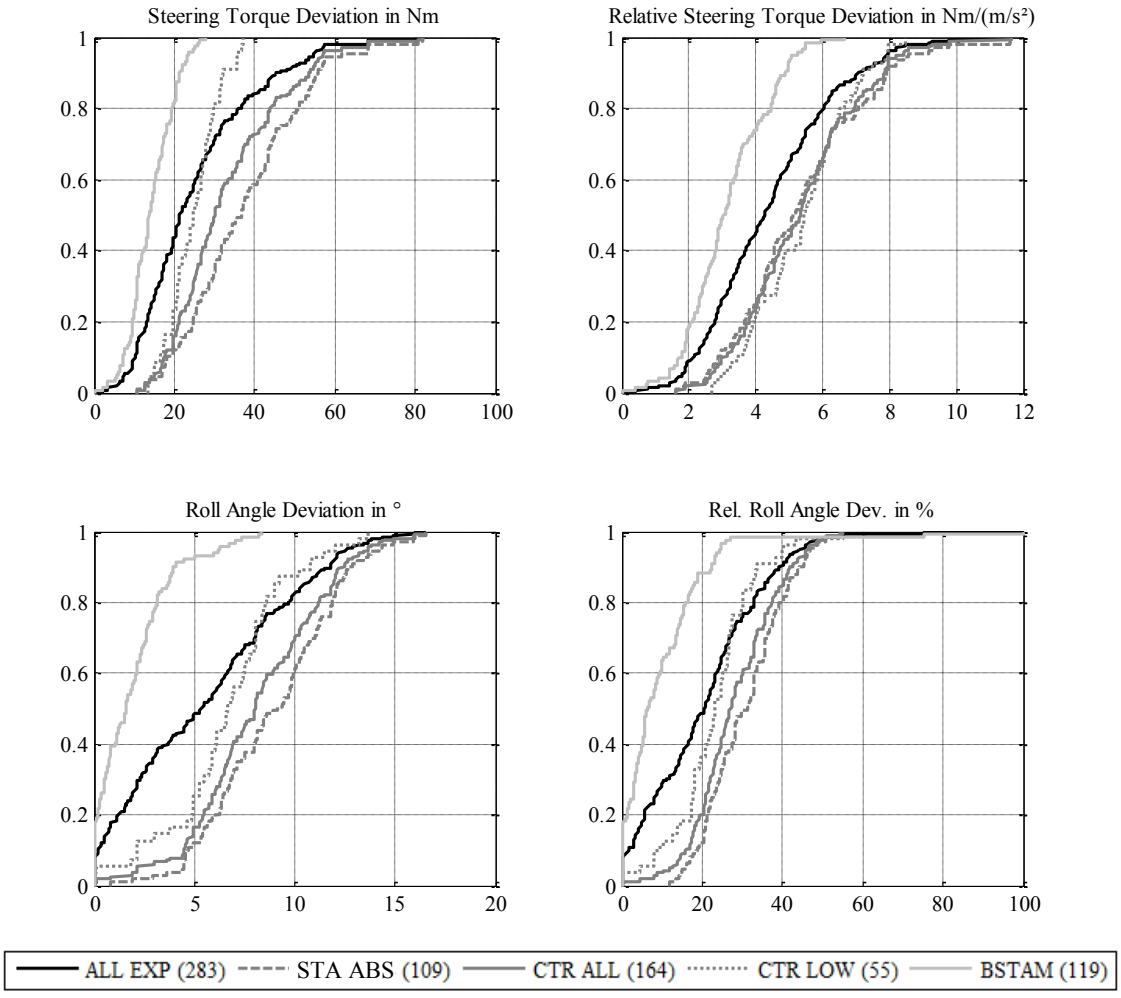

Figure A.12: Additional characteristic values of the global analysis in CDF-plot format, cf. Figure 5.6

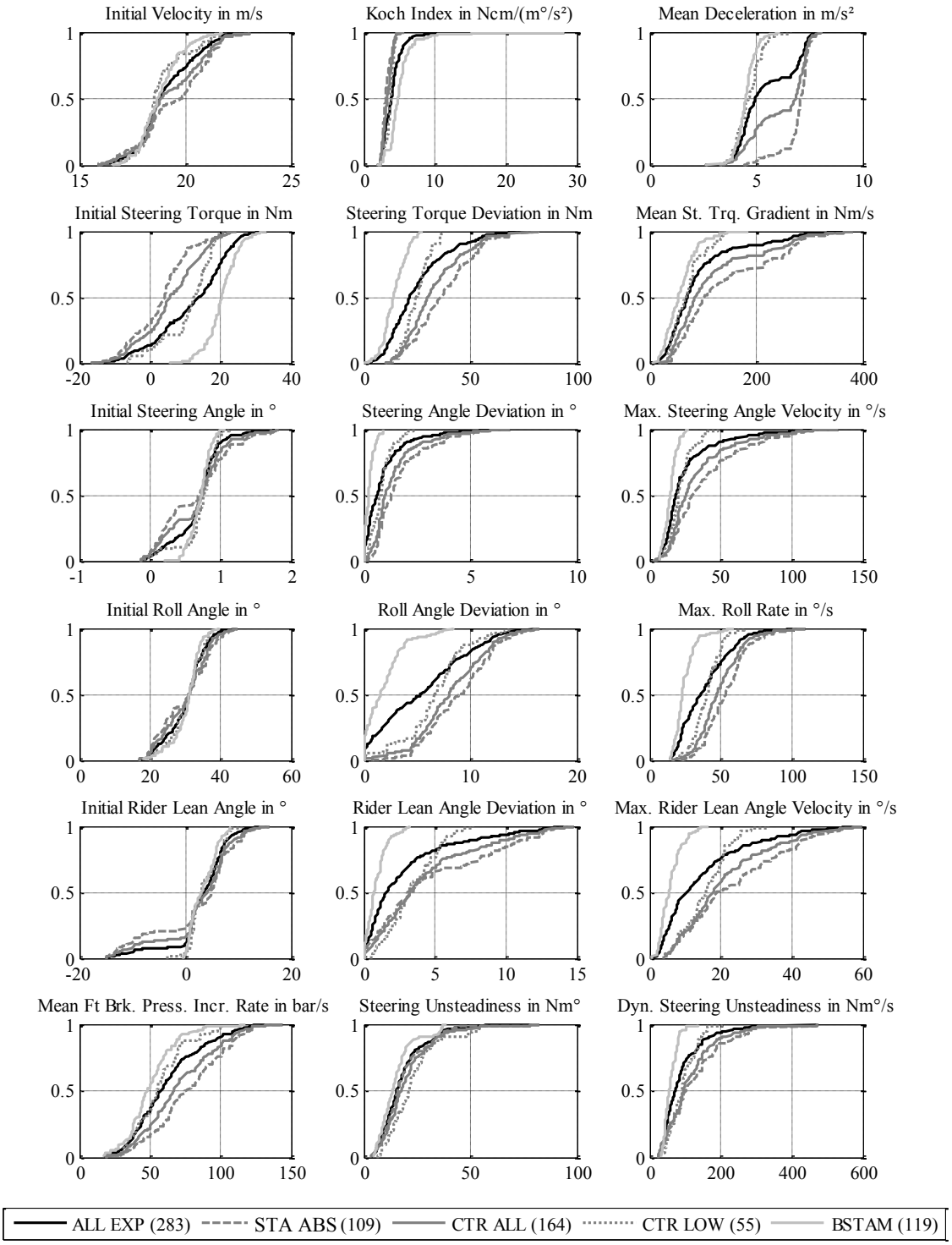

Figure A.13: Main characteristic values of global analysis in CDF-plot format, cf. Figure 5.6

The following three sections contain the full correlation tables of characteristic values for three experiment groups of the global analysis according to chapter 5.3.1:

- All experiments (ALL EXP)
- All experiments with centered steering axis (ALL CTR = STA + BPC)
- All experiments with BSTAM active ((ALL) BSTAM)

A.5.2 Correlation Tables for ALL Experiments

Note: High R-values are indicated darker, low p-values are lighter.

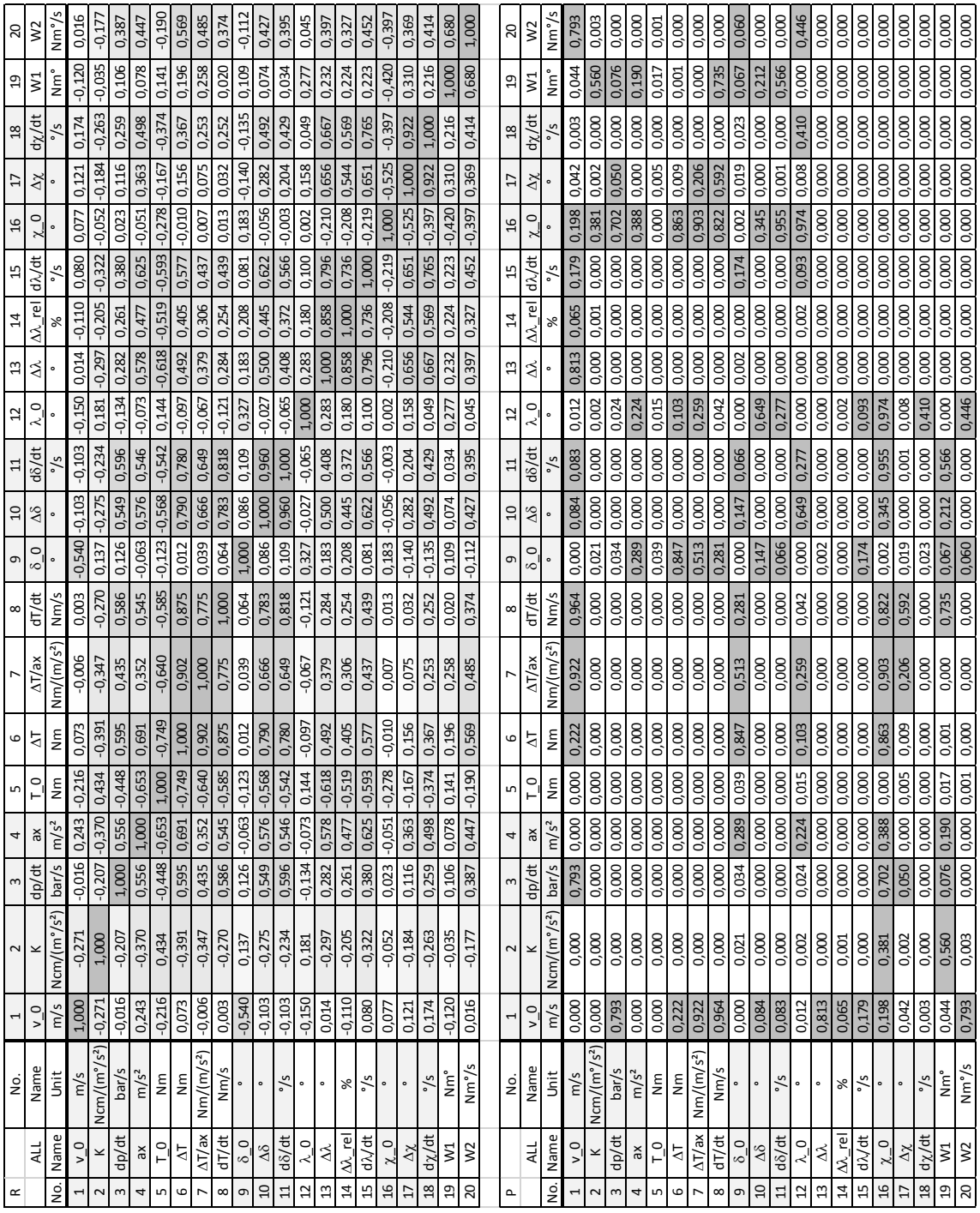

R		No.	1	2	3	4	5	6	7	8	9	10	11	12	13	14	15	16	17	18	19	20
	ALL	Name	v_0	K	dp/dt	ax	T_0	ΔT	ΔT/ax	dT/dt	δ_0	Δδ	dδ/dt	λ_0	Δλ	Δλ_rel	dλ/dt	χ_0	Δχ	dχ/dt	W1	W2
No.	Name	Unit	m/s	Ncm/(m°/s²)	bar/s	m/s²	Nm	Nm	Nm/(m/s²)	Nm/s	°	°	°/s	°	°	%	°/s	°	°	°/s	Nm°	Nm°/s
1	v_0	m/s	1,000	-0,271	-0,016	0,243	-0,216	0,073	-0,006	0,003	-0,540	-0,103	-0,103	-0,150	0,014	-0,110	0,080	0,077	0,121	0,174	-0,120	0,016
2	K	Ncm/(m°/s²)	-0,271	1,000	-0,207	-0,370	0,434	-0,391	-0,347	-0,270	0,137	-0,275	-0,234	0,181	-0,297	-0,205	-0,322	-0,052	-0,184	-0,263	-0,035	-0,177
3	dp/dt	bar/s	-0,016	-0,207	1,000	0,556	-0,448	0,595	0,435	0,586	0,126	0,549	0,596	-0,134	0,282	0,261	0,380	0,023	0,116	0,259	0,106	0,387
4	ax	m/s²	0,243	-0,370	0,556	1,000	-0,653	0,691	0,352	0,545	-0,063	0,576	0,546	-0,073	0,578	0,477	0,625	-0,051	0,363	0,498	0,078	0,447
5	T_0	Nm	-0,216	0,434	-0,448	-0,653	1,000	-0,749	-0,640	-0,585	-0,123	-0,568	-0,542	0,144	-0,618	-0,519	-0,593	-0,278	-0,167	-0,374	0,141	-0,190
6	ΔT	Nm	0,073	-0,391	0,595	0,691	-0,749	1,000	0,902	0,875	0,012	0,790	0,780	-0,097	0,492	0,405	0,577	-0,010	0,156	0,367	0,196	0,569
7	ΔT/ax	Nm/(m/s²)	-0,006	-0,347	0,435	0,352	-0,640	0,902	1,000	0,775	0,039	0,666	0,649	-0,067	0,379	0,306	0,437	0,007	0,075	0,253	0,258	0,485
8	dT/dt	Nm/s	0,003	-0,270	0,586	0,545	-0,585	0,875	0,775	1,000	0,064	0,783	0,818	-0,121	0,284	0,254	0,439	0,013	0,032	0,252	0,020	0,374
9	δ_0	°	-0,540	0,137	0,126	-0,063	-0,123	0,012	0,039	0,064	1,000	0,086	0,109	0,327	0,183	0,208	0,081	0,183	-0,140	-0,135	0,109	-0,112
10	Δδ	°	-0,103	-0,275	0,549	0,576	-0,568	0,790	0,666	0,783	0,086	1,000	0,960	-0,027	0,500	0,445	0,622	-0,056	0,282	0,492	0,074	0,427
11	dδ/dt	°/s	-0,103	-0,234	0,596	0,546	-0,542	0,780	0,649	0,818	0,109	0,960	1,000	-0,065	0,408	0,372	0,566	-0,003	0,204	0,429	0,034	0,395
12	λ_0	°	-0,150	0,181	-0,134	-0,073	0,144	-0,097	-0,067	-0,121	0,327	-0,027	-0,065	1,000	0,283	0,180	0,100	0,002	0,158	0,049	0,277	0,045
13	Δλ	°	0,014	-0,297	0,282	0,578	-0,618	0,492	0,379	0,284	0,183	0,500	0,408	0,283	1,000	0,858	0,796	-0,210	0,656	0,667	0,232	0,397
14	Δλ_rel	%	-0,110	-0,205	0,261	0,477	-0,519	0,405	0,306	0,254	0,208	0,445	0,372	0,180	0,858	1,000	0,736	-0,208	0,544	0,569	0,224	0,327
15	dλ/dt	°/s	0,080	-0,322	0,380	0,625	-0,593	0,577	0,437	0,439	0,081	0,622	0,566	0,100	0,796	0,736	1,000	-0,219	0,651	0,765	0,223	0,452
16	χ_0	°	0,077	-0,052	0,023	-0,051	-0,278	-0,010	0,007	0,013	0,183	-0,056	-0,003	0,002	-0,210	-0,208	-0,219	1,000	-0,525	-0,397	-0,420	-0,397
17	Δχ	°	0,121	-0,184	0,116	0,363	-0,167	0,156	0,075	0,032	-0,140	0,282	0,204	0,158	0,656	0,544	0,651	-0,525	1,000	0,922	0,310	0,369
18	dχ/dt	°/s	0,174	-0,263	0,259	0,498	-0,374	0,367	0,253	0,252	-0,135	0,492	0,429	0,049	0,667	0,569	0,765	-0,397	0,922	1,000	0,216	0,414
19	W1	Nm°	-0,120	-0,035	0,106	0,078	0,141	0,196	0,258	0,020	0,109	0,074	0,034	0,277	0,232	0,224	0,223	-0,420	0,310	0,216	1,000	0,680
20	W2	Nm°/s	0,016	-0,177	0,387	0,447	-0,190	0,569	0,485	0,374	-0,112	0,427	0,395	0,045	0,397	0,327	0,452	-0,397	0,369	0,414	0,680	1,000

P		No.	1	2	3	4	5	6	7	8	9	10	11	12	13	14	15	16	17	18	19	20
	ALL	Name	v_0	K	dp/dt	ax	T_0	ΔT	ΔT/ax	dT/dt	δ_0	Δδ	dδ/dt	λ_0	Δλ	Δλ_rel	dλ/dt	χ_0	Δχ	dχ/dt	W1	W2
No.	Name	Unit	m/s	Ncm/(m°/s²)	bar/s	m/s²	Nm	Nm	Nm/(m/s²)	Nm/s	°	°	°/s	°	°	%	°/s	°	°	°/s	Nm°	Nm°/s
1	v_0	m/s	0,000	0,000	0,793	0,000	0,000	0,222	0,922	0,964	0,000	0,084	0,083	0,012	0,813	0,065	0,179	0,198	0,042	0,003	0,044	0,793
2	K	Ncm/(m°/s²)	0,000	0,000	0,000	0,000	0,000	0,000	0,000	0,000	0,021	0,000	0,000	0,002	0,000	0,001	0,000	0,381	0,002	0,000	0,560	0,003
3	dp/dt	bar/s	0,793	0,000	0,000	0,000	0,000	0,000	0,000	0,000	0,034	0,000	0,000	0,024	0,000	0,000	0,000	0,702	0,050	0,000	0,076	0,000
4	ax	m/s²	0,000	0,000	0,000	0,000	0,000	0,000	0,000	0,000	0,289	0,000	0,000	0,224	0,000	0,000	0,000	0,388	0,000	0,000	0,190	0,000
5	T_0	Nm	0,000	0,000	0,000	0,000	0,000	0,000	0,000	0,000	0,039	0,000	0,000	0,015	0,000	0,000	0,000	0,000	0,005	0,000	0,017	0,001
6	ΔT	Nm	0,222	0,000	0,000	0,000	0,000	0,000	0,000	0,000	0,847	0,000	0,000	0,103	0,000	0,000	0,000	0,863	0,009	0,000	0,001	0,000
7	ΔT/ax	Nm/(m/s²)	0,922	0,000	0,000	0,000	0,000	0,000	0,000	0,000	0,513	0,000	0,000	0,259	0,000	0,000	0,000	0,903	0,206	0,000	0,000	0,000
8	dT/dt	Nm/s	0,964	0,000	0,000	0,000	0,000	0,000	0,000	0,000	0,281	0,000	0,000	0,042	0,000	0,000	0,000	0,822	0,592	0,000	0,735	0,000
9	δ_0	°	0,000	0,021	0,034	0,289	0,039	0,847	0,513	0,281	0,000	0,147	0,066	0,000	0,002	0,000	0,174	0,002	0,019	0,023	0,067	0,060
10	Δδ	°	0,084	0,000	0,000	0,000	0,000	0,000	0,000	0,000	0,147	0,000	0,000	0,649	0,000	0,000	0,000	0,345	0,000	0,000	0,212	0,000
11	dδ/dt	°/s	0,083	0,000	0,000	0,000	0,000	0,000	0,000	0,000	0,066	0,000	0,000	0,277	0,000	0,000	0,000	0,955	0,001	0,000	0,566	0,000
12	λ_0	°	0,012	0,002	0,024	0,224	0,015	0,103	0,259	0,042	0,000	0,649	0,277	0,000	0,000	0,002	0,093	0,974	0,008	0,410	0,000	0,446
13	Δλ	°	0,813	0,000	0,000	0,000	0,000	0,000	0,000	0,000	0,002	0,000	0,000	0,000	0,000	0,000	0,000	0,000	0,000	0,000	0,000	0,000
14	Δλ_rel	%	0,065	0,001	0,000	0,000	0,000	0,000	0,000	0,000	0,000	0,000	0,000	0,002	0,000	0,000	0,000	0,000	0,000	0,000	0,000	0,000
15	dλ/dt	°/s	0,179	0,000	0,000	0,000	0,000	0,000	0,000	0,000	0,174	0,000	0,000	0,093	0,000	0,000	0,000	0,000	0,000	0,000	0,000	0,000
16	χ_0	°	0,198	0,381	0,702	0,388	0,000	0,863	0,903	0,822	0,002	0,345	0,955	0,974	0,000	0,000	0,000	0,000	0,000	0,000	0,000	0,000
17	Δχ	°	0,042	0,002	0,050	0,000	0,005	0,009	0,206	0,592	0,019	0,000	0,001	0,008	0,000	0,000	0,000	0,000	0,000	0,000	0,000	0,000
18	dχ/dt	°/s	0,003	0,000	0,000	0,000	0,000	0,000	0,000	0,000	0,023	0,000	0,000	0,410	0,000	0,000	0,000	0,000	0,000	0,000	0,000	0,000
19	W1	Nm°	0,044	0,560	0,076	0,190	0,017	0,001	0,000	0,735	0,067	0,212	0,566	0,000	0,000	0,000	0,000	0,000	0,000	0,000	0,000	0,000
20	W2	Nm°/s	0,793	0,003	0,000	0,000	0,001	0,000	0,000	0,000	0,060	0,000	0,000	0,446	0,000	0,000	0,000	0,000	0,000	0,000	0,000	0,000

The nomenclature is as follows:

- R = correlation coefficient
- p = probability value (check for $p < 0.05$)
- g_1 and g_2 → slope and axis intercept parameters of the regression lines

Refer to the relevant (dark) correlations, to spot out values of interest.

G1		No.	1	2	3	4	5	6	7	8	9	10	11	12	13	14	15	16	17	18	19	20
	ALL	Name	v_0	K	dp/dt	ax	T_0	ΔT	ΔT/ax	dT/dt	δ_0	Δδ	dδ/dt	λ_0	Δλ	Δλ_rel	dλ/dt	χ_0	Δχ	dχ/dt	W1	W2
No.	Name	Unit	m/s	Ncm/(m°/s²)	bar/s	m/s²	Nm	Nm	Nm/(m/s²)	Nm/s	°	°	°/s	°	°	%	°/s	°	°	°/s	Nm°	Nm°/s
1	v_0	m/s	1,000	-0,404	-0,285	0,231	-1,598	0,775	-0,008	0,139	-0,131	-0,079	-1,513	-0,596	0,043	-1,172	1,041	0,290	0,284	1,571	-0,986	0,772
2	K	Ncm/(m°/s²)	-0,182	1,000	-2,518	-0,236	2,153	-2,789	-0,329	-9,387	0,022	-0,142	-2,304	0,484	-0,607	-1,467	-2,812	-0,132	-0,289	-1,595	-0,192	-5,854
3	dp/dt	bar/s	-0,001	-0,017	1,000	0,029	-0,182	0,348	0,034	1,668	0,002	0,023	0,481	-0,029	0,047	0,153	0,272	0,005	0,015	0,129	0,048	1,047
4	ax	m/s²	0,256	-0,580	10,624	1,000	-5,072	7,732	0,523	29,706	-0,016	0,464	8,414	-0,304	1,852	5,363	8,544	-0,204	0,896	4,731	0,676	23,121
5	T_0	Nm	-0,029	0,088	-1,101	-0,084	1,000	-1,078	-0,123	-4,125	-0,004	-0,059	-1,076	0,078	-0,255	-0,750	-1,045	-0,142	-0,053	-0,457	0,157	-1,263
6	ΔT	Nm	0,007	-0,055	1,017	0,062	-0,520	1,000	0,120	4,272	0,000	0,057	1,075	-0,036	0,141	0,407	0,706	-0,004	0,034	0,312	0,151	2,631
7	ΔT/ax	Nm/(m/s²)	-0,004	-0,365	5,584	0,237	-3,346	6,782	1,000	28,590	0,007	0,361	6,730	-0,190	0,817	2,316	4,018	0,019	0,125	1,614	1,500	16,881
8	dT/dt	Nm/s	0,000	-0,008	0,206	0,010	-0,083	0,179	0,021	1,000	0,000	0,012	0,232	-0,009	0,017	0,052	0,110	0,001	0,001	0,044	0,003	0,356
9	δ_0	°	-2,232	0,844	9,452	-0,248	-3,745	0,507	0,228	13,745	1,000	0,274	6,628	5,373	2,308	9,179	4,351	2,859	-1,354	-5,025	3,703	-22,787
10	Δδ	°	-0,134	-0,534	13,003	0,713	-5,470	10,950	1,227	52,751	0,027	1,000	18,333	-0,141	1,988	6,195	10,552	-0,277	0,863	5,792	0,797	27,373
11	dδ/dt	°/s	-0,007	-0,024	0,739	0,035	-0,273	0,566	0,063	2,886	0,002	0,050	1,000	-0,018	0,085	0,271	0,503	-0,001	0,033	0,264	0,019	1,325
12	λ_0	°	-0,038	0,068	-0,610	-0,017	0,267	-0,259	-0,024	-1,571	0,020	-0,005	-0,238	1,000	0,217	0,482	0,327	0,002	0,093	0,112	0,571	0,561
13	Δλ	°	0,005	-0,145	1,681	0,180	-1,498	1,717	0,176	4,813	0,015	0,126	1,961	0,370	1,000	3,007	3,398	-0,260	0,504	1,974	0,625	6,408
14	Δλ_rel	%	-0,010	-0,029	0,443	0,042	-0,359	0,403	0,041	1,226	0,005	0,032	0,510	0,067	0,245	1,000	0,897	-0,074	0,119	0,481	0,172	1,504
15	dλ/dt	°/s	0,006	-0,037	0,530	0,046	-0,337	0,472	0,047	1,744	0,002	0,037	0,638	0,031	0,187	0,605	1,000	-0,063	0,117	0,531	0,141	1,708
16	χ_0	°	0,020	-0,021	0,110	-0,013	-0,544	-0,029	0,003	0,185	0,012	-0,011	-0,013	0,002	-0,169	-0,589	-0,754	1,000	-0,326	-0,948	-0,916	-5,168
17	Δχ	°	0,052	-0,117	0,902	0,147	-0,526	0,706	0,045	0,705	-0,014	0,092	1,274	0,268	0,852	2,479	3,611	-0,845	1,000	3,548	1,088	7,752
18	dχ/dt	°/s	0,019	-0,043	0,521	0,053	-0,306	0,433	0,040	1,444	-0,004	0,042	0,696	0,022	0,225	0,673	1,102	-0,166	0,239	1,000	0,197	2,259
19	W1	Nm°	-0,015	-0,006	0,233	0,009	0,127	0,253	0,044	0,127	0,003	0,007	0,061	0,134	0,086	0,290	0,353	-0,193	0,088	0,237	1,000	4,070
20	W2	Nm°/s	0,000	-0,005	0,143	0,009	-0,028	0,123	0,014	0,393	-0,001	0,007	0,118	0,004	0,025	0,071	0,119	-0,030	0,018	0,076	0,114	1,000

G2		No.	1	2	3	4	5	6	7	8	9	10	11	12	13	14	15	16	17	18	19	20
	ALL	Name	v_0	K	dp/dt	ax	T_0	ΔT	ΔT/ax	dT/dt	δ_0	Δδ	dδ/dt	λ_0	Δλ	Δλ_rel	dλ/dt	χ_0	Δχ	dχ/dt	W1	W2
No.	Name	Unit	m/s	Ncm/(m°/s²)	bar/s	m/s²	Nm	Nm	Nm/(m/s²)	Nm/s	°	°	°/s	°	°	%	°/s	°	°	°/s	Nm°	Nm°/s
1	v_0	m/s	0,000	11,841	67,493	1,067	42,520	10,440	4,599	89,325	3,183	2,420	54,071	41,701	4,724	42,931	19,205	-2,462	-2,560	-15,364	36,933	76,736
2	K	Ncm/(m°/s²)	19,847	0,000	72,437	6,457	3,131	36,731	5,798	130,645	0,594	1,497	34,681	28,332	8,050	26,602	50,675	3,619	4,051	21,204	18,896	115,616
3	dp/dt	bar/s	19,149	5,174	0,000	3,677	23,302	3,613	2,341	-11,587	0,582	-0,526	-4,665	32,148	2,608	11,040	22,207	2,779	1,927	6,652	15,138	26,492
4	ax	m/s²	17,693	7,303	3,804	0,000	39,818	-17,162	1,573	-71,071	0,774	-1,633	-20,949	31,993	-4,609	-8,851	-7,764	4,194	-2,053	-11,313	14,397	-35,292
5	T_0	Nm	19,447	3,072	75,270	6,492	0,000	38,177	5,912	141,214	0,734	1,622	38,102	29,394	8,608	29,562	51,632	4,779	3,496	20,110	16,217	106,647
6	ΔT	Nm	18,923	5,504	36,405	3,923	25,134	0,000	1,416	-16,191	0,679	-0,525	-1,950	31,245	1,987	10,290	21,277	3,166	1,994	6,766	14,290	25,100
7	ΔT/ax	Nm/(m/s²)	19,114	5,746	37,259	4,433	26,867	-4,884	0,000	-35,408	0,656	-0,691	-4,700	31,169	1,918	10,270	21,240	2,987	2,304	7,459	11,446	16,521
8	dT/dt	Nm/s	19,095	4,835	43,150	4,569	19,573	8,843	2,523	0,000	0,657	-0,151	3,902	31,175	4,014	15,753	28,960	2,985	2,731	10,612	17,811	58,904
9	δ_0	°	20,626	3,545	55,572	5,653	14,576	24,883	4,284	82,571	0,000	0,726	20,637	26,643	3,963	14,258	36,099	1,113	3,788	18,073	15,566	107,102
10	Δδ	°	19,218	4,611	50,176	4,831	17,006	15,229	3,320	43,638	0,661	0,000	8,436	30,456	3,729	14,893	29,443	3,327	2,071	9,337	17,377	66,474
11	dδ/dt	°/s	19,273	4,723	43,435	4,591	18,895	10,966	2,862	19,164	0,640	-0,353	0,000	30,771	3,408	13,721	26,421	3,095	2,038	7,978	17,621	58,112
12	λ_0	°	20,235	2,070	80,565	6,008	3,897	33,094	5,165	139,629	0,084	1,072	32,413	0,000	-1,031	5,948	29,179	3,017	0,043	11,245	0,792	74,455
13	Δλ	°	19,070	4,928	52,730	4,484	20,317	15,712	3,466	65,257	0,605	0,215	14,308	28,275	0,000	3,876	20,242	4,512	0,062	3,681	14,640	55,946
14	Δλ_rel	%	19,307	4,709	52,944	4,610	19,382	16,948	3,607	66,753	0,589	0,257	14,694	28,952	0,514	0,000	20,656	4,584	0,405	4,750	14,570	60,562
15	dλ/dt	°/s	18,855	5,564	41,327	3,699	25,179	6,799	2,585	23,747	0,627	-0,521	0,253	29,131	-1,745	-3,080	0,000	5,554	-1,726	-6,112	12,601	24,706
16	χ_0	°	19,033	4,187	61,715	5,523	13,681	25,320	4,432	91,419	0,650	0,949	25,222	30,321	6,065	22,362	41,399	0,000	3,861	17,542	20,920	107,362
17	Δχ	°	18,948	4,457	59,474	5,062	13,513	23,213	4,310	89,966	0,727	0,649	21,539	29,561	3,108	13,465	28,758	5,489	0,000	4,483	14,994	69,310
18	dχ/dt	°/s	18,814	4,759	54,437	4,715	16,482	18,904	3,861	70,820	0,739	0,301	15,004	30,010	2,252	10,703	22,959	5,500	-0,643	0,000	15,227	58,441
19	W1	Nm°	19,360	4,237	57,827	5,319	9,710	20,651	3,637	89,684	0,628	0,788	24,075	27,902	3,990	15,294	32,699	6,568	1,257	10,334	0,000	17,792
20	W2	Nm°/s	19,067	4,614	48,993	4,693	14,614	13,988	3,165	56,002	0,736	0,304	14,432	29,991	3,295	14,064	28,157	5,856	1,249	7,675	7,709	0,000

Refer to chapter 5.3.1 for a detailed explanation on the correlation analysis and chapter 5.2 for a definition of the characteristic values that are correlated in the tables.

A.5.3 Correlation Tables for Exp. with Centered Steering Axis

Note: High R-values are indicated darker, low p-values are lighter.

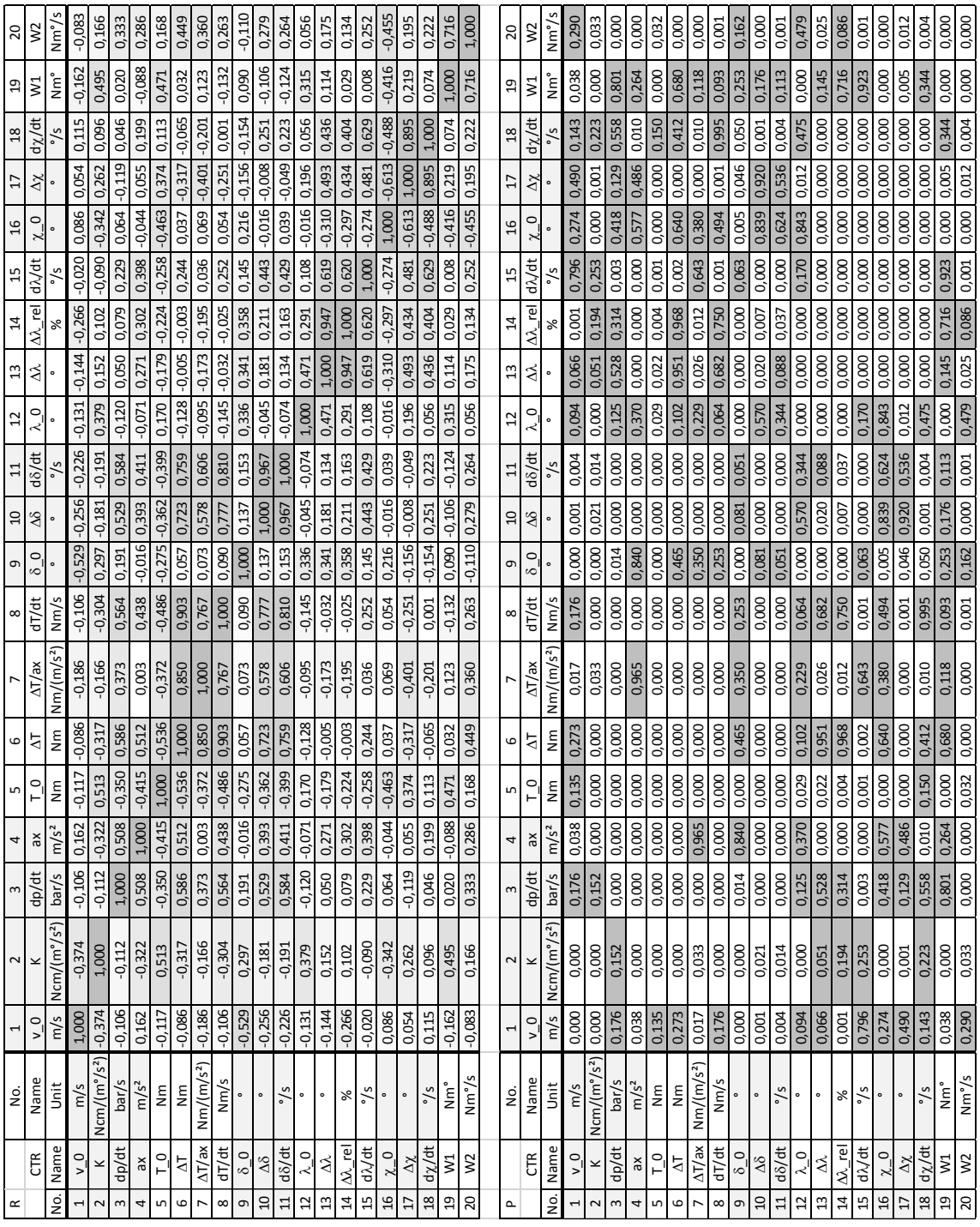

R		No.	1	2	3	4	5	6	7	8	9	10	11	12	13	14	15	16	17	18	19	20
	CTR	Name	v_0	K	dp/dt	ax	T_0	ΔT	ΔT/ax	dT/dt	δ_0	Δδ	dδ/dt	λ_0	Δλ	Δλ_rel	dλ/dt	χ_0	Δχ	dχ/dt	W1	W2
No.	Name	Unit	m/s	Ncm/(m°/s²)	bar/s	m/s²	Nm	Nm	Nm/(m/s²)	Nm/s	°	°	°/s	°	°	%	°/s	°	°	°/s	Nm°	Nm°/s
1	v_0	m/s	1,000	-0,374	-0,106	0,162	-0,117	-0,086	-0,186	-0,106	-0,529	-0,256	-0,226	-0,131	-0,144	-0,266	-0,020	0,086	0,054	0,115	-0,162	-0,083
2	K	Ncm/(m°/s²)	-0,374	1,000	-0,112	-0,322	0,513	-0,317	-0,166	-0,304	0,297	-0,181	-0,191	0,379	0,152	0,102	-0,090	-0,342	0,262	0,096	0,495	0,166
3	dp/dt	bar/s	-0,106	-0,112	1,000	0,508	-0,350	0,586	0,373	0,564	0,191	0,529	0,584	-0,120	0,050	0,079	0,229	0,064	-0,119	0,046	0,020	0,333
4	ax	m/s²	0,162	-0,322	0,508	1,000	-0,415	0,512	0,003	0,438	-0,016	0,393	0,411	-0,071	0,271	0,302	0,398	-0,044	0,055	0,199	-0,088	0,286
5	T_0	Nm	-0,117	0,513	-0,350	-0,415	1,000	-0,536	-0,372	-0,486	-0,275	-0,362	-0,399	0,170	-0,179	-0,224	-0,258	-0,463	0,374	0,113	0,471	0,168
6	ΔT	Nm	-0,086	-0,317	0,586	0,512	-0,536	1,000	0,850	0,903	0,057	0,723	0,759	-0,128	-0,005	-0,003	0,244	0,037	-0,317	-0,065	0,032	0,449
7	ΔT/ax	Nm/(m/s²)	-0,186	-0,166	0,373	0,003	-0,372	0,850	1,000	0,767	0,073	0,578	0,606	-0,095	-0,173	-0,195	0,036	0,069	-0,401	-0,201	0,123	0,360
8	dT/dt	Nm/s	-0,106	-0,304	0,564	0,438	-0,486	0,903	0,767	1,000	0,090	0,777	0,810	-0,145	-0,032	-0,025	0,252	0,054	-0,251	0,001	-0,132	0,263
9	δ_0	°	-0,529	0,297	0,191	-0,016	-0,275	0,057	0,073	0,090	1,000	0,137	0,153	0,336	0,341	0,358	0,145	0,216	-0,156	-0,154	0,090	-0,110
10	Δδ	°	-0,256	-0,181	0,529	0,393	-0,362	0,723	0,578	0,777	0,137	1,000	0,967	-0,045	0,181	0,211	0,443	-0,016	-0,008	0,251	-0,106	0,279
11	dδ/dt	°/s	-0,226	-0,191	0,584	0,411	-0,399	0,759	0,606	0,810	0,153	0,967	1,000	-0,074	0,134	0,163	0,429	0,039	-0,049	0,223	-0,124	0,264
12	λ_0	°	-0,131	0,379	-0,120	-0,071	0,170	-0,128	-0,095	-0,145	0,336	-0,045	-0,074	1,000	0,471	0,291	0,108	-0,016	0,196	0,056	0,315	0,056
13	Δλ	°	-0,144	0,152	0,050	0,271	-0,179	-0,005	-0,173	-0,032	0,341	0,181	0,134	0,471	1,000	0,947	0,619	-0,310	0,493	0,436	0,114	0,175
14	Δλ_rel	%	-0,266	0,102	0,079	0,302	-0,224	-0,003	-0,195	-0,025	0,358	0,211	0,163	0,291	0,947	1,000	0,620	-0,297	0,434	0,404	0,029	0,134
15	dλ/dt	°/s	-0,020	-0,090	0,229	0,398	-0,258	0,244	0,036	0,252	0,145	0,443	0,429	0,108	0,619	0,620	1,000	-0,274	0,481	0,629	0,008	0,252
16	χ_0	°	0,086	-0,342	0,064	-0,044	-0,463	0,037	0,069	0,054	0,216	-0,016	0,039	-0,016	-0,310	-0,297	-0,274	1,000	-0,613	-0,488	-0,416	-0,455
17	Δχ	°	0,054	0,262	-0,119	0,055	0,374	-0,317	-0,401	-0,251	-0,156	-0,008	-0,049	0,196	0,493	0,434	0,481	-0,613	1,000	0,895	0,219	0,195
18	dχ/dt	°/s	0,115	0,096	0,046	0,199	0,113	-0,065	-0,201	0,001	-0,154	0,251	0,223	0,056	0,436	0,404	0,629	-0,488	0,895	1,000	0,074	0,222
19	W1	Nm°	-0,162	0,495	0,020	-0,088	0,471	0,032	0,123	-0,132	0,090	-0,106	-0,124	0,315	0,114	0,029	0,008	-0,416	0,219	0,074	1,000	0,716
20	W2	Nm°/s	-0,083	0,166	0,333	0,286	0,168	0,449	0,360	0,263	-0,110	0,279	0,264	0,056	0,175	0,134	0,252	-0,455	0,195	0,222	0,716	1,000

P		No.	1	2	3	4	5	6	7	8	9	10	11	12	13	14	15	16	17	18	19	20
	CTR	Name	v_0	K	dp/dt	ax	T_0	ΔT	ΔT/ax	dT/dt	δ_0	Δδ	dδ/dt	λ_0	Δλ	Δλ_rel	dλ/dt	χ_0	Δχ	dχ/dt	W1	W2
No.	Name	Unit	m/s	Ncm/(m°/s²)	bar/s	m/s²	Nm	Nm	Nm/(m/s²)	Nm/s	°	°	°/s	°	°	%	°/s	°	°	°/s	Nm°	Nm°/s
1	v_0	m/s	0,000	0,000	0,176	0,038	0,135	0,273	0,017	0,176	0,000	0,001	0,004	0,094	0,066	0,001	0,796	0,274	0,490	0,143	0,038	0,290
2	K	Ncm/(m°/s²)	0,000	0,000	0,152	0,000	0,000	0,000	0,033	0,000	0,000	0,021	0,014	0,000	0,051	0,194	0,253	0,000	0,001	0,223	0,000	0,033
3	dp/dt	bar/s	0,176	0,152	0,000	0,000	0,000	0,000	0,000	0,000	0,014	0,000	0,000	0,125	0,528	0,314	0,003	0,418	0,129	0,558	0,801	0,000
4	ax	m/s²	0,038	0,000	0,000	0,000	0,000	0,000	0,965	0,000	0,840	0,000	0,000	0,370	0,000	0,000	0,000	0,577	0,486	0,010	0,264	0,000
5	T_0	Nm	0,135	0,000	0,000	0,000	0,000	0,000	0,000	0,000	0,000	0,000	0,000	0,029	0,022	0,004	0,001	0,000	0,000	0,150	0,000	0,032
6	ΔT	Nm	0,273	0,000	0,000	0,000	0,000	0,000	0,000	0,000	0,465	0,000	0,000	0,102	0,951	0,968	0,002	0,640	0,000	0,412	0,680	0,000
7	ΔT/ax	Nm/(m/s²)	0,017	0,033	0,000	0,965	0,000	0,000	0,000	0,000	0,350	0,000	0,000	0,229	0,026	0,012	0,643	0,380	0,000	0,010	0,118	0,000
8	dT/dt	Nm/s	0,176	0,000	0,000	0,000	0,000	0,000	0,000	0,000	0,253	0,000	0,000	0,064	0,682	0,750	0,001	0,494	0,001	0,995	0,093	0,001
9	δ_0	°	0,000	0,000	0,014	0,840	0,000	0,465	0,350	0,253	0,000	0,081	0,051	0,000	0,000	0,000	0,063	0,005	0,046	0,050	0,253	0,162
10	Δδ	°	0,001	0,021	0,000	0,000	0,000	0,000	0,000	0,000	0,081	0,000	0,000	0,570	0,020	0,007	0,000	0,839	0,920	0,001	0,176	0,000
11	dδ/dt	°/s	0,004	0,014	0,000	0,000	0,000	0,000	0,000	0,000	0,051	0,000	0,000	0,344	0,088	0,037	0,000	0,624	0,536	0,004	0,113	0,001
12	λ_0	°	0,094	0,000	0,125	0,370	0,029	0,102	0,229	0,064	0,000	0,570	0,344	0,000	0,000	0,000	0,170	0,843	0,012	0,475	0,000	0,479
13	Δλ	°	0,066	0,051	0,528	0,000	0,022	0,951	0,026	0,682	0,000	0,020	0,088	0,000	0,000	0,000	0,000	0,000	0,000	0,000	0,145	0,025
14	Δλ_rel	%	0,001	0,194	0,314	0,000	0,004	0,968	0,012	0,750	0,000	0,007	0,037	0,000	0,000	0,000	0,000	0,000	0,000	0,000	0,716	0,086
15	dλ/dt	°/s	0,796	0,253	0,003	0,000	0,001	0,002	0,643	0,001	0,063	0,000	0,000	0,170	0,000	0,000	0,000	0,000	0,000	0,000	0,923	0,001
16	χ_0	°	0,274	0,000	0,418	0,577	0,000	0,640	0,380	0,494	0,005	0,839	0,624	0,843	0,000	0,000	0,000	0,000	0,000	0,000	0,000	0,000
17	Δχ	°	0,490	0,001	0,129	0,486	0,000	0,000	0,000	0,001	0,046	0,920	0,536	0,012	0,000	0,000	0,000	0,000	0,000	0,000	0,005	0,012
18	dχ/dt	°/s	0,143	0,223	0,558	0,010	0,150	0,412	0,010	0,995	0,050	0,001	0,004	0,475	0,000	0,000	0,000	0,000	0,000	0,000	0,344	0,004
19	W1	Nm°	0,038	0,000	0,801	0,264	0,000	0,680	0,118	0,093	0,253	0,176	0,113	0,000	0,145	0,716	0,923	0,000	0,005	0,344	0,000	0,000
20	W2	Nm°/s	0,290	0,033	0,000	0,000	0,032	0,000	0,000	0,001	0,162	0,000	0,001	0,479	0,025	0,086	0,001	0,000	0,012	0,004	0,000	0,000

The nomenclature is as follows:

- R = correlation coefficient
- p = probability value (check for $p < 0.05$)
- g_1 and g_2 → slope and axis intercept parameters of the regression lines

Refer to the relevant (dark) correlations, to spot out values of interest.

G1		No.	1	2	3	4	5	6	7	8	9	10	11	12	13	14	15	16	17	18	19	20
	CTR	Name	v_0	K	dp/dt	ax	T_0	ΔT	ΔT/ax	dT/dt	δ_0	Δδ	dδ/dt	λ_0	Δλ	Δλ_rel	dλ/dt	χ_0	Δχ	dχ/dt	W1	W2
No.	Name	Unit	m/s	Ncm/(m°/s²)	bar/s	m/s²	Nm	Nm	Nm/(m/s²)	Nm/s	°	°	°/s	°	°	%	°/s	°	°	°/s	Nm°	Nm°/s
1	v_0	m/s	1,000	-0,161	-1,779	0,132	-0,648	-0,770	-0,218	-5,552	-0,142	-0,191	-3,382	-0,528	-0,308	-1,813	-0,205	0,357	0,124	0,939	-1,312	-4,227
2	K	Ncm/(m°/s²)	-0,870	1,000	-4,376	-0,609	6,589	-6,588	-0,454	-36,951	0,186	-0,313	-6,642	3,551	0,759	1,615	-2,106	-3,306	1,394	1,817	9,312	19,677
3	dp/dt	bar/s	-0,006	-0,003	1,000	0,025	-0,115	0,313	0,026	1,758	0,003	0,024	0,520	-0,029	0,006	0,032	0,138	0,016	-0,016	0,022	0,010	1,012
4	ax	m/s²	0,200	-0,170	10,459	1,000	-2,821	5,622	0,005	28,134	-0,005	0,360	7,549	-0,349	0,713	2,524	4,937	-0,224	0,154	2,002	-0,872	17,896
5	T_0	Nm	-0,021	0,040	-1,060	-0,061	1,000	-0,866	-0,079	-4,590	-0,013	-0,049	-1,080	0,124	-0,069	-0,276	-0,470	-0,348	0,155	0,167	0,689	1,543
6	ΔT	Nm	-0,010	-0,015	1,098	0,047	-0,331	1,000	0,112	5,277	0,002	0,060	1,268	-0,058	-0,001	-0,002	0,275	0,017	-0,081	-0,059	0,029	2,556
7	ΔT/ax	Nm/(m/s²)	-0,158	-0,061	5,322	0,002	-1,750	6,475	1,000	34,135	0,017	0,367	7,708	-0,325	-0,316	-1,133	0,313	0,244	-0,780	-1,397	0,845	15,611
8	dT/dt	Nm/s	-0,002	-0,003	0,181	0,007	-0,051	0,154	0,017	1,000	0,000	0,011	0,232	-0,011	-0,001	-0,003	0,049	0,004	-0,011	0,000	-0,020	0,256
9	δ_0	°	-1,972	0,476	11,913	-0,048	-5,672	1,914	0,321	17,488	1,000	0,380	8,502	5,049	2,722	9,085	5,464	3,349	-1,326	-4,674	2,708	-20,778
10	Δδ	°	-0,344	-0,104	11,900	0,429	-2,689	8,675	0,911	54,509	0,049	1,000	19,384	-0,242	0,521	1,926	5,996	-0,089	-0,024	2,751	-1,154	19,077
11	dδ/dt	°/s	-0,015	-0,006	0,654	0,022	-0,148	0,454	0,048	2,832	0,003	0,048	1,000	-0,020	0,019	0,074	0,290	0,011	-0,007	0,122	-0,067	0,899
12	λ_0	°	-0,033	0,040	-0,500	-0,014	0,234	-0,284	-0,028	-1,881	0,022	-0,008	-0,275	1,000	0,250	0,492	0,269	-0,016	0,111	0,114	0,633	0,702
13	Δλ	°	-0,067	0,031	0,388	0,103	-0,462	-0,020	-0,095	-0,787	0,043	0,063	0,933	0,887	1,000	3,012	2,915	-0,603	0,526	1,665	0,432	4,159
14	Δλ_rel	%	-0,039	0,006	0,195	0,036	-0,182	-0,004	-0,034	-0,192	0,014	0,023	0,357	0,172	0,298	1,000	0,918	-0,182	0,146	0,485	0,034	1,003
15	dλ/dt	°/s	-0,002	-0,004	0,381	0,032	-0,141	0,216	0,004	1,307	0,004	0,033	0,636	0,043	0,131	0,419	1,000	-0,113	0,109	0,510	0,006	1,273
16	χ_0	°	0,021	-0,035	0,256	-0,009	-0,614	0,079	0,019	0,675	0,014	-0,003	0,139	-0,015	-0,160	-0,487	-0,663	1,000	-0,337	-0,958	-0,809	-5,564
17	Δχ	°	0,024	0,049	-0,872	0,020	0,905	-1,239	-0,206	-5,740	-0,018	-0,003	-0,318	0,346	0,462	1,293	2,123	-1,115	1,000	3,198	0,776	4,349
18	dχ/dt	°/s	0,014	0,005	0,094	0,020	0,076	-0,071	-0,029	0,003	-0,005	0,023	0,407	0,028	0,114	0,337	0,777	-0,249	0,250	1,000	0,074	1,380
19	W1	Nm°	-0,020	0,026	0,041	-0,009	0,321	0,036	0,018	-0,850	0,003	-0,010	-0,230	0,157	0,030	0,024	0,010	-0,214	0,062	0,075	1,000	4,501
20	W2	Nm°/s	-0,002	0,001	0,110	0,005	0,018	0,079	0,008	0,270	-0,001	0,004	0,078	0,004	0,007	0,018	0,050	-0,037	0,009	0,036	0,114	1,000

G2		No.	1	2	3	4	5	6	7	8	9	10	11	12	13	14	15	16	17	18	19	20
	CTR	Name	v_0	K	dp/dt	ax	T_0	ΔT	ΔT/ax	dT/dt	δ_0	Δδ	dδ/dt	λ_0	Δλ	Δλ_rel	dλ/dt	χ_0	Δχ	dχ/dt	W1	W2
No.	Name	Unit	m/s	Ncm/(m°/s²)	bar/s	m/s²	Nm	Nm	Nm/(m/s²)	Nm/s	°	°	°/s	°	°	%	°/s	°	°	°/s	Nm°	Nm°/s
1	v_0	m/s	0,000	6,453	104,712	3,634	18,440	48,064	9,580	223,629	3,410	5,067	98,196	40,392	14,110	63,220	53,478	-4,027	1,895	2,861	45,644	196,783
2	K	Ncm/(m°/s²)	22,210	0,000	85,037	8,223	-16,142	55,279	6,892	240,254	0,047	2,435	55,187	18,307	5,634	22,824	56,570	13,939	-0,380	14,902	-10,864	49,316
3	dp/dt	bar/s	19,742	3,552	0,000	4,447	14,045	11,218	3,531	-7,244	0,454	-0,270	-3,685	32,239	7,729	25,967	39,809	1,754	5,431	19,406	19,654	44,022
4	ax	m/s²	18,062	4,401	5,713	0,000	23,369	-1,547	5,340	-57,464	0,702	-0,840	-13,737	32,361	3,768	12,627	18,992	4,254	3,336	8,610	25,719	4,572
5	T_0	Nm	19,422	3,113	76,660	6,545	0,000	38,346	5,838	143,695	0,748	1,677	39,341	29,463	8,587	29,865	52,305	4,931	3,371	19,999	16,245	106,074
6	ΔT	Nm	19,616	3,856	33,928	4,636	16,927	0,000	1,662	-58,770	0,612	-0,615	-9,185	32,120	8,214	28,311	40,382	2,299	6,980	22,946	19,353	30,344
7	ΔT/ax	Nm/(m/s²)	20,147	3,677	41,801	6,170	15,323	-1,559	0,000	-66,830	0,579	-0,584	-8,451	31,943	9,874	34,316	47,835	1,554	8,477	28,488	15,789	31,386
8	dT/dt	Nm/s	19,533	3,641	49,334	5,389	11,910	15,225	3,364	0,000	0,615	0,096	5,970	31,504	8,329	28,612	43,847	2,369	5,568	20,978	22,701	85,389
9	δ_0	°	20,616	3,031	62,408	6,215	9,722	31,932	5,156	104,787	0,000	1,133	27,252	26,821	6,354	22,152	45,861	0,626	5,176	24,115	18,515	129,125
10	Δδ	°	19,773	3,494	53,871	5,587	9,657	21,176	4,106	40,865	0,601	0,000	6,048	30,535	7,453	25,560	41,199	2,991	4,322	17,170	21,928	88,754
11	dδ/dt	°/s	19,795	3,531	48,829	5,446	10,795	18,256	3,803	23,191	0,579	-0,201	0,000	30,861	7,544	25,789	39,971	2,513	4,534	16,979	22,545	85,606
12	λ_0	°	20,278	2,130	85,489	6,613	-1,131	41,794	6,201	173,289	-0,007	1,637	41,260	0,000	0,623	13,383	41,387	3,352	0,927	17,554	1,207	94,016
13	Δλ	°	19,845	3,099	67,205	5,342	9,707	33,379	6,148	122,921	0,319	0,872	25,314	22,951	0,000	3,610	25,690	7,795	-0,015	7,378	16,797	81,218
14	Δλ_rel	%	20,401	3,168	64,880	5,165	11,056	33,329	6,321	121,923	0,270	0,736	22,857	25,332	-0,234	0,000	23,590	8,001	0,171	7,309	19,367	86,891
15	dλ/dt	°/s	19,396	3,539	51,531	4,592	12,925	22,511	5,160	51,773	0,477	-0,233	1,443	28,069	1,670	7,507	0,000	8,462	-1,112	-4,244	20,024	52,198
16	χ_0	°	19,237	3,451	69,645	6,208	7,688	32,986	5,315	114,554	0,629	1,396	32,544	30,243	8,633	29,627	51,420	0,000	5,253	23,733	22,648	131,175
17	Δχ	°	19,194	3,138	74,118	6,099	2,046	38,527	6,252	141,102	0,748	1,398	34,306	28,715	6,195	22,685	40,415	7,650	0,000	7,271	17,000	96,571
18	dχ/dt	°/s	19,001	3,244	68,397	5,766	4,325	34,695	5,976	116,422	0,775	0,907	24,398	29,619	5,775	21,169	33,220	8,083	-0,968	0,000	18,783	86,251
19	W1	Nm°	19,704	2,815	69,547	6,362	-0,606	32,485	5,009	133,767	0,609	1,586	37,607	27,005	7,561	27,742	49,324	7,219	3,030	19,463	0,000	23,731
20	W2	Nm°/s	19,484	3,187	57,735	5,655	3,826	24,117	4,412	85,341	0,736	0,916	24,002	29,692	7,326	26,160	43,752	7,160	3,276	16,884	7,200	0,000

Refer to chapter 5.3.1 for a detailed explanation on the correlation analysis and chapter 5.2 for a definition of the characteristic values that are correlated in the tables.

A.5.4 Correlation Tables for Exp. with BSTAM Active

Note: High R-values are indicated darker, low p-values are lighter. .

R		No.	1	2	3	4	5	6	7	8	9	10	11	12	13	14	15	16	17	18	19	20
	BSTAM	Name	v_0	K	dp/dt	ax	T_0	ΔT	ΔT/ax	dT/dt	δ_0	Δδ	dδ/dt	λ_0	Δλ	Δλ_rel	dλ/dt	χ_0	Δχ	dχ/dt	W1	W2
No.	Name	Unit	m/s	Ncm/(m°/s²)	bar/s	m/s²	Nm	Nm	Nm/(m/s²)	Nm/s	°	°	°/s	°	°	%	°/s	°	°	°/s	Nm°	Nm°/s
1	v_0	m/s	1,000	-0,279	-0,048	0,275	-0,213	0,135	0,060	0,104	-0,684	-0,140	-0,141	-0,199	-0,273	-0,333	-0,195	0,099	-0,115	-0,091	-0,181	0,093
2	K	Ncm/(m°/s²)	-0,279	1,000	-0,023	-0,144	0,149	-0,220	-0,186	-0,100	0,162	-0,011	0,078	0,206	0,039	0,116	-0,002	0,029	-0,044	-0,089	-0,088	-0,184
3	dp/dt	bar/s	-0,048	-0,023	1,000	0,093	0,067	0,044	0,004	0,284	0,030	-0,168	0,153	-0,175	-0,241	-0,062	-0,093	-0,048	-0,142	-0,097	0,006	-0,136
4	ax	m/s²	0,275	-0,144	0,093	1,000	-0,137	0,197	-0,064	0,094	-0,217	-0,044	-0,198	-0,084	-0,148	-0,251	-0,088	0,118	-0,018	0,057	-0,116	-0,054
5	T_0	Nm	-0,213	0,149	0,067	-0,137	1,000	-0,611	-0,585	-0,297	0,067	0,031	0,105	0,203	-0,300	-0,026	0,040	-0,307	-0,016	-0,078	0,341	0,113
6	ΔT	Nm	0,135	-0,220	0,044	0,197	-0,611	1,000	0,961	0,614	0,132	0,318	0,145	0,013	0,246	0,067	0,231	-0,072	0,335	0,363	0,225	0,269
7	ΔT/ax	Nm/(m/s²)	0,060	-0,186	0,004	-0,064	-0,585	0,961	1,000	0,578	0,184	0,362	0,205	0,035	0,302	0,152	0,267	-0,104	0,354	0,355	0,269	0,284
8	dT/dt	Nm/s	0,104	-0,100	0,284	0,094	-0,297	0,614	0,578	1,000	0,160	-0,007	0,319	-0,003	-0,011	0,093	0,151	-0,139	0,074	0,128	0,177	0,023
9	δ_0	°	-0,684	0,162	0,030	-0,217	0,067	0,132	0,184	0,160	1,000	0,199	0,184	0,317	0,345	0,344	0,347	-0,174	0,375	0,320	0,362	0,101
10	Δδ	°	-0,140	-0,011	-0,168	-0,044	0,031	0,318	0,362	-0,007	0,199	1,000	0,432	0,294	0,408	0,275	0,265	-0,439	0,548	0,379	0,407	-0,022
11	dδ/dt	°/s	-0,141	0,078	0,153	-0,198	0,105	0,145	0,205	0,319	0,184	0,432	1,000	0,064	0,017	0,163	0,046	-0,314	0,118	0,072	0,308	-0,001
12	λ_0	°	-0,199	0,206	-0,175	-0,084	0,203	0,013	0,035	-0,003	0,317	0,294	0,064	1,000	0,384	0,207	0,405	0,090	0,395	0,346	0,213	0,147
13	Δλ	°	-0,273	0,039	-0,241	-0,148	-0,300	0,246	0,302	-0,011	0,345	0,408	0,017	0,384	1,000	0,526	0,443	0,037	0,428	0,283	0,011	-0,067
14	Δλ_rel	%	-0,333	0,116	-0,062	-0,251	-0,026	0,067	0,152	0,093	0,344	0,275	0,163	0,207	0,526	1,000	0,530	-0,138	0,262	0,254	0,250	0,055
15	dλ/dt	°/s	-0,195	-0,002	-0,093	-0,088	0,040	0,231	0,267	0,151	0,347	0,265	0,046	0,405	0,443	0,530	1,000	-0,146	0,516	0,462	0,437	0,316
16	χ_0	°	0,099	0,029	-0,048	0,118	-0,307	-0,072	-0,104	-0,139	-0,174	-0,439	-0,314	0,090	0,037	-0,138	-0,146	1,000	-0,252	-0,138	-0,504	0,139
17	Δχ	°	-0,115	-0,044	-0,142	-0,018	-0,016	0,335	0,354	0,074	0,375	0,548	0,118	0,395	0,428	0,262	0,516	-0,252	1,000	0,821	0,474	0,254
18	dχ/dt	°/s	-0,091	-0,089	-0,097	0,057	-0,078	0,363	0,355	0,128	0,320	0,379	0,072	0,346	0,283	0,254	0,462	-0,138	0,821	1,000	0,345	0,334
19	W1	Nm°	-0,181	-0,088	0,006	-0,116	0,341	0,225	0,269	0,177	0,362	0,407	0,308	0,213	0,011	0,250	0,437	-0,504	0,474	0,345	1,000	0,483
20	W2	Nm°/s	0,093	-0,184	-0,136	-0,054	0,113	0,269	0,284	0,023	0,101	-0,022	-0,001	0,147	-0,067	0,055	0,316	0,139	0,254	0,334	0,483	1,000

P		No.	1	2	3	4	5	6	7	8	9	10	11	12	13	14	15	16	17	18	19	20
	BSTAM	Name	v_0	K	dp/dt	ax	T_0	ΔT	ΔT/ax	dT/dt	δ_0	Δδ	dδ/dt	λ_0	Δλ	Δλ_rel	dλ/dt	χ_0	Δχ	dχ/dt	W1	W2
No.	Name	Unit	m/s	Ncm/(m°/s²)	bar/s	m/s²	Nm	Nm	Nm/(m/s²)	Nm/s	°	°	°/s	°	°	%	°/s	°	°	°/s	Nm°	Nm°/s
1	v_0	m/s	0,000	0,002	0,608	0,002	0,020	0,142	0,518	0,262	0,000	0,129	0,127	0,030	0,003	0,000	0,033	0,285	0,212	0,324	0,049	0,313
2	K	Ncm/(m°/s²)	0,002	0,000	0,803	0,117	0,107	0,016	0,043	0,282	0,078	0,904	0,402	0,024	0,672	0,211	0,980	0,758	0,631	0,333	0,344	0,045
3	dp/dt	bar/s	0,608	0,803	0,000	0,315	0,468	0,633	0,962	0,002	0,745	0,068	0,096	0,057	0,008	0,503	0,312	0,607	0,124	0,292	0,952	0,141
4	ax	m/s²	0,002	0,117	0,315	0,000	0,136	0,032	0,490	0,314	0,018	0,638	0,031	0,363	0,108	0,006	0,342	0,200	0,847	0,535	0,209	0,557
5	T_0	Nm	0,020	0,107	0,468	0,136	0,000	0,000	0,000	0,001	0,470	0,736	0,256	0,027	0,001	0,777	0,666	0,001	0,862	0,401	0,000	0,222
6	ΔT	Nm	0,142	0,016	0,633	0,032	0,000	0,000	0,000	0,000	0,151	0,000	0,116	0,892	0,007	0,467	0,012	0,439	0,000	0,000	0,014	0,003
7	ΔT/ax	Nm/(m/s²)	0,518	0,043	0,962	0,490	0,000	0,000	0,000	0,000	0,045	0,000	0,025	0,702	0,001	0,098	0,003	0,262	0,000	0,000	0,003	0,002
8	dT/dt	Nm/s	0,262	0,282	0,002	0,314	0,001	0,000	0,000	0,000	0,084	0,944	0,000	0,973	0,907	0,318	0,102	0,135	0,428	0,166	0,056	0,807
9	δ_0	°	0,000	0,078	0,745	0,018	0,470	0,151	0,045	0,084	0,000	0,030	0,045	0,000	0,000	0,000	0,000	0,058	0,000	0,000	0,000	0,275
10	Δδ	°	0,129	0,904	0,068	0,638	0,736	0,000	0,000	0,944	0,030	0,000	0,000	0,001	0,000	0,002	0,004	0,000	0,000	0,000	0,000	0,811
11	dδ/dt	°/s	0,127	0,402	0,096	0,031	0,256	0,116	0,025	0,000	0,045	0,000	0,000	0,490	0,850	0,076	0,619	0,001	0,202	0,439	0,001	0,989
12	λ_0	°	0,030	0,024	0,057	0,363	0,027	0,892	0,702	0,973	0,000	0,001	0,490	0,000	0,000	0,024	0,000	0,331	0,000	0,000	0,020	0,110
13	Δλ	°	0,003	0,672	0,008	0,108	0,001	0,007	0,001	0,907	0,000	0,000	0,850	0,000	0,000	0,000	0,000	0,690	0,000	0,002	0,906	0,470
14	Δλ_rel	%	0,000	0,211	0,503	0,006	0,777	0,467	0,098	0,318	0,000	0,002	0,076	0,024	0,000	0,000	0,000	0,134	0,004	0,005	0,006	0,553
15	dλ/dt	°/s	0,033	0,980	0,312	0,342	0,666	0,012	0,003	0,102	0,000	0,004	0,619	0,000	0,000	0,000	0,000	0,114	0,000	0,000	0,000	0,000
16	χ_0	°	0,285	0,758	0,607	0,200	0,001	0,439	0,262	0,135	0,058	0,000	0,001	0,331	0,690	0,134	0,114	0,000	0,006	0,135	0,000	0,131
17	Δχ	°	0,212	0,631	0,124	0,847	0,862	0,000	0,000	0,428	0,000	0,000	0,202	0,000	0,000	0,004	0,000	0,006	0,000	0,000	0,000	0,005
18	dχ/dt	°/s	0,324	0,333	0,292	0,535	0,401	0,000	0,000	0,166	0,000	0,000	0,439	0,000	0,002	0,005	0,000	0,135	0,000	0,000	0,000	0,000
19	W1	Nm°	0,049	0,344	0,952	0,209	0,000	0,014	0,003	0,056	0,000	0,000	0,001	0,020	0,906	0,006	0,000	0,000	0,000	0,000	0,000	0,000
20	W2	Nm°/s	0,313	0,045	0,141	0,557	0,222	0,003	0,002	0,807	0,275	0,811	0,989	0,110	0,470	0,553	0,000	0,131	0,005	0,000	0,000	0,000

The nomenclature is as follows:

- R = correlation coefficient
- p = probability value (check for $p < 0.05$)
- g_1 and g_2 → slope and axis intercept parameters of the regression lines

Refer to the relevant (dark) correlations, to spot out values of interest.

G1		No.	1	2	3	4	5	6	7	8	9	10	11	12	13	14	15	16	17	18	19	20
	BSTAM	Name	v_0	K	dp/dt	ax	T_0	ΔT	ΔT/ax	dT/dt	δ_0	Δδ	dδ/dt	λ_0	Δλ	Δλ_rel	dλ/dt	χ_0	Δχ	dχ/dt	W1	W2
No.	Name	Unit	m/s	Ncm/(m°/s²)	bar/s	m/s²	Nm	Nm	Nm/(m/s²)	Nm/s	°	°	°/s	°	°	%	°/s	°	°	°/s	Nm°	Nm°/s
1	v_0	m/s	1,000	-0,749	-0,837	0,132	-0,965	0,745	0,073	3,072	-0,100	-0,031	-0,637	-0,810	-0,510	-4,200	-1,512	0,241	-0,083	-0,282	-1,488	1,806
2	K	Ncm/(m°/s²)	-0,104	1,000	-0,152	-0,026	0,251	-0,452	-0,085	-1,096	0,009	-0,001	0,131	0,313	0,027	0,544	-0,007	0,026	-0,012	-0,103	-0,268	-1,328
3	dp/dt	bar/s	-0,003	-0,004	1,000	0,003	0,017	0,014	0,000	0,476	0,000	-0,002	0,039	-0,041	-0,026	-0,044	-0,041	-0,007	-0,006	-0,017	0,003	-0,150
4	ax	m/s²	0,574	-0,809	3,415	1,000	-1,300	2,266	-0,163	5,817	-0,066	-0,020	-1,876	-0,716	-0,578	-6,617	-1,419	0,604	-0,027	0,371	-1,988	-2,202
5	T_0	Nm	-0,047	0,088	0,261	-0,015	1,000	-0,744	-0,158	-1,994	0,002	0,002	0,105	0,182	-0,124	-0,073	0,068	-0,165	-0,003	-0,053	0,619	0,483
6	ΔT	Nm	0,025	-0,107	0,141	0,017	-0,503	1,000	0,213	3,377	0,004	0,013	0,119	0,009	0,083	0,154	0,324	-0,032	0,044	0,204	0,335	0,947
7	ΔT/ax	Nm/(m/s²)	0,049	-0,409	0,063	-0,025	-2,174	4,340	1,000	14,349	0,022	0,066	0,763	0,118	0,462	1,575	1,689	-0,207	0,208	0,900	1,807	4,510
8	dT/dt	Nm/s	0,004	-0,009	0,170	0,002	-0,044	0,112	0,023	1,000	0,001	0,000	0,049	0,000	-0,001	0,040	0,040	-0,011	0,002	0,013	0,049	0,015
9	δ_0	°	-4,671	2,972	3,619	-0,709	2,069	4,984	1,533	32,278	1,000	0,305	5,687	8,823	4,407	29,685	18,303	-2,908	1,838	6,748	20,279	13,358
10	Δδ	°	-0,625	-0,133	-13,220	-0,093	0,632	7,823	1,972	-0,868	0,130	1,000	8,741	5,349	3,411	15,525	9,151	-4,785	1,758	5,228	14,924	-1,918
11	dδ/dt	°/s	-0,031	0,046	0,596	-0,021	0,105	0,176	0,055	2,074	0,006	0,021	1,000	0,057	0,007	0,455	0,079	-0,169	0,019	0,049	0,558	-0,005
12	λ_0	°	-0,049	0,136	-0,757	-0,010	0,226	0,017	0,011	-0,022	0,011	0,016	0,071	1,000	0,177	0,641	0,769	0,054	0,070	0,262	0,429	0,701
13	Δλ	°	-0,146	0,056	-2,264	-0,038	-0,727	0,724	0,197	-0,171	0,027	0,049	0,042	0,836	1,000	3,550	1,829	0,048	0,164	0,468	0,048	-0,692
14	Δλ_rel	%	-0,026	0,025	-0,086	-0,010	-0,009	0,029	0,015	0,216	0,004	0,005	0,059	0,067	0,078	1,000	0,324	-0,027	0,015	0,062	0,163	0,084
15	dλ/dt	°/s	-0,025	-0,001	-0,213	-0,005	0,023	0,164	0,042	0,576	0,007	0,008	0,027	0,213	0,107	0,865	1,000	-0,046	0,048	0,185	0,464	0,792
16	χ_0	°	0,040	0,031	-0,344	0,023	-0,570	-0,162	-0,052	-1,672	-0,010	-0,040	-0,582	0,150	0,028	-0,714	-0,461	1,000	-0,074	-0,175	-1,694	1,104
17	Δχ	°	-0,160	-0,166	-3,474	-0,012	-0,101	2,567	0,601	3,031	0,076	0,171	0,743	2,238	1,114	4,599	5,553	-0,857	1,000	3,533	5,417	6,846
18	dχ/dt	°/s	-0,029	-0,078	-0,555	0,009	-0,114	0,647	0,140	1,223	0,015	0,027	0,105	0,455	0,171	1,039	1,156	-0,109	0,191	1,000	0,916	2,092
19	W1	Nm°	-0,022	-0,029	0,012	-0,007	0,189	0,151	0,040	0,634	0,006	0,011	0,170	0,106	0,002	0,385	0,412	-0,150	0,042	0,130	1,000	1,141
20	W2	Nm°/s	0,005	-0,025	-0,123	-0,001	0,026	0,077	0,018	0,035	0,001	0,000	0,000	0,031	-0,006	0,036	0,126	0,018	0,009	0,053	0,205	1,000

G2		No.	1	2	3	4	5	6	7	8	9	10	11	12	13	14	15	16	17	18	19	20
	BSTAM	Name	v_0	K	dp/dt	ax	T_0	ΔT	ΔT/ax	dT/dt	δ_0	Δδ	dδ/dt	λ_0	Δλ	Δλ_rel	dλ/dt	χ_0	Δχ	dχ/dt	W1	W2
No.	Name	Unit	m/s	Ncm/(m°/s²)	bar/s	m/s²	Nm	Nm	Nm/(m/s²)	Nm/s	°	°	°/s	°	°	%	°/s	°	°	°/s	Nm°	Nm°/s
1	v_0	m/s	0,000	19,287	66,336	2,041	38,555	0,202	1,785	0,107	2,594	0,850	26,474	45,749	11,522	89,012	53,149	-1,181	2,448	11,166	43,047	24,763
2	K	Ncm/(m°/s²)	19,359	0,000	51,365	4,652	19,089	16,579	3,597	63,619	0,663	0,265	13,808	28,878	1,778	7,145	24,736	3,222	0,952	6,398	16,434	65,646
3	dp/dt	bar/s	18,956	5,368	0,000	4,390	19,518	13,531	3,143	33,867	0,696	0,368	12,492	32,552	3,214	12,217	26,776	3,692	1,183	6,728	14,912	66,318
4	ax	m/s²	16,225	8,846	35,147	0,000	26,264	3,992	3,893	31,612	1,008	0,352	22,966	33,738	4,533	39,865	31,111	0,630	1,011	4,185	24,024	68,702
5	T_0	Nm	19,778	3,396	45,262	4,814	0,000	29,392	6,373	98,368	0,664	0,229	12,348	26,788	4,450	11,461	23,312	6,729	0,942	6,943	2,431	48,911
6	ΔT	Nm	18,470	6,716	48,565	4,275	27,548	0,000	0,129	9,464	0,658	0,077	12,795	30,371	0,732	7,775	20,093	3,809	0,269	2,965	10,271	45,281
7	ΔT/ax	Nm/(m/s²)	18,665	6,481	50,378	4,597	27,257	0,526	0,000	12,230	0,639	0,051	12,080	30,129	0,459	4,995	19,366	4,012	0,233	3,019	9,336	44,512
8	dT/dt	Nm/s	18,621	5,714	40,743	4,437	22,840	7,881	1,837	0,000	0,661	0,265	11,672	30,504	1,949	7,628	22,372	4,031	0,781	5,083	12,172	57,972
9	δ_0	°	22,129	3,084	48,013	5,020	18,925	10,700	2,072	35,110	0,000	0,045	10,459	24,252	-1,202	-11,063	11,733	5,418	-0,412	1,082	0,676	49,291
10	Δδ	°	18,982	5,224	54,019	4,542	20,226	12,195	2,645	58,160	0,675	0,000	12,213	29,110	1,032	5,928	22,319	4,603	0,433	4,502	11,159	59,255
11	dδ/dt	°/s	19,269	4,524	41,948	4,821	18,871	11,683	2,357	27,845	0,622	-0,049	0,000	29,670	1,815	3,378	23,563	5,807	0,620	5,155	6,953	58,834
12	λ_0	°	20,309	1,045	73,683	4,820	13,510	13,714	2,834	58,617	0,361	-0,233	12,318	0,000	-3,465	-9,583	1,249	1,713	-1,235	-2,141	1,955	37,361
13	Δλ	°	19,099	5,082	54,925	4,591	21,787	12,842	2,781	58,258	0,657	0,167	14,407	28,898	0,000	3,153	21,190	3,265	0,575	4,965	14,951	60,084
14	Δλ_rel	%	19,082	4,945	51,439	4,613	20,485	13,939	3,012	55,783	0,669	0,212	13,904	29,838	1,142	0,000	21,467	3,623	0,742	5,242	13,421	57,915
15	dλ/dt	°/s	19,444	5,210	55,831	4,652	19,813	10,172	2,119	43,715	0,546	0,071	13,822	25,237	-0,726	-11,394	0,000	4,493	-0,294	1,297	3,593	39,185
16	χ_0	°	18,684	5,084	51,732	4,440	22,303	14,774	3,332	63,560	0,744	0,395	16,444	29,999	1,825	12,365	26,250	0,000	1,139	6,449	20,731	55,049
17	Δχ	°	18,962	5,337	53,671	4,529	20,481	11,946	2,623	55,251	0,641	0,108	13,826	28,510	0,928	5,875	19,757	4,120	0,000	2,717	10,221	52,660
18	dχ/dt	°/s	18,992	5,645	53,831	4,466	21,058	10,441	2,336	50,757	0,620	0,100	13,873	27,834	0,915	3,879	17,921	3,996	-0,228	0,000	9,674	46,492
19	W1	Nm°	19,152	5,620	50,398	4,620	17,555	11,958	2,557	48,416	0,611	0,093	11,928	28,914	1,882	4,174	18,509	5,612	0,266	3,908	0,000	41,584
20	W2	Nm°/s	18,537	6,685	57,827	4,597	18,840	9,735	2,108	55,902	0,664	0,275	14,506	28,683	2,299	7,867	17,288	2,328	0,337	2,735	3,015	0,000

Refer to chapter 5.3.1 for a detailed explanation on the correlation analysis and chapter 5.2 for a definition of the characteristic values that are correlated in the tables.

Bibliography

ACEM (European Association of Motorcycle Manufacturers): MAIDS: Motorcycle Accidents In Depth Study – In-depth investigations of accidents involving powered two wheelers. www.maids-study.eu, Final Report 2.0, April 2009

ARX – virtual: www.armodelling.com, last access: 2014-05-06

Bald, Stefan; Stumpf, Katja: Hinweise für das Anbringen von Verkehrszeichen und Verkehrseinrichtungen (HAV) Verkehrstechnischer Kommentar. Kirschbaum Verlag, Bonn, 2014, ISBN 978-37812-1700-3

Bauer, Klaus; Peldschus, Steffen; Schick, Sylvia: Retrospective analysis of fatal motorcycle accidents and derivation of protective measures in complex braking maneuvers. In: Proceedings of the 10th International Motorcycle Conference 2014, pp. 116-127, Institute for Motorcycle Safety e.V., Essen, 2014

Bayer, Bernward: Das Pendeln und Flattern von Krafträdern. Forschungshefte Zweiradsicherheit Nr. 4, Institut für Zweiradsicherheit e.V., Bochum, 1986, ISBN 3-88314-549-1

Bergmann, Guido: Kurvenwunder. In: Motorrad News 11/2013, Technik, pp. 10-11, Syburger Verlag, Unna, 2013

BMVBS (Federal Ministry of Transport, Building and Urban Development): Road Safety Programme 2011, 2011-12-01, www.bmvbs.de, last access: 2014-04-16

BOSCH: Improved safety on two wheels | Bosch motorcycle stability control goes into series production | Controlled braking – also in bends. Bosch Press-Release PI 8314 CC, September 2013

BOSCH: Powerful and compact | New Bosch ABS for all motorcycle types | Safe braking with ABS. Bosch Press-Release PI 7438 CC, July 2011

BOSE – virtual: http://www.bose.com/prc.jsp?url=/automotive/bose_suspension/, last access: 2016-11-11

Breuer, Bert; Karlheinz Bill (Ed.): Brake Technology Handbook. SAE International, 2008, ISBN 978-0-7680-1787-8

Breuer, Bert; Karlheinz Bill (Ed.): Bremsenhandbuch. ATZ/MTZ-Fachbuch, Vieweg+Teubner, Wiesbaden, 2012, ISBN 978-3-8348-1796-9

Cossalter, Vittore: Motorcycle Dynamics (2nd English edition), LuLu Enterprises, Inc., USA, 2006, ISBN 978-1-4303-0861-4

Cossalter, V.; Lot, R.; Massaro, M.; Peretto, M.: Motorcycle Steering Torque Decomposition. In: Proceedings of the World Congress on Engineering 2010 (WCE 2010), Vol. II., London, 2010, ISBN 978-988-18210-7-2

DEKRA: Verkehrssicherheitsreport Motorrad 2010, DEKRA Automobil GmbH, Stuttgart, 2010

DESTATIS (Statistisches Bundesamt): Verkehrsunfälle Zeitreihen 2013, 2014, www.destatis.de, last access: 2014-11-15

DESTATIS (Statistisches Bundesamt): Zweiradunfälle im Straßenverkehr 2013, www.destatis.de, 2014, last access: 2014-11-15

European Commission: Road Safety Programme 2011-2020: detailed measures. MEMO/10/343, 2010-07-20, http://europa.eu/rapid/press-release_MEMO-10-343_en.htm, last access: 2014-04-30

European Commission: Towards a European road safety area: policy orientations on road safety 2011-2020, COM(2010) 389 final, 2010-07-20

European Parliament and Council: Regulation (EU) No. 168/2013 of the European Parliament and of the Council of 15 January 2013 on the approval and market surveillance of two- or three-wheel vehicles and quadricycles, eur-lex.europa.eu, last access: 2014-04-30

Evangelou, S.; Limebeer, D. J. N.; Sharp, R. S.; Smith, M. C.: Steering compensation for high-performance motorcycles. Proceedings of the 43rd IEEE Conference on Decision and Control, Bahamas, Dec. 14-17, 2004, pp. 749-754.

Ferrero, Thomas: Fahrverhalten und Unfallgeschehen auf typischen Motorradstrecken. Vertieferarbeit am Fachgebiet Straßenentwurf und Straßenbetrieb der Technischen Hochschule Darmstadt, Darmstadt, 1988.

FGSV (Forschungsgesellschaft für Straßen- und Verkehrswesen): Merkblatt zur Verbesserung der Verkehrssicherheit auf Motorradstrecken (MVMot R2). FGSV Verlag, Köln, 2007, ISBN 978-3-939715-31-3

FGSV (Forschungsgesellschaft für Straßen- und Verkehrswesen): Richtlinien für die Anlage von Landstraßen (RAL 2012). FGSV Verlag, Köln, 2012, ISBN 978-3-86446-039-5

Flacke, Emil: Gyrostatic Mechanism. Patent Application US1048817A, 1910/12

Foale, Tony: Motorcycle Handling and Chassis Design, The Art and Science. Tony Foale Dynamics, 2002, ISBN 84-933286-3-4.

Foale – virtual: www.tonyfoale.com, last access: 2014-11-30

Funke, Joachim: Belastung und Beanspruchung von Motorradfahrern bei der Bremsung mit verschiedenen Bremssystemen. Fortschritt-Berichte VDI Reihe 12 Nr. 633, VDI-Verlag, Düsseldorf, 2007, ISBN 3-18-363312-8

Funke, J.; Savaresi, S.; Spelta, C.: Electrorheological Dampers as a Basis for semi-active Motorcycle Suspensions. In: Proceedings of the 8th International Motorcycle Conference 2010, pp. 211-224, Institute for Motorcycle Safety e.V., Essen, 2010

Guth, Sebastian: Motorrad-Fahrsimulation zur Absicherung von Anzeige-Bedien-Konzepten und informierenden Assistenzsystemen. In: Proceedings of the 10th International Motorcycle Conference 2014, pp. 440-459, Institute for Motorcycle Safety e.V., Essen, 2014

Harmonic Drive – virtual: www.harmonicdrive.de, last access: 2014-12-01

Hikichi, T.; Kiyota, S.; Tagami, T.; Araki, M.: Motorcycle steering system. Patent Application EP2085307A1, 2008/09

Hossack – virtual: www.hossack-design.com, last access: 2014-11-30.

Hurt, H. H.; Ouellet, J. V.; Thom, D. R.: Motorcycle Accident Cause Factors and Identification of Countermeasures Volume I: Technical Report. U.S. Department of Transportation, National Highway Traffic Safety Administration, Washington, D.C. 20590, Final Report, January 1981

International Traffic Safety Data and Analysis Group (IRTAD): Road Safety Annual Report 2013, OECD International Transport Forum, 2013, www.internationaltransportforum.org, last access: 2014-04-30

Kim, Daniel Kee Young: Dynamically balanced flywheel. Patent Application US20130233100A1, 2013/13

Kim, D. K. Y.; Bretney, K.; Shao, A.; Tsang, A. L.: Electronic control system for gyroscopic stabilized vehicle. Patent Application US8532915B2, 2010/13

King, L. W.; Pizzey, J. K.: Motor Bicycle Assemblies. Patent Application GB1319703A, 1971/73

Kooijman, J. D. G.; Meijaard, J. P.; Papadopoulos, J. M.; Ruina, A; Schwab, A. L.: A bicycle can be self-stable without gyroscopic or caster effects. Science Magazine, Vol. 332 no. 6027 pp. 339-342, April 15, 2011, DOI: 10.1126/science.1201959

Koch, Jochim: Experimentelle und Analytische Untersuchungen des Motorrad-Fahrer-Systems. Fortschritt-Berichte VDI Reihe 12 Nr. 40, VDI-Verlag, Düsseldorf, 1980, ISBN 3-18-144012-4.

Kompass, K.; Osendorfer, H.; Rauscher, S.: The Safety Concept of BMW C1. In: Proceedings of the 2nd International Motorcycle Conference 1998, pp. 223-241, Institute for Motorcycle Safety e.V., Essen, 1998

Kühn, Matthias: Analyse des Motorradunfallgeschehens - Interdisziplinäre Analyse der Sicherheitslage von Motorradfahrern in Deutschland. Unfallforschung der Versicherer (UDV) im Gesamtverband der Deutschen Versicherungswirtschaft e.V. (GDV), Präsentation, UDV Jahrestagung, 2008

Landerl, Christian; Deissinger, Felix; Wagner, Hans-Albert; Jahreiss, Hans-Jürgen: Enhanced rider assistance via connection of the Engine- and Suspension Control Systems of the BMW S 1000 RR. In: Proceedings of the 8th International Motorcycle Conference 2010, pp. 362-377, Institute for Motorcycle Safety e.V., Essen, 2010

Lattke, Benedikt: Ein kommunikationsbasiertes Gefahrstellenwarnsystem für Motorräder. Fortschritt-Berichte VDI Reihe 12 Nr. 757, VDI-Verlag, Düsseldorf, 2012, ISBN 978-3-18-375712-1

LIT Motors – virtual: litmotors.com, last access: 2016-11-11

Matschl, Gerald; Mörbe, Matthias; Gröger, Christian: Motorcycle Stability Control – MSC, Der nächste Schritt zur Fahrsicherheit für Motorräder. In: Proceedings of the 10th International Motorcycle Conference 2014, pp. 128-154, Institute for Motorcycle Safety e.V., Essen, 2014

Mercedes Benz – virtual: www.fanmercedesbenz.com/2001-mercedes-benz-f400-carving/, last access: 2016-09-08

Merziger, Gerhard; Mühlbach, Günter; Wille, Detlef; Wirth, Thomas: Formeln + Hilfen zur höheren Mathematik. Binomi Verlag, Springer, 2001, ISBN 3-923 923-35-X

MonoTracer – virtual: https://peraves.wordpress.com/, last access: 2016-11-11

Murri, Raphael; Martinbianco, Roberto; Gerster, Bernhard: Sicherheitsgurt für Motorradfahrer. In: Proceedings of the 7th International Motorcycle Conference 2008, pp. 418-429, Institute for Motorcycle Safety e.V., Essen, 2008

Nishikawa, Yutaka; Nanri, Takehiko; Takenouchi, Kazuya; Takayanagi, Shinji; Tani, Kazuhiko; Fukaya, Syuichi: Experimental Study of Pitching Control of Large Motorcycles with Short Wheelbases using a Brake-by-Wire System. In: Proceedings of the 7th International Motorcycle Conference 2008, pp. 430-446, Institute for Motorcycle Safety e.V., Essen, 2008

Nishimoto, Yukimasa; Iwashita, Kanau; Tsuchida, Tetsuo; Thiem, Michael: Research on Combined Brake System for Motorcycle. In: Proceedings of the International Motorcycle Conference 1991, pp. 327-345, Institute for Motorcycle Safety e.V., Bochum, 1991, ISBN 3-923994-11-7

Osborn, F. J.; Wood, N. F.: Lenkvorrichtung – insbesondere für Motorräder. Patent Application DE494664A, 1928/30

Pacejka, Hans: Tire and Vehicle Dynamics (3rd edition), Butterworth-Heinemann, 2012, ISBN 978-0080970165

Pieve M.; Santucci, M. D.; Di Tanna, O.: Safety In Motion (SIM). Integrated approach for motorcycle safety. In: Proceedings of the 8th International Motorcycle Conference 2010, pp. 167-185, Institute for Motorcycle Safety e.V., Essen, 2010

PISa – virtual: www.pisa-project.eu, last access: 2014-11-20

Präckel, Jürgen: Die Motorradbremsung im System Mensch / Maschine / Umgebung. Fortschritt-Berichte VDI Reihe 12 Nr. 384, VDI-Verlag, Düsseldorf, 1999, ISBN 3-18-338412-4

Quinny – virtual: "Automatic Safe Steering". http://dohnal.comnex.net/... ...jogger/quinny.htm, last access: 2014-05-06

Roll, Georg; Hoffmann, Oliver: Evaluation of the safety benefits of electronic brake-control systems in single-track vehicles. In: Proceedings of the 8th International Motorcycle Conference 2010, pp. 423-513, Institute for Motorcycle Safety e.V., Essen, 2010

SafeRider – virtual: www.saferider-eu.org, last access: 2014-11-20

Schneider, Ralf: Vollbremsung in Schräglage. In: Motorrad 23/2013, Test + Technik, pp. 52-55, Motor Presse Stuttgart, Stuttgart, 2013

Schneider, Ralf: Schrecklage und Schrägbremsen. In: Motorrad 04/2014, Test + Technik, pp. 38-41, Motor Presse Stuttgart, Stuttgart, 2014

Seidl, Josef: Lenkung für ein Fahrzeugrad (EN: Front wheel steering for motorcycle - incorporates horizontal forks and linked steering arms). Patent Application DE3914050A1, 1989/90

Seidl, Josef: Motorrad. Patent Application DE102006024326A1, 2006/07

Seidl, J.; Heyl, G.: Kugelgelenk mit aktiver Dämpfungsverstellung (EN: Ball joint e.g. for front suspension of vehicle has adjustable tensioning device to vary pre-tension between joint body and bearing parts). Patent Application DE10245983A1, 2002/04

Seiniger, Patrick: Erkennbarkeit und Vermeidbarkeit von ungebremsten Motorrad-Kurvenunfällen. Fortschritt-Berichte VDI Reihe 12 Nr. 707, VDI-Verlag, Düsseldorf, 2009, ISBN 978-3-18-370712-9

Seiniger, Patrick; Winner, Hermann; Schröter, Kai; Kolb, Friedrich; Eckert, Alfred; Hoffmann, Oliver: Development of a roll angle sensor technology for future brake systems. In: Proceedings of the 6th International Motorcycle Conference 2006, Institute for Motorcycle Safety e.V., Essen, 2006

Smith, Malcom Clive: Force-controlling mechanical device. Patent Applications WO2003005142A1, 2002/03; EP1402327B1, 2002/10; US20050034943, 2004/05; US7316303B2, 2004/08, and others

Spiegel, Bernt: The Upper Half of the Motorcycle – on the unity of rider and machine. Whitehorse Press, Center Conway, New Hampshire, 2010, ISBN 978-1-884313-75-2

Stern, Wolfgang: Motorcycle Safety Trips – Experience with motorcycle safety trainings in real traffic situations. In: Proceedings of the 6th International Motorcycle Conference 2006, Institute for Motorcycle Safety e.V., Essen, 2006

Stoffregen, Jürgen: Motorradtechnik (7., überarbeitete u. erweiterte Auflage). Vieweg + Teubner Verlag, Wiesbaden, 2010, ISBN 978-3834806987

Suzuki, Osamu: Steering assist system for motorcycle. Patent Application US2009/0139793A1, 2008/09

Tani, Kazuhiko; Toda, Makoto; Takenouchi, Kazuya; Fukaya; Shuichi: Research on Brake-by-Wire System for Super-Bike Race Motorcycle. In: Proceedings of the 8th International Motorcycle Conference 2010, pp. 378-395, Institute for Motorcycle Safety e.V., Essen, 2010

TIER – virtual: www.tiermotor.com, last access: 2014-11-15

Thiers, Jean-Michel: Motorcycle Steering. Patent Application US7887077B2, 2007/11

Uden, Edgar: Lenkungsdämpfer mit veränderbarer Wirkung für Kraftfahrzeuge und andere Fahrzeuge mit nur einem gelenkten Vorderrad. Patent Application DE102006036135B4, 2006/10

Unger, Martin: Sicherheitskonzept zum Schutz von Motorradfahrern. In: Proceedings of the 8th International Motorcycle Conference 2010, pp. 2-48, Institute for Motorcycle Safety e.V., Essen, 2010

Wakabayashi, T.; Sakai, K.: Development of electronically controlled hydraulic rotary steering damper for motorcycles. In: Proceedings of the 5th International Motorcycle Conference 2004, pp. 489-509, Institute for Motorcycle Safety e.V., Essen, 2004

Weidele, Alois: Motorradlenkung (EN: Compensated Steering for Motorcycle). Patent Application DE3933058A1, 1989/1990

Weidele, Alois: Untersuchungen zum Bremsverhalten von Motorrädern unter besonderer Berücksichtigung der ABS-geregelten Kurvenbremsung. Fortschritt-Berichte VDI Reihe 12 Nr. 210, VDI-Verlag, Düsseldorf, 1994, ISBN 3-18-321012-6.

Weidele, Alois: Skriptum Motorräder 2014. Material for the lecture "Motorcycles" at TU Darmstadt, Institute of Automotive Engineering (*FZD*), Darmstadt, 2014

Weidele, A.; Schmieder, M.: Research on the power transfer between motorcycle tyres and real road surfaces. In: Proceedings of the 23rd FISITA-Congress, 1990, paper 905213

Weldy, R. A.: Steering and suspension system for the front wheel of a three-wheeled vehicle. Patent Application US4353567A, 1980/82

Will, S.; Pleß, R.; Guth, S.: Bringing single track vehicle dynamics to motorcycle riding simulators – results of a pilot study. In: Proceedings of the Bicycle and Motorcycle Dynamics Conference – BMD 2016, Milwaukee, USA, 2016

Willig, R.; Lemejda, M.: A New Inertial Sensor Unit for Dynamic Stabilizing Systems of Powered Two Wheelers. In: Proceedings of the 9th International Motorcycle Conference 2012, pp. 66-84, Institute for Motorcycle Safety e.V., Essen, 2012

Winkelbauer, Martin: Riding Left Hand Corners: Facts and Measures. In: Proceedings of the 10th International Motorcycle Conference 2014, pp. 44-61, Institute for Motorcycle Safety e.V., Essen, 2014

Winner, H.; Hakuli, S.; Lotz, F.; Singer, C. (Ed.): Handbook of Driver Assistance Systems, Springer International Publishing, 2016, ISBN 978-3-319-12351-6

Winner, H.; Hakuli, S.; Lotz, F.; Singer, C. (Ed.): Handbuch Fahrerassistenzsysteme, ATZ/MTZ-Fachbuch, Springer Wiesbaden, 2015, ISBN 978-3-658-05734-3

World Health Organization (WHO): Global status report on road safety 2013: supporting a decade of action, 2013, ISBN 978-92-4-156456-4, www.who.int, last access: 2014-04-30

Wunderlich – virtual: BMW R1200GS LC Hybrid, www.wunderlich.de/action/... ...konzeptfahrzeuge/r/wunderlich-r-1200-gs-lc-hybrid/, last access: 2016-09-08

Yildirim, Fevzi; Mörbe, Matthias: Modern Brake Control Systems and Sensor Systems for Power Two Wheeler (PTW). In: Proceedings of the EuroBrake Conference 2013, FISITA (UK) Ltd., London, 2013

Own Publications

Publications as Main Author

Schröter, K.; Bunthoff, J.; Fernandes, F.; Schröder, T.; Winner, H.; Seiniger, P.; Tani, K.; Fuchs, O.: Brake Steer Torque Optimized Corner Braking of Motorcycles. In: Proceedings of the 8th International Motorcycle Conference 2010, pp. 396-422, Institute for Motorcycle Safety e.V., Essen, 2010

Schröter, K.; Wallisch, M.; Vasylyev, O.; Schleiffer, J.-E.; Pleß, R.; Winner, H.; Tani, K.; Fuchs, O.: Update on Brake Steer Torque Optimized Corner Braking of Motorcycles. In: Proceedings of the 9th International Motorcycle Conference 2012, pp. 2-46, Institute for Motorcycle Safety e.V., Essen, 2012

Schröter, K.; Wallisch, M.; Weidele, A.; Winner, H.: Bremslenkmomentoptimierte Kurvenbremsung von Motorrädern. In: ATZ Automobiltechnische Zeitschrift 05/2013, „Special Motorrad“, pp. 436-443, Springer Vieweg, Wiesbaden, 2013, ISSN 0001-2785

Schröter, K.; Fuchs, O.; Winner, H.: Braking while Cornering on a Motorcycle with Brake Steer Torque Avoidance Mechanism. In: EuroBrake 2013, Book of Abstracts, p. 28ff, FISITA (UK) Ltd., 2013, ISBN 978-0-9572076-3-9

Schröter, K.; Seiniger, P.; Pleß, R.: Fahrdynamikregelsysteme für Motorräder. In: Winner, H.; Hakuli, S.; Lotz, F.; Singer, C. (Ed.): Handbuch Fahrerassistenzsysteme, ATZ/MTZ-Fachbuch, Springer Wiesbaden, 2015, DOI: 10.1007/978-3-658-05734-3_42

Schröter, K.; Seiniger, P.; Pleß, R.: Vehicle Dynamics Control Systems for Motorcycles. In: Winner, H.; Hakuli, S.; Lotz, F.; Singer, C. (Ed.): Handbook of Driver Assistance Systems, Springer International Publishing, 2016, ISBN 978-3-319-12351-6

Co-Authored Publications

Seiniger, P.; Winner, H.; Schröter, K.; Kolb, F.; Eckert, A.; Hoffmann, O.: Development of a roll angle sensor technology for future brake systems. In: Proceedings of the 6th International Motorcycle Conference 2006, pp. 369-388, Institute for Motorcycle Safety e.V., Essen, 2006

Seiniger, P.; Schröter, K.; Gail, J.: Perspectives for Motorcycle Stability Control Systems, International Conference on Safety and Mobility of Vulnerable Road Users (VRU): Pedestrians, Motorcyclists, and Bicyclists, Jerusalem, Israel, 2010

Winner, H.; Lattke, B.; Schröter, K.: Active Safety Approaches for Motorcycles. Proceedings of the 2011 International Conference on Advances in Construction Machinery and Vehicle Engineering (ICACMVE'2011), Shanghai, 2011

Seiniger, P.; Schröter, K.; Gail, J.: Perspectives for Motorcycle Stability Control Systems, in Accident Analysis & Prevention (AA&P), Volume 44, Issue 1, January 2012, Pages 74-81, journal homepage: www.elsevier.com/locate/aap, DOI: 10.1016/j.aap.2010.11.018

Lattke, B.; Schröter, D.; Schröter, K.; Winner, H.; Schlipsing, M.; Salmen, J.: Roll Angle Estimation: Evaluation of Approaches based on Vehicle Dynamics and Video Sensors. In: Proceedings of the 9th International Motorcycle Conference 2012, pp. 49-65, Institute for Motorcycle Safety e.V., Essen, 2012

Schlipsing, M.; Salmen, J.; Lattke, B.; Schröter, K.; Winner, H.: Roll Angle Estimation for Motorcycles; IEEE Intelligent Vehicles Symposium (IV) 2012, Alcalá de Henares, Spain, 2012, DOI: 10.1109/IVS.2012.6232200

Pleß, R.; Schröter, K.; Kranz, I.; Deforth, J.; Hummel, N.; Winner, H.: Quo Vadis, Darmstadt Method for Abrasive Testing. In: Proceedings of the 10th International Motorcycle Conference 2014, pp. 485-505, Institute for Motorcycle Safety e.V., Essen, 2014

Student Research Work

Student Research Work advised by the Author

Pleß, Simon: Validation of a Motorcycle Simulation Model. Studienarbeit[197] No. 982/08, 2009

Schröder, Timm: Design and Construction of a Prototype-Braking-System for a Research-Motorcycle. Bachelor-Thesis No. 1004/09, 2009

Fernandes, Felipe: Experimental Identification of Parameters for Driver-Optimal Braking of a Motorcycle in Turns. Bachelor-Thesis No. 1005/09, 2009

Bunthoff, Jan: Equipment of a Research-Motorcycle with a Brake-Steer-Torque-Avoidance-Mechanism. Bachelor-Thesis No. 1015/09, 2010

Römer, Timm: Development and Evaluation of alternative Concepts of Brake-Steer-Torque-Avoidance-Mechanisms for Motorcycles. Bachelor-Thesis No. 1020/09, 2010

Hämel, Tobias: Survey on the Corner Braking Behavior of Motorcycle Riders. Bachelor-Thesis No. 1031/10, 2010

Kalden, Alexander: Literature and Patent Research on Technical Counter Measures against the Brake-Steer-Torque on PTW. Bachelor-Thesis No. 1055/10, 2011

Magiera, Nils: Simulation Model for the Prediction of Steering Torque in PTW with Brake Steer Torque Avoidance Mechanism. Bachelor-Thesis No. 1073/11, 2011

Frisch, Simon: Countermeasures against Brake-Steer-Torque in Three Wheel Tilting Vehicles. Bachelor-Thesis No. 1074/11, 2011

Vasylyev, Oleg: Multi Body Simulation of a Motorcycle with Brake Steer Torque Avoidance Mechanism (BSTAM). Bachelor-Thesis No. 1095/11, 2012

Vollmuth, Thomas: Kinematic Analysis of a Multi-Lever-Front-Suspension for Powered-Two-Wheelers. Fahrzeugtechnische Projektarbeit[198] 1/11, 2012

Schaede, Carsten; Schleiffer, Jean-Eric; Stritzke, Felix: Optimization of a Research-Motorcycle with regards to Construction, Measurement Setup and Data Processing. Advanced Design Project No. 39/12, 2012

---

[197] At TU Darmstadt, a "Studienarbeit" is a student research project equivalent to a Bachelor-Thesis.

[198] A special form of student research project in vehicle technology for technical instructors.

Wallisch, Michael: Evaluation of Driving Tests with a Motorcycle with and w/o Brake Steer Torque Avoidance Mechanism (BSTAM). Master-Thesis Nr. 507/12, 2012

Fischer, Kilian: Investigations on a Motorcycle's Coupling of Steer and Roll Motion using the Example of Corner Braking. Bachelor-Thesis 1159/13

Rivera, Alex: Automated Evaluation of Abrasion Tests of Motorcyclists' Protective Clothing. US National Science Foundation Research Experience for Undergraduates Project, 2011

Ritter, Stefan: Modernization of the Darmstadt Test Rig for Impact-Abrasion-Testing of Motorcyclists' Protective Clothing. Diplomarbeit[199] No. 516/13, 2014

Historical Student Research Work on BSTAM at TU Darmstadt

The following student research projects were advised by Alois Weidele, Martin Schmieder, and Wolfram Seibert under leadership of Professor Bert Breuer in the 1990s.

Biermann, Michael: Entwurf einer Lösung zur Verhinderung des Bremslenkmoments an Motorrädern, Studienarbeit No. 388/89, 1990

Thiel, Norman: Entwurf einer Ansteuerung für den FZD-Motorrad-Bremslenkmomentverhinderer, Konstruktiver Entwurf[200] No. 459/90, 1991

Gross, Martin: Bau des FZD-Motorrad-Bremslenkmomentverhinderers, Studienarbeit No. 485/91, 1992

Wittmann, Justus: Konzeption, Bau und Inbetriebnahme einer Ansteuerung für den Motorrad-Bremslenkmomentverhinderer (BLMV) mit einem Gleichstrommotor, Diplomarbeit No. 225/91, 1992

Hermsdorf, Jörg: Konstruktion und Bau einer Vorrichtung zur Messung der Lenkermomente bei Einsatz des Bremslenkmomentverhinderers (BLMV) am FZD-Versuchsmotorrad, Diplomarbeit No. 227/91, 1992

Dörr, Andreas: Konzeption und Aufbau einer Ansteuerung für den Bremslenkmomentverhinderer (BLMV), Studienarbeit No. 489/91, 1992

Homann, Jörg: Konstruktion des FZD-Bremslenkmomentverhinderers und Analyse der Kinematik, Studienarbeit / Konstruktiver Entwurf No. 499/91, 1992

Scharting, Stefan: Endmontage und praktische Erprobung des FZD-Bremslenkmomentverhinderers (BLMV), Studienarbeit No. 545/92, 1993

---

[199] At TU Darmstadt, a "Diplomarbeit" is a student research project equivalent to a Master-Thesis.

[200] At TU Darmstadt, a "Konstruktiver Entwurf" is a student research project equivalent to a Bachelor-Thesis, with focus on layout and detailed design of mechanical components ready for manufacturing.